Study of Building Material Emissions and Indoor Air Quality

by

Xudong Yang

M.E., Thermal Energy Engineering

Tsinghua University, 1993

Submitted to the Department of Architecture
on August 6, 1999 in partial fulfillment of the
requirements for the Degree of Doctor of Philosophy in the field of
Architecture: Building Technology

at the

Massachusetts Institute of Technology

September 1999

Signature of Author_____
Department of Architecture
August 6, 1999

Certified by ___
Qingyan Chen
Associate Professor of Building Technology
Thesis supervisor

Accepted by _____
Stanford Anderson
Chairman, Departmental Committee on Graduate Students
Head, Department of Architecture

Thesis Committee:

Leon R. Glicksman, Professor of Building Technology and Mechanical Engineering
Ain A. Sonin, Professor of Mechanical Engineering
Leslie K. Norford, Associate Professor of Building Technology

Study of Building Material Emissions and Indoor Air Quality

by

Xudong Yang

Submitted to the Department of Architecture
on August 6, 1999 in partial fulfillment of the
requirements for the Degree of Doctor of Philosophy in the field of
Architecture: Building Technology

ABSTRACT

Building materials and furnishings emit a wide variety of indoor pollutants, such as volatile organic compounds (VOCs). At present, no accurate models are available to characterize material emissions and sorption under realistic indoor conditions. The objective of this thesis is to fill that gap.

Using the emission data measured in small-scale and full-scale environmental chambers, this investigation has developed a numerical model for simulating emissions of "wet" materials applied to porous substrates. This model considers VOC mass transfer processes in the air, material-air interface, material film, and the substrate. The model can predict "wet" material emissions under different environmental conditions (i.e., temperature, velocity, turbulence, and VOC concentration in the air) with reasonable accuracy.

We developed two models for simulating VOC emissions from dry materials. One is a numerical model for short-term predictions, the other is an analytical model for long-term predictions. The models have been successfully used to examine the VOC emissions from two particleboard samples and a polypropene Styrene-Butadiene Rubber (SBR) carpet.

A VOC sorption model has also been developed to analytically solve the VOC sorption rate as a function of air-phase concentrations. The model has been validated using an analytical solution as well as data obtained from sorption experiments.

The emission and sorption models that we developed have been further used to study indoor air quality (IAQ) in a small office with different ventilation systems. The results show that displacement ventilation may not provide better IAQ than mixing systems if the VOC sources are from the floor. Further, our study shows sink effects from internal walls of gypsum board.

Thesis Supervisor: Qingyan Chen
Title: Associate Professor of Building Technology

ACKNOWLEDGEMENTS

I would like to thank my supervisor, Professor Qingyan (Yan) Chen. For the past three years, he has been a constant source of guidance and support. His insightful comments and helpful discussions are invaluable to this work. I am especially grateful for his understanding, support, and encouragement when I face difficulties and failure. With his high standards in research, teaching, and personal integrity, Yan has been a role model for me.

My thanks also extend to the members of my thesis committee, Professors Leon Glicksman, Ain Sonin, and Leslie Norford. They give me valuable comments and insightful feedback in every phase of my research.

I am also grateful to the National Research Council (NRC) of Canada for allowing me to use their test facilities. Special thanks are given to Dr. Jianshun Zhang, Dr. John Shaw, Dr. Jie Zeng, Mr. Gang Nong, Dr. Jiping Zhu, Mr. Bob Magee, Ms. Ewa Lusztyk, Dr. Yan An, and Dr. Awad Bodalal for their cooperation, assistance, and helpful discussions.

My sincere thanks are also given to Professor Yi Jiang of Tsinghua University, Professor Shuzo Murakami of University of Tokyo, Professor John Spengler of Harvard School of Public Health, Drs. John Chang and Zhishi Guo of U.S. Environmental Protection Agency, Dr. Xiaoxiong (John) Yuan of Applied Materials, Inc., and Dr. Philomena Bluyssen of TNO (the Netherlands) for their advise, encouragement, and helpful discussions.

I would also like to express my appreciation to all staff members and colleagues of the Building Technology Program for their help and support. Especially, I want to thank Dorrit Schuchter, Kathleen Ross, Chunxin Yang, Jelena Srebric, Weiran Xu, Wei Zhang, Shiping (George) Hu, Junjie Liu, and Yi Jiang.

Finally, I am deeply indebted to my parents, my wife, and my brothers for their love, support, and encouragement all the time.

DEDICATION

To my parents, Yong Yang and Shuxian Zhang and

To my wife, Qing Shi

CONTENTS

Chapter 1

Introduction

Indoor air quality (IAQ) is currently of great public concern. This chapter reviews the problems associated with IAQ and current methodology in measuring and modeling the volatile organic compound (VOC) emissions from various building materials and furnishings. The review indicates a need for developing advanced models to fully characterize building material emissions and their impact on IAQ, which comprises the major objective of this thesis.

1.1 Overview of Problems Associated with Indoor Air Quality

Every day we breathe 10 m^3 of air. This amount is equivalent to 10 housefuls a year, yet this number can increase a factor of 10 via physical activities. This partly explains why people have been extremely concerned about air quality since ancient times. For a long time, however, the concern was almost exclusively with air quality in ambient air. Although some hygienists studied indoor air in 1800's (*e.g.*, Pettenkofer, 1872), concern about the effects of indoor air on human health arose in the past 20 years.

Today, indoor air pollution has been identified by the U.S. Environmental Protection Agency (EPA) and World Health Organization (WHO) as one of the top environmental risks to the nations' health (WHO, 1989; US EPA, 1990). The high risk from exposure to indoor pollution reflects the elevated concentration of indoor contaminants, the large number of people exposed to indoor air pollution, and the amount of time spent indoors.

The causes of elevated indoor contaminant concentrations are mainly due to two reasons. First, with the advancement of modern technology, the types and amounts of contaminants released into the indoor environment have increased dramatically. New buildings contain many synthetic building materials and furnishings from walls to carpets to air conditioning systems. Use of these new materials and furnishings have resulted in a large number of new indoor pollutants in greater concentrations (van der Wal *et al.*, 1991; Brown *et al.*, 1994). On the other hand, in order to save energy, the air tightness of buildings has been improved and the supply of fresh air (by either natural or mechanical ventilation) has been reduced (Maga and Gammage, 1985; Esmen, 1985). The effects of these two factors combined have increased the indoor air pollutant levels significantly. Studies indicate that indoor air is far more polluted than outdoor air. As evidence, a series of long-term EPA studies of human exposure to air pollutants indicated that indoor levels of many pollutants may be 25 times, and occasionally more than 100 times, higher than outdoor levels (US EPA, 1988).

As a result of deteriorated IAQ, numerous cases of health complaints among employees in office buildings have been lodged with federal and state agencies. An EPA report (1991) suggested that up to 30 percent of new and remodeled buildings worldwide have been the subject of a significant number of complaints related to IAQ. The complaints

can be divided into two categories: sick building syndrome (SBS) and multiple chemical sensitivity (MCS) (Ashford, 1991). SBS is said to affect otherwise healthy persons whose adverse symptoms are related to time spent in a particular building and which wane when the affected persons leave a suspected problematic indoor air environment. MCS sufferers exhibit similar symptoms, but they are not restricted to a single environment and they manifest as symptoms of continuous discomfort and illness. SBS is better characterized than MCS, but both suffer from imprecise definitions, a lack of consistent health effect markers, and an understanding of causative mechanisms. According to the US EPA (1991), indications of SBS include:

- Significant complaints from building occupants of acute discomfort, *e.g.*, headache; eye, nose, or throat irritation; dry cough; dry or itchy skin; dizziness and nausea; difficulty in concentrating; fatigue; and sensitivity to odors.
- The cause of symptoms is not known.
- Most of the complaints report relief soon after leaving the building.

In addition to health problems associated with poor IAQ, indoor air pollution also has economic effects including loss of worker productivity, direct medical costs, and materials and equipment damage. Fisk and Rosenfeld (1997) estimated that the annual economic cost from poor IAQ for the United States is $6 billion to $19 billion from respiratory diseases, $1 billion to $4 billion from allergies and asthma, $10 billion to $20 billion from sick building syndrome symptoms, and $12 billion to $125 billion from reduced worker performance. Haymore and Odom (1993) have also estimated that the overall economic impact of poor indoor air quality in the United States alone is a staggering $40 billion per year.

In non-industrial buildings, the most common contaminants that can cause SBS and MCS are the Volatile Organic Compounds (VOCs), a broad range of compounds with boiling points from less than 0 °C to about 400 °C. Indoor VOCs come from a wide variety of sources such as building materials, ventilation systems, household and consumer products, office equipment, and outdoor related activities (traffic, neighborhood industry) (Wolkoff, 1995).

Among the sources mentioned above, building materials, furnishings, and consumer products have received considerable attention. A review by De Bellis *et al.* (1995) indicated that more than 60% of indoor VOCs are emitted from building materials. These materials include, but are not limited to, wood stain (Chang and Guo, 1992; Zhang *et al.*, 1999), latex paints (Guo *et al.*, 1996), floor wax (Chang, 1992), carpet materials (Hodgson *et al.*, 1993), PVC flooring (Christianson *et al.*, 1993), gypsum wallboard (Matthews *et al.*, 1987), insulation materials (Wallace *et al.*, 1987), and heating, ventilating, and air-conditioning (HVAC) systems (EC, 1997). Public officials are gradually acknowledging VOC sources as pollutants in various new national standards (DIN-1946 1994, SBE 1995), in European guidelines (CEC 1992), in the European draft

pre-standard (EDP 1994), and in the new draft of ASHRAE 62 ventilation standard (ASHRAE 1996).

Due to the large amount of materials used in buildings and their constant exposure to indoor air, there is a growing concern about the effects of these indoor pollutants on the health and comfort of building occupants. Over two hundred VOCs have been identified in the indoor environment (Brown *et al.*, 1994; Wolkoff, 1995). The presence of VOCs in indoor air, as defined by the WHO (1989), has in the past decade often been associated with adverse health effects such as sensory irritation, odor and the more complex set of symptoms of SBS. Also researchers have found that neurotoxic effects may follow from low level exposures to air pollutants (Molhave *et al.*, 1993). Reactions include runny eyes and nose, high frequency of airway infections, asthma-like symptoms among non-asthmatics, along with odor or taste complaints (WHO, 1989; Molhave *et al.*, 1998). More recently, scientists have suggested a possible link between the increase in allergies throughout the industrialized areas of the world and exposure to elevated concentrations of VOCs.

1.2 Methods for Measuring Building Material Emissions

Since building materials are the primary sources of VOCs in indoor environments, it is important to characterize their emissions and obtain reliable emission rate. Table 1.1 lists three types of methods widely used for measuring chemical emissions from building materials and furnishings: laboratory studies, dynamic chamber studies, and field studies (Tichenor, 1996).

1.2.1 Laboratory studies

Laboratory studies are usually conducted to determine emission compositions of materials. An example of laboratory studies is the static headspace analysis (Merrill *et al.*, 1987). In the headspace analysis, a specimen of material is placed in a small, airtight container made of inert, emission-free material. Samples of the air inside the container (*i.e.*, headspace) are analyzed by gas chromatography (GC) with mass spectrometry to identify the compounds and determine the compound concentrations emitted from the material. Static headspace analyses are normally conducted at ambient temperature (*e.g.*, 23 °C) and atmospheric pressure. However, in some cases higher temperatures are also used. One example is to determine the saturated vapor pressure of a "wet" material as a function of temperature.

Table 1.1: Typical emission testing methods (modified from Tichenor, 1996).

Name	Method	Pros	Cons
Laboratory Studies	Static headspace analysis	• Provide information on emission composition	• Does not provide emission rate data
Dynamic chamber studies	Measure emissions in small-scale chambers	• Provide emission composition and emission rate data under controlled environmental conditions • Cheap compared to full-scale chambers	• Chamber size may limit the use for some material sources (*e.g.*, furniture, work stations)
	Measure emissions in full-scale chambers	• Provide emission composition and emission rate data under actual environmental conditions	• Expensive compared to small-scale chambers • Difficult to control local environmental parameters (*e.g.*, local velocity)
Field studies	Measure emissions in actual buildings	• Provide integrated emission profile of all sources and sinks under uncontrolled conditions	• Emission rate determinations generally not possible • Differentiating between same emissions and sink re-emissions extremely difficult

1.2.2 Dynamic chamber studies

Although information on the composition of potential emissions can be obtained via laboratory studies, the information is not sufficient for characterizing building material emissions. The reason is that laboratory studies such as the headspace analysis do not provide the dynamic behavior of emissions. Dynamic chambers are usually used to obtain the emission data. Two types of chambers are commonly employed for emission testing: small-scale chambers and full-scale chambers.

Compared to full-scale chambers, small-scale test chambers (ASTM, 1990) are less expensive and widely used. The chamber size varies from 3.5×10^{-5} m^3 for the field and laboratory emission cells (Wolkoff *et al.*, 1993) to up to 1 - 2 m^3. The entire chamber system includes an environmental test chamber, an environmental enclosure to house the chamber, equipment for supplying clean and conditioned air to the chamber, and outlet fittings for sampling the air from the chamber's exhaust. To avoid possible emission from the chamber itself, all materials and components in contact with the panel specimen or air system from the chamber inlet to the sample collection point should be chemically inert.

Suitable materials include stainless steel and glass. All gaskets and flexible components should also be made from chemically inert materials.

Small chambers have obvious limitations. First, the flow and thermal conditions in a small-scale test chamber can not adequately represent the whole range of conditions in a real building. For materials whose emission characteristics are sensitive to flow and thermal conditions (*e.g.*, "wet" materials such as paints and wood stain), emission data measured using a small-scale chamber may not be applicable to buildings. Secondly, small chambers are generally not applicable for testing large material samples, equipment, whole pieces of furniture, and processes of applying emission materials (*e.g.*, painting process). Full-scale chambers are used to overcome the limitations of small chambers noted above.

A full-scale chamber usually consists of a full-size stainless steel room and an HVAC system with stainless steel components (*e.g.*, fan, ducts, dampers, coils, diffusers). Similar to small-scale chambers, a full-scale chamber also consists of a data acquisition system for sampling and analyzing the VOCs emitted from testing materials/products. Hence, a full-scale chamber is much more expensive and difficult to operate than a small-scale chamber. Currently, few national labs (US EPA, NRC in Canada, CSIRO in Australia) use a full-scale chamber for material emission studies.

The measurement of material emissions in a small-scale or full-scale chamber can be either direct or indirect. An example of direct measurement is the use of an electronic balance to monitor the weight decay of an emission source as a function of time (Zhang *et al.*, 1999). Although this measurement provides the most direct information on emissions, it also has limitations. For instance, the method is only applicable for sources that have a large emission rate and fast decay, in particular, "wet" materials. For many dry materials the emission rates are so low that the weight decay cannot be accurately detected by an electronic balance even with a high resolution. In these cases indirect measurements are used. Indirect measurement monitors time-dependent concentration changes in the chamber resulting from emissions of a test material. Since the measured data indirectly reflect the emission rates, an emission model is required to calculate the emission rates based on the measured concentration data. The methods of calculating emissions based on the measured concentration data will be discussed in Section 1.3.

1.2.3 Field studies

While dynamic chamber studies are useful for determining emission rates of indoor materials under controlled conditions, they still cannot measure the contaminant exposures in actual buildings. Actual buildings may be composed of thousands of different materials and it would be impossible to conduct controlled experiments using an environmental chamber. Field studies provide an opportunity to monitor the air pollution level and evaluate factors such as variable air exchange rates, operating of HVAC systems, room-to-room air movement, and occupant activities on indoor air pollution.

Literally hundreds of field studies have been conducted to investigate indoor air pollution problems. Unfortunately, many indoor sources share common emission profiles in terms of compounds emitted. Thus, isolating the source of common indoor pollutants based on indoor measurements may be impossible. In addition, re-emissions from indoor sinks can cause elevated indoor concentrations of some pollutants long after the original source of the pollutants has been depleted or removed. Thus, field study results generally only provide an integrated assessment of IAQ from a multitude of sources and re-emitting sinks under uncontrolled conditions. Using field study results to determine the emission rates of individual sources is extremely difficult, if not impossible.

1.3 Methods for Modeling Building Material Emissions

The purpose of modeling emission sources is to predict the emission rates of various VOCs as a function of time under typical indoor air conditions. Source models are useful for analyzing the emission data obtained from test chambers, for extrapolating the test results beyond the test period, for developing simplified methods and procedures for emission testing, and for evaluating the impact of various building materials on VOC concentrations in buildings.

Before discussing the emission models for different building materials, it is worthwhile to briefly mention the factors that may affect material emissions. VOC emission rates of building materials and furnishings are affected by many factors such as product type ("wet", dry), chemical compounds used, manufacturing process, product age, environmental conditions (temperature, air velocity and turbulence, humidity, air phase VOC concentration), and the way they are packaged, transported, stored, and used in buildings. In general, these factors can be classified into two categories:

(1) Internal factors: the inherent properties (*e.g.*, physical properties, chemical properties) of a material.

(2) External factors (or environmental conditions): the surrounding conditions, such as temperature, air velocity, turbulence, relative humidity, and air phase VOC concentration. These factors exist independent of the material.

Theoretically, the emission characteristics of a building material can be predicted with sufficient knowledge of each individual factor, internal and external. However, this is very difficult (if not impossible) because in most cases a material in general behaves like a black "box". Material emissions observed by experiments reflect very few perspectives from outside the "box", resulting from interactions of numerous internal and external factors.

Therefore, an emission model must be developed based on experimental data (*e.g.*, by environmental chamber tests). The purpose of the experimental data is to provide some

knowledge on the impact of influencing factors, either internal or external, on emissions. In practice, two modeling approaches are usually employed.

The first approach is to derive a mathematical model based solely on the observation and statistical analysis of emission data obtained from environmental chamber testing. A model like this (so-called empirical model) is nothing more than a simple representation of the experimental data. The impact of each internal or external factor on emissions are all lumped together. A common example is the widely used first-order decay model (*e.g.*, Chang and Guo, 1992; Colombo *et al.*, 1992). The model assumes that the emission rate from a material follows an empirical first-order equation. The empirical constants used by the model are obtained by matching the model prediction with the experimental data.

An empirical emission model is simple and easy to use. However, it is not able to provide insight into the physical emission mechanisms. It does not allow separation of internal factors from external ones and therefore, does not allow scaling of the results from chamber to building conditions.

The second approach is to develop models based on the mass transfer theory. This type of model is developed in light of the notion that VOC emissions from building materials are governed by well-established mass transfer principles and hence are predictable using mechanistic mathematical models. From a mass transfer point of view, two main mechanisms contribute to material emissions: VOC diffusion in a material as a result of a concentration gradient, and interfacial mass transfer due to the interaction of the material surface with the adjacent air. In general, the internal factors of a material can be attributed to a few physical properties (*e.g.*, diffusivity) that govern the internal diffusion, while the external factors govern the interfacial mass transfer. Unlike the empirical models, mass transfer-based models allow separation of internal and external factors. This allows scaling the model parameters developed from chamber experiments (which should be independent of the chamber) to buildings.

Currently, several mass transfer-based models are available for predicting emissions from different types of building materials and furnishings. However, these models have limitations, as we highlight below.

Based on the emission characteristics, building materials can be broadly categorized into "wet" coating materials and dry materials. VOC emissions from "wet" coating materials could result from interfacial mass transfer and/or internal diffusion. Currently, we lack a complete emission model that considers both the internal diffusion and the interaction between the material and its environment. Much progress has been made in developing mass transfer models for the evaporation dominant process. Guo and Tichenor (1992) did pioneer work by developing an evaporative mass transfer model, the Vapor pressure and Boundary layer (VB) model, for VOC emissions from interior architectural coatings. The VB model has been widely used for simulating early-stage emissions of "wet" materials. However, it requires the gas phase mass transfer coefficient as an input. The gas phase

mass transfer coefficient is usually determined by the flow field, such as air velocity, flow direction, and turbulence. Sparks *et al.* (1996) developed a correlation of the gas phase mass transfer coefficient with the flow Reynolds number (Re) and the VOC Schmidt number (Sc). However, the correlation was based on small-scale chamber tests and may not be applicable to buildings in which the flow conditions usually cannot be represented by a single Reynolds number. Therefore, Yang *et al.* (1997, 1998a) and Topp et al, (1997) developed models to numerically calculate the dynamic mass transfer coefficient by using the computational fluid dynamics (CFD) technique.

Despite the above progress, not much work has been done on the material side. The VB model assumes a uniform VOC concentration in the material film and neglects internal diffusion. Hence, such a model applies only when evaporation is dominant. Recently, researchers have proposed both empirical models (Guo *et al.*, 1996a) and semi-empirical models (Sparks *et al.*, 1999) to examine the entire process (from "wet" to dry). However, the use of empirical factors limits the general applicability of these models. Further, all the existing models fail to consider the impact of substrates on emissions.

Unlike the models for "wet" materials, most existing models for dry materials assume that emissions are exclusively dominated by internal diffusion. The existing models, so-called diffusion models, use Fick's law to solve VOC diffusions in a solid under simple initial and boundary conditions. For example, Dunn (1987) calculates diffusion-controlled compound emissions from a semi-infinite source. Little *et al.* (1994) simulates the VOC emissions from new carpets using the assumption that the VOCs originate predominately in a uniform slab of polymer backing material. These models, though based on the sound mass transfer mechanisms of VOC species, still have limitations:

(1) They presume that the only mass transfer mechanism is the diffusion through the source material. The models neglect the mass transfer resistance through the air phase boundary layer and also the air phase concentration on emissions. Although this may be true for some dry materials, the assumption as a general one has not been well justified.

(2) They tend to solve the VOC diffusion problem analytically. These models usually apply only to a 1-D diffusion process with simple boundary and initial conditions. In practice, emissions can be 3-D with complicated initial and boundary conditions.

The above indicates that, although there is general agreement that emissions from indoor sources can be described by fundamental mass transfer theories, a generalized model that has been validated with experimental data for detailed emission study is not yet available. This suggests a need for developing advanced models to fully characterize building material emissions and their impact on IAQ, as will be described in the next section.

1.4 Aim of the Present Work

In recent years, VOC emissions from building materials have been the subject of considerable studies. However, due to the complexity of the emission processes, the studies are still mainly by experimental approach. In the past, many environmental chamber tests have been conducted to identify the VOCs emitted from different building materials. The ultimate goal of such studies should be to provide accurate and sufficient information for designing a healthy indoor environment. Unfortunately, very few studies have been focused on that goal and in particular, have answered the following questions:

- What do the emission data measured from a standard emission chamber mean in actual buildings whose environmental and boundary conditions are usually significantly different from those of the test chamber?
- How can we predict the actual indoor contaminant exposures, given that several emission sources and sinks usually co-exist in buildings?
- How can we reduce indoor contaminant levels using control or mitigation strategies, such as selecting effective ventilation systems?

The purpose of this thesis is to address the three questions mentioned above. This requires further research in the following areas:

(1) To understand the mechanisms of VOC emissions from different types of building materials and furnishings, and to develop comprehensive mathematical models for simulating the building material emissions under actual environmental conditions.

(2) To study the characteristics of VOC sorption by building materials. In addition to emitting VOCs, building materials may adsorb some compounds emitted by other materials, releasing them at a later time. This complicates the investigation of material emissions in actual rooms.

(3) To study the combined impact of material emissions, sorption, and air movement on IAQ and indoor pollutant exposures.

This thesis is organized as follows. In Chapter 2, the VOC emissions of two "wet" materials (a commercial wood stain and a decane) are measured. The purpose of the study is to understand systematically the effects of environmental conditions (*e.g.*, temperature, velocity, and velocity fluctuation) and substrate on "wet" material emissions. In Chapter 3, a numerical model using CFD techniques is developed to simulate the "wet" material emission processes. The experimental data measured in Chapter 2 are used to obtain the model parameters and also to validate the numerical model. In Chapter 4, we focus on emission modeling of dry sources, specifically, how to use the small-scale chamber data for both short-term and long-term emission predictions.

We use two particle boards and a polypropene styrene-butadiene rubber (SBR) carpet to demonstrate the modeling procedures and the effect of temperature on carpet emissions. Since sorption of VOCs by different materials can also affect VOC concentrations in indoor environments, Chapter 5 presents a new VOC sorption model for homogeneous building materials. The model solves analytically the VOC mass transfer rate at the material-air interface as a function of air phase concentration. It can be used as a "wall function" for solving the VOCs by a CFD program to study indoor air quality. Then in Chapter 6, we combine the material emission, sorption, and a two-layer turbulence model for a detailed study of IAQ and exposures in a room with different ventilation systems. Finally, Chapter 7 gives general conclusions and recommendations based on the entire research and experiments presented in this thesis.

Chapter 2

Measurements of VOC Emissions from "Wet" Coating Materials

In this chapter, the VOC emissions from "wet" coating materials are measured. The purpose of the study is to systematically investigate the effects of environmental conditions (temperature, velocity, turbulence, and VOC concentration in the air) and substrates on VOC emissions. We measured the VOC emissions from a decane and a wood stain coating using a small-scale ($0.4m^3$) and a full-scale ($55m^3$) environmental chamber. The results indicate that both the environmental conditions and the substrate significantly impact "wet" material emissions. The measured data are used for developing and validating a new emission model to be developed in Chapter 3.

2.1 Introduction

Interior architectural coatings such as wood stains, vanishes, and paints are widely used in buildings. In the United States, over 1 billion gallons (~3.8×10^9 liters) of paint are sold each year for industrial and residential purposes (Guo *et al.*, 1996a). Similar amounts of other coating materials are purchased by commercial and residential users. These materials are generally called "wet" materials because they are wet when applied onto a substrate and then gradually dry.

Most "wet" materials such as paints, varnishes, and wood stain contain petroleum-based solvents and thus emit a wide variety of VOCs. These VOCs can increase indoor air pollution (WHO, 1989). Hence, understanding the emission characteristics of "wet" materials is important for preventing indoor air pollution problems.

The types and amounts of VOCs emitted from "wet" materials are usually measured using environmental chambers. Previous studies have indicated that the emission process of "wet" materials appears to have three phases (Zhang *et al.*, 1999). The first phase represents the period shortly after the material is applied but is still relatively wet. The VOC emissions in this phase are characterized by high emission rates but fast decay. It appears that emissions are related to evaporation at the surface of the material. In the second phase, the material dries as emissions transition from an evaporation-dominant phase to an internal-diffusion controlled phase. In the third phase the material becomes relatively dry. In this phase the VOC off-gassing rate decreases and so does the decay rate. The dominant emission mechanism in this phase is believed to be the internal diffusion of VOCs through the substrate (Chang and Guo, 1992; Wilkes *et al.*, 1996; Zhang *et al.*, 1996a).

To fully understand the emission characteristics of "wet" materials, the factors that affect emissions must be identified and evaluated. Using environmental chambers, previous studies have found that the emissions of "wet" materials are likely to depend on environmental conditions (*e.g.*, temperature, air velocity, turbulence, humidity, VOC

concentration in air) and also physical properties of the material and the substrate (*e.g.*, diffusivity).

Among the factors that may affect "wet" material emissions, environmental conditions deserve special attention because the environmental conditions around a "wet" material in a building are usually different from those in a small-scale chamber (which is cheap and widely used for measuring material emissions). A small-scale chamber usually has simple flow boundary conditions and controlled iso-thermal conditions, while conditions in a room (uncontrolled turbulent and non-isothermal flow) can be more complicated and significantly different from the standard test conditions.

Currently, a wide variety of experimental data on the emission characteristics of "wet" coating materials can be found in the literature. However, most of the data were obtained under one set of environmental conditions (*e.g.*, 23 °C, 50% relative humidity, 1 air exchange per hour) from a small-scale environmental chamber. Although some investigations have either measured or addressed the impact of environmental parameters such as temperature and relative humidity on "wet" materials emissions (Zhang *et al.*, 1997; Haghighat *et al.*, 1998), detailed data are not available to systematically address such an impact to a large extent. In addition, the existing data are also difficult to use for developing and validating advanced emission models due to the lack of detailed information of flow and VOC boundary conditions and necessary physical properties.

Therefore, we have conducted experiments to measure material VOC emissions using a small-scale ($0.4m^3$) and a full-scale ($55m^3$) environmental chamber under different environmental conditions. A majority of the measurements were conducted in the small-scale chamber. We used the full-scale chamber to approximate airflows in an actual room or office. Data obtained from the full-scale chamber is used to validate a new emission model developed in Chapter 3. The following section discusses the experimental methods for measuring VOC emissions, a description of the testing results and analysis follows.

2.2 Experimental Method

In this section, the test materials, test facility, test conditions and cases, and the test procedure are presented sequentially. An analysis on the measured data is presented at the end of this section.

2.2.1 Test materials

The "wet" materials selected for emission tests were a commercial oil-based wood stain and a single compound (decane). Wood stain is a common architectural coating material with well-known emissions characteristics (Chang and Guo, 1992; Sparks *et al.*, 1996; Yang *et al.*, 1998a; Zhang *et al.*, 1999), although different wood stains may contain different compounds and exhibit different emission characteristics. The wood stain we tested contains evaporative VOCs and non-evaporative additives. Several dozen cans of

wood stain with the same product serial number (manufactured and filled on the same day) were purchased from a local store. Each can was used for only one measurement. The single compound decane was also tested because its emission characteristics can be compared with those of the wood stain as reference data.

In order to obtain useful and realistic emission data, these "wet" materials must be applied to an appropriate substrate. Two types of substrates were used for the emission measurements: oak board and glass plate. The oak board, a common building material, has a porous surface and absorbs liquid. Glass, on the other hand, is not permeable to VOCs. The purpose of using a glass substrate was to identify the possible substrate effect on emissions.

For each test, the "wet" material was applied to one side of the substrate. The emission area was 0.06 m^2 (0.24m $\times$ 0.25 m).

2.2.2 Test facility

Experiments were conducted in a small-scale and a full-scale environmental chamber at the National Research Council (NRC) of Canada. The following sections briefly describe the two environmental chambers and the corresponding emission measurement systems.

2.2.2.1 The small-scale environmental chamber system

The small-scale chamber (Zhang *et al.*, 1996a) consisted of an inner and an outer chamber, both made of stainless steel (Figure 2.1). The outer chamber (1.0 m long $\times$ 0.8 m wide $\times$ 0.5 m high or 0.4 m^3 in air volume) facilitates the control of temperature and humidity. Conditioned air was supplied to the outer chamber to maintain a constant temperature and humidity (ASTM, 1990). The inner chamber in which the test material was placed acted like a wind tunnel that provided controls for the local velocity over the surface of material samples under testing. The local velocity was controlled by a stainless tube-axial fan. The fan drew air through the inner chamber and discharged it through the holes into the outer chamber. A microcomputer was used to monitor and control the test conditions, including the air-exchange rate, temperature, and humidity within the chamber, air velocity above the material, ambient air temperature and relative humidity.

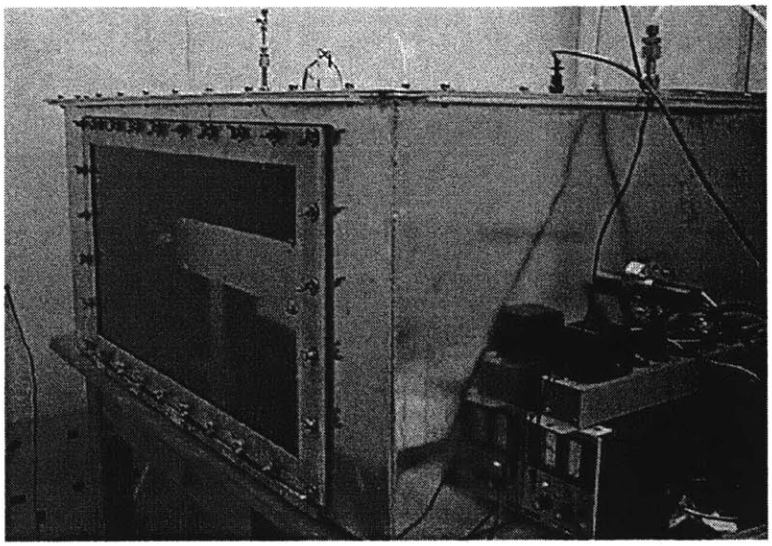

(a)

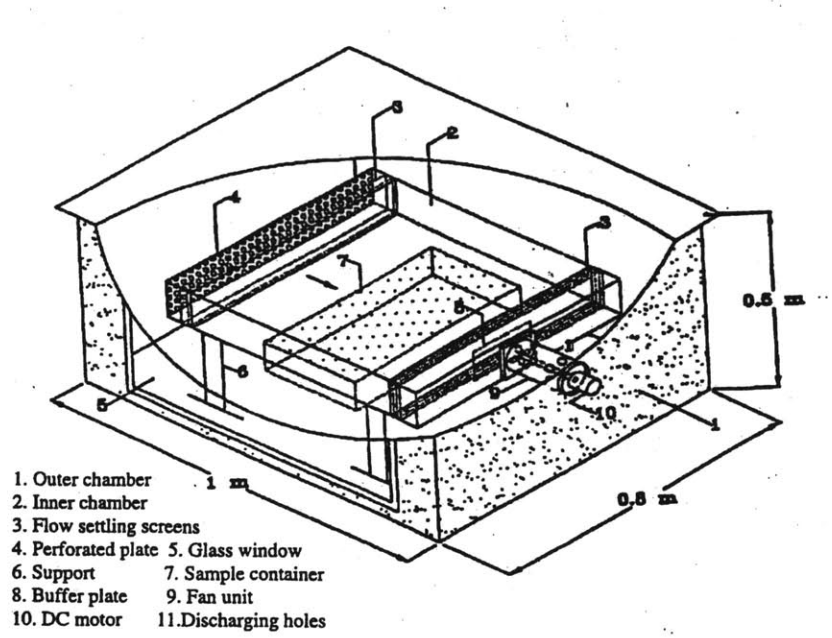

(b)

Figure 2.1 The small-scale chamber for emission measurements: (a) Photo of the chamber, (b) Sketch of the chamber.

For both the wood stain and decane, all the evaporable components were VOCs. An electronic balance was used to monitor the weight loss of the material due to the total VOC (TVOC) emissions from the test materials. The resolution of the electronic balance was 1.0 mg. During the experiment, the weight of the substrate specimen was measured every 10 seconds during the first 15 minutes. The measurement frequency was reduced to every 30 seconds between the 15^{th} minute to 1 hour period, and every 1 minute after 1 hour of the test. Data were recorded by a micro-computer that was connected to the electronic balance via an RS232 communication cable.

The weight decay data from the electronic balance provide the time-dependent TVOC emissions directly. However, no information on the emissions of single VOCs can be inferred from the data. The emissions of single VOCs were indirectly measured by tube sampling and gas chromatography (GC) analysis. Figure 2.2 shows the tube sampling process using a sampling pump with a controlled sampling rate. The sampling period and sampling volume were determined based on the estimated VOC concentrations in the chamber. In order to catch the high concentration variation in the first few hours, the chamber air was sampled every 5 to 15 minutes for the first 4 to 8 hours, and every 1 to 5 hours thereafter. The sampled tubes were analyzed using a Varian 3400cx GC with a flame ionization detector (FID) equipped with a multiposition thermal desorption and pre-concentration unit. The GC/FID was calibrated routinely using a mixture of benzene-toluene-xylene gas. The GC/FID analysis rendered the measured concentrations at each sampling time for both single VOCs and TVOC.

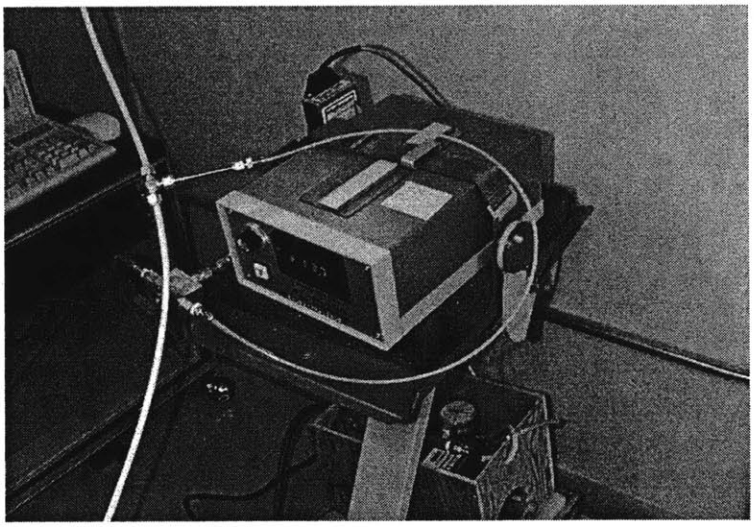

Figure 2.2 Sampling of chamber air using a sampling pump.

2.2.2.2 The full-scale environmental chamber system

The full-scale chamber test system (Zhang *et al.*, 1996b) consists of a stainless steel room and a heating, ventilating and air-conditioning (HVAC) system with stainless steel components (*e.g.*, fan, ducts, dampers, coils, etc.), as shown in Figure 2.3. The system provides controlled temperature, humidity, airflow rates and airflow patterns in the chamber with minimal contamination from the HVAC system itself. The full-scale chamber was used to evaluate the emissions under realistic flow conditions similar to those in office buildings.

The full-scale chamber is 5 m long × 4 m wide × 2.75 m high (55 m^3) as shown in Figure 2.3. A square air diffuser was located at the center of the ceiling and an exhaust opening was located at the edge of the ceiling. The air supply from the diffuser flowed along the ceiling and then mixed with the chamber air. The wood stain or decane applied to the substrate was placed 1.0 m from a side wall at the central section of the chamber (Figure 2.4) as the airflow there was expected to be approximately parallel to the substrate surface.

The TVOC emission rates, taken after the weight loss from the substrate, were also measured using the electronic balance. In order to identify the mixing condition and possible sink effect of the chamber, the TVOC concentrations in the full-scale chamber were measured using a gas monitor at several locations including the return/exhaust air duct, and center (x = 2 m, y = 1.4 m, z = 2.5 m) and one corner (x = y = z = 0.3 m) of the chamber. Figure 2.5 shows the Bruel & Kjaer Type 1302 multigas monitor for the TVOC measurements. The multigas monitor was calibrated by using cyclohexane (C_6H_{12}) as the reference gas. In addition, the TVOC and single VOC concentrations in the chamber exhaust were also analyzed using the GC/FID method.

For each test, the chamber was set at isothermal conditions so the measurement of temperature distributions in the chamber was not needed. The distributions of velocity and velocity fluctuations in the full-scale chamber were measured using a fast-response hot-wire anemometer and 24 hot-sphere anemometers. Results of the velocity measurements will be presented in Chapter 3, when the CFD simulation of air distributions is compared with the measured data.

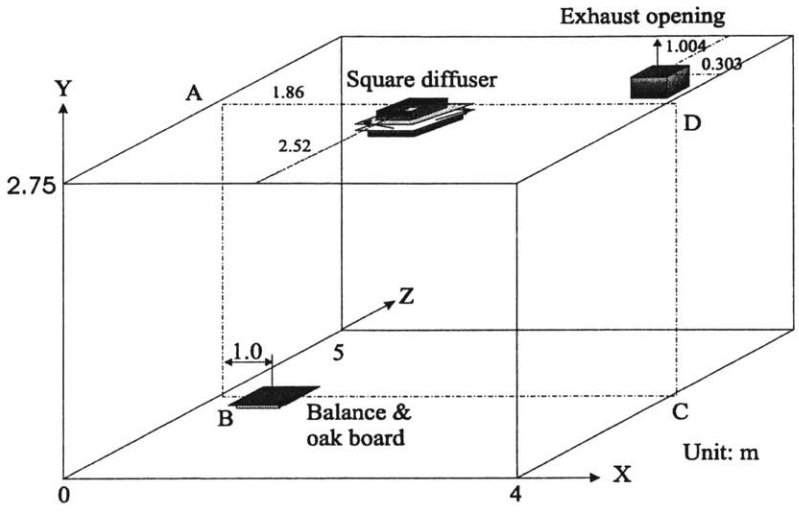

(a)

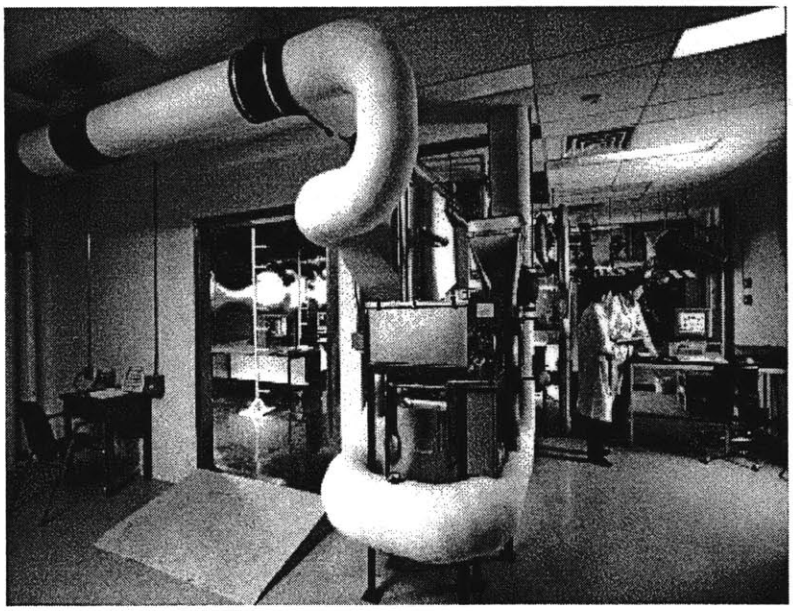

(b)

Figure 2.3 The full-scale chamber for emission measurements: (a) Sketch of the full-scale chamber, (b) An outside view of the full-scale chamber.

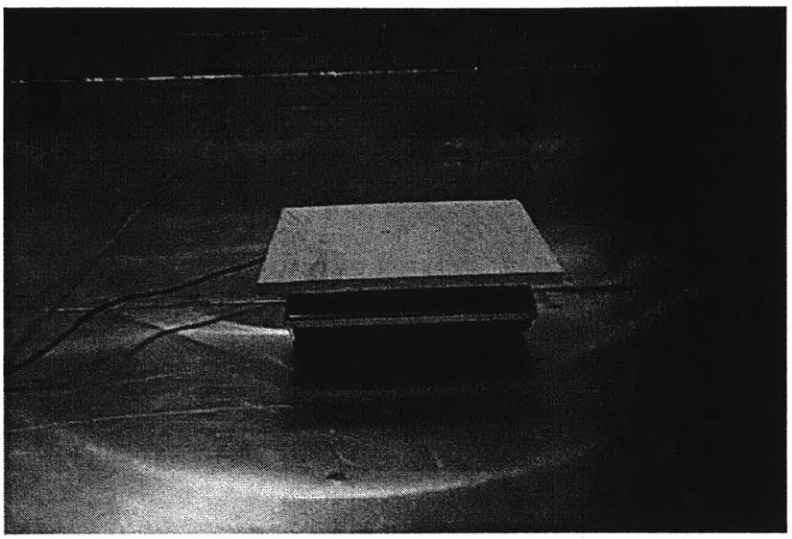

Figure 2.4 A test material in the full-scale chamber.

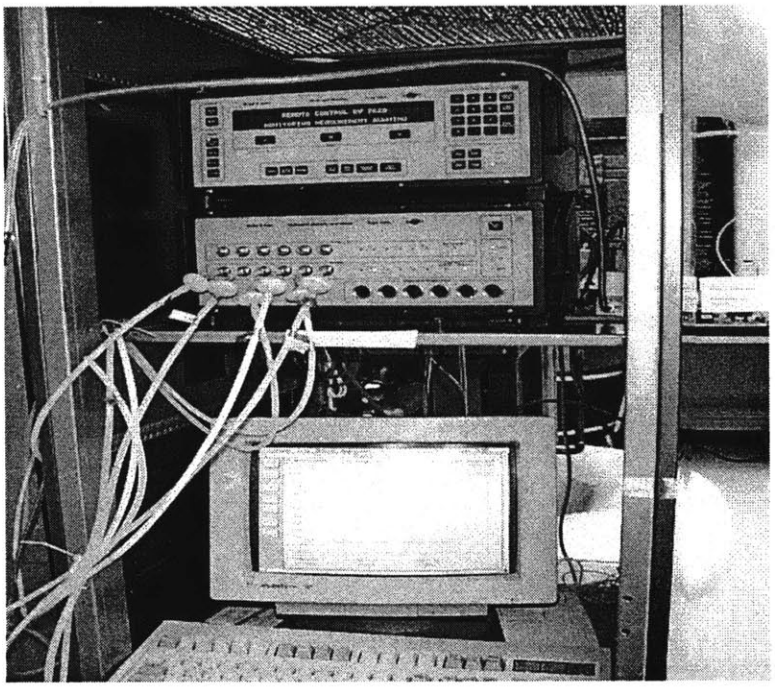

Figure 2.5 The multi-gas monitor for measuring TVOC concentrations in the full-scale chamber.

2.2.3 Test conditions and cases

For both decane and wood stain, we measured emissions under different temperature and airflow conditions by using the small-scale and full-scale chambers.

The small-scale chamber was used to measure the effects of temperature on emissions. The chamber was operated at four temperatures, *i.e.*, 20.5±0.5°C, 23.5±0.5°C, 27.5±0.5°C, and 31.5±0.5°C, representing low to high indoor temperatures. To measure the influence of different substrates on emissions, both the oak board and glass substrate were used. The air velocity above the material at the center of the inner chamber was controlled at approximately 0.15 m/s in the experiments, which corresponds to a common air velocity found indoors (Hart and Int-Hout, 1980; Zhang *et al.*, 1995). The air exchange rate of the entire chamber was 1.0 air change per hour (ACH) and the relative humidity in the chamber was controlled at 50±2%.

The full-scale chamber was used to measure the "wet" material emissions under realistic flow conditions and to compare the results with those from a small-scale chamber. We produced turbulent airflow with different distributions of velocity and velocity fluctuation above the test material by changing the air ventilation rates in the full-scale chamber. The full-scale chamber was operated at three different air exchange rates, *i.e.*, 1 ACH, 5 ACH and 9 ACH, to represent various situations in actual buildings. We measured the air velocities flowing around the material using a fast response hot-wire anemometer and registered about 0.04m/s, 0.10m/s, and 0.15m/s for 1ACH, 5ACH and 9ACH, respectively. Higher velocity fluctuations were observed with larger air exchange rates. The full-scale chamber was operated at a fixed temperature of 23.5±0.5°C and relative humidity of 50±2%.

A headspace analysis was also conducted on the commercial wood stain to (a) identify the most abundant VOCs emitted by the material, and (b) obtain the equilibrium air phase concentrations for the compounds identified (used in Chapter 3 to calculate the partition coefficient for VOCs). In the procedure of headspace analysis, a sample of wood stain was placed in a small airtight glass container. Three duplicate samples of the air inside the container (*i.e.*, headspace) were then analyzed by the GC/FID.

Table 2.1 summarizes the total 18 test cases.

Table 2.1 Test cases.

Case No.	Environmental conditions				Emission material	Substrate (0.24m×0.25m)
	Chamber size	Air change rate (ACH)	Temperature (°C)	Relative humidity (%)		
Case 0-1b	Headspace analysis		23.5±0.5		Wood stain	
Case 0-2b						
Case 0-3b						
Case 1-1a	Small-scale (1.0m×0.8m× 0.5m=0.4m^3)	1	20.5±0.5	50±2	Decane	Oak
Case 1-1b					Wood stain	
Case 1-2a			23.5±0.5		Decane	
Case 1-2b					Wood stain	
Case 1-3a			27.5±0.5		Decane	
Case 1-3b					Wood stain	
Case 1-4a			31.5±0.5		Decane	
Case 1-4b					Wood stain	
Case 1-5b			20.5±0.5		Wood stain	Glass
Case 1-6b			23.5±0.5			
Case 1-7b			27.5±0.5			
Case 2-1b	Full-scale (5.0m×4.0m× 2.75m=55m^3)	1	23.5±0.5	50±2	Wood stain	Oak
Case 2-2a		5	23.5±0.5		Decane	
Case 2-2b			23.5±0.5		Wood stain	
Case 2-3b		9	23.5±0.5		Wood stain	

2.2.4 Test procedures

The procedures for each test were as follows:

(1) We flushed the chamber with clean air until the TVOC background concentration was below 20 μg/m^3, which is less than 1% of the VOC concentration measured during the emission test. This ensured that all the VOCs adsorbed by the chamber walls were removed. At the same time, we controlled the air temperature, relative humidity, and air exchange rate to the pre-defined values as given in Table 2.1.

(2) After a steady state temperature and relative humidity had been reached in the chamber, the oak or glass substrate was then placed in the environmental chamber for pre-conditioning. This equalized the temperature and moisture content of the substrate with the ambient air as indicated by an almost constant reading of the electronic balance (indicating that no more moisture was lost or gained). During this period, we found that the electronic balance reading was very sensitive to the relative humidity fluctuation in the chamber, especially at temperatures higher than room temperature. Although the control system of the chamber was improved to reach a relative humidity fluctuation of less than 2% (5% in a common emission measurement), it was still difficult to achieve moisture equilibrium between the chamber air and the substrate, especially at high

temperatures (>27.5 C). We expected this to affect the emission data measured by the electronic balance.

(3) The conditioned substrate was then quickly removed from the chamber and the "wet" material was applied to the substrate outside the chamber. A guideline by Zhang *et al.* (1999) was followed in this process. The substrate was then placed on the electronic balance. For a small-chamber test, the specimen was placed inside the sample holder in the inner chamber, so that the emission surface was flush with the bottom surface of the inner chamber. The whole process took approximately 2 to 3 minutes to complete. The test start time ($\tau = 0$) began when the chamber door was closed.

2.2.5 Test data analysis

The time-dependent VOC emission rates can be obtained from the measured weight data.

For the oil-based wood stain, the weight loss was due entirely to the VOC emitted from the test materials. The emission rate can be calculated directly from weight data through the following equation:

$$E(\tau_{i+1/2}) = \frac{W(\tau_i) - W(\tau_{i+1})}{\tau_{i+1} - \tau_i} \tag{2.1}$$

where
$E(\tau_{i+1/2})$ = average emission rate between τ_i and τ_{i+1}, g/h
τ_i, τ_{i+1} = two adjacent sampling times, h
$W(\tau_i)$, $W(\tau_{i+1})$ = weights at the corresponding sampling times, g

This is the "direct calculation method." Based on differential theory, a shorter $\Delta\tau$ ($= \tau_{i+1} - \tau_i$) gives a more accurate emission rate. However, the resolution of the electronic balance was 1.0 mg. This means that a weight loss smaller than 1.0 mg could not be detected in the balance. Generally, the emission rates of a "wet" coating material change dramatically during the emission process. Thus it is usually difficult to determine a suitable $\Delta\tau$ in which to balance these two factors. Furthermore, a slight signal oscillation due to mechanical vibration or flow fluctuation can result in considerable weight fluctuations. This problem increases when a material is tested in a flow field with a high velocity and large turbulence. In order to obtain accurate emission rates, we used the following exponential-power equation to represent the measured weight data:

$$W(\tau) = ae^{-b\tau} + c(\tau + d)^f + g \tag{2.2}$$

where
$W(\tau)$ = weight of the "wet" material remaining in the substrate, g

a, b, c, d, f = constants determined by the Least Square Regression Analysis
g = weight of non-VOC content, g.

Eq. (2.2) contains three parts. The first part, $ae^{-b\tau}$, is a first-order decay model that accounts for the evaporation-controlled period. The second one, $c(\tau+d)^f$, is an empirical power-law model that accounts for the internal diffusion-controlled period. The last part, g, signifies the total weight of non-evaporable content.

In Eq. (2.2) g=0 for decane and g=15.6% of the initial mass of wood stain applied (estimated by using the weight loss of wood stain applied on a glass plate over a period of 96 hours). The TVOC emission rate can then be calculated by:

$$E(\tau) = -d[W(\tau)]/d\tau = abe^{-b\tau} - cf(\tau+d)^{f-1} \tag{2.3}$$

Previously, other empirical equations, such as a double-exponential equation, were used to represent the weight data (Zhang *et al.*, 1999). The double-exponential equation expresses the weight data in two exponential terms as follows:

$$W(\tau) = c_1 e^{-k_1\tau} + c_2 e^{-k_2\tau} + g \tag{2.4}$$

where c_1, c_2, k_1, and k_2 are constants whose values are obtained by the Least Square Regression Analysis.

We will demonstrate in section 2.3.2 that the exponential-power equation more accurately describes the weight data and hence the emission rates than the double-exponential equation.

2.3 Results and Discussion

2.3.1 Headspace results of the wood stain

A partial list of the compounds identified via the headspace analysis is given in Table 2.2. The results indicate that the wood stain contains four major compounds: nonane, decane, undecane, and octane. All these compounds belong to the same chemical category: the aliphatic hydrocarbon. Table 2.3 lists the vapor pressure and boiling point of these compounds. Generally, a compound with a higher vapor pressure or a lower boiling point is more volatile. Hence, Table 2.3 shows a descending volatility for octane, nonane, decane, and undecane, respectively.

Table 2.2 List of the identified compounds in the wood stain.

Peak No.	Peak Name	Retention Time (min)	Area (counts)	Concentration (mg/m^3)
1	Octane	12.23	334	31.7146
2	Nonane	16.751	26142	1495.602
3	Decane	22.826	35848	1977.007
4	Undecane	29.451	296	28.5036

Total Volatile Organic Compound (TVOC) concentration = 17131.4 mg/m^3

Table 2.3 Properties of major compounds from the wood stain (23 °C).

Compound	Formula	Molecular Weight	Vapor Pressure (mm Hg)	Boiling Point (°C)
Octane	C_8H_{18}	114.2	12.07	125
Nonane	C_9H_{20}	128.3	3.93	151
Decane	$C_{10}H_{22}$	142.3	1.25	174
Undecane	$C_{11}H_{24}$	156.3	0.35	196

The last column of Table 2.2 contains the equilibrium headspace concentrations for each compound and also for TVOC. The measured data will be used to calculate another important property: the partition coefficient that will be discussed in Chapter 3.

2.3.2 Emission rates obtained from the electronic balance

The regression results of *a*, *b*, *c*, *d*, and *f* for the test cases are summarized in Table 2.4. The regression coefficients R^2 were higher than 0.99, indicating that Eq. (2.2) represents the measured weight data.

Table 2.4 Regression data on $W(\tau)$ achieved through the exponential-power equation (Eq. 2.2).

Case No.	Initial mass (g)	a	b	c	d	f	g	Regression coefficient R^2
Case 1-1a	3.9225	2.7712	0.7454	7.0348	8.5287	-0.8128	0.0	0.9989
Case 1-1b	4.6914	0.5524	1.0255	2.6534	0.3066	-0.2090	0.7313	1.0000
Case 1-2a	4.3464	1.5436	0.9609	34.6272	4.4442	-1.6855	0.0	0.9977
Case 1-2b	4.5083	1.2904	1.9768	3.2826	1.9266	-0.4200	0.7028	0.9999
Case 1-3a	4.1322	2.6084	1.1230	35.4540	13.4632	-1.1901	0.0	0.9995
Case 1-3b	4.2760	0.5391	6.3675	3.1436	1.0427	-0.3785	0.6666	0.9990
Case 1-4a	4.0950	2.7420	1.4792	103.7674	25.2570	-1.3190	0.0	0.9983
Case 1-4b	3.7100	0.1463	8.4318	1.5828	0.3348	-0.4809	0.5783	0.9983
Case 1-5b	3.6252	3.0872	1.3725	5.8338E-2	3.3967	-5.6017	0.5612	1.0000
Case 1-6b	3.4231	2.9440	1.7752	1.1639	20.6933	-2.0168	0.534	0.9999
Case 1-7b	2.9990	1.4668	1.2499	3.4751	1.5545	-2.6407	0.4640	0.9999
Case 2-1b	4.5270	1.4434	1.7273	2.9565	1.9276	-0.2108	0.7057	0.9992
Case 2-2a	4.7660	3.2428	1.1942	2.3068	2.7613	-0.3132	0.0	0.9989
Case 2-2b	4.1860	0.8024	2.1436	2.1424	0.1595	-0.1173	0.6525	0.9965
Case 2-3b	4.9453	2.0753	0.0013	1.0190	0.2465	-0.5469	0.7709	0.9921

To assess whether the exponential-power equation (Eq. 2.2) represents the weight data better than the common double-exponential equation (Eq. 2.4), we can examine Figure 2.6, which illustrates an example of the measured weight data from the electronic balance. Figure 2.7 gives the relative weight error caused by the regression analysis using the exponential-power equation and double-exponential equation, respectively. Results show that although both equations appear to represent the weight data (relative error $<\pm 5\%$), the double-exponential equation generated a much higher weight error than the exponential-power equation. Since the emisison rates will be calculated based on the regressed equation, a small weight error may result in a significant error in the emisison rate, especially during the initial period. For example, the double-exponential equation underestimated the initial weight at a maximum 4%. As a result, the initial emission rates could be under-predicted by nearly 50%, as shown in Figure 2.8. The weight error found with the exponential-power equation was lower than 0.7% during the 24 hour period. The emission rates obtained from the exponential-power equation well represented those from the "direct calculation method," as illustrated in Figure 2.8.

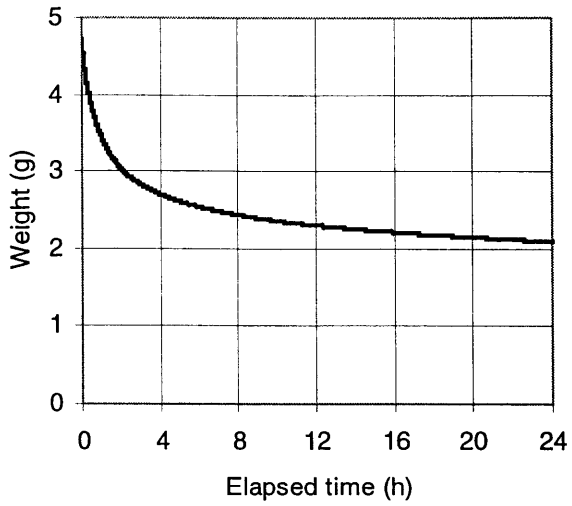

Figure 2.6 Measured weight data of Case 1-1b.

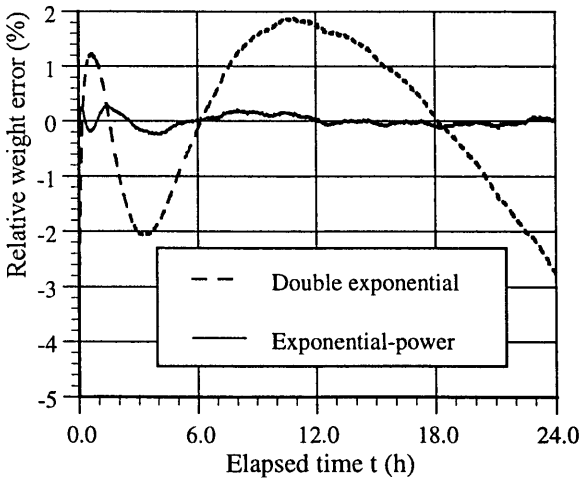

Figure 2.7 Relative weight error found by using different equations to represent the weight data (Case 1-1b).

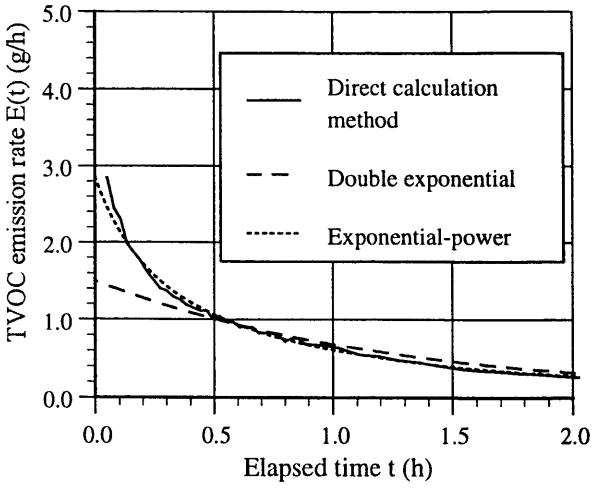

(a)

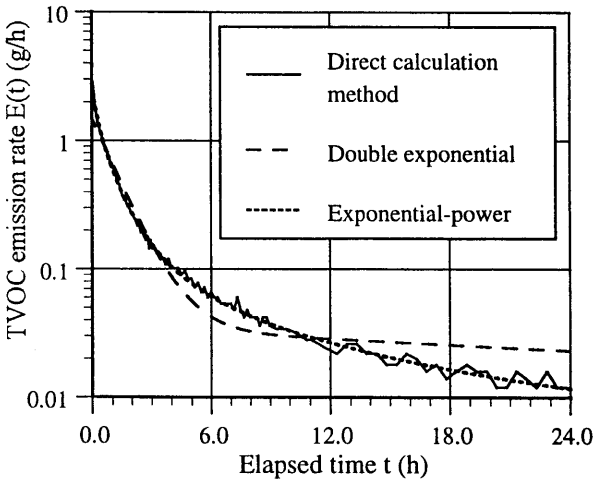

(b)

Figure 2.8 Comparison of emission rates obtained from three different methods (Case 1-1b): (a) 0 - 2 hours, (b) 0 - 24 hours.

The following sections examine the effects of substrate, airflow, and temperature on TVOC emissions. The analysis is based mainly on the weight data from the electronic balance.

2.3.3 Effects of substrate on emission characteristics

A glass substrate with the same surface area as that of oak was used to identify the substrate effect. Since it was difficult to apply the wood stain in the glass substrate uniformly, only the measured data within the first few hours (when most of the wood stain on the glass substrate was still wet) were reliable. After the first few hours, a portion of the area became dry while the rest remained "wet" (due to the non-uniform wood stain film on the glass); the measured weight data thus became less reliable.

Figure 2.9 shows the measured TVOC emission rates during the 6-hour test period from the wood stain applied to the two different substrates at 23.5 °C. A significant substrate effect on VOC emissions was evidenced by comparing the VOC emission rates of the oak board and glass substrate tests. The figure indicates that both the initial emission rate and emission decay rate of the glass substrate were considerably higher than those of the oak substrate during the 6-hour test period. When the wood stain was applied to the oak board instead of the non-permeable glass plate, the TVOC emission rates during the first 2 hours decreased by as much as 60%, while the emission period significantly increased.

The differences are also reflected by the amount of VOCs emitted in the 6-hour test period. We discovered that most of the TVOCs (>99.5%) were emitted for the cases with glass as the substrate. However, only 54.7% (20.5 °C), 63.9% (23.5 °C), and 52.4% (27.5 °C) of the TVOCs were emitted during the same period when oak board was the substrate.

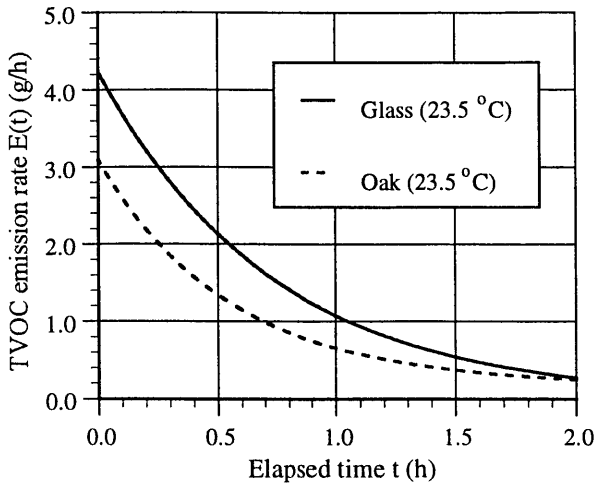

(a)

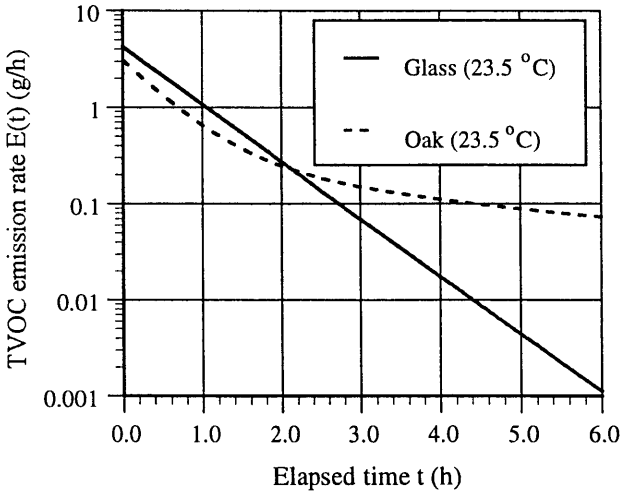

(b)

Figure 2.9 Comparison of measured emission rates at 23.5 °C: (a) 0 - 2 hours, (b) 0 - 6 hours.

The above results are similar to those observed by Chang *et al.* (1997) who measured VOC emissions from latex paint using a gypsum board and a stainless steel panel as the substrates. Based on their measurements, Chang *et al.* recommended that investigators use "real" substrates such as wood and gypsum board instead of "ideal" substrates such

as glass or stainless steel to evaluate the time-varying VOC emissions and drying mechanisms of wet products. Hereafter, our studies will use a realistic substrate such as oak board.

2.3.4 Effects of airflow on emission characteristics

As mentioned before, the effects of airflow on emissions were measured using the full-scale chamber. The full-scale chamber does not directly control local velocity or turbulence. Different airflow conditions were achieved by changing the air exchange rate of the chamber. By doing so, the VOC concentration in air, which also affects emissions, was inadvertently changed as well. Hence, the emission rates measured using a full-scale chamber reflect the combined effects of multiple factors (velocity, turbulence, flow direction, and VOC concentration in air) on emissions. The following sections provide the measurement results for both wood stain and decane.

2.3.4.1 Wood stain

Figure 2.10 presents the measured TVOC emission rates of wood stain using the electronic balance. Cases 2-1b, 2-2b and 2-3b were conducted in the full-scale chamber with air exchange rates of 1 ACH, 5 ACH, and 9 ACH, respectively. As a comparison, the measured TVOC emission rates of wood stain in the small-scale chamber (Case1-2b, velocity 0.15 m/s) are also shown in Figure 2.10. To analyze the differences among these cases, the 24-hour test period can further be divided into three periods: the initial period (0 - 0.2 h), the second period (0.2 h - 6 h), and the third period (> 6 h).

In the initial period (0 - 0.2 h) when the emissions were likely to be dominated by evaporation at the material surface, emission rates of the cases with greater velocity and turbulence (*e.g.*, Case2-3b, 9ACH) were higher than those with lower velocity and turbulence (*e.g.*, Case2-1b, 1ACH). This may be explained by two factors. First, the flow field with larger velocity and velocity fluctuation generated a larger mass transfer coefficient, and resulted in a larger initial emission rate. Secondly, a larger air exchange rate resulted in smaller air phase VOC concentrations. Based on the mass transfer theory, reducing VOC concentrations in the air phase can also enhance the air phase mass transfer. Note that Cases 2-2b (full-scale chamber, 5ACH) and 2-3b (full-scale chamber, 9ACH) had higher initial emission rates than Case 1-2b (small-scale chamber, 0.15m/s), although Cases 2-2b and 2-3b had slightly lower local velocity than Case 1-2b (0.15 m/s). This may be attributed to the effects of turbulence and VOC concentrations in the air on the boundary layer mass transfer. The flow was turbulent for Cases 2-2b and 2-3b, while laminar for Case 1-2b. On the other hand, the full-scale chamber had much smaller loading ratio than the small-scale chamber (0.011 vs. 0.15) and higher air exchange rates (5 vs. 1), resulting in much smaller air phase concentrations in the full-scale chamber. Contrary to the above results, the initial emission rates of Case 1-2b were larger than those of Case 2-1b (full-scale chamber, 1ACH). This was due to the local air velocity of

the former case (0.15 m/s), which was much higher than that of Case2-1b (<0.04 m/s), although Case 2-1b had a turbulent flow and much smaller air phase concentrations.

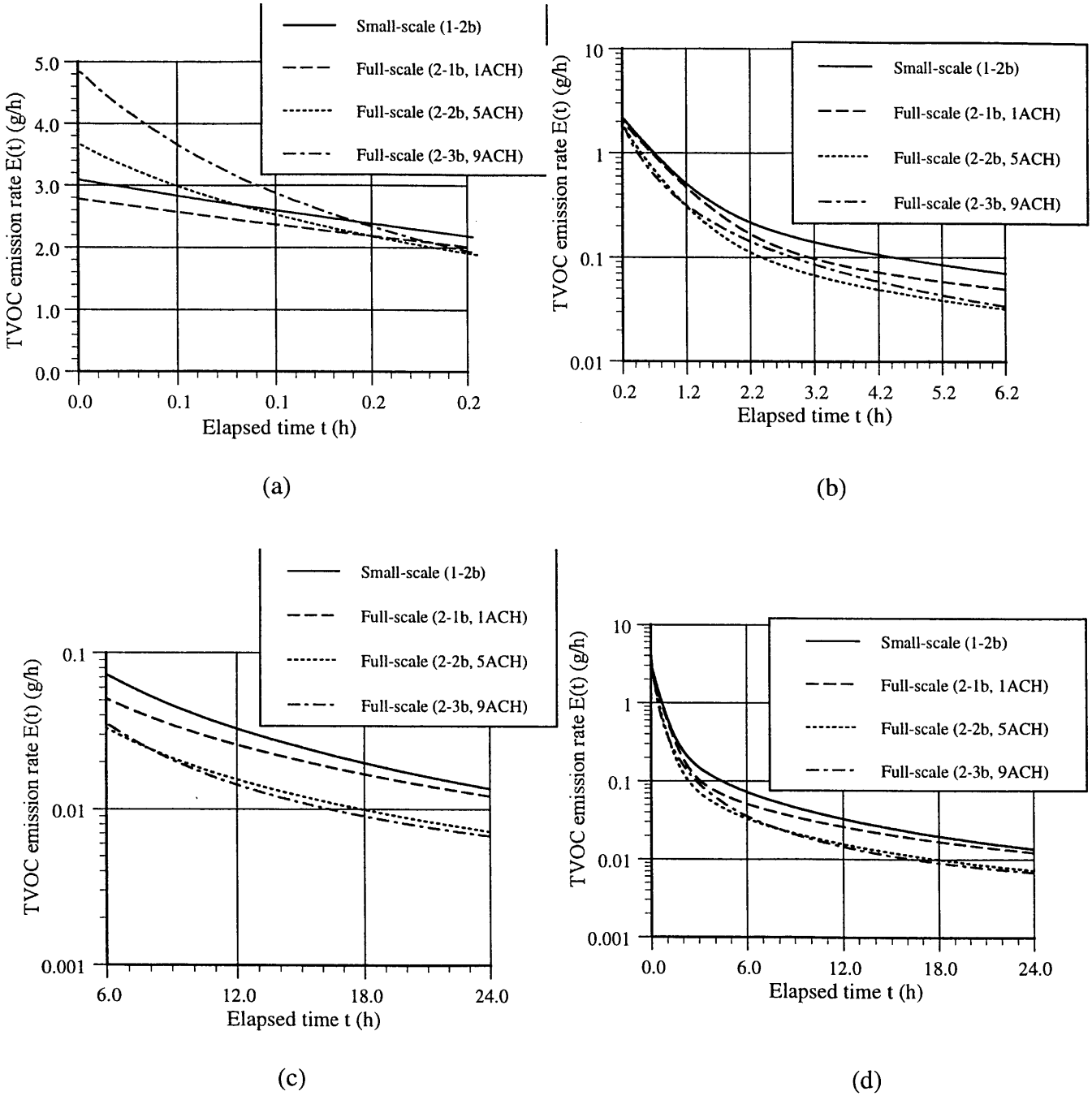

Figure 2.10 Measured TVOC emission rates of wood stain in different chambers: (a) 0 - 0.2 hour, (b) 0.2 - 6 hours, (c) 6 - 24 hours, (d) 0-24 hours.

In the second period (0.2-6 h), the emission rates of the cases with larger initial emission rates (*e.g.*, Cases 2-2b and 2-3b) decayed faster. At 6 hours, Cases 1-2b and 2-1b had higher emission rates than those of Cases 2-2b and 2-3b.

In the third period (> 6 h), the cases whose initial emission rates were higher (*e.g.*, Case 2-3b) had smaller emission rates. However, at 24 hours Cases 1-2b and 2-1b, and Cases 2-2b and 2-3b had approximately the same emission rates. Emissions during this period were likely affected by several factors. First, as more VOCs were off-gassed, emission rates changed from evaporation dominant to internal diffusion dominant. Therefore, the impact of local airflow lessened. Second, the "wet" films, for cases with higher initial emission rates, also dried faster at the material surface. So the surface concentration decreased at a later time. Third, the applied mass of wood stain was not exactly the same for every case. The different applied mass may also have affected the emission rates in the third period. Finally, the weight decay in the third period decreased by two or three orders of magnitude from the initial period. The measured weight data was more easily affected by factors such as moisture and velocity fluctuations, rendering the emission rates obtained from the balance data less reliable.

2.3.4.2 Decane

Two cases, one using the small-scale chamber (Case1-1a, 0.15 m/s above the material) and the other using the full-scale chamber (Case2-2a, 5ACH), were conducted to measure the emissions for decane under different chamber and airflow conditions. Comparing the counterpart cases for wood stain (Cases 1-1b and 2-2b), similar phenomena also occurred with the decane. Figure 2.11 provides the emission rates of these two cases. From 0-1.2 h, the emission rates in the full-scale chamber were greater than those in the small-scale one. But from the 1.2 hour point, the process reversed.

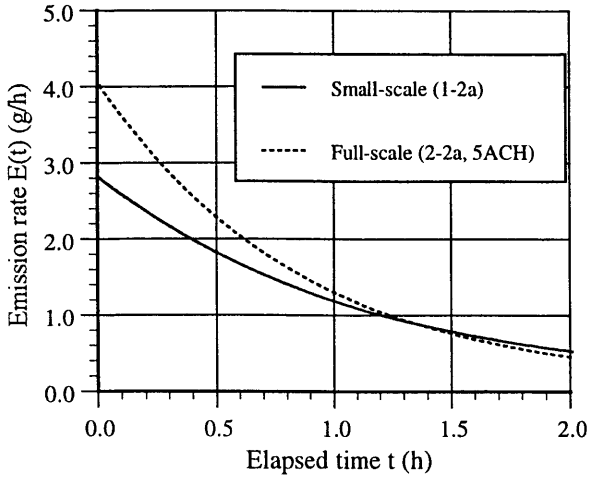

(a)

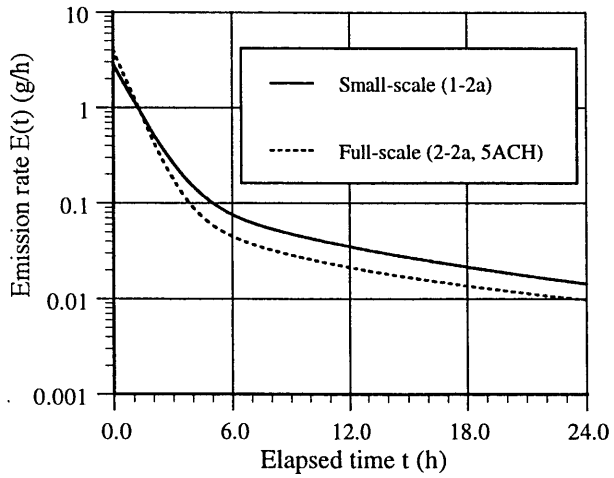

(b)

Figure 2.11 Measured emission rates of decane in the small-scale and full-scale chambers: (a) 0 - 2 hours, (b) 0 - 24 hours.

Based on the above results, the effect of airflow on the third (internal diffusion dominant) period remains unclear. This third period will be further studied in Chapter 3 by using a detailed emission model.

2.3.5 Effects of temperature on emission characteristics

2.3.5.1 Wood stain

Figure 2.12 shows the TVOC emission rates of wood stain at four different temperatures during the 24-hour emission period. The results show that the temperature impacted the emission rates differently during different emission periods.

During the first period (0 - 0.2 h), higher emission rates and faster decays were observed for higher temperatures. The emissions during this period were likely dominated by evaporation. Thus the emission rate depended on the equilibrium vapor pressure of VOC, which was higher at a higher air temperature.

During the second period (0.2 - 8 h), the phenomena became complicated. The emission rates of Case 1-2b (23.5°C) were higher than those of Case 1-1b (20.5°C) from 0.2 h point to the 1 h point. Both cases, however, had almost the same emission rates from the 1 h point to the 4 h point. From the 4 h point the emission rates of Case 1-2b were higher than those of Case 1-1b again. A similar tendency occurred between Cases 1-3b (27.5°C) and 1-4b (31.5°C).

For the third period (from the 8 h point), it appears that the temperature impact was similar to that during the first period, *i.e.*, the emission rates were higher for higher temperatures. However, an examination of the TVOC concentration measured by GC/FID (Figure 2.13) did not support this conclusion. Figure 2.13 shows that higher emissions for higher temperatures were not observed during the third period, and the GC/FID results do not show a clear temperature effect on emission rates.

The above ambiguity may again be due to the fact that during the second and third periods, emissions were likely affected by multiple factors. Also the measurement error of the wood stain weight, due to moisture and velocity fluctuations, could be more pronounced. These combined factors could have masked the impact of temperature on emission rates.

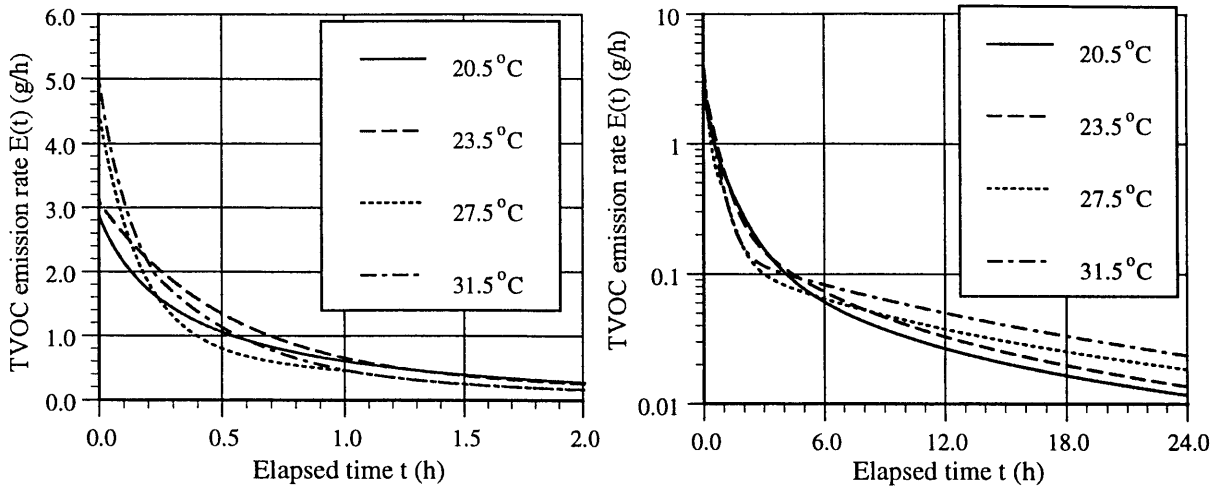

Figure 2.12 TVOC emission rates of wood stain at different temperatures: (a) 0 - 2 hours, (b) 0 - 24 hours.

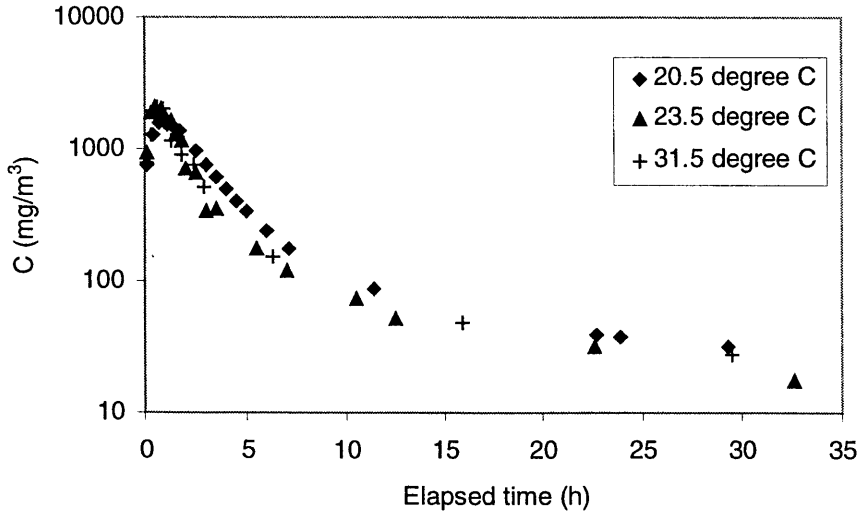

Figure 2.13 TVOC concentrations measured by GC/FID at different temperatures.

2.3.5.2 Decane

The single compound decane was also measured at four temperatures (20.5°C, 23.5°C, 27.5°C, and 31.5°C) respectively. Figure 2.14 illustrates the measured emission rates. In general, the temperature effects on emission rates of decane were similar to those of wood stain. The differences of emission rates during the third period, for the cases at temperatures 23.5°C, 27.5°C, and 31.5°C were not significant compared to those of wood stain.

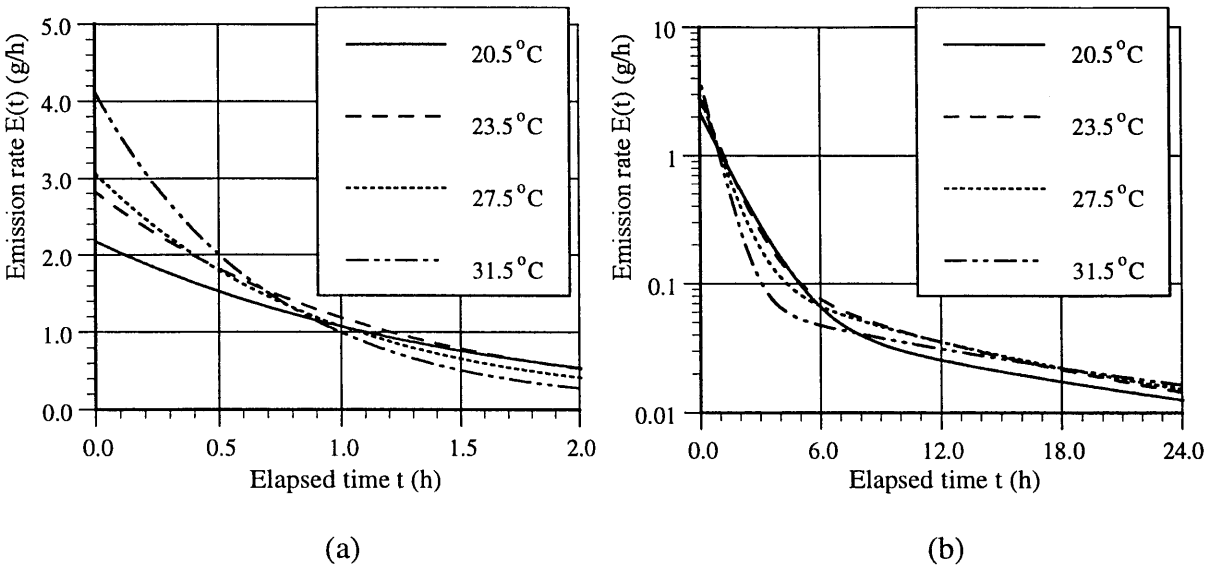

Figure 2.14 Emission rates of decane at different temperatures: (a) 0 - 2 hours, (b) 0 - 24 hours.

The results from the experimental measurements indicate that both environmental conditions (airflow and temperature) and the substrate may significantly affect both the short-term (observed) and long-term (expected) emissions of a "wet" material. Because the flow and thermal conditions in small-scale chambers are usually different from those in buildings, the emission rates obtained from the chambers may not be applied directly to analysis of indoor air quality in buildings. In Chapter 3, we develop a numerical model using computational fluid dynamics (CFD) to fully characterize the effects of both environmental conditions and the substrate on "wet" material emissions. The experimental results obtained in this chapter will serve as the primary data for developing and validating the model.

2.4 Conclusions

This chapter presents the results of an investigation of the emission characteristics of "wet" materials measured using a small-scale (0.4 m^3) and a full-scale (55 m^3) environmental chamber. A commercial oil-based wood stain and a single compound (decane) applied to both oak and glass substrates were selected for emission testing. Emission rates were measured by monitoring the weight loss with an electronic balance as well as by sampling the VOC concentrations in the chamber's exhaust. The effects of environmental conditions (temperature and airflow) and the substrate on "wet" material emissions were investigated by comparing the measured emission data between different cases. The following conclusions can be made based on the experimental measurements:

(1) Results of the measured TVOC emission rates from the wood stain applied to two different substrates (oak board and glass) confirmed that substrate can significantly affect "wet" material emissions. Both the initial emission rate and emission decay rate resulting from the glass substrate were considerably higher than those from the oak substrate. When the wood stain was applied to the oak board (instead of the non-permeable glass plate), the TVOC emission rates during the first 2 hours decreased as much as 60%, while the emission term was significantly prolonged. In order to evaluate the time-varying VOC emission characteristics of "wet" products, a realistic substrate such as wood should be used.

(2) Airflow (velocity and velocity fluctuation) distributions created different impacts on the "wet" material emissions during the three different emission periods. In the first and second period (0 - 6 h for wood stain), the cases with larger velocity and velocity fluctuation demonstrated a larger initial emission rate and also a faster decay rate. No general trend could be observed during the third period.

(3) Temperature also impacted "wet" material emissions differently during the three periods. In the first period (0 to 0.2 h for wood stain), higher emission rates and faster decay were observed for higher temperatures. The impact of temperature during the second period (0.2 - 8 h for wood stain) could not be identified, although it appeared that the cases with higher temperatures also decayed faster. During the third period (> 8 h), results obtained based on the electronic balance and GC/FID analysis did not agree. Further investigations are needed for this period.

Chapter 3

Modeling of VOC Emissions from "Wet" Coating Materials Applied to Porous Substrates

VOC emissions from "wet" coating materials result from evaporation and internal-diffusion processes. In this chapter, a numerical model using computational fluid dynamics (CFD) has been developed to numerically simulate "wet" material emissions. The model considers the VOC mass transfer process in the air and material-air interface, and diffusion in the material film and also in the substrate. The numerical model developed can predict emissions under different environmental conditions (temperature, velocity, turbulence). Our numerical simulations further confirmed that the emissions from "wet" materials applied to an absorptive substrate are dominated by evaporation at the beginning followed by internal diffusion, which had been hypothesized based on previous experimental data. The numerical model has the potential to simulate "wet" material emissions in actual building environments based on the data from inexpensive small-scale chamber tests.

3.1 Introduction

The experimental measurements presented in Chapter 2 revealed that the emission behavior of "wet" materials can be affected by environmental conditions (temperature, velocity and velocity fluctuation) and the substrate. Hence, the emission data from environmental chambers under defined standard conditions may not be applied directly to buildings in which environmental conditions may significantly differ from those in the test chambers. It would also be too expensive to investigate the emissions under the actual building conditions. A feasible way to investigate emissions would be to develop computer models to simulate the emission processes in buildings based on the data from inexpensive small-scale chamber tests.

The review of method for modeling building material emissions given in Chapter 1 indicates that we currently lack a comprehensive emission model that applies to the entire emission process of a "wet" material applied to a realistic substrate such as oak. In this chapter, a numerical model using CFD has been developed to fill that gap. The model considers VOC mass transfer in the air and material-air interface, diffusion in the material film, and also diffusion in the substrate. It is able to predict the VOC emission rates of a "wet" material under different environmental conditions. The use of this numerical model requires the thermodynamic properties of compounds or materials. With the thermodynamic properties, the model can simulate "wet" material emissions in buildings.

The following section (3.2) analyzes the emission mechanisms for "wet" materials applied to a porous, absorptive substrate (*e.g.*, oak board). In sections 3.3 and 3.4, the mathematical model and numerical methods for simulating the "wet" material emissions are provided. Section 3.5 discusses the method to obtain the necessary physical properties

used by the model, and validates the emission model based on the experimental data obtained in Chapter 2. Finally, section 3.6 presents the findings from these processes.

3.2 The Emission Mechanisms

This section examines the VOC emission mechanisms of "wet" materials. However, since there are many types of "wet" materials on the market, it is impossible to study all of them. Rather, we focus on a typical material that best represents the mechanisms of "wet" material emissions.

The scenario considered is a "wet" coating material applied to a wood substrate. Wood is a porous material comprised of tubular hollow cells bound together with lignin. These cells communicate with one another through small openings in the cell wall called pits. For simplicity, we assume that the amount of coating material is small so that all the liquids will be absorbed by the porous substrate after application. VOCs can be contained in the substrate as free liquid in the cell cavities or bound VOCs held in the cell walls.

When the substrate with applied "wet" coating material is exposed to air, VOCs will gradually be off-gassed from the film surface. During the emission process, several mechanisms of external and internal VOC mass transfer occur. These mechanisms include evaporation at the material surface, movement of free or bound VOCs, VOC vapor diffusion in the material film, and VOC diffusion from the material film to the substrate. Each of these mechanisms, shown in Figure 3.1, will now be discussed.

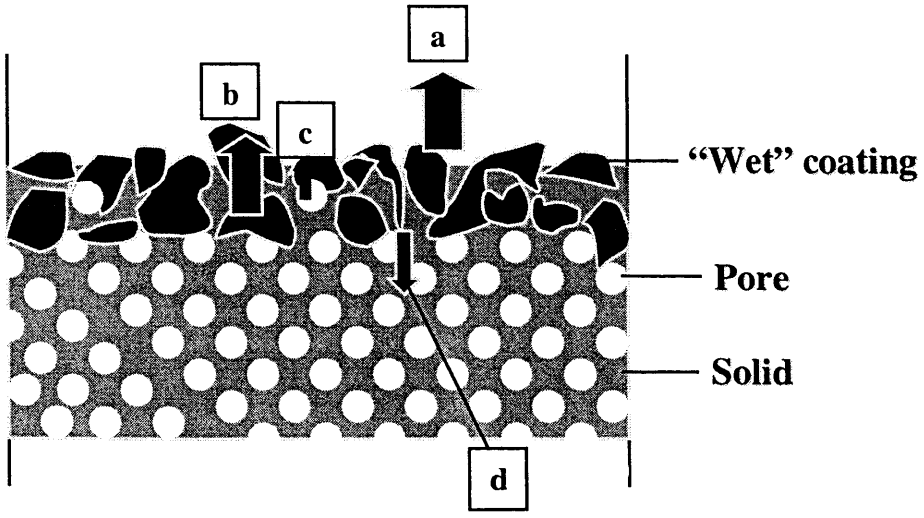

Figure 3.1 Schematic representation of the emission mechanisms of a "wet" material embedded in a porous substrate. (a) = evaporation; (b) = movement of free and bound VOCs; (c) = vapor flow; (d) = diffusion to substrate.

3.2.1 Evaporation

After a "wet" material is applied to a substrate, the VOCs will evaporate at the material-air interface. In general, the rate of evaporation of a partially saturated porous medium to a convective medium depends on the phase distributions on, and adjacent to, the interface. Figure 3.1 shows that, from a microscopic point of view, the interface of a macroscopically flat surface is not planar. The distribution of the liquid phases on this interface is very complex and depends on a solid topology, the degree of roughness of the surface, and the amount of "wet" material applied, etc. The phase distributions on the air-exposed side are governed by environmental conditions, *i.e.*, temperature, airflow, relative humidity, and the air phase VOC concentration. At the beginning of the emission process, the liquid phase is close to saturation, so environmental conditions dominate the rate of evaporation. As more VOCs are off-gassed, the surface saturation decreases along with the vapor pressure and emission rates. At the same time, the dominant emission resistance gradually changes from evaporation to internal mass transfer, such as the movement of free or bound VOCs and vapor flow.

3.2.2 Movement of free and bound VOCs

The compounds absorbed by the substrate are either free liquids stored in the pore cavities or bound to the cell walls. Free liquids may develop immediately after the application. They are then more likely to be bound to the cell walls by physical or chemical forces.

Movement of free or bound VOCs cannot be simply defined as a diffusion process. Rather, this is due to capillary motion along very fine capillaries. However, extensive literature on a similar phenomena of movement of bound water in a porous material uses an analogous form of Fick's second law to describe the process (*e.g.*, Sherwood, 1929; Wijeysundera *et al.*, 1996). In this approach, movement of free or liquid moisture is usually described by well-defined mass transfer equations. All the mechanisms characterizing this process depend on a single property: the diffusivity of the moisture. Clearly, diffusivity depends on the microscopic structure of the material. Moreover, evidence shows that diffusivity is also a strong function of temperature and water content (Chirife, 1983; Chen and Pei, 1989). Similarly, the movement of free and bound VOCs is also affected by the substrate structure, temperature, and VOC concentrations in the material.

3.2.3 Vapor flow

During the emission process, liquid or bound VOCs may also evaporate inside the substrate, resulting in the vapor flow through the voids of porous material by convection and diffusion. Two kinds of diffusion are key to this process: molecular diffusion and Knudsen diffusion. When the capillary size is large compared to the mean molecular free

path of VOC, λ, molecular diffusion prevails. On the other hand, when the capillary size is smaller than λ, the Knudsen diffusion predominates.

The vapor flow from a "wet" coating material applied to a wood substrate are expected to be much less than the bound VOC flow due to two reasons. First, the material film absorbed by the substrate is usually very thin. The internal cavities of the substrate are mostly occupied by the liquids when the material is applied so there is not enough "room" for evaporation to take place inside the cavities. Second, for most surface coating materials the additives on the material surface quickly dries and hardens to prevent vapor VOCs from filtrating through the material surface. Hence, the effect of vapor flow will not be considered in our subsequent study.

3.2.4 VOC diffusion from the material film to the substrate

The existence of VOC diffusion from the material film to the substrate is based on the assumption that once the "wet" material is applied to a substrate, a recognizable front will form between the material film and the rest of the substrate. At the beginning of the emission process, the pore space is filled with liquid above the front but is free from the liquid below the front. Hence, VOCs will also diffuse to the substrate from the material film due to the concentration gradient located on the boundary.

Because of the porous property of the substrate, the VOC diffusion to the substrate is also a sum of diffusion processes including dissolution into and permeation through the cell walls and diffusion through the cell walls from one wall to the next. In addition, VOCs may also evaporate in the cell cavities and diffuse through the holes in the cell walls. A microscopic view of the entire diffusion processes will yield a picture that is too complicated to be solved. Hence, simplified approaches are needed to characterize the in-substrate diffusion. A popular approach, a continuum model, has been used to study the mass transfer of chlorofluorocarbon gases (CFCs) through the cellular structure of rigid foam (*e.g.*, Svanstrom, 1997). Similar to the approach for describing the movement of free or bound VOCs from a material film, the continuum model treats the material as a homogeneous medium that can be characterized by an effective diffusion coefficient, D_{eff}. Introduction of D_{eff} allows the use of Fick's law to predict the mass transfer within a porous material. Recognizing that VOC diffusion in the substrate is so complicated that detailed mechanistic models are impossible to use, the continuum model will also be used in our study to address the in-substrate diffusion. Such a model, though, cannot distinguish individual differences between mechanisms, but can be employed to address the in-substrate diffusion due to its simplicity.

3.3 The Mathematical Model

Based on the discussion of the emission mechanisms in the previous section, a mathematical model that describes the mass transfer processes for a "wet" material

applied to a porous substrate can be established. In addressing this problem, we make the following assumptions:

(1) The amount of coating material applied is small so that the material is quickly absorbed by the porous substrate after the application, and a wet layer with a uniform initial VOC concentration is formed inside the substrate. The upper boundary of the wet layer is exposed to ambient airflow and the lower boundary is the substrate initially unaffected by the wet film.

(2) Both the material film and substrate can be treated, from a macroscopic point of view, as homogeneous. Hence, it is possible to define an effective VOC mass diffusivity (including TVOC).

(3) During the emission process, VOCs in the material film and the VOC vapor pressure are in thermodynamic equilibrium at the material-air interface. The VOC off-gassing only occurs at the material-air interface.

(4) The VOC gradients are considered as the only driving force for mass transfer.

(5) The mass transfer rate between the air and material is very small. Hence, heat generation/release associated with the emissions is negligible.

(6) The VOCs are passive contaminants and have no impact on airflow.

(7) There is no chemical reaction inside the material film or the substrate to generate or consume VOCs.

Figure 3.2 shows that VOC emissions from a "wet" material are governed by mass transfer in four different layers: the material film, the substrate, the material-air interface, and the air phase. The following sections present the governing equations of VOC mass transfer in these layers.

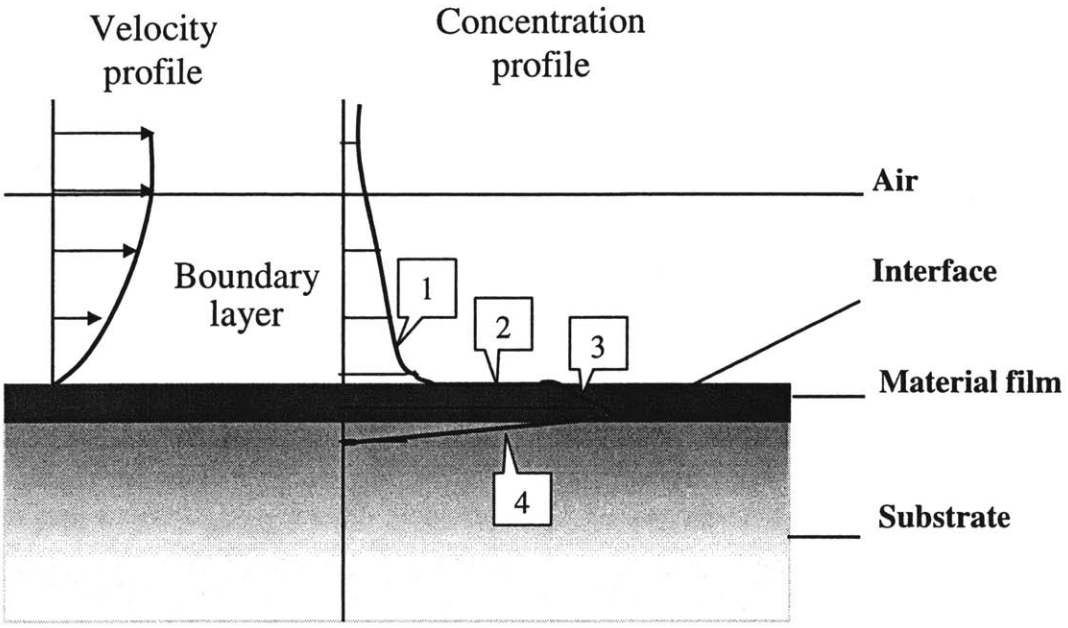

Figure 3.2: Physical configuration of VOC emission mechanisms for a "wet" material applied onto an absorptive substrate. 1 = boundary layer diffusion; 2 = phase change; 3 = in-film diffusion; 4 = in-substrate diffusion.

3.3.1 Material Film

Based on the discussion in section 3.2.2, the transient VOC diffusion process in the material film can be expressed in a form analogous to Fick's law:

$$\frac{\partial C_m}{\partial \tau} = \frac{\partial}{\partial x_j}\left(D_m \frac{\partial C_m}{\partial x_j}\right) \tag{3.1}$$

where

C_m = VOC concentration in the material film, mg/m^3

τ = time, sec

x_j = coordinates (j=1,2,3)

D_m = effective diffusion coefficient in the material film, m^2/s

The key to using Eq. (3.1) effectively is to determine the D_m. Section 3.2.2 indicates that D_m is a function of the pore structure, the material type, compound properties, temperature, and the VOC concentration in the material film. For a given "wet" material-substrate-VOC system, the D_m is considered a thermally activated process and can be expressed by the following Arrhenius-type equation:

$$D_m(C,T) = D(C)\exp(-\frac{E_d}{RT}) \qquad (3.2)$$

where
D(C) = diffusion coefficient at concentration C
E_d = activation energy, J/mol
R = universal gas constant (= 8.3145 $Jmol^{-1}K^{-1}$)
T = absolute temperature (K).

Crank and Park (1968) explained that the activation energy will be larger for bigger molecules. Glasstone *et al.* (1941) showed that the E_d may be related to the energy of evaporation for the solute molecules. Limited data obtained by Crank and Park (1968) suggested that the E_d for different gasses in polymers varies within a limited range (4.0 ~ 12.0 kcal/mole), which agrees with the results given by others (*e.g.*, Barrer, 1957; Van Amerongen, 1950 and1964). For example, Barrer (1957) cited the E_d values for CO_2 ranging from 7.3 Kcal/mole in polybutadiene to 14.4 kcal/mole in isoprene acrylonitrile rubbers. Van Amerongen (1950, 1964) found the E_d of N_2 and O_2 in three different polymers ranging from 6.8 to 12.4 Kcal/mole. However, too little data have been collected over a wide range of materials to allow definitive conclusions to be drawn.

The temperature for indoor applications only vary within a small range. Hence, it may be possible to estimate the E_d using the above results as reference data. For example, Chen and Lin (1998) used (for unknown reasons) E_d =7.3 Kcal/mole for moisture in polymer solution. Later in section 3.6.2, we present the results when the same value of E_d is used for VOCs.

The determination of the dependence level of D_m on VOC concentrations, however, will involve major difficulties. Currently, theories for calculating liquid-state diffusion coefficients are quite idealized, and none is satisfactory in providing relations for calculating the correct diffusion coefficient (Reid *et al.*, 1977). Because of the limitation of the theoretical approaches for estimating diffusivity, diffusion coefficients in polymer-solvent systems have been measured by several researchers (Crank and Park, 1968; Okazaki *et al.*, 1974; Cantrel *et al.*, 1997). However, most data have represented a specific solute-solvent system and the results between these different systems have been quite diverse. Without entering into the question of the reliability of the published data, we present some of those published data (dependence of D_m on the mass fraction of the solute in the solution, w) in Table 3.1. It can be seen that the same solute content may vary in the order of magnitude, which is not unexpected in view of the different physical/chemical interactions among these systems. A "wet" material such as wood stain contains different compositions, and the dependence of D_m on the VOC content could be more complicated than the binary solvent-solute system mentioned above.

Table 3.1 Examples of systems that show the dependence of D_m on the relative solvent content, w.

System	D_m (m^2/s) at				Reference
	w=0.9	w=0.5	w=0.1	w=0.05	
Skim milk-water	4.04E-10	1.71E-10	1.06E-12	4.46E-14	Sano and Yamamoto, 1989
Polyvinyl alcohol-water	8.56E-11	5.27E-11	2.98E-12	4.95E-13	Sano and Yamamoto, 1989
Polyvinyl alcohol-water	4.86E-11	3.04E-11	4.20E-13	5.97E-14	Okazaki *et al.*, 1973

Another factor hindering the determination of the D_m for VOC is the presence of the substrate. Since the "wet" material is embedded in a porous substrate, VOC diffusion with the presence of a substrate is generally slower than diffusion in a material film without the substrate. There are two reasons for the lower effective diffusion coefficient. First, during diffusion through the porous substrate, part of the VOCs are retained by the internal surface of the substrate. This tends to slow or retard the mass transfer through the substrate. Second, due to the tortuous nature of the internal diffusion path in the substrate, it takes VOCs longer to diffuse through the substrate. As evidence, Adham *et al.* (1991) showed that the molecular diffusion coefficients of aqueous materials in activated carbon particles were many orders of magnitude less than the diffusion coefficient in pure water.

Due to the above reasons, a theoretical or experimental determination of the D_m as a function of VOC concentrations is extremely difficult. It is beyond the scope of this thesis to develop a correlation for different types of "wet" materials (if such a correlation exists at all). In the numerical study that follows, we use a third-power empirical equation to describe the dependence of D_m on VOC concentration in the material film:

$$D(C) = D_0\left(\frac{C_m}{C_{m,0}}\right)^3 \tag{3.3}$$

where

D_0 = initial diffusion coefficient in the material film, m^2/s

$C_{m,0}$ = initial VOC concentration in the material film, mg/m^3

Eq. (3.3) is proposed after a study of the dependence of moisture transfer on moisture content in a hygroscopic material (Chen and Pei, 1989). Note the equation may not apply for a very small $C_m/C_{m,0}$ (when material film is totally dry) in that it will lead to an infinitely small D_m as $C_m/C_{m,0}$ approaches 0. The VOC diffusivity in a dry film needs to be measured directly or estimated with long-term (*e.g.*, several weeks or months)

experimental data. As an approximation, the VOC diffusion coefficient in the substrate (see below) can be used as an asymptote of D_m at low C_m.

Clearly, the physical meaning of Eq. (3.3) is weak. Introduction of the empirical correlation for VOC diffusivity is a major weakness of the current study. However, this can be remedied with additional theoretical or experimental work.

For the convenience of future applications, Eqs. (3.2) and (3.3) can be rewritten as:

$$D_m(C,T) = D_{m,0}(\frac{C_m}{C_{m,0}})^3 \tag{3.4}$$

and

$$D_{m,0} = D_0 \exp(-\frac{E_d}{RT}) \tag{3.5}$$

where for a specific material film and VOC, $D_{m,0}$ at a reference temperature needs to be determined by experimental data. The $D_{m,0}$ at a temperature different from the reference temperature can be calculated using Eq. (3.5).

3.3.2 Substrate

By using the "continuum model" (see section 3.2.4) and Fick's law, the transient VOC diffusion process in the substrate may be described by:

$$\frac{\partial C_s}{\partial \tau} = \frac{\partial}{\partial x_j}(D_s \frac{\partial C_s}{\partial x_j}) \tag{3.6}$$

where
C_s = VOC concentration in the substrate, mg/m^3
D_s = VOC diffusion coefficient in the substrate, m^2/s

Similar to the diffusivity in the material film, the dependence of D_s on temperature and VOC concentration should also be considered. However, Schwope *et al.* (1989) has suggested that the concentration dependence on the diffusion coefficient may be ignored below a concentration ratio (a dimensionless ratio of the VOC concentration in the material to the material density) of 1%. Recognizing that the VOC concentration in the substrate will be small, the dependence of the D_s on the VOC concentration can thus be ignored. The dependence of D_s on temperature is assumed to follow the Arrhenius equation as:

$$D_s = D_{s,0} \exp(-\frac{E_d}{RT}) \tag{3.7}$$

The VOC flux, q (mg/m^2s), at an arbitrary displacement, y, of material and time τ is given by:

$$q = -D_s \frac{\partial C_s}{\partial x_j} \tag{3.8}$$

In general, the VOC diffusion rate in a substrate can be solved numerically. However, the D_s in most solid substrates is usually very small. If a direct numerical simulation of VOC diffusion in the substrate is used, a very fine grid distribution in the substrate is needed to eliminate the false numerical diffusion. Such a solution requires a fast computer with large capacity. To avoid this, we developed a new sorption model to analytically solve the VOC mass transfer rate. In this way, no numerical grid in the substrate is needed. The sorption model, detailed in Chapter 5, calculates the time-dependent VOC mass transfer (sorption) rate by the substrate as (Figure 3.3):

$$q(\tau_n) = X_0 C_s(\tau_n) + \tilde{q}(\tau_{n-}) \tag{3.9}$$

where

$q(\tau_n)$ = VOC mass transfer (sorption) rate at time $\tau = n\Delta\tau$, n means the n^{th} time step

$\Delta\tau$ = time step (sec)

X_0 = coefficient that is determined by the diffusion coefficient of the substrate (D_s), thickness of the substrate (L_s), and $\Delta\tau$

$C_s(\tau_n)$ = VOC concentration at the film-substrate interface at the current time ($n\Delta\tau$)

$\tilde{q}(\tau_{n-})$ = a value that is determined by the history of C_s as well as D_s, L_s, and $\Delta\tau$

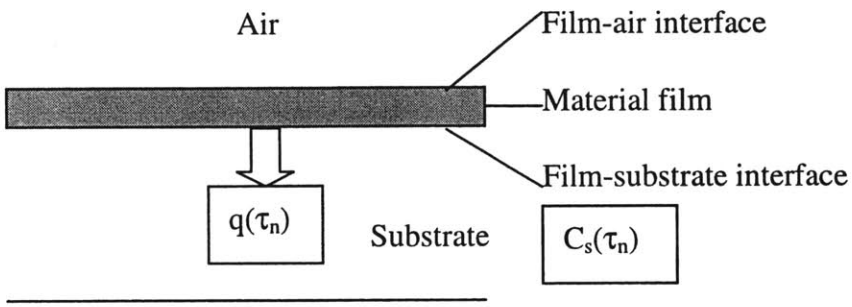

Figure 3.3 Description of the VOC sorption by the substrate.

Eq. (3.9) links the VOC sorption rate with the VOC concentration at current time step, $C_s(\tau_n)$, and the effect of its history on sorption, $\tilde{q}(\tau_{n^-})$, in a linear form. The sorption model can serve as a boundary condition to the numerical cell of the material film. In this way, no numerical grids in the substrate are needed.

3.3.3 Material-air interface

At the material-air interface, the VOC changes phase from the material (liquid or solid) side to the air side. Henry's Law states that at equilibrium, the ratio of the concentration of a volatile solute in a solvent, C_m (mg/m^3), to the solute's concentration in the vapor phase above the solvent-solute mixture, C_a (mg/m^3), is a constant. Although Henry's Law is valid only for low-solute concentrations, it can also be applied to a wide range of gases and VOCs of environmental interest (Clark, 1996). When the same units are used for both C_m and C_a, Henry's Law can be expressed as:

$$C_m = K_{ma} C_a \tag{3.10}$$

where K_{ma} is a constant, which frequently is called the dimensionless material-air partition coefficient. It is a material property and can be obtained from physical data or by static headspace analysis. The method for calculating K_m will be discussed in Section 3.5.1.

3.3.4 Air

The VOC transport in the air is determined by diffusion through the boundary layer at the material-air interface. Since the boundary condition at the material-air interface, C_a, cannot be determined a priori, the problem should be posed and solved as a conjugate mass transfer. Hence, a complete set of room airflow and VOC transport equations in the air phase are needed in order to fully describe the VOC transport process in the air. For an incompressible and Newtonian flow, the conservation equations for continuity, momentum (using Boussenisseq approximation for buoyancy), energy, and VOC species are as follows:

Continuity equation:

$$\frac{\partial}{\partial x_j}(\rho u_j) = 0 \tag{3.11}$$

Momentum equation:

$$\frac{\partial}{\partial \tau}(\rho u_i) + \frac{\partial}{\partial x_j}(\rho u_j u_i) = \frac{\partial}{\partial x_j}(\mu \frac{\partial u_i}{\partial x_j}) - \frac{\partial p}{\partial x_i} - \rho g_i \beta (T - T_{ref}) \quad (i=1,2,3) \tag{3.12}$$

Energy equation:

$$\frac{\partial}{\partial \tau}(\rho T) + \frac{\partial}{\partial x_j}(\rho u_j T) = \frac{\partial}{\partial x_j}(\frac{\mu}{Pr}\frac{\partial T}{\partial x_j}) + \frac{1}{c_p} S_T \tag{3.13}$$

Air phase VOC transport equation:

$$\frac{\partial}{\partial \tau}(\rho C_a) + \frac{\partial}{\partial x_j}(\rho u_j C_a) = \frac{\partial}{\partial x_j}(\frac{\mu}{Sc}\frac{\partial C_a}{\partial x_j}) + \rho S \tag{3.14}$$

where in Eqs. (3.11) - (3.14):

x_j (j=1,2,3) = coordinate. In a cartecine coordinate, x_1=x, x_2=y, x_3=z

ρ = air density, kg/m^3

u_j (j=1,2,3) = three components of air velocity. In a Cartesian coordinate, u_1 = u (velocity in x direction), u_2 = v (velocity in y direction), u_3 = w (velocity in z direction)

μ = molecular viscosity of air, Pa.s

P = air pressure, Pa

C_a = air phase VOC concentration (mg/m^3)

Sc = Schmidt number of VOC

S = VOC source term, mg/m^{3}s. S = 0 if there are no additional sources or sinks

For laminar flow (*e.g.*, flow in a small-scale chamber), Eqs. (3.11) - (3.14) can be solved numerically to obtain the distributions of air velocity and temperature. However, the airflow in a typical ventilated room (*e.g.*, the full-scale chamber) is turbulent. In such a case we also need a suitable turbulence model so that we can simulate the airflow and VOC transport on a personal computer. There are many turbulence models available. The "standard" k-ε model (Launder and Spalding 1974) is probably most widely used in engineering calculations due to its relative simplicity. However, the model sometimes provides poor results for indoor airflow. Many modifications have been applied to the standard model. However, the modified models are not generally applicable for indoor airflow. The applicability of different models depends largely on the flow type, *i.e.*, natural, forced, and mixed convection. Chen (1995 and 1996) calculated the indoor flows with eight different turbulence models. He concluded that the Re-Normalization Group (RNG) k-ε model (Yokhot *et al.* 1992) performed slightly better than others, although none of them accurately predicted both air velocity and turbulence. The model is used here. The governing equations for the RNG k- ε model can be generalized as:

$$\frac{\partial}{\partial \tau}(\rho \phi) + \frac{\partial}{\partial x_j}(\rho u_j \phi) = \frac{\partial}{\partial x_j}(\Gamma_\phi \frac{\partial \phi}{\partial x_j}) + S_\phi \tag{3.15}$$

where

ϕ = 1 for mass continuity

ϕ = u_j (j = 1, 2, and 3) for three components of momentum (u,v,w)

ϕ = k for kinetic energy of turbulence

ϕ = ε for the dissipation rate of turbulence energy

ϕ = T for temperature

ϕ = C for VOC concentrations

$\Gamma_{\phi,eff}$ = effective diffusion coefficient for ϕ

S_ϕ = source term for ϕ

The ϕ, Γ_ϕ and S_ϕ are shown in Table 3.2.

Table 3.2 Values of ϕ, Γ_ϕ and S_ϕ in Eq. (3.15).

ϕ	Γ_ϕ	S_ϕ
1	0	0
u_i	$\mu + \mu_t$	$-\frac{\partial p}{\partial x_i} - \rho g_i \beta (T - T_0)$
k	$\mu + \mu_t/\sigma_k$	$G - \rho\varepsilon + G_B$
ε	$\mu + \mu_t/\sigma_\varepsilon$	$(C_{\varepsilon 1} G - C_{\varepsilon 2}\rho\varepsilon + C_{\varepsilon 3} G_B)\varepsilon/k + R$
T	$\mu/Pr + \mu_t / Pr_t$	S_T
C	$\mu/Sc + \mu_t/ Sc_t$	S_c

where

μ = laminar viscosity

$\mu_t = \rho C_\mu \frac{k^2}{\varepsilon}$ is turbulent viscosity

$G = \mu_t \frac{\partial u_i}{\partial x_j}\left(\frac{\partial u_i}{\partial x_j} + \frac{\partial u_j}{\partial x_i}\right)$ is turbulent production

$G_B = -g_i \beta \frac{\mu_t}{Pr_t}\frac{\partial T}{\partial x_i}$ is turbulent production due to buoyancy

$R = \frac{C_\mu \eta^3 (1 - \eta/\eta)}{1 + \beta\eta^3}\frac{\varepsilon^2}{k}$ is the source term from renormalization

$\eta = S\frac{k}{\varepsilon}$, $S = (2S_{ij} S_{ij})^{1/2}$, $S_{ij} = \frac{1}{2}\left(\frac{\partial u_i}{\partial x_j} + \frac{\partial u_j}{\partial x_i}\right)$

C_μ =0.0845, $C_{\varepsilon 1}$ = 1.42, $C_{\varepsilon 2}$ = 1.68, $C_{\varepsilon 3}$ = 1.0, σ_k = 0.7194, σ_ε = 0.7194 are the model constants

Pr= 0.71, Pr_t = 0.9 are the laminar and turbulent Prandtl numbers

Sc, Sc_t=1.0 are the molecular and turbulent Schmidt numbers

3.3.5 Boundary conditions

Appropriate boundary conditions for velocities, temperature, and VOC species are needed in order to close the governing equations. The common velocity and temperature boundary conditions, including inlet, outlet, and walls, can be found in the literature (*e.g.*, Yuan *et al.*, 1999) and will not be discussed here.

The boundary conditions for VOCs are:

$$C_{a,inlet}=0 \qquad \text{at the air inlet} \tag{3.16}$$

$$-D_m \frac{\partial C_m}{\partial y} = -D_a \frac{\partial C_a}{\partial y} \qquad \text{at the material-air interface} \tag{3.17}$$

$$-D_m \frac{\partial C_m}{\partial y} = -D_s \frac{\partial C_s}{\partial y} \qquad \text{at the film-substrate interface} \tag{3.18}$$

$$C_m = C_s \qquad \text{at the film-substrate interface} \tag{3.19}$$

$$C_{s,y=L_a} = 0 \qquad \text{at the other side of the substrate} \tag{3.20}$$

where in Eq. (3.17) D_a is the VOC diffusion coefficient in the air (m^2/s) and y is the normal direction of the film surface. The VOC boundary conditions are also illustrated in Figure 3.4.

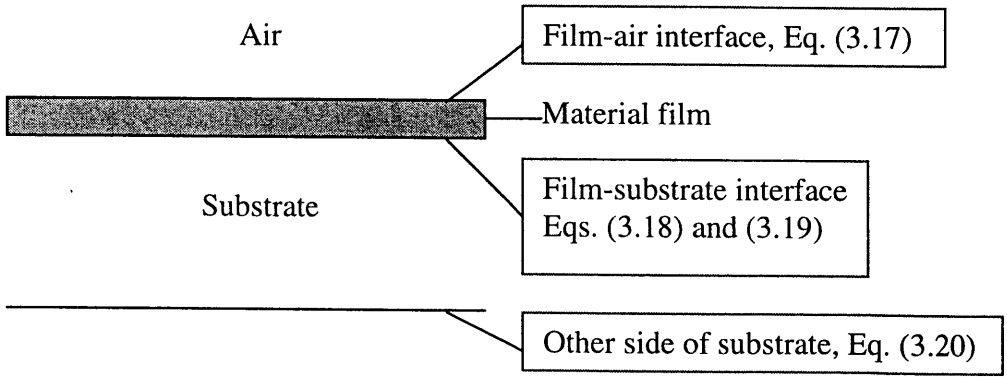

Figure 3.4 Explanation of the VOC boundary conditions (Eqs. (3.17) – (3.20)).

The RNG k-ε model uses wall functions for the near-wall region. Patankar and Spalding (1970) derived the wall functions of velocity and temperature for the Couette flow. In their wall functions, the near wall region is divided into a laminar region and a log-law region. The viscous effect dominates in the laminar region and the Prandtl's mixing length hypothesis is applied in the log-law region. The wall functions may be expressed as:

$$u^+ = y^+ \qquad \text{for } y^+ \le 11.5 \qquad (3.21a)$$

$$u^+ = \frac{1}{\kappa}\ln(Ey^+) \qquad \text{for } y^+ > 11.5 \qquad (3.21b)$$

$$T^+ = \mathrm{Pr}\, y^+ \qquad \text{for } y^+ \le 11.5 \qquad (3.22a)$$

$$T^+ = \mathrm{Pr}_t[u^+ + E(\frac{\mathrm{Pr}}{\mathrm{Pr}_t} - 1)(\frac{\mathrm{Pr}_t}{\mathrm{Pr}})^{1/4}] \qquad \text{for } y^+ > 11.5 \qquad (3.22b)$$

where

$$y^+ = \frac{y u_\tau \rho}{\mu}$$

$$u_\tau = \sqrt{\frac{\tau_w}{\rho}}$$

$$u^+ = \frac{u}{u_\tau}$$

$$T^+ = \frac{(T_{a,int} - T_a)u_\tau}{Q_{int}}$$

$T_{a,int}$ = surface temperature, °C
Q_{int} = heat transfer rate, W/m^2
y = distance between the first grid node and the wall, m
u = velocity parallel to the wall at the first grid node, m/s
τ_w = wall shear stress, kg/ms^2
κ = von Karman constant (0.435)
E = constant, E=9 for a moderate pressure-gradient flow on a smooth surface

Based on Eqs. (3.22a) and (3.22b), the analogous wall function for VOC is:

$$C_a^+ = \mathrm{Sc}\, y^+ \qquad \text{for } y^+ \le 11.5 \qquad (3.23a)$$

$$C_a^+ = \mathrm{Sc}_t[u^+ + E(\frac{\mathrm{Sc}}{\mathrm{Sc}_t} - 1)(\frac{\mathrm{Sc}_t}{\mathrm{Sc}})^{1/4}] \qquad \text{for } y^+ > 11.5 \qquad (3.23b)$$

where

$$C_a^+ = \frac{(C_{a,int} - C_a)u_\tau}{q_{int}}$$

$C_{a,int}$ = air phase VOC concentration at material-air interface, mg/m^3

q_{int} = VOC mass transfer rate at material-air interface, mg/m^2s

3.3.6 Initial conditions

The VOC initial conditions are:

$$C_{a,\tau=0} = 0 \quad \text{in the room air} \tag{3.24}$$

$$C_{m,\tau=0} = C_{l,0}/\alpha \quad \text{in the material film} \tag{3.25}$$

$$C_{s,\tau=0} = 0 \quad \text{in the substrate} \tag{3.26}$$

where $C_{l,0}$ is the initial VOC concentration in the "wet" source before the source is applied to the substrate. In Eq. (3.25) the liquid expansion factor (α) was introduced to represent the absorptivity of the substrate. Physically, α means that once a "wet" material is applied to an absorptive substrate, the volume of the liquid film absorbed by the substrate will expand by a factor of α to the initial volume, and the initial VOC concentration in the film will decrease by a factor of α. The method for estimating α is discussed in Section 3.5.3.

3.4 Numerical Method

The numerical simulation of the above equations requires a simultaneous solution together with the room airflow and VOC transport equations. However, since VOC emissions have a negligible impact on air flow and heat transfer, the process can be separated into two parts as shown in Figure 3.5. First, we simulate the room airflow and obtain the steady-state distributions of air temperature, velocity and turbulent intensity using a CFD program. The flow and temperature results are then incorporated into the VOC mass-transfer equations for simulating emissions.

Eq. (3.15) indicates that the governing equations for both laminar and turbulent flow can be generalized as the same form. The following section discusses the numerical technique for solving the governing equations for VOC transport. The discretization and solving procedure for the flow and temperature components can be found in the literature (*e.g.*, CHAM, 1996) and will not be discussed here.

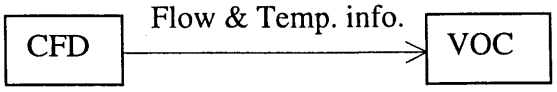

Figure 3.5 Schematic procedure for simulating VOC emissions from "wet" materials.

3.4.1 Discretization of the equations

In order to solve the governing equations numerically, they have to be replaced by their discrete counterparts by means of discretization. There are several approaches to carry out for discretization, *e.g.*, finite elements, finite difference, and finite volume. Among the three, the finite volume method is both mathematically simple and uses physical conservation; thus it is used in the present investigation.

The finite volume method divides the solution domain into a finite number of sub-domains (volumes). Following this, the conservation equations are integrated over these finite volumes. For simplicity, we explain the discretization process in a 2-D rectangular grid system as shown in Figure 3.6 (the discretization is conducted for 3-D). The scalar variables (P, T, k, ε, and C) are specified in the center of the control volume and the velocity components are specified on the faces of the volume (this means that the control volume for the velocity components is not the same as that for the scalar variables). This is the so-called staggered-grid system, which has advantages in discretizing the pressure gradients in combination with the continuity equation (Harlow and Welch, 1965).

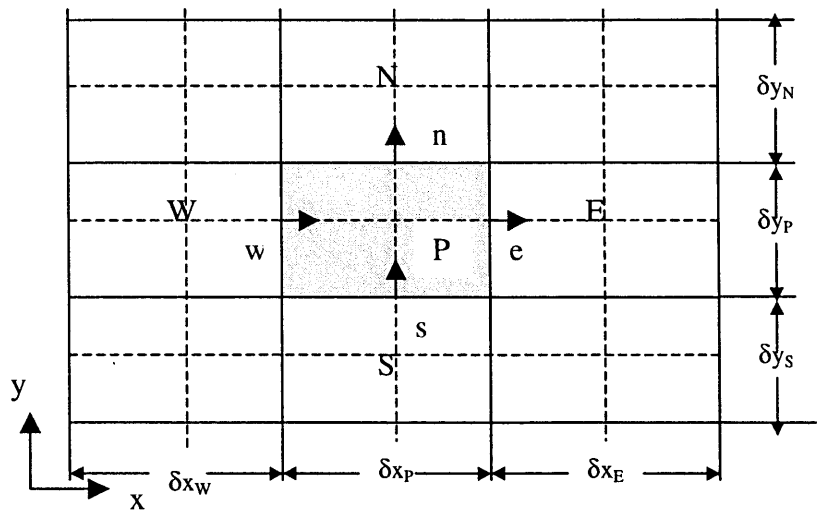

Figure 3.6 A 2-D illustration of the staggered-grid system for the discretization of VOC-governing equations. The shaded area represents the control volume of VOC concentration; capital letters refer the concentrations at the current cell (P) and west (W), east (E), north (N), and south (S) neighbor cells; lower-case letters refer the west (w), east (e), north (n), and south (s) face of the current cell. The third dimension (z) is not shown in the figure.

The second step of the finite-volume discretization is to integrate Eq. (3.15) over a control volume and approximate the integrals. Due to the staggered grid system, the derivation of the discrete equations for the scalar variables is different from that for the velocity components. The following derivations apply to the concentration as well as other scalar variables (P, T, K, and ε).

Applying Gauss's divergence theorem, and presuming all variables and fluid properties are independent of their position within a control volume and all quantities are uniform over volume faces, the integration over a control volume will result in:

$$\begin{aligned}&\int_V \frac{\partial}{\partial \tau}(\rho\phi)dV + \int_w^e \frac{\partial}{\partial A}(\rho u\phi)dA + \int_s^n \frac{\partial}{\partial A}(\rho v\phi)dA + \int_l^h \frac{\partial}{\partial A}(\rho w\phi)dA \\ &= \int_w^e \frac{\partial}{\partial A}(\Gamma_\phi \frac{\partial \phi}{\partial x})dA + \int_s^n \frac{\partial}{\partial A}(\Gamma_\phi \frac{\partial \phi}{\partial y})dA + \int_l^h \frac{\partial}{\partial A}(\Gamma_\phi \frac{\partial \phi}{\partial z})dA + \int_V S_\phi dV\end{aligned} \tag{3.27}$$

where:

V = volume of the cell
A = area of the face
x,y,z = coordinates

The e,w,n,s,h,l in Eq. (3.27) refer to, respectively, direction in east (+x), west (-x), north (+y), south (-y), high (+z), and low (–z).

In Eq. (3.27), ϕ and its gradients at volume faces must be related to the values at the nodal points by way of an interpolation assumption. The fully implicit upwind scheme is one of the most stable discretization schemes. Under this scheme, the values of the scalar variables at the volume face are those at the nearest nodal point on the 'upwind' side of the face at the new time level:

$$\int_w^e \frac{\partial}{\partial A}(\rho u\phi)dA = \| F_e, 0 \| \phi_P - \| -F_e, 0 \| \phi_E - (\| F_w, 0 \| \phi_W - \| -F_w, 0 \| \phi_P) \tag{3.28}$$

where F_e and F_w are the momentum flux on the east and west surfaces of the cell as given in Table 3.3; ||a,b|| stands for the greater of a and b, and ϕ_E, ϕ_W, and ϕ_P are the ϕ in cells E, W, or P, as shown in Table 3.3.

Similarly, we have

$$\int_s^n \frac{\partial}{\partial A}(\rho v\phi)dA = \| F_n, 0 \| \phi_P - \| -F_n, 0 \| \phi_N - (\| F_s, 0 \| \phi_S - \| -F_s, 0 \| \phi_P) \tag{3.29}$$

$$\int_l^h \frac{\partial}{\partial A}(\rho w\phi)dA = \| F_h,0 \| \phi_P - \| -F_h,0 \| \phi_H - (\| F_l,0 \| \phi_L - \| -F_l,0 \| \phi_P) \qquad (3.30)$$

Assuming that ϕ varies linearly and Γ_ϕ is the weighted average (by length) of those on either side of the volume faces, the diffusion terms (the first three terms in the RHS of Eq. (3.27)) can be expressed as:

$$\int_w^e \frac{\partial}{\partial A}(\Gamma_\phi \frac{\partial \phi}{\partial x})dA = D_e(\phi_E - \phi_P) - D_w(\phi_P - \phi_W) \qquad (3.31)$$

$$\int_s^n \frac{\partial}{\partial A}(\Gamma_\phi \frac{\partial \phi}{\partial y})dA = D_n(\phi_N - \phi_P) - D_s(\phi_P - \phi_S) \qquad (3.32)$$

$$\int_l^h \frac{\partial}{\partial A}(\Gamma_\phi \frac{\partial \phi}{\partial z})dA = D_h(\phi_H - \phi_P) - D_l(\phi_P - \phi_L) \qquad (3.33)$$

where D_e, D_w, D_n, D_s, D_h, and D_l are listed in Table 3.3.

Table 3.3 Formula for F's and D's.

Cell face	**Convective flux F**	**Diffusive coefficient D**
e	$\rho u_e A_e$	$\frac{2A_e(\Gamma_{\phi,P}\delta x_P + \Gamma_{\phi,E}\delta x_E)}{(\delta x_P + \delta x_E)^2}$
w	$\rho u_w A_w$	$\frac{2A_w(\Gamma_{\phi,P}\delta x_P + \Gamma_{\phi,W}\delta x_W)}{(\delta x_P + \delta x_W)^2}$
n	$\rho v_n A_n$	$\frac{2A_n(\Gamma_{\phi,P}\delta y_P + \Gamma_{\phi,N}\delta y_N)}{(\delta y_P + \delta y_N)^2}$
s	$\rho v_s A_s$	$\frac{2A_s(\Gamma_{\phi,P}\delta y_P + \Gamma_{\phi,S}\delta y_S)}{(\delta y_P + \delta y_S)^2}$
h	$\rho w_h A_h$	$\frac{2A_h(\Gamma_{\phi,P}\delta z_P + \Gamma_{\phi,H}\delta z_H)}{(\delta z_P + \delta z_H)^2}$
l	$\rho w_l A_l$	$\frac{2A_l(\Gamma_{\phi,P}\delta z_P + \Gamma_{\phi,L}\delta z_L)}{(\delta z_P + \delta z_L)^2}$
τ	$\rho V_p/\delta_\tau$	

For the unsteady term, we have:

$$\int_V \frac{\partial}{\partial \tau}(\rho\phi)dV = C_\tau(\phi_P - \phi_{P-}) \tag{3.34}$$

where ϕ_P and ϕ_{P-} are the values at the current time (τ) and the previous time step (τ-δ_τ,), respectively.

Finally, the source term may be expressed in a linear form:

$$\int_V S_\phi dV = S_{\phi,c} + S_{\phi,p}\phi_p \tag{3.35}$$

Substituting Eqs. (3.28) - (3.35) into (3.27) yields:

$$(a_{\phi,P} - S_{\phi,P})\phi_P = a_{\phi,E}\phi_E + a_{\phi,W}\phi_W + a_{\phi,N}\phi_N + a_{\phi,S}\phi_S + a_{\phi,H}\phi_H + a_{\phi,L}\phi_L + a_{\phi,\tau}\phi_{P-} + S_{\phi,c} \tag{3.36}$$

where the coefficients

$a_{\phi,E} = \| -F_e, 0 \| + D_e$

$a_{\phi,W} = \| F_w, 0 \| + D_w$

$a_{\phi,N} = \| -F_n, 0 \| + D_n$

$a_{\phi,S} = \| F_s, 0 \| + D_s$

$a_{\phi,H} = \| -F_h, 0 \| + D_h$

$a_{\phi,L} = \| F_l, 0 \| + D_l$

$a_{\phi,\tau} = F_\tau$

$a_{\phi,P} = a_{\phi,E} + a_{\phi,W} + a_{\phi,N} + a_{\phi,S} + a_{\phi,H} + a_{\phi,L} + a_{\phi,\tau}$

The above equations also apply to the VOC diffusion in the material. For these cells the convection terms (F_e, F_w, F_n, F_s, F_h, and F_l) are 0. However, special treatments are needed for the following cells:

- Cells at the material-air interface (both on the material and air side)
- Cells associated with sinks (*e.g.*, material cells near the substrate)
- Cells with additional sources or boundary conditions (*e.g.*, sources with known flux or surface concentration, or inlets)

The following two sections discuss the treatment of these special cells.

3.4.2 Solving the interfacial mass transfer at the material-air interface

Figure 3.7 shows the interfacial grids, both on the material side and the air side. The discretized mass transfer equations for these cells are based on the governing equations of VOC diffusion inside the material, VOC phase changes at the material-air interface, and VOC mass transfer in the air-phase boundary layer.

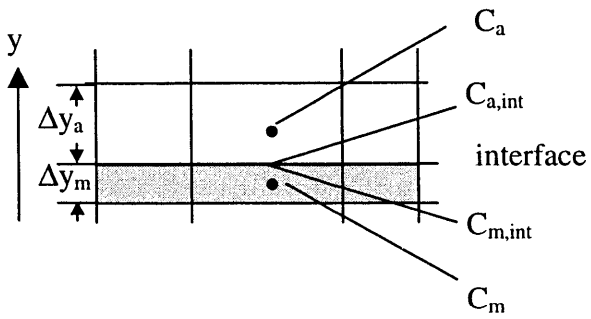

Figure 3.7 Grid notation and the grid configuration at the material-air interface

(a) VOC diffusion inside the material. Assuming emission occurred in the y direction, the mass transfer rate, from the material side to air, is:

$$q_{m,int} = D_m \frac{C_m - C_{m,int}}{\frac{1}{2}\Delta y_m} \tag{3.37}$$

where

D_m = the diffusion coefficient on the material side
C_m = the material-side concentration for the first near-interface grid
$C_{m,int}$ = the surface concentration on the material side
Δy_m = the grid size (in y direction) of the first near-interface grid

(b) VOC phase change at the material-air interface (Eq. 3.10):

$$C_{m,int} = K_{ma} C_{a,int} \tag{3.38}$$

where $C_{a,int}$ is the surface concentration on the air side

(c) VOC mass transfer in the air phase boundary layer. The mass transfer rate is:

$$q_{a,int} = D_{a,eff} \frac{C_{a,int} - C_a}{\frac{1}{2}\Delta y_a} \tag{3.39}$$

where

$D_{a,eff}$ = the effective air phase diffusion coefficient (see below)
C_a = air phase concentration in the first near-interface grid

The $D_{a,eff}$ in Eq. (3.39) depends on the airflow status and is given as follows:

- For laminar flow:

$$D_{a,eff} = D_a \tag{3.40}$$

where D_a is the laminar diffusivity of VOC.

- For turbulent flow using wall functions (see Eqs. (3.23a) and (3.23b)):

$$D_{a,eff} = D_a \qquad \text{for } y^+ \le 11.5 \tag{3.41a}$$

$$D_{a,eff} = \frac{1}{2} \frac{\Delta y_a u_\tau}{Sc_t[u^+ + E(\frac{Sc}{Sc_t} - 1)(\frac{Sc_t}{Sc})^{1/4}]} \qquad \text{for } y^+ > 11.5 \tag{3.41b}$$

- For turbulent flow using no wall functions (*e.g.*, Low Reynolds Number k-ε model or two-layer model):

$$D_{a,eff} = D_a + \frac{\mu_t}{Sc_t} \tag{3.42}$$

From mass conservation and Eqs. (3.37) - (3.42), we can obtain:

$$q_{m,int} = q_{a,int} = D_{a,eff} \frac{\frac{\frac{D_{a,eff}}{\Delta y_a} C_a + \frac{D_m}{\Delta y_m} C_m}{\frac{D_{a,eff}}{\Delta y_a} + K_{ma} \frac{D_m}{\Delta y_m}} - C_a}{\frac{1}{2}\Delta y_a} \tag{3.43}$$

On the other hand, the mass transfer rate at the material-air interface can be written in another form:

$$q_{m,int} = q_{a,int} = D_{int} \frac{C_m - C_a}{\frac{1}{2}(\Delta y_a + \Delta y_m)} \tag{3.44}$$

The purpose of introducing Eq. (3.44) is to express the interfacial mass transfer in a conventional format whereby the interfacial cells in the two phases are taken as normal cells of others. The only difference is that these cells have a different diffusivity, D_{int}, compared to the others.

From Eqs. (3.43) and (3.44), we identify D_{int} as follows

$$D_{int} = \frac{D_m D_{a,eff}(\Delta y_m + \Delta y_a)}{D_{a,eff}\Delta y_m + K_{ma} D_m \Delta y_a} \frac{C_m - K_{ma} C_a}{C_m - C_a} \tag{3.45}$$

A special case to Eq. (3.45) is K_{ma}=1, where the concentration at the material-air interface is continuous. D_{int} can then be simplified into:

$$D_{int} = \frac{D_m D_{a,eff}(\Delta y_m + \Delta y_a)}{D_{a,eff}\Delta y_m + D_m \Delta y_a} \tag{3.46}$$

Eq. (3.46) is the "harmonious diffusivity" derived by Patankar (1980) when solving conjugate heat transfer problems. Note that in the VOC mass transfer problem, D_{int} is determined not only by the material properties and grid distributions, but also by the VOC concentrations in both the interfacial material and air cell. Hence, it can be seen that the K_{ma} introduces numerically challenging non-linear couplings for the interfacial mass transfer. During the numerical simulation, an iteration method must be adopted for each time step to solve the above D_{int}. After this process, the discretized equation of the interfacial cells will be the same as the normal cells.

3.4.3 General form for VOC sources and sinks

Broadly speaking, both the VOC sink (*e.g.*, the material cell near the substrate) and other boundary conditions can be treated as additional source terms. These terms can be expressed, in general, as linearized sources with the following form:

$$q_s = COEF * (VAL - C_P) \tag{3.47}$$

where

q_s = source term

COEF = coefficient
VAL = value
C_p = VOC concentration in the cell associated with a source or sink

For the common boundaries, *i.e.*, air inlet, impermeable (adiabatic) walls, constant surface concentration, and constant surface flux, the values of COEF and VAL are given in Table 3.4. VOC sorption by permeable materials is expressed as a negative source, (see Eq. (3.9)) that is:

$$q_s = -(X_0 C_P + \tilde{q}) \tag{3.48}$$

where $\tilde{q}$ is known at the current time step.

From Eqs. (3.37) and (3.48):

$$q_s = -(X_0 C_{P,int} + \tilde{q}) = D_m \frac{C_{p,int} - C_p}{\frac{1}{2}\Delta y_m} \tag{3.49}$$

Comparing Eq. (3.49) with Eq. (3.47) for the sink:

$$COEF = \frac{2D_m / \Delta y_m}{1 + 2D_m / (X_0 \Delta y_m)} \tag{3.50}$$

$$VAL = -\frac{\tilde{q}}{X_0} \tag{3.51}$$

Eqs. (3.50) and (3.51) are also listed in Table 3.4.

Table 3.4 Coefficients and values in Eq. (3.47) for various boundary conditions.

Boundary condition	**Inlet**	**Impermeable wall**	**Fixed surface concentration**	**Fixed surface flux**	**Associated sink**
COEF	V_{inlet}	0.0	2E10	2E-10	$\frac{2D_m/\Delta y_m}{1+2D_m/(X_0\Delta y_m)}$
VAL	C_{inlet}	0.0	C_s	Q_{flux}/2E-10	$-\frac{\tilde{q}}{X_0}$

3.4.4 Solving the VOC equations in the whole computational domain

By using the above discretization method, all the computational cells, including those of the air and the material, can be expressed in the same form as Eq. (3.36). For each dependent variable, there are as many algebraic equations as there are control volumes in the integration domain. These algebraic equations can be solved by the Tri-Diagonal Matrix Algorithm (TDMA); see Patankar (1980) for details.

The above mathematical model is based solely on the mass transfer mechanisms during each phase. Theoretically, the model can predict VOC emissions provided that the physical properties of the compounds and substrate are given. Although the properties such as the material-air partition coefficient can be experimentally measured, others, such as the effective diffusivities in the material film and substrate, are more difficult to obtain accurately. Very recently, Bodalal *et al.* (1999) developed an experimental method to measure VOC diffusivity in several solid materials. However, the diffusivities for "wet" coating materials and oak wood substrate are not yet available. Methods for determining the material properties for numerical simulation will be discussed in the following section.

3.5 Determination of Material Properties for Numerical Simulation

In order to simulate VOC emissions from the "wet" material, the following material properties for each compound are needed:

(a) VOC initial concentration in the liquid material, $C_{l,0}$
(b) VOC partition coefficient in the material-air interface, K_{ma}
(c) Liquid expansion factor in the substrate, α
(d) VOC diffusivities

- In the air, D_a
- In the material film (initial), $D_{m,0}$
- In the substrate, D_s

In this study, we assume that the TVOC mixture has lumped properties as if it were a single compound. Based on this assumption, one question must first be resolved: how do we determine the properties (*e.g.*, the diffusivity) of TVOC? We propose to use the properties of the most dominant component in the solvent mixture to approximate the average properties of the TVOC mixture. This is clearly an approximation because the composition of the mixture changes over time. However, US EPA researchers (Guo *et al.*, 1999) have shown that the assumption is adequate for petroleum-based "wet" sources such as wood stains.

The following section discusses the method for determining the aforementioned parameters.

3.5.1 The VOC initial concentration in the "wet" source

For a pure compound (*e.g.*, decane), $C_{l,0}$ is the density of the saturated liquid at the temperature tested. For a mixture such as wood stain, $C_{l,0}$ for TVOC can be measured by monitoring the weight loss of the VOC using a glass substrate for a long period (*e.g.*, 3 days), while $C_{l,0}$ for a single compound in the material can be obtained by integrating the measured compound concentrations using a small-scale test chamber.

3.5.1 The partition coefficient

By definition, the partition coefficient represents the ratio of concentrations between two different phases assuming the equilibrium at the interface is achieved instantaneously. For a compound in the material film, K_{ma} can be calculated by:

$$K_{ma} = \frac{C_{l,0}}{C_{a,0}} \tag{3.52}$$

where $C_{a,0}$ is the equilibrium vapor phase concentration (mg/m^3).

Two methods can be used to determine the $C_{a,0}$ of a compound: by headspace analysis or by theoretical calculation.

The headspace analysis measures the $C_{a,0}$ directly for both TVOC and a single compound in a "wet" material. Eq. (3.52) can be used to calculate K_{ma}. This method is suitable for obtaining $C_{a,0}$ at room temperature (*e.g.*, 23 °C). To obtain $C_{a,0}$ (and hence K_{ma}) at different temperatures, theoretical calculations are usually employed.

Several equations have been proposed to calculate the vapor pressure for a pure compound (Reid *et al.*, 1977). For the application of petroleum-based "wet" coating materials, Chang and Guo (1992) suggested the use of following equation:

$$\log_{10} P = -0.2185\frac{A}{T} + B \tag{3.53}$$

where
P = vapor pressure, mmHg
T = temperature, K
A, B = properties of compounds. The values for the major VOCs identified as emitted from the wood stain are given in Table 3.5.

Table 3.5 Values of the coefficients used by Eq. (3.53) (Chang *et al.*, 1992).

Compound	A	B
Nonane	10456.9	8.332532
Decane	10912.0	8.248089
Undecane	11481.7	8.260477

The ideal gas law can be used to calculate $C_{a,0}$ based on P:

$$C_{a,0} = \frac{1.33\times10^{8}P}{8314T/M} \tag{3.54}$$

where M is the molecular weight of the compound.

By combining Eqs. (3.53) and (3.54), $C_{a,0}$ can be calculated based on the temperature (T), molecular weight (M), and properties of the compound (A,B).

For a "wet" coating material that emits different VOCs, the headspace analysis is usually used to determine K_{ma} at a reference temperature (*e.g.*, 23 °C) and Eqs. (3.53) and (3.54) to determine the dependence of K_{ma} on temperature. Assuming the K_{ma} at the reference temperature, T_{ref}, is $K_{ma}(T_{ref})$, the K_{ma} at a different temperature, T, will be:

$$K_{ma}(T) = K_{ma}(T_{ref})\frac{T}{T_{ref}}10^{0.2185A(\frac{1}{T}-\frac{1}{T_{ref}})} \tag{3.55}$$

3.5.3 The liquid expansion factor (α)

Eq. (3.25) indicates that due to the liquid expansion factor (α), the initial VOC concentration (and hence the equilibrium air phase concentration) of the "wet" material film being absorbed into the substrate will be smaller than that of the "wet" source. Since it is difficult to measure α directly, its value can be estimated by assuming that when a "wet' material is applied to a porous substrate emissions at the beginning must be evaporation dominated and hence the VB model applies for the beginning. The following procedures provide the details.

(1) Assume an initial VOC concentration in the material film absorbed by the substrate, $C_{l,ini}$. The value could be equal to or smaller than $C_{l,0}$ (the VOC concentration in the "wet" source).

(2) Calculate the equilibrium air phase concentration corresponding to $C_{l,ini}$ by using Eq. (3.38).

(3) Calculate the VOC emission rate by using the VB model. Adjust the $C_{1,ini}$ until the initial emission rate (*e.g.*, from 0 - 0.2 h), as calculated by the VB model, agree with the measured data. The α can then be calculated by:

$$\alpha = \frac{C_{1,0}}{C_{1,ini}}$$

It should be noted that the key to using this approach is to provide the correct mass transfer coefficient when using the VB model. In our study, we used CFD to calculate the average mass transfer and used the value for the VB model.

After obtaining all of the above parameters independently, we still had three unknowns: D_a, $D_{m,o}$ and D_s. D_a can be easily found in the literature (*e.g.*, Reid *et al.*, 1977). However, no sufficient information is available regarding the $D_{m,o}$ and D_s. In this study, they are obtained by fitting the predicted VOC emission rates with the measured data, as will be discussed in section 3.6.1.2.

3.6 Results and Discussion

This section presents the results of simulating "wet" material emissions by using the numerical model described above. In the following, two small-scale chamber cases (one for decane and the other for wood stain) tested in Chapter 2 are used to obtain the unknown diffusion coefficients based on the measured emission rates of these two cases. The diffusivity values are then used for other small-scale and full-scale chamber cases without further adjustment. The purpose of these simulations is to further validate the model for simulating the effects of various environmental conditions (temperature, velocity, velocity fluctuation) on "wet" material emissions.

3.6.1 Simulation of the reference cases

The reference cases selected were Case1-2a for decane and Case 1-2b for wood stain. The test conditions for both cases were as follows:

- Temperature: 23.5 ± 0.5 °C
- Relative humidity: 50 ± 2 %
- Air exchange rate: 1.0 ± 0.05 ACH
- Air velocity at the mid-height of the inner chamber: 0.15 m/s
- Inlet and outlet size: 0.0063 m in diameter
- Substrate of tested material: 0.24 m (long) by 0.25 m (wide) oak board

3.6.1.1 Characteristics of flow fields

We started the reference cases by first simulating the airflows in the small-scale chamber. The Reynolds number of the flow, Re_h, in the inner chamber was:

$$Re_h = Vh\rho/\mu \tag{3.56}$$

where

V = air velocity at the center of the inner chamber, m/s
h = inner chamber height, m
ρ = air density, kg/m^3
μ = molecular viscosity of air, $N \cdot s/m^2$

For the reference cases, V = 0.15 m/s and h = 0.08 m. The Re_h was only 800, which means the flow was laminar. The simulated airflow patterns using a commercial CFD code (CHAM, 1996) in a section over the material are shown in Figure 3.8. Figure 3.9 gives the simulated velocity distribution by CFD above the material in the inner chamber. The air exchange rates in the inner chamber was about 1800 air changes per hour (ACH) based on the air velocity in the inner chamber (0.15 m/s). However, the air exchange rate in the whole chamber was only 1.0 ACH. The exhaust fan in the inner chamber exhausted the contaminated air to the outer chamber, resulting in a bulk velocity of about 0.01 m/s for the outer chamber. (The bulk velocity due to the net 1.0 ACH air exchange rate for the whole chamber was very small.)

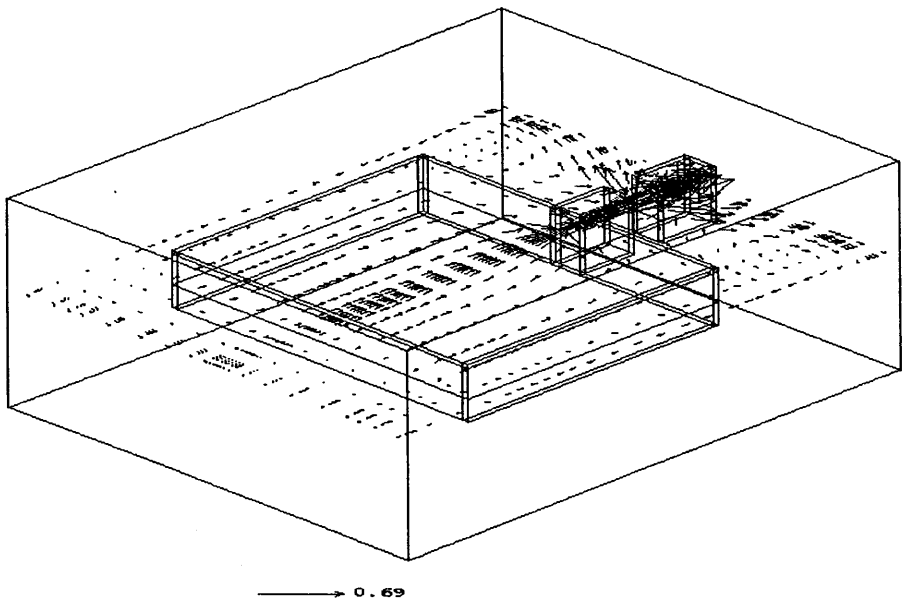

Figure 3.8 Predicted velocity vectors in the small-scale chamber.

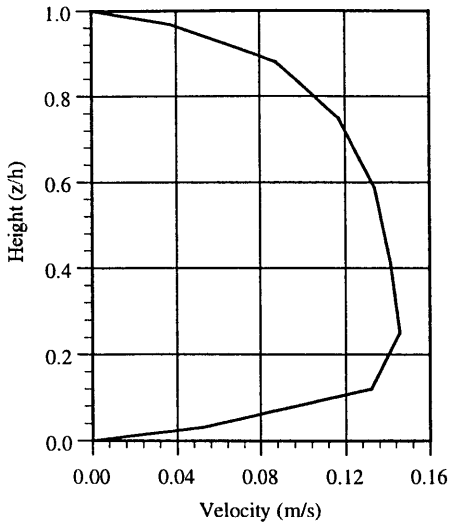

Figure 3.9 Simulated velocity distribution above the material in the inner chamber of the small-scale chamber, h = 0.08 m (inner chamber height).

3.6.1.2 Material properties used in the numerical simulation

Table 3.6 lists the physical properties of decane, and Table 3.7 gives the properties for wood stain (TVOC and three single compounds) required by the numerical model. Most of the parameters in the tables are the properties of the material or the compounds. Among others, the partition coefficient for both TVOC and single compounds, $C_{l,0}$ and α, were obtained following the procedures discussed in section 3.5. The properties most difficult to determine are the diffusivities of VOCs in the material film ($D_{m,0}$) and in the substrate (D_s). The values listed in Tables 3.6 and 3.7 were obtained by fitting the predicted VOC emission rates to the small-scale experimental data. The following section discusses the procedure in detail.

Table 3.6: Physical properties of decane applied to oak substrates (23.5 °C).

Property	Symbol (unit)	Value
Liquid density	ρ_l (mg/m^3) [a]	7.3×10^8
Initial VOC concentration in liquid	$C_{l,0}$ (mg/m^3)	7.3×10^8
VOC vapor pressure	$C_{a,0}$ (mg/m^3) [b]	12466
Partition coefficient	K_{ma} (-) [c]	58559.3
Liquid expansion factor in substrate	α (-) [d]	1.2
Initial VOC concentration in film	$C_{m,0}$ (mg/m^3) [e]	6.083×10^8
VOC Schmidt number	Sc (-) [f]	2.6
Initial VOC diffusivity in film	$D_{m,0}$ (m^2/s) [g]	1×10^{-11}
VOC diffusivity in substrate	D_s (m^2/s) [g]	1×10^{-14}

[a] Lide 1995
[b] Eqs. (3.53) and (3.54)
[c] $K_{ma} = C_{l,0}/C_{a,0}$
[d] Obtained by using the VB model for the initial period (0 - 0.2 h) and comparing the calculated initial emission rate with the small-scale chamber data (Case1-2a)
[e] $C_{m,0} = C_{l,0}/\alpha$
[f] Sparks *et al.*, 1996
[g] Obtained by matching the simulated emission rates with the small-scale chamber data (Case1-2a)

Table 3.7: Physical properties of wood stain applied to oak substrates (23.5 °C)

Property	Symbol (unit)	TVOC	Nonane	Decane	Undecane
Liquid density	ρ_l (mg/m^3)	8.18×10^{8} [a]	7.176×10^{8} [b]	7.3×10^{8} [b]	7.402×10^{8} [b]
Initial VOC concentration in liquid	$C_{l,0}$ (mg/m^3) [c]	6.9092×10^{8}	3.364×10^{7}	5.974×10^{7}	2.581×10^{7}
VOC vapor pressure	$C_{a,0}$ (mg/m^3)	17131.7 [d]	29532.8 [e]	12466 [e]	5362.3 [e]
Partition coefficient	K_{ma} (-)	40330 [f]	24298.4 [g]	58559.3 [g]	138033 [g]
Liquid expansion factor in substrate	α (-) [h]	1.33	1.33	1.33	1.33
Initial VOC concentration in film	$C_{m,0}$ (mg/m^3) [i]	5.195×10^{8}	2.529×10^{7}	4.492×10^{7}	1.941×10^{7}
VOC Schmidt number	Sc (-) [j]	2.6	2.6	2.6	2.6
Initial VOC diffusivity in film	$D_{m,0}$ (m^2/s) [k]	1×10^{-11}	1×10^{-11}	1×10^{-11}	1×10^{-11}
VOC diffusivity in substrate	D_s (m^2/s) [k]	1×10^{-14}	1×10^{-14}	1×10^{-14}	1×10^{-14}

[a] For wood stain; lab measurement
[b] For pure compound; Lide 1995
[c] Lab measurement using glass substrates
[d] Headspace analysis
[e] For pure compound; Eqs. (3.53) and (3.54)
[f] $K_{ma} = C_{l,0}/C_{a,0}$
[g] $K_{ma} = \rho_l/C_{a,0}$
[h] Obtained by using the VB model for the initial period (0 - 0.2 h) and comparing the calculated initial emission rate with the small-scale chamber data (Case1-2b)
[i] $C_{m,0} = C_{l,0}/\alpha$
[j] Sparks *et al.*, 1996
[k] Obtained by matching the simulated emission rates with the small-scale chamber data (Case1-2b)

The diffusivity estimation is a "reverse" process of the emission simulations. In emission simulations, we know the material properties and the non-linear mathematical model calculates the VOC distributions (or equivalently, emission rates) as a function of time. In diffusivity estimation, we estimate some of the unknown constants based on the most appropriate match, *i.e.*, adjusting the diffusivities until an agreement between the model prediction and the experimental data is achieved. This approach is also useful for two

reasons:

(1) It can verify the adequacy of the assumptions used in the model. For example, if the model involves some unrealistic assumptions (*e.g.*, neglect the internal diffusion in the material film), we may never get the correct data fit no matter how we adjust the unknown parameters. If our model is correct, the residuals should exhibit tendencies that tend to confirm the assumptions we have made, or, at least, should not exhibit a denial of these assumptions.

(2) It can serve as the sensitivity study needed to examine how the emission characteristics will be affected by the changes in the diffusivities. Because the diffusivities in the material film and the substrate are always coupled, independent determination (by experimental measurements or theoretical calculation) of these diffusivities is extremely difficult. If the estimation error of these diffusivities exists, the sensitivity study can predict how the actual emission rates will change accordingly.

Since the diffusivity estimation involves obtaining two unknowns using one set of measured data (emission rates), we must ensure that the parameter values obtained are unique. In general, a "good" agreement between the measured and predicted emission rates may be the result of three possibilities for $D_{m,0}$ and D_s:

1) Both values are correct
2) Only one value is correct
3) Both values are incorrect

The first option should yield the correct regression of $D_{m,0}$ and D_s. The second one may indicate that the measured emission rates are not sensitive to one parameter in some range, and the last option indicates there could be multiple solutions to the differential equation, and that the regression process has failed. To obtain reasonable diffusivities, the first result is ideal, the second may be acceptable, and the last is unacceptable.

To estimate $D_{m,0}$ and D_s simultaneously by one regression, intuitively the last option may be possible because changing $D_{m,0}$ and D_s may lead to the same trend to the emission rates. For instance, increasing the $D_{m,0}$ may increase the decay rate of the emissions, while increasing D_s may create the same trend. A preliminary analysis has been conducted in an attempt to confine both values within a small range, as will be discussed below.

First, list the possible range for $D_{m,0}$ and D_s in terms of order of magnitude. Physically, $D_{m,0}$ should be within a certain range, say, from 10^{-9} to 10^{-13} (m^2/s), and D_s should be within, say, 10^{-11} to 10^{-16}. Considering these possibilities in terms of order of magnitude we can obtain a parametric matrix as shown in Table 3.8. Each element in the matrix shows a different case. So now we have a total of $6 \times 5=30$ cases.

Table 3.8 Screening cases that include all the possible combinations of $D_{m,0}$ and D_s in terms of order of magnitude. The subscript under C in a table cell indicates a case number.

Column number		C1	C2	C3	C4	C5	C6
Line number	D_s(m^2/s) / $D_{m,0}$ (m^2/s)	10^{-16}	10^{-15}	10^{-14}	10^{-13}	10^{-12}	10^{-11}
L1	10^{-13}	C_{11}	C_{12}	C_{13}	C_{14}	C_{15}	C_{16}
L2	10^{-12}	C_{21}	C_{22}	C_{23}	C_{24}	C_{25}	C_{26}
L3	10^{-11}	C_{31}	C_{32}	C_{33}	C_{34}	C_{35}	C_{36}
L4	10^{-10}	C_{41}	C_{42}	C_{43}	C_{44}	C_{45}	C_{46}
L5	10^{-9}	C_{51}	C_{52}	C_{53}	C_{54}	C_{55}	C_{56}

Next we wanted to screen these 30 cases to see if any multiple regions with the same good data fit exists. To do that, we did not need to simulate all these cases. Instead, we started from several extreme cases, *i.e.*, C21, C26, C41, and C46. Figure 3.10 gives the results of the first-round data fit. The results are discussed here.

- C21 ($D_{m,0} = 10^{-12}$, $D_s = 10^{-16}$) and C26 ($D_{m,0} = 10^{-12}$, $D_s = 10^{-11}$). C21 predicted too low early stage (0 - 0.2 h) emissions, indicating that $D_{m,0}$ is too small even with a negligible substrate diffusion ($D_s = 10^{-16}$). Increasing D_s tends to make the early-stage emissions even smaller (results of C26 confirm). Hence, the value of $D_{m,0}$ should not be lower than 10^{-12} m^2/s.
- C41 ($D_{m,0} = 10^{-10}$, $D_s = 10^{-16}$) and C46 ($D_{m,0} = 10^{-10}$, $D_s = 10^{-11}$). C41 predicted the correct initial emission rate but a too fast decay, indicating that $D_{m,0}$ is too large even with a negligible D_s (= 10^{-16} m^2/s). Again, increasing D_s will increase the decay even more and produce incorrect emission rates during the later stage (> 4 hour, results of C46 confirm). Hence, the value of $D_{m,0}$ should not be larger than 10^{-10} m^2/s.

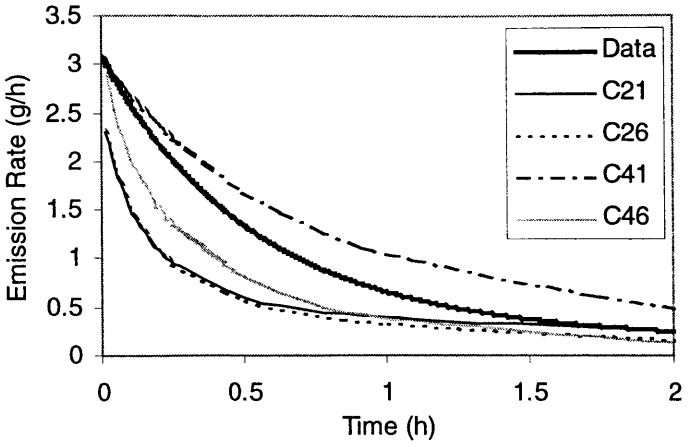

(a)

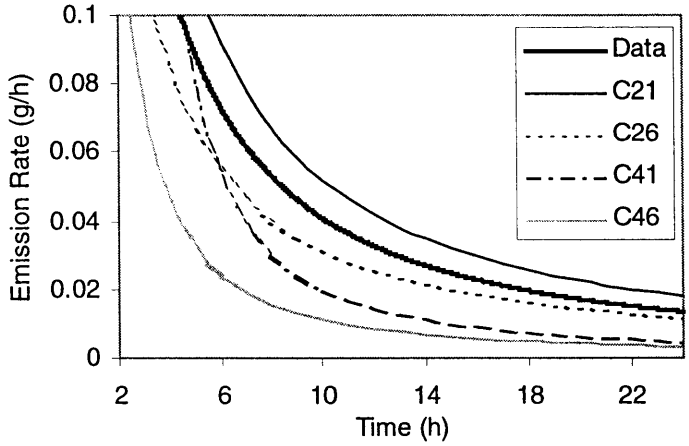

(b)

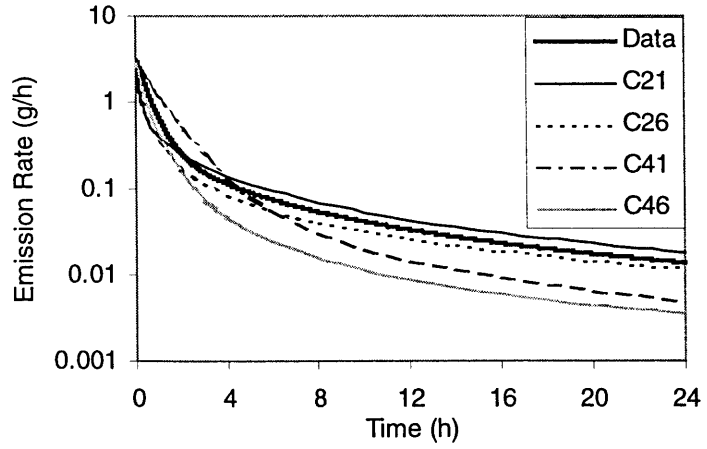

(c)

Figure 3.10 A comparison of measured and simulated emission rates with different diffusion coefficients. See Table 3.8 for the diffusion coefficients for each case: (a) 0 - 2 hour, (b) 2 - 24 hour, (c) 0 - 24 hour.

The above indicates that all the cases in L1, L2, L4, and L5 can be eliminated because these cases either have a too small $D_{m,0}$ (L1 and L2) or too large $D_{m,0}$ (L4 and L5). After eliminating these cases, we have only the six cases in L3 left.

Now it is possible to simulate all the six remaining cases in L3. The results, as shown in Figure 3.11, indicate that:

- C34 ($D_s = 10^{-13}$), C35 ($D_s = 10^{-12}$), and C36 ($D_s = 10^{-11}$) predicted too small emissions and too fast decay rates throughout the entire period, indicating that D_s is too large for these cases (too much VOC has been diffused into the substrate).
- Among the remaining three cases, C31 ($D_s = 10^{-16}$) and C32 ($D_s = 10^{-15}$) predicted almost identical emission rates during the 24-hour period. Both cases preformed slightly better for $\tau > 5$ hours than C33 ($D_s = 10^{-14}$) but worse during 0.5-5 hours. All these cases, however, predicted a relatively good agreement of the emissions with the measured data.

The above results indicate that the order of magnitude of $D_{m,0}$ should be around 10^{-11} m^2/s. However, the D_s could vary by three orders of magnitude, *i.e.*, $10^{-14} \sim 10^{-16}$ m^2/s. In other words, the predicted emissions are not sensitive to D_s when its value is within $10^{-14} \sim 10^{-16}$ m^2/s.

To further test the sensitivity of emissions to $D_{m,0}$, we set D_s to 10^{-14} m^2/s and varied $D_{m,0}$ from within 5×10^{-12} - 2×10^{-11} m^2/s. The results, as given in Figure 3.12, show that the predicted emission rates began to deviate from the measured values when $D_{m,0}$ was beyond this range.

Hence, from the above preliminary study we concluded that, based on the above data-fitting and sensitivity study, we cannot obtain the exact values of $D_{m,0}$ and D_s. Instead, we found that we may obtain a relatively small region in which the parameter accuracy cannot be considerably improved. The values of $D_{m,0}$ and D_s in Tables 3.6 and 3.7 simply reflect a possible combination within such a region.

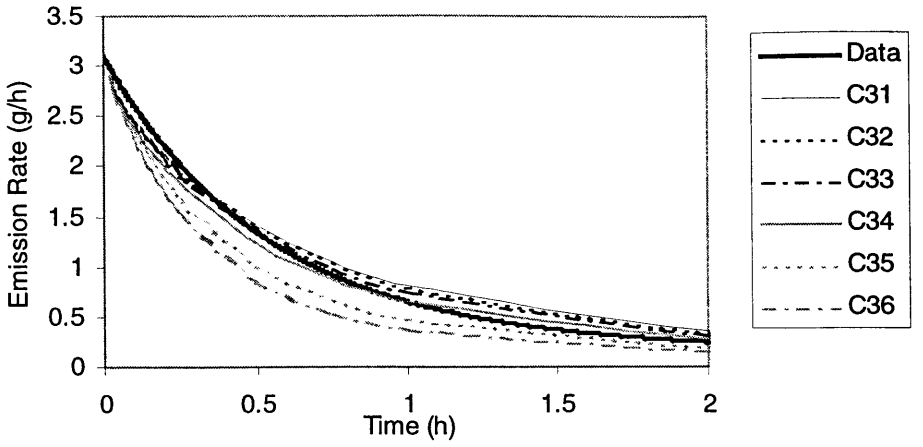

(a)

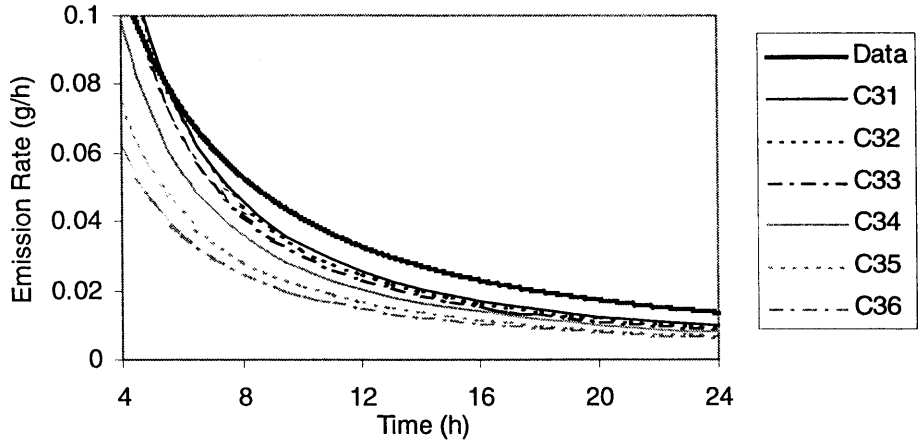

(b)

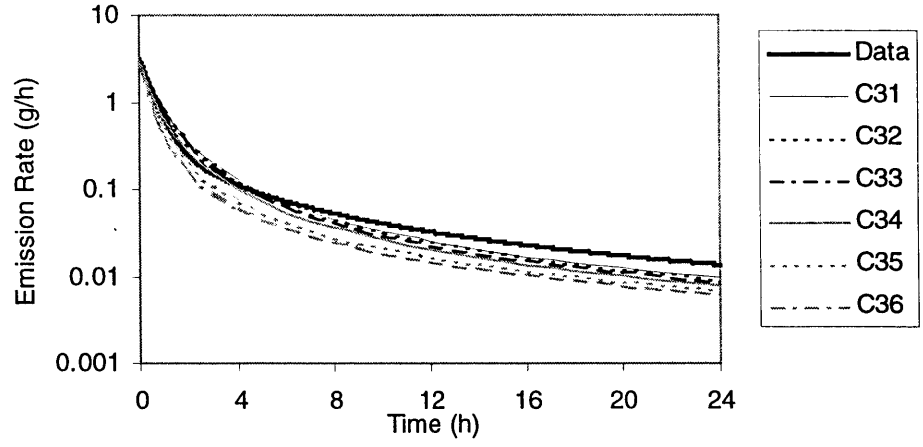

(c)

Figure 3.11 A comparison of measured and simulated emission rates with different diffusion coefficients. See Table 3.8 for the diffusion coefficients for each case: (a) 0 - 2 hour, (b) 2 - 24 hour, (c) 0 - 24 hour.

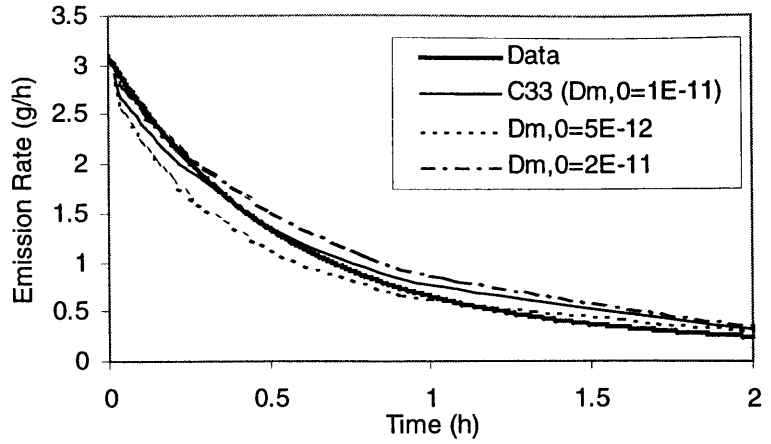

(a)

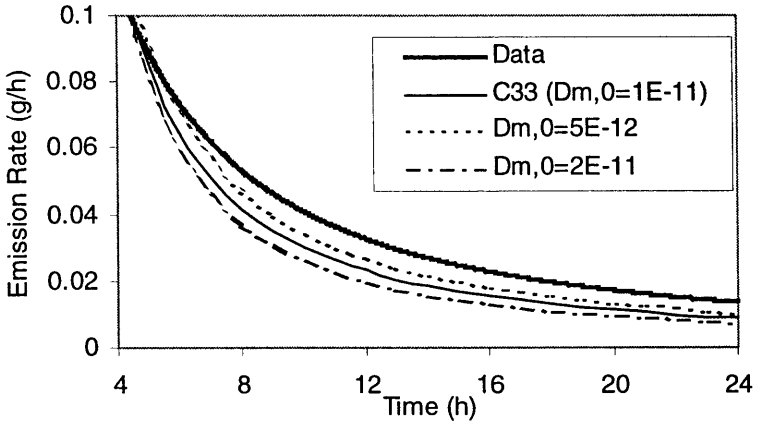

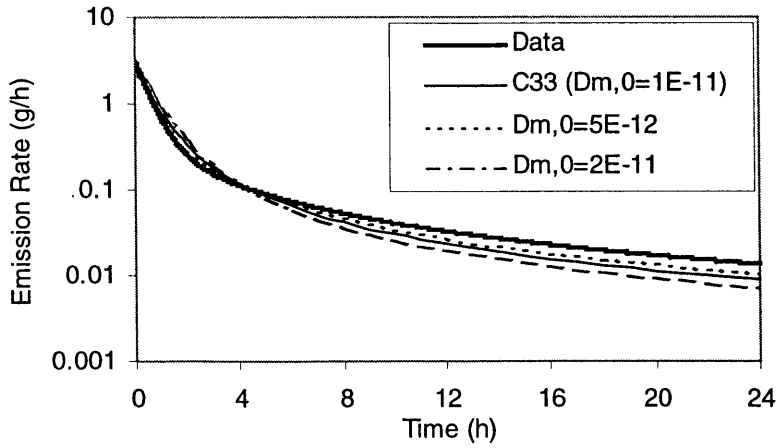

(c)

Figure 3.12 A comparison of measured and simulated emission rates with different diffusion coefficients: (a) 0 - 2 hour, (b) 2 - 24 hour, (c) 0 - 24 hour.

3.6.1.3 Prediction of TVOC emissions

As soon as the material properties are obtained or estimated, theses properties can be used in the numerical model to predict emissions. Figures 3.13 and 3.14 compare the measured and simulated TVOC emission rates in the small-scale chamber for Cases 1-2a and 1-2b, respectively using both the numerical model and the VB model. The average air phase mass transfer coefficient used in the VB model was 4.03 m/h (V = 0.15 m/s). The value was obtained by CFD simulation. Since the VB model assumes no internal diffusion in the material film and the substrate, it only applies to the period when the emissions are dominated by evaporation. The difference of the emission rates predicted by the VB and numerical models indicates the effects of diffusion. The results show that evaporation dominated the emission process during the first 2 hours for decane, while only the first 0.2 hour for the wood stain. After that, emissions gradually became internal-diffusion-controlled which rendered the VB model invalid. The results confirmed that emissions from "wet" materials applied to an absorptive substrate are dominated by evaporation at the beginning and internal diffusion afterwards, which had been hypothesized based on previous experimental data.

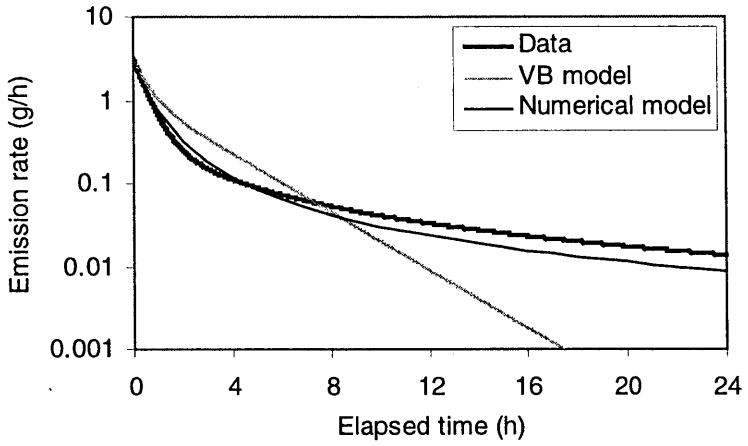

Figure 3.13 Comparison of measured and simulated TVOC emission rates from the wood stain in the small-scale chamber.

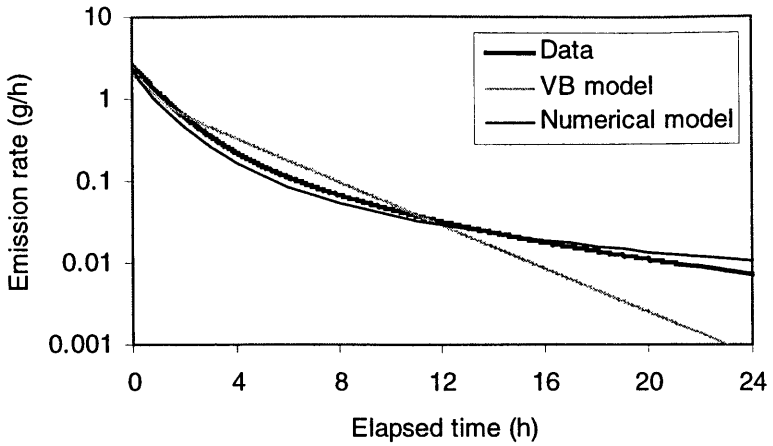

Figure 3.14 Comparison of measured and simulated TVOC emission rates from decane in the small-scale chamber.

An analysis of VOC mass balance during the emission process further helped us to quantitatively characterize the "wet" material emissions and the substrate effect. Figure 3.15 gives the predicted percentages of the TVOC mass emitted from the material, diffused from the film to the substrate, and remaining in the material film, respectively. At the beginning, VOC emitted very quickly. About 63% of the TVOC were emitted within the first 4 hours, while about 5% of the VOCs were diffused into the substrate. After that, both the emission amount and substrate sorption amount increased slowly. At τ=24 hour the percentage of TVOC emitted, diffused (to the substrate), and remaining inside the film were 78.1%, 6.1%, and 15.8%, respectively. This means that after 24 hours, only about 15% of the TVOC remained in the material film. Emissions from this small amount, however, is expected to last for a long period of time due to slow diffusion inside the material film and the substrate.

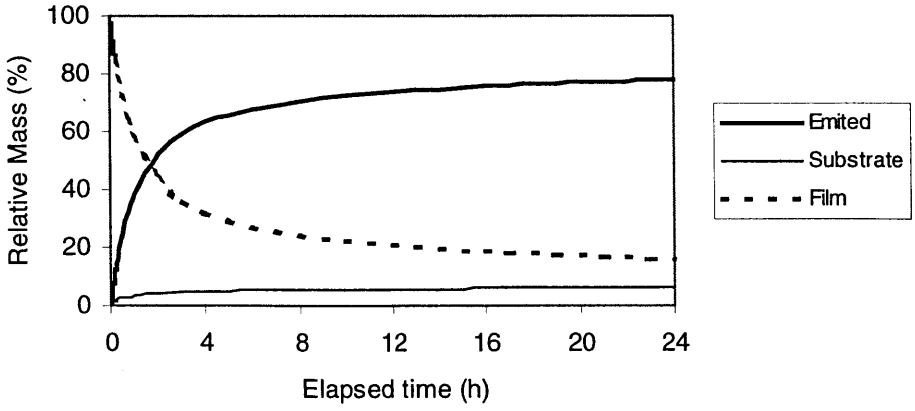

Figure 3.15 Predicted percentages of TVOC mass emitted from the material, diffused from the film to the substrate, and left in the material film.

By using the numerical model, it is also possible to examine the VOC distributions in different mass transfer layers as illustrated in Figure 3.2. Figure 3.16 shows the relative TVOC concentration distributions in the material film ($y/\delta<1$), at the material-air interface ($y/\delta=1$), and the air phase boundary layer ($y/\delta>1$) at different times. The VOC distributions in the substrate was not shown because the concentrations in the substrate were not calculated directly. (The mass transfer to the substrate was calculated using the sorption model; see Section 3.3.1.2 for details.)

Figure 3.16 depicts the VOC evolution in different layers. At the beginning (*e.g.*, 0 - 15 minutes), the VOC concentration in the material film was close to the initial concentration ($C/C_0 \rightarrow 1$). The concentration gradient in the film was small. At the same time, the VOC concentration in the air was also small except in the area very close to the interface ($y/\delta<10$). Emissions in this period were dominated by the VOC phase change at the interface and gas phase mass transfer. As time goes on, the concentration gradient in the material film especially near the interface became larger while the gradient in the air phase boundary layer became smaller. This indicated that diffusion began to dominate the gas phase mass transfer. The above results support our previous conclusions based on the VOC emission rates. During this process ($\tau>15$ min), the air phase concentration in the boundary layer first increased due to the air phase mass transfer, and then decreased due to the decreasing emission rates from the source.

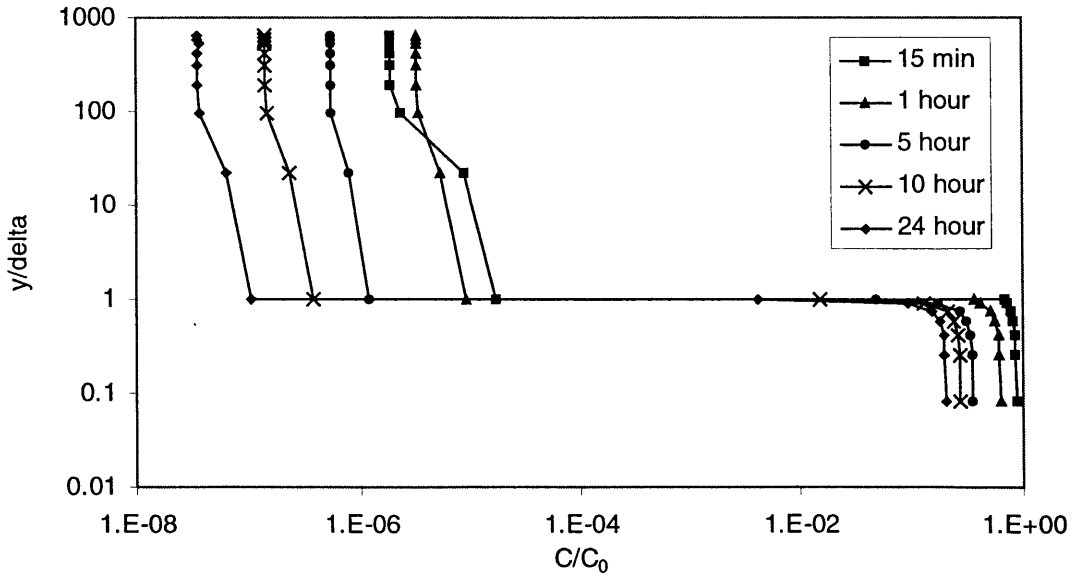

Figure 3.16 Predicted TVOC distributions in the material film (y/delta (δ) < 1), material-air interface ($y/\delta=1$), and the air phase boundary layer ($y/\delta>1$).

3.6.1.4 Prediction of single VOC emissions

In addition to predicting TVOC emission rates, the numerical model can also be used to calculate the emissions of a single VOC. Figure 3.17 compares the simulated concentrations of three single compounds (nonane, decane, undecane) emitted from the wood stain with the measured data. Note that the same values of $D_{m,0}$ and D_s for TVOC were used for single VOCs (the K_{ma} and C_0 were different). This was done to examine to what extent the diffusivities obtained from TVOC data could be applied to single compounds. As shown in Figure 3.17, the predicted results generally agree with the experimental data. The most important feature, that a more volatile compound (*e.g.*, nonane) emits faster than a less volatile compound (*e.g.*, undecane), was correctly predicted. The prediction error for undecane was significantly higher than that for the other two compounds. This again demonstrates that different single compounds may have different diffusivities in the material film and the substrate. It seems that the diffusivity of TVOC is approximately equal to the most abundant compounds (nonane and decane in this case) but not all of the compounds.

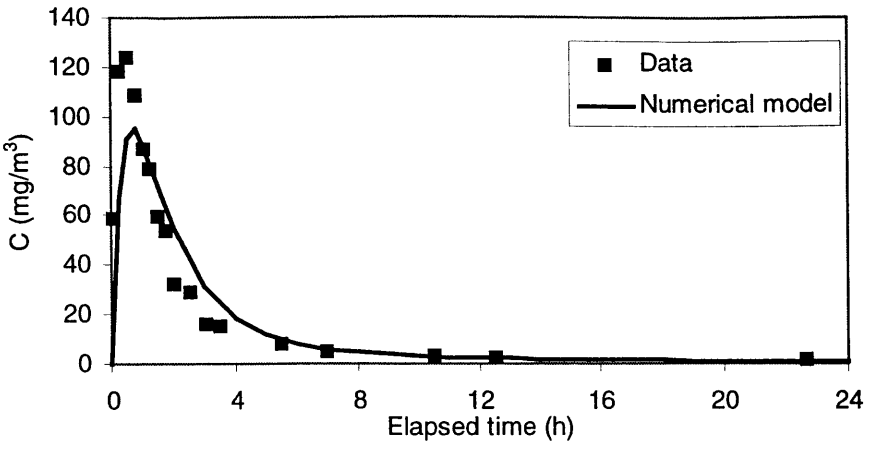

(a)

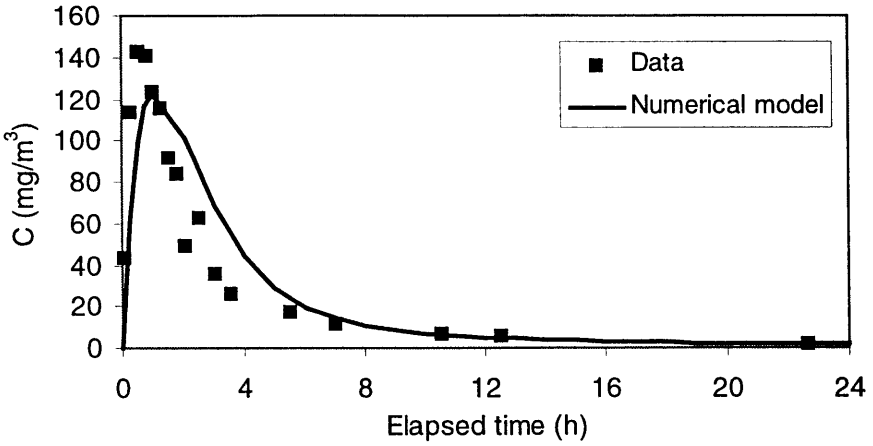

(b)

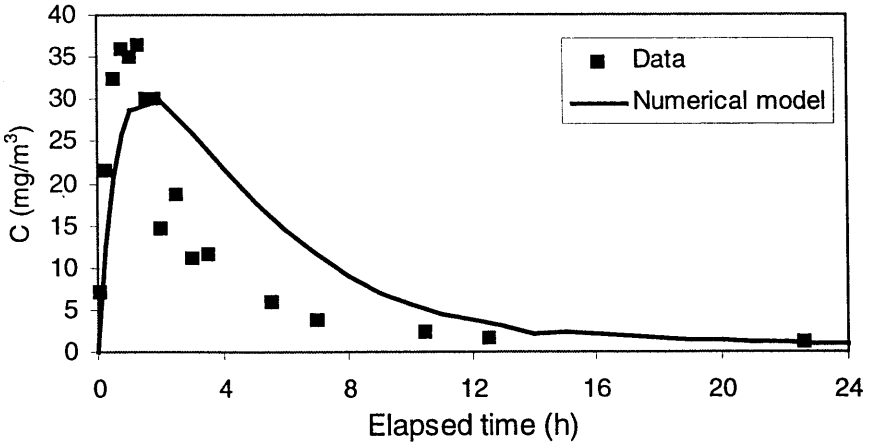

(c)

Figure 3.17 Comparison of the measured and simulated single VOC concentrations at the chamber exhaust: (a) Nonane, (b) Decane, (c) Undecane.

3.6.2 Validation of the model based on the small-scale chamber data

As discussed earlier, we obtained the unknown diffusivities, $D_{m,0}$ and D_s, based on the measured data of the reference cases. With the property values, the model should apply to any environmental conditions (velocity, turbulence, ventilation rate, temperature) without further adjustments of the diffusivities. In Chapter 2, we measured emissions from both decane and wood stain under different environmental conditions. It is natural to evaluate the numerical model by using those data. The following section presents the results of the small-scale chamber cases other than the reference case, while in Section 3.6.3 the model is further validated by the full-scale chamber cases. The purpose of the full-scale chamber validation is to make sure that the model developed based on small-scale chamber data can be scaled up to buildings.

Chapter 2 shows the measured emissions from both the wood stain and decane under four different temperatures, 20.5 °C, 23.5 °C, 27.5 °C, and 31.5 °C. In this section, we will test whether the model can correctly predict the emissions at different temperatures. Using the partition coefficient (K_{ma}) and diffusion coefficients ($D_{m,0}$ and D_s) for both decane and wood stain at 23.5 °C as the reference data (which have been obtained), K_{ma}, $D_{m,0}$, and D_s at different temperatures, as calculated using Eqs. (3.5), (3.7), and (3.55), are listed in Table 3.9. A value of 7.3 Kcal/mole for activation energy (E_d) was used to calculate the temperature dependence of $D_{m,0}$ and D_s.

Table 3.9 Values of partition coefficient (K_{ma}) and diffusion coefficients ($D_{m,0}$ and D_s) for wood stain and decane under different temperatures.

Temperature	**Wood stain (TVOC)**			**Decane**		
(°C)	K_{ma}	$D_{m,0}$ (m^2/s)	D_s (m^2/s)	K_{ma}	$D_{m,0}$ (m^2/s)	D_s (m^2/s)
20.5	49112	0.87×10^{-11}	0.87×10^{-14}	71311	0.87×10^{-11}	0.87×10^{-14}
23.5	40330	1×10^{-11}	1×10^{-14}	58559	1×10^{-11}	1×10^{-14}
27.5	31953	1.18×10^{-11}	1.18×10^{-14}	46396	1.18×10^{-11}	1.18×10^{-14}
31.5	25476	1.38×10^{-11}	1.38×10^{-14}	36991	1.38×10^{-11}	1.38×10^{-14}

Figure 3.18 compares the measured and simulated TVOC emission rates (using both numerical and VB model) of wood stain at different temperatures. The results of the numerical model generally agree with the data. However, a large discrepancy was found for the high temperature cases (27.5 °C and 31.5 °C) especially during the diffusion dominant period (τ > 10 h). Possible reasons for this could derive from both simulation and experimental errors. Eqs. (3.5), (3.7), and (3.55) may not be accurate for high temperatures (*e.g.*, 31.5 °C). On the other hand, the measurement data gathered at a higher temperature could be affected by moisture fluctuations during this period, as discussed in Chapter 2. Despite such discrepancies, the results from the numerical simulation match the experimental data much better than results derived form the VB model.

Similar phenomena also occurred with decane. Figure 3.19 compares the three temperatures tested: 20.5 °C, 27.5 °C, and 31.5 °C. For higher temperatures, the simulated emission rates of decane agree with the data slightly better than those of wood stain.

3.6.3 Validation of the model by the full-scale chamber data

As indicated earlier, the flow conditions in the full-scale chamber are close to those found in buildings. The numerical model, after we validated it using a full-scale chamber, can be used with confidence in buildings.

To simulate VOC emissions in a full-scale chamber, the airflow should first be correctly simulated. The following sections compare the airflow distributions and VOC emission rates from experimental measurements and numerical simulations.

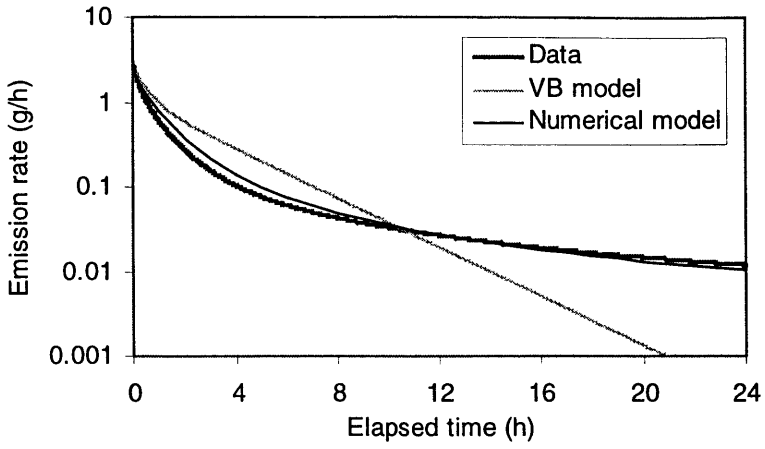

(a)

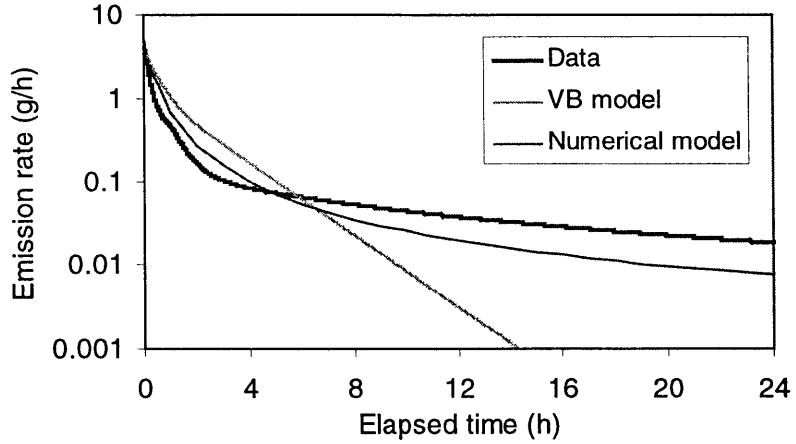

(b)

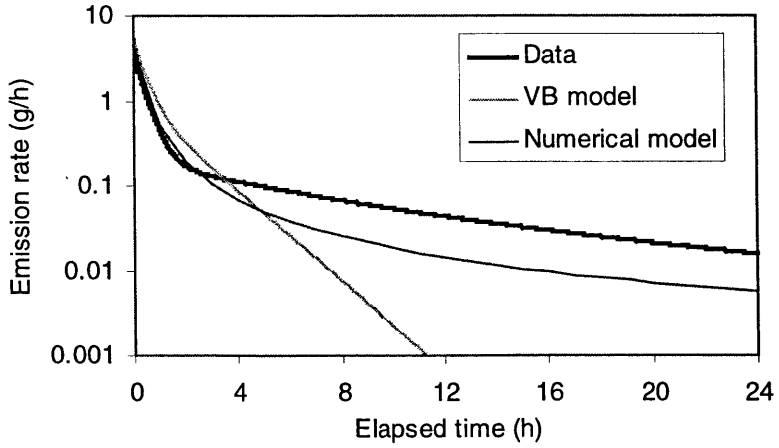

(c)

Figure 3.18 Comparison of measured and simulated TVOC emission rates of wood stain under different temperatures: (a) 20.5 °C, (b) 27.5 °C, (c) 31.5 °C.

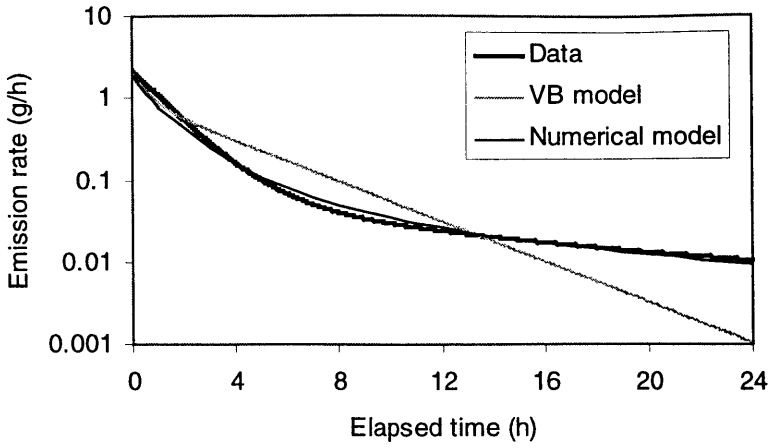

(a)

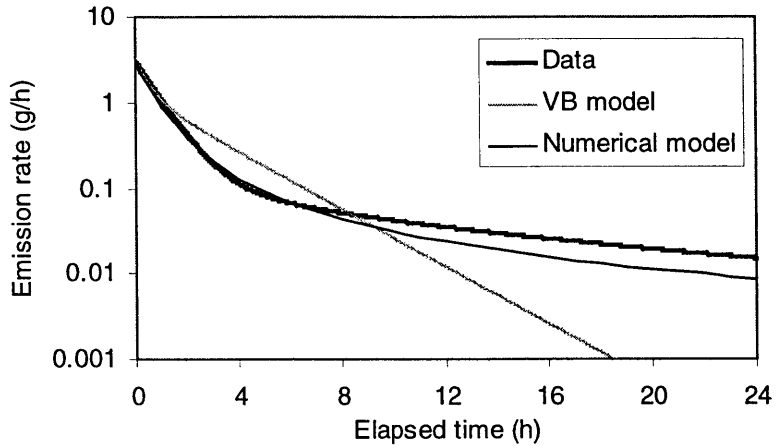

(b)

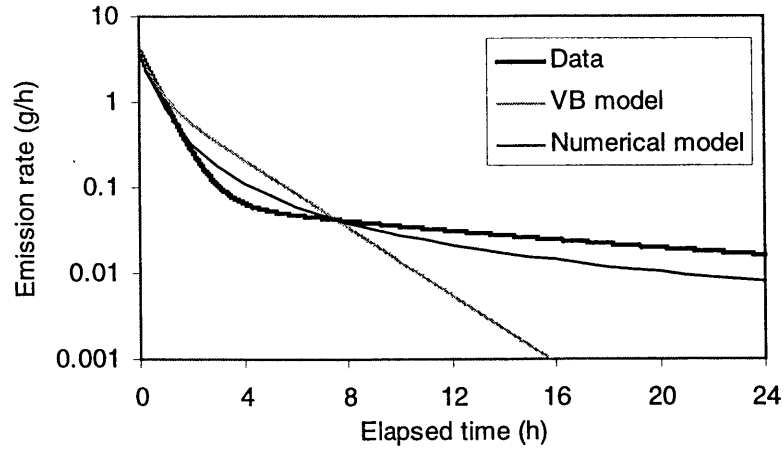

(c)

Figure 3.19 Comparison of measured and simulated emission rates of decane under different temperatures: (a) 20.5 °C, (b) 27.5 °C, (c) 31.5 °C.

3.6.3.1 Airflow distributions

The configuration of the full-scale chamber and the emission measurements using the full-scale chamber for wood stain and decane have been discussed in Chapter 2. Figure 3.20 shows the simulated air flow patterns in one section of the full-scale chamber for 5 ACH using the RNG k-ε model, and Figures 3.21(a) and 3.21(b) respectively present, the measured and computed velocity and velocity fluctuation in several locations in the section. The computed velocity fluctuation was defined as $\sqrt{2k/3}$, where k is the turbulent kinetic energy. The measurements were done with seven poles, each pole carried eight hot-sphere anemometer sensors. In addition, an automatic traversal system that carried a fast-response hot-wire anemometer was also used to measure the velocity and velocity fluctuation distributions in the same locations. To obtain the correct velocity boundary condition at the inlet diffuser, we used a calibrated hand-held velocimeter to measure the velocity distributions and used the measured data as the boundary condition for flow simulation. Figure 3.22 shows the measured inlet boundary condition for the case with ACH = 5. The height of the inlet slot was adjusted as 0.00875 m, 0.015 m, and 0.025 m for ACH = 1, 5, and 9, respectively, to obtain a reasonable supply velocity and mixing.

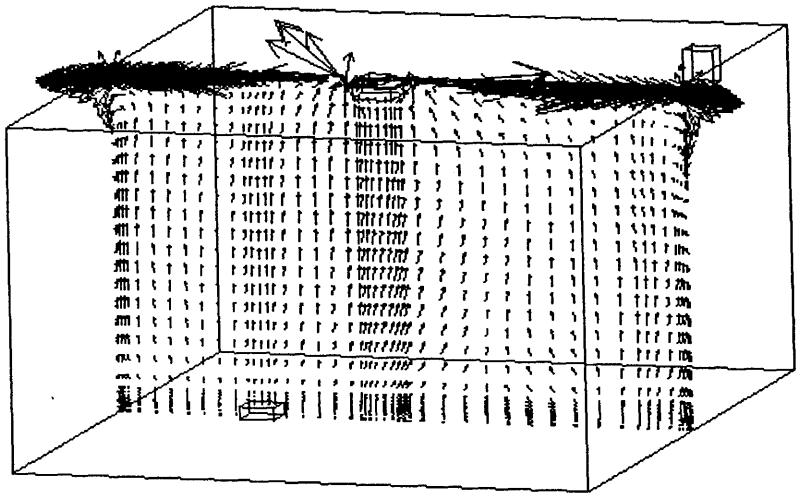

Figure 3.20 Simulated velocity vectors in one section in the full-scale chamber.

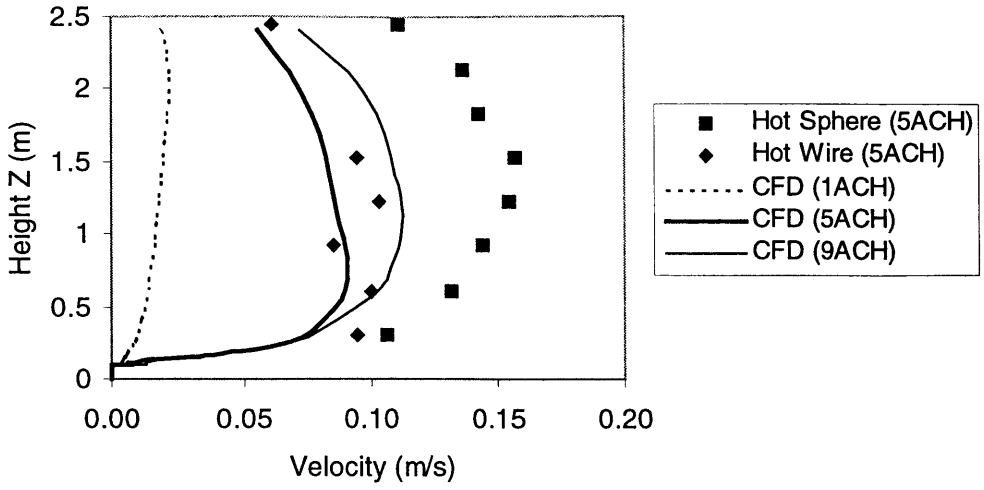

(a)

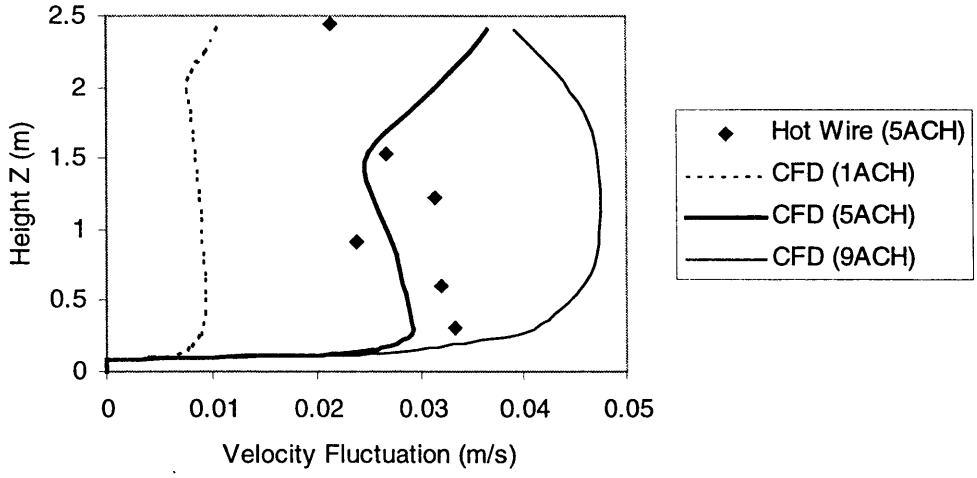

(b)

Figure 3.21 Measured and simulated airflow distributions above the material in the full-scale chamber: (a) velocity, (b) velocity fluctuation.

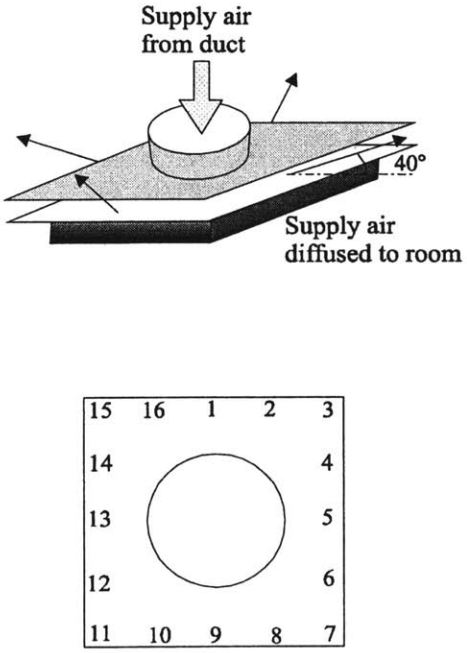

Measured points (top view)

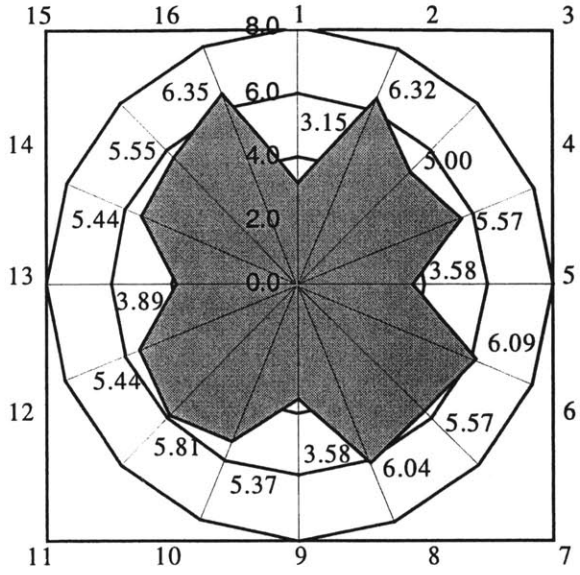

Velocity distribution
around the diffuser (m/s)

Figure 3.22 Measured inlet flow boundary condition in the full-scale chamber with 5 ACH.

Figure 3.21 shows that in the full-scale chamber, a larger ventilation rate created larger local velocity and turbulence distributions near the test material. The small-scale chamber had a maximum velocity similar to the full-scale chamber with 9 ACH but with a different turbulence level, *i.e.*, laminar flow in the small-scale chamber but turbulent flow in the full-scale chamber. Because the local flow characteristics in the small-scale chamber and in the full-scale chamber (with different ventilation rates) were different, experimental results from Chapter 2 show that the resulting emissions were also different.

There are discrepancies between the computed velocity, the velocity fluctuation distributions and the measured data. Note even the measured velocities using the hot-sphere and hot-wire anemometers do not always agree. This is because the velocity in most of the space is small (< 0.2 m/s) except near the diffusers. The hot-sphere or hot-wire anemometers may fail to provide accurate results in such low velocities. The numerical simulation may also have errors especially for such complicated inlet boundary conditions. Nevertheless, the general trend of the simulated distributions of velocity and velocity fluctuation above the test material (substrate) follows those of the measured data.

After validating the air distributions, the following section presents the results of the VOC emission rates in the full-scale chamber.

3.6.3.2 VOC emission rates

Figure 3.23 compares the simulated VOC emission rates from the wood stain with the measured data for 5 ACH in the full-scale chamber (Case2-2b). Comparison of the wood stain emissions at other ventilation rates (1 ACH, 9 ACH) between the simulated and measured results, shows the similar trends. Again, the numerical model performed better than the VB model especially during the diffusion-controlled period. The full-scale chamber simulation used the same material property data obtained from the small-scale chamber. The relatively large discrepancy during 0.25 - 7 hours may be attributed to the simulation error caused from inaccurate estimation of material properties, and the simulation error of velocity and turbulence distributions. In addition, the electronic balance also experienced fluctuations due to the turbulent flow and moisture fluctuation in the full-scale chamber, so the measured weight decay data could also have some error. Taking these combined factors into consideration, the simulated emission rates agreed reasonably with the measured data.

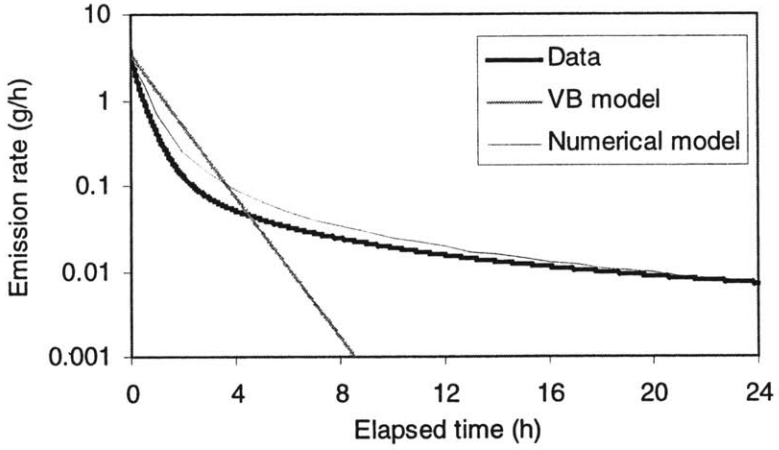

Figure 3.23 Comparison of measured and simulated TVOC emission rates of wood stain in the full-scale chamber (5 ACH).

Figure 3.24 further compares the simulated and measured TVOC distributions (using both the Brul&Kjar multi-gas monitor and GC/FID) at several locations (the exhaust, a corner, and the center) in the full-scale chamber for Case2-2b. Note that although the ventilation system of the chamber was operated in full-exhaust mode, VOC concentrations still did not reach zero at the inlet air. The TVOC data shown in the figure was obtained by subtracting the inlet concentration measured at the corresponding time from the measured data at different locations in the chamber. In general, the concentrations simulated by the numerical model agree with the measured data. The relatively large discrepancy noted during 0.25 - 7 hours again reflects the simulation error of the emission rates by the numerical model. Further, results from the simulation and measurements show that the concentrations measured at these three locations are close to each other, indicating a relatively good mixing of VOC in the chamber.

(a) Exhaust
(b) Corner (x = y = z = 0.3 m)
(c) Center (x = 2 m, y = 1.4 m, z = 2.5 m)

The above results indicate that the numerical model is suitable for predicting "wet" material emissions in both small-scale (laminar flow) and full-scale (turbulent flow) chambers. The emission characteristics of a "wet" material will change when the environmental conditions change. The model can address the effects of the environmental conditions (velocity, turbulence, etc.) on emissions provided that the material properties are known. With the property data, the numerical model can be used to study "wet" material emissions in actual building environments based solely on the data from inexpensive small-scale chamber tests.

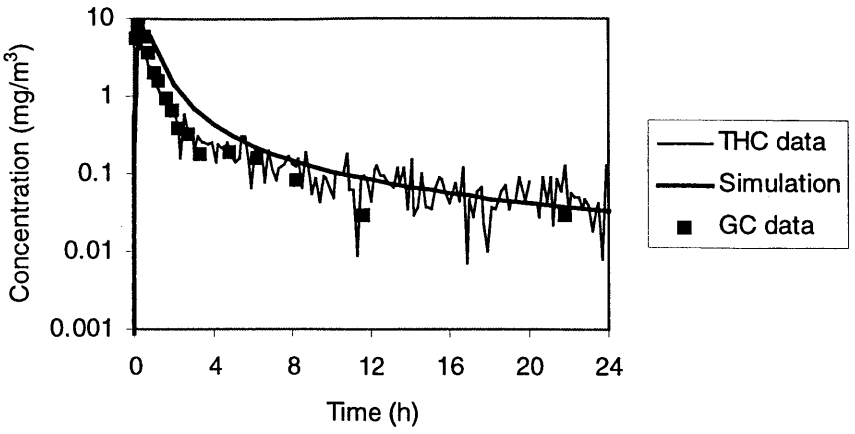

(a)

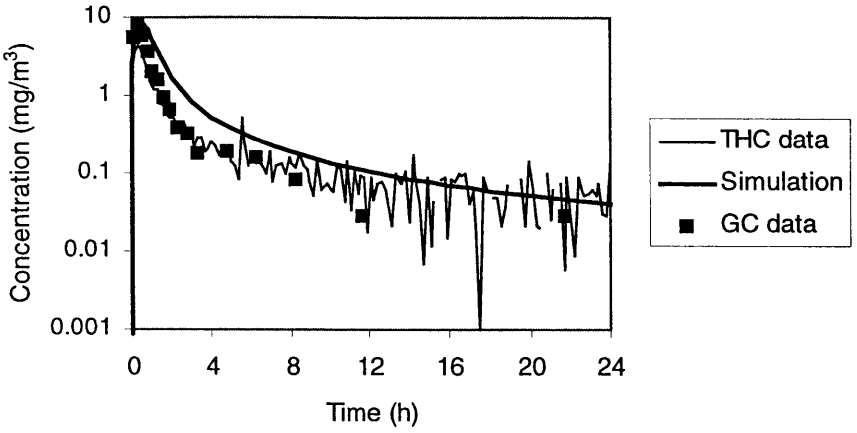

(b)

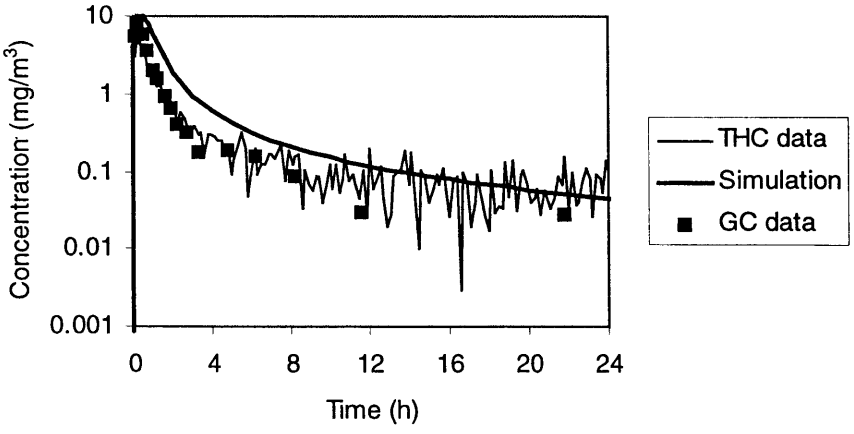

(c)

Figure 2.24 Comparison of the measured and simulated TVOC concentration distributions at different locations in the full-scale chamber. See Figure 2.3 in Chapter 2 for the locations: (a) at the exhaust, (b) at the corner, (c) at the room center

3.6.4 Effects of air velocity, film thickness, temperature, and sample application time on "wet" material emissions

The results of the experimental measurements given in Chapter 2 have demonstrated the influencing factors on "wet" material emissions. However, some of the results actually reflect the effects of multiple factors, instead of one single factor, on emissions. The problem arises because in the experiments we usually could not control many factors to their "idealized" conditions. An example is that when we intend to measure the effect of temperature on emissions, ideally all the factors except for temperature should be unchanged between different experiments. This however is very difficult to achieve because it's hard to maintain consistency with some factors, such as sample application time and film thickness between different experiments. If the emissions are also sensitive to these factors, the actual temperature effect may be masked and the results could be misleading. Hence, it is important to reveal the relative importance of each single factor on "wet" material emissions.

The following sections discuss the effects of air velocity, film thickness, temperature, and sample application time on "wet" material emissions.

3.6.4.1 Impact of air velocity on emissions

In Chapter 2, we have measured the VOC emissions of "wet" materials under different flow conditions. The measured results actually reflect the combined effects of air velocity, turbulence, flow direction, and VOC concentrations on emissions. This section examines the effect of a single factor – air velocity on "wet" material emissions. To do this, a series of numerical simulations have been conducted in which all the parameters were kept the same as the reference case (Case1-2b) except the air velocity above the source. The range of the air velocity studied was 0.15 m/s to 0.5 m/s; the results are presented in Figure 3.25.

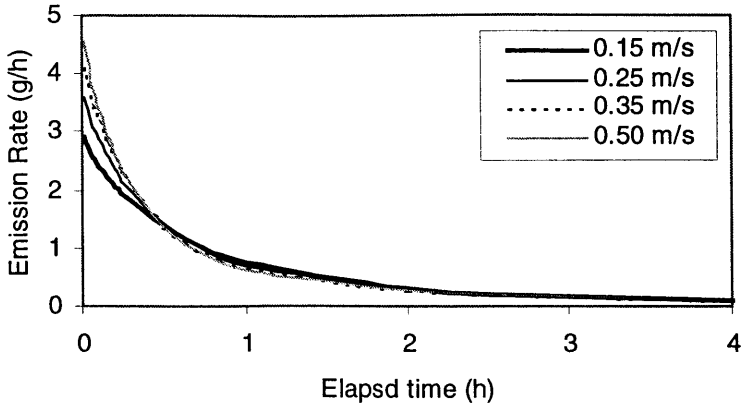

(a)

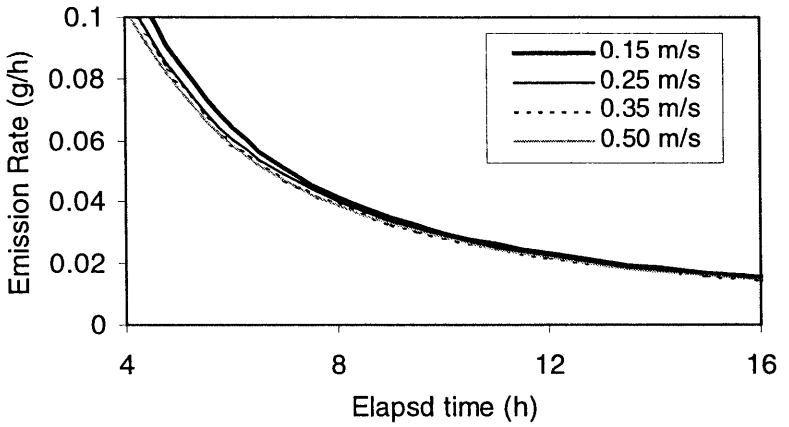

(b)

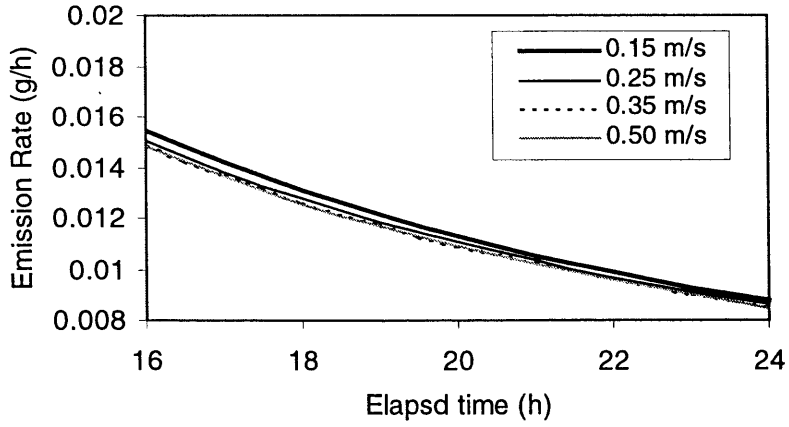

(c)

Figure 3.25 Simulated TVOC emission rates from wood stain under four different velocities: (a) 0 – 4 hour, (b) 4 – 16 hour, (c) 16 – 24 hour.

The above results indicate that at the beginning (0 – 2 h), cases with higher air velocity emit faster but also decay faster. This agrees with the findings obtained in Chapter 2. Greater air velocity will generate a larger mass transfer coefficient and thus higher initial emission rates. However, simulation results show that the impact of air velocity becomes small when $\tau > 8$ h. This is due to the fact that from about the 8th hour point, internal diffusion begins to dominate the interfacial mass transfer rendering air velocity less influential.

Since air velocity affects emissions through the air phase boundary layer, its effect on the gas phase mass transfer coefficient was studied next. The mass transfer coefficient, h_c (m/h), can be calculated based on the local VOC emission rate R (mg/m^{2}h) and the difference in the overall VOC concentration between the material surface, C_s (mg/m^3), and the air in the bulk flow, C_∞ (mg/m^3), via:

$$h_c=R/(C_s - C_\infty) \tag{3.57}$$

The h_c may also be expressed by a dimensionless Sherwood number, Sh:

$$Sh=h_cL/(3600D_a) \tag{3.58}$$

where L is the characteristic length of the source (m) and D the molecular diffusion coefficient of VOC (m^2/s). Sparks *et al.* (1996) suggested the use of the square root of the source area as the characteristic length. Since the airflow is unidirectional in the inner chamber, it is more appropriate to use the length of emission source in the present study.

The results show that for each given velocity, the h_c does not change with time. The h_c calculated were 4.02, 5.11, 5.87, and 6.65 (m/h) for velocities of 0.15, 0.25, 0.35, and 0.50 m/s, respectively.

Correlations are available to relate the Sherwood number, Sh, with the Reynolds number, Re_L, and the Schmidt number, Sc. For VOC species transfer over a flat plate, Sparks *et al.* (1996) obtained the following formula based on the data from chambers and a test house with constant synthetic stain and moth cakes:

$$Sh=0.28Re_L^{0.65}Sc^{0.333} \tag{3.59}$$

where L is used as the characteristic length for Re_L:

$$Re_L=VL\rho/\mu \tag{3.60}$$

Axley (1991) suggested the following correlations by using the heat and mass transfer analogy:

$$Sh=0.664Re_L^{0.5}Sc^{0.333} \quad \text{for } Re_L < 500{,}000 \tag{3.61}$$

$$Sh=0.037Re_L^{0.8}Sc^{0.333} \quad \text{for } Re_L > 500{,}000 \tag{3.62}$$

For the cases studied, the Sh for TVOC calculated by Eqs. (3.59) and (3.61) and those by numerical simulation are shown in Figure 3.26. The results indicate that the mass transfer coefficient obtained by numerical simulation was very close to that of Eq. (3.61), but was considerably lower than Sparks's result with Eq. (3.59). One possible reason is that Eq. (3.59) was not developed with a controlled, parallel flow over the material surface. Hence, the correlation may not apply to the small-scale chamber used.

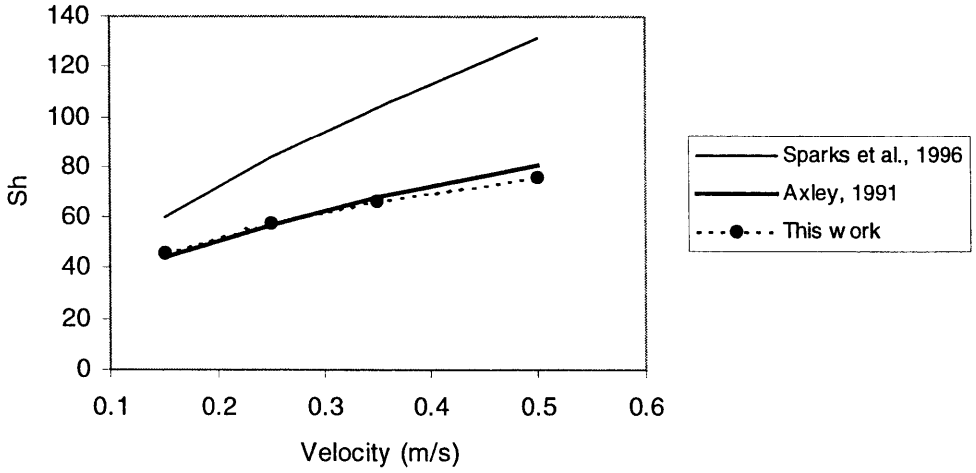

Figure 3.26 Predicted Sh in the small-scale chamber under different velocities.

3.6.4.2 Impact of film thickness on emissions

The effect of film thickness on the emission rates has not received as much attention as air velocity, but preliminary observations indicate that it could be as important as air velocity (Guo *et al.*, 1996b). Understanding the impact of film thickness on emissions is critical for both the emission measurements and study of material emissions in buildings.

To investigate the potential effect of film thickness, we conducted two additional numerical simulations of wood stain emissions. In the simulations, different film thickness were achieved by assuming various applied masses of wood stain. The nominal film thickness of the reference case (Case 1-2b) is 1.2238×10^{-4} m, calculated based on the applied mass (4.5162 g), density of the wood stain (818 kg/m^3), applied area (0.06 m^2), and the liquid expansion factor (1.33). Two more cases, one with a film thickness of 1.1014×10^{-4} m (10% lower than that of the reference case), and the other case with a film thickness of 1.3462×10^{-4} m (10% higher than that of the reference case) will be simulated.

Figure 3.27 gives the simulated emission rates for the above three cases. The results indicate that all these cases had approximately the same emission rates during the first hour. After that, the emission rates began to deviate. Cases with larger film thickness had higher emission rates and also slower decay rates than cases with smaller film thickness. The difference tends to be more pronounced as time goes on. A change of 10% in film thickness may also result in a change of approximately 10% in emission rate at τ = 24 hours. This indicates that the film thickness does not influence the early stage emissions but will affect the long-term emission profiles. This may be explained by two factors. First, for a "wet" material, the emission rates during the initial period are mainly dominated by evaporation. Hence, the film thickness is immaterial. As time goes on, a thinner film depletes faster, resulting in smaller concentrations in both the material phase and the material-air interface. The emission rates for smaller film thickness will thus be smaller.

The above results indicate that when comparative experiments are conducted to identify the impact of a specific factor on emissions, the film thickness must be controlled within a very small range, 5 - 10%, in order to obtain repeatable and comparable results.

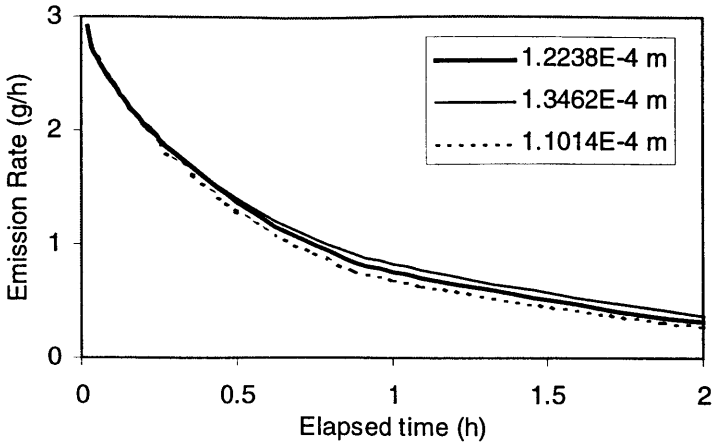

(a)

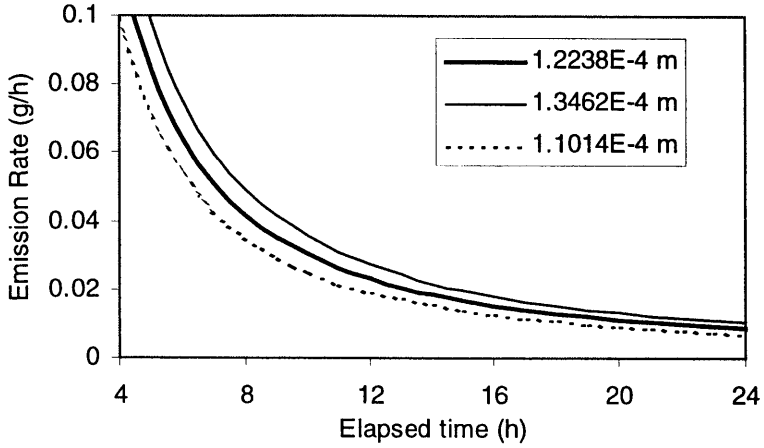

(b)

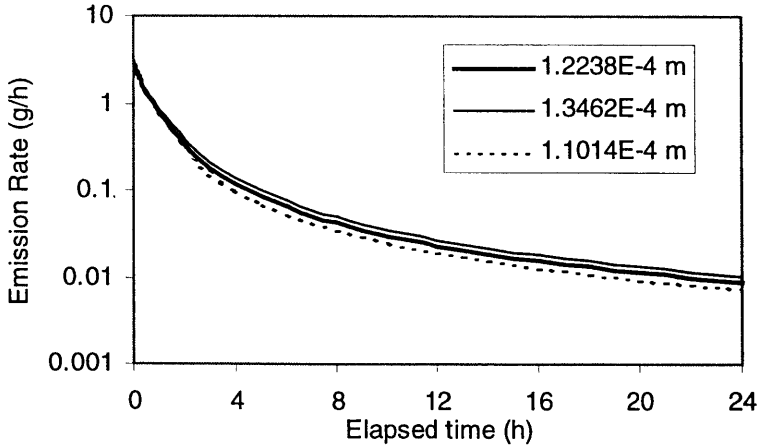

(c)

Figure 3.27 Predicted emission rates in the small-scale chamber under different film thickness: (a) 0 - 2 hour, (b) 4 - 24 hour, (c) 0 – 24 hour.

3.6.4.3 Impact of temperature on emissions

The impact of temperature on emissions has been measured using the small-scale chamber (Chapter 2). However, due to the difficulty in accurately controlling the amount of wood stain applied, the measurement was not conducted with the same film thickness. Further, the measurements may be subject to measurement errors especially during the diffusion dominant periods. Thus, it is necessary to evaluate the temperature effect again by using the same film thickness.

Figure 3.28 presents simulated emissions from the wood stain for the four different temperatures, 20.5 °C, 23.5 °C, 27.5 °C, and 31.5 °C. Other conditions including the film thickness were the same as the reference case (Case1-2b). The results show that temperature can affect the emissions throughout the 24-hour period. In the initial (evaporation dominant) period, the simulated temperature effect agrees with that concluded based on the small-scale chamber measurements in Chapter 2. However, simulations show that smaller emissions result with higher temperature during the diffusion-dominant period, which was not clearly measured by our experiments.

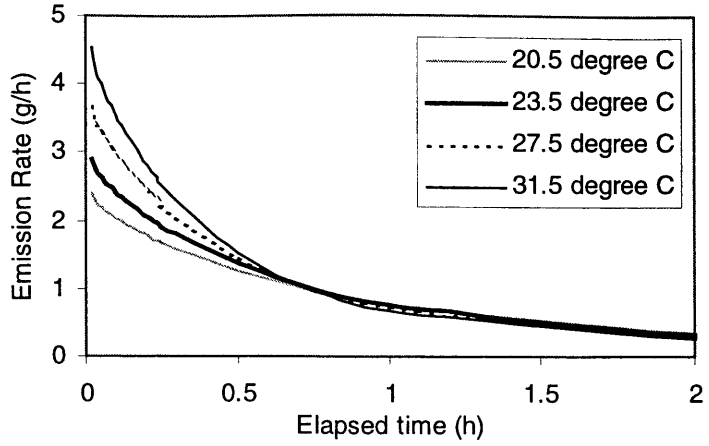

(a)

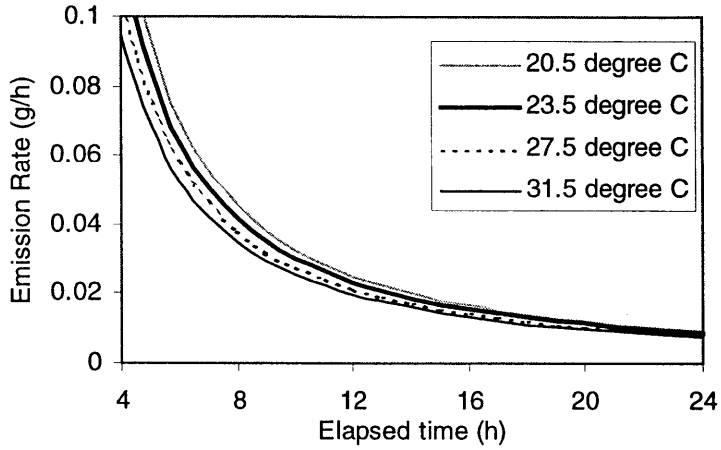

(b)

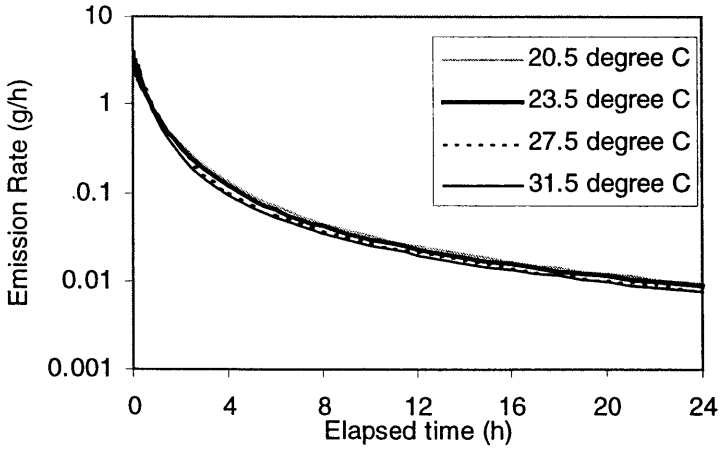

(c)

Figure 3.28 Predicted emission rates in the small-scale chamber under different temperatures: (a) 0 - 2 hour, (b) 4 - 24 hour, (c) 0 – 24 hour.

3.6.4.4 Impact of sample application time on emissions

When an indoor coating material is tested in a chamber, it must be applied to an appropriate substrate before the testing. This procedure usually takes several minutes, sometimes longer. If the source is highly evaporative, losses of volatile components during the application could cause errors in the estimation of the emission rates.

In order to determine the impact of the sample application time on the emission measurements, computer simulations were performed for the wood stain reference case. Since the emission process during the sample application can be very complicated, an accurate simulation of such a process is very difficult. To demonstrate the approach, the "wet" material emissions during the application time were simulated by assuming the material was in the small-scale chamber ($v = 0.15$ m/s above the material). A numerical simulation was conducted for that period. The concentration distributions in the material film (which was not uniform) were then used as the initial conditions for a new simulation. Results of the new simulation give the emissions by considering the VOC loss during the application period.

Figure 3.29 demonstrates the simulated TVOC emission rates for these three application times and an idealized zero application time (that is, uniform initial concentration in the material film). The results show that potential loss of VOCs during sample preparation significantly affects emissions during the early phase. A longer application time yields smaller early-stage emission rates. The application time, on the other hand, has virtually no impact for $\tau > 3$ hours. Considering the importance of early-stage emissions for highly evaporative coating material such as wood stain, the application period should be kept as short as possible in order to obtain good repeatability and reproducibility (current standards use 2 - 3 minutes).

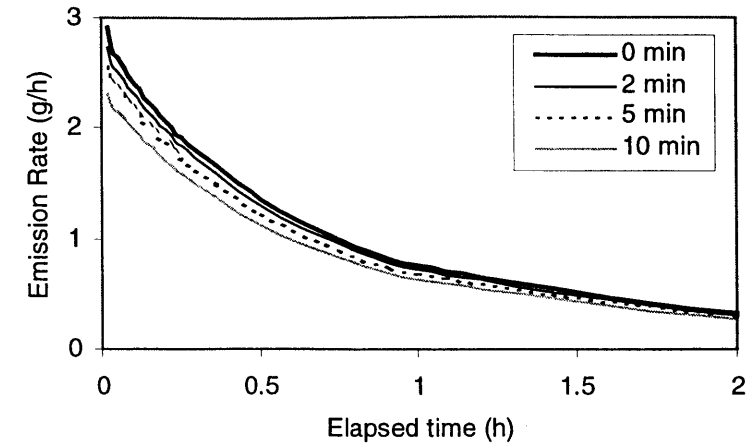

(a)

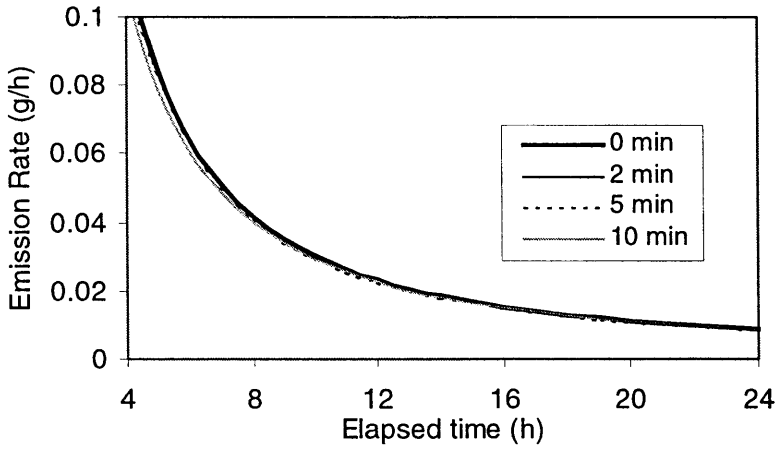

(b)

Figure 3.29 Predicted emission rates in the small-scale chamber with different sample application times: (a) 0 - 2 hour, (b) 4 - 24 hour.

Before concluding, it should be mentioned that the emphasis in this chapter is on developing a complete mass transfer model to obtain parameters based on minimum experimental data. The general approach, though, was based on a relatively simple scenario of "wet" material emissions, and can be extended to consider more complicated situations in the future research.

3.7 Conclusions

A numerical model using computational fluid dynamics (CFD) has been developed to simulate the VOC emissions from "wet" coating materials. The model is different from other existing emission models in that it is based on the VOC mass transfer of the entire "wet" material-substrate system. The system includes four layers: air, material-air interface, material film, and the substrate. The model is a detailed prediction tool to account for the interaction of different mechanisms, such as internal diffusion and evaporation, and their impact on emissions. It can also be used to quantitatively evaluate the effects of a single factor, such as air velocity and sample application time on emissions. The use of the model could also significantly reduce the need of chamber measurements, which are expensive, time consuming, and may be subject to measurement errors. The use of the numerical model leads to the following conclusions:

(1) The numerical simulations have confirmed that the emissions from the "wet" materials applied to an absorptive substrate are dominated by evaporation at the beginning and internal diffusion afterwards, which had been hypothesized based on previous experimental data.

(2) The use of the numerical model requires material properties such as VOC diffusivities in the material film and the substrate. The current study used small-scale chamber data to obtain these properties. With these property values, the numerical model can be used to study "wet" material emissions in actual building environments. The numerical model has been validated in a full-scale environmental chamber.

(3) By using the numerical model that we developed, the effects of air velocity, film thickness, temperature, and sample application time on "wet" material emissions have been investigated independently. For the wood stain studied, simulation results indicate that air velocity and sample application time only significantly affect the emission profiles in the early stage (0 - 4 hours). Film thickness, on the other hand, affects long-term ($\tau > 0.2$ h) emissions. Temperature can affect both the short-term and long-term emissions. In order to obtain repeatable and reproducible measurements, all these parameters must be well controlled.

Chapter 4

Modeling of VOC Emissions from Dry Materials

This chapter presents two models for simulating VOC emissions from dry materials. One is a numerical model using the Computational Fluid Dynamics (CFD) technique for short-term predictions, the other is an analytical model for long-term predictions. The models were used to examine the VOC emissions from two particleboards and a polypropene Styrene-Butadiene Rubber (SBR) bitumen-backed carpet. The emission study for the particleboards shows that a fairly good agreement of VOC concentrations between the model prediction and experimental data can be achieved by pre-calculating the partition coefficient (K_{ma}) and material age (AGE) and adjusting the diffusion coefficient (D_m) and initial concentration (C_0). Further, the study finds that K_{ma} only affects short-term emissions while D_m influences both the short-term and long-term emissions. The short-term predictions of the carpet show that the VOC emissions under different temperatures can be modeled solely by changing the carpet diffusion coefficients. A formulation of the Arrhenius relation was used to correlate the dependence of the carpet diffusion coefficient with temperature. The long-term predictions of the carpet show that it would take several years to bake out the VOCs, and temperature would have a major impact on the bake-out time.

4.1 Introduction

Numerous field and laboratory studies have found that commonly used dry materials such as wood products, floor coverings (carpet, vinyl), wall coverings (wallpaper, fabric), ceiling materials (acoustic tiles, subfloors), and insulation materials (fiberglass, rigid foam) emit a variety of VOCs. Emissions from dry materials are important to indoor air quality because of their large surface area and permanent exposure to indoor air. Therefore, they should be studied and rated so that only those with low emission rates are used in buildings.

In the past, VOC emissions from several hundred types of dry materials have been tested. These have been done mainly for screening purposes, *i.e.*, identifying the major VOCs emitted from a particular source and its time-varying emission dynamics. A majority of the tests use a small-scale test chamber under controlled environmental conditions (*e.g.*, 23 °C temperature, 50% relative humidity, and 1 air exchange per hour). A large body of measurement results can be found in the literature, and recently, have been included in the emission database of indoor materials (EC, 1997; NRC, 1999).

In addition to screening materials, the measurements should also:

(1) facilitate material ranking. Industries use the emission data to rank a material as a high, medium, or low emission source. This information can be given to material manufacturers for improving their products as well as to building designers to select the least toxic or non-toxic materials.

(2) help us understand emission characteristics. Contrary to "wet" materials, the emission rates of dry materials are usually small and decay slowly. This means that their emissions can last much longer than "wet" materials. The data would also help us to better understand emission mechanisms (*e.g.*, diffusion-controlled instead of evaporation-controlled).

(3) provide data for indoor air quality studies. Because limiting all the materials to zero- or low-emissions is either impractical or quite expensive, information on how to transfer the data from an environmental chamber to buildings is needed for indoor environment design.

The first two objectives can be easily achieved. The last one, however, cannot be inferred directly from the measured data due to the following two reasons:

(1) To obtain useful emission data for dry material, the test period must be sufficiently long. The real measurements cannot cover the entire emission life of a material. Material emissions beyond the period of measurement remain unknown.

(2) A chamber test usually measures a material sample. While in buildings, both the geometry (*e.g.*, the thickness of the material) and boundary conditions may be different from the test sample. Further, the environmental conditions in buildings may not be the same as those in a test chamber. Even though airflow may have a negligible effect, the diffusion process may be significantly affected by other factors, such as temperature. Hence, the measured data from an environmental chamber may not be valid in buildings.

Appropriate emission models are needed to solve the above problems. Existing models, as indicated in Chapter 1, are usually inadequate due to their limitations. This chapter first applies a similar approach to the numerical model developed in Chapter 3 to developing a comprehensive mass transfer model without neglecting the mechanisms affecting dry material emissions. The model is a general one that applies to broad purposes, from obtaining useful material properties based on environmental chamber test data to studying material emissions in buildings. Next, a simplified model that can quickly evaluate the emission behavior of dry materials is also developed.

Section 4.2 presents the numerical model that uses the CFD technique for short-term predictions, and section 4.3 discusses an analytical model for long-term emissions.

4.2 The Numerical Method for Short-term Predictions

Chapter 3 presented a numerical model using CFD that can simultaneously consider several major mechanisms associated with the VOC mass transfer process. The model can also deal with complicated initial and boundary conditions and physically address the effect of environmental parameters on emissions. Using the same assumptions for "wet"

materials given in Section 3.3, the following section provides the mathematical model for emissions from dry materials.

4.2.1 The mathematical model

Similar to a "wet" material, the VOC emission process from a dry source also involves mass transfer in three different regions:

- The bulk air
- The material-air interface
- The solid material

For a dry material, the VOC governing equations for the material-air interface and air phase remain the same as those for "wet' materials. The VOC diffusion inside the material is governed by:

$$\frac{\partial C_m}{\partial \tau} = \frac{\partial}{\partial x_j}(D_m \frac{\partial C_m}{\partial x_j}) \tag{4.1}$$

where:

C_m = VOC concentration in the solid material, $\mu g/m^3$

τ = time, sec

x_j = coordinates (j = 1,2,3)

D_m = diffusion coefficient of the VOC in the solid material, m^2/s

Here, the dependence of D_m on the VOC concentration is neglected. This is based on the fact that VOC concentrations in a dry source are usually very small (*e.g.*, the ratio of the initial VOC concentration to the material density is much less than the threshold 1%, as suggested by Schwope *et al.* (1989)). The dependence of D_m on temperature is again assumed to follow an Arrhenius type (Jost, 1960):

$$D_m = D_{m,0} \exp(-\frac{E_d}{RT}) \tag{4.2}$$

For a composite material composed of two or more layers of homogeneous materials, applying Eq. (4.1) to each layer yields:

$$\frac{\partial C_{s,i}}{\partial \tau} = \frac{\partial}{\partial x_j}(D_{s,i} \frac{\partial C_{s,i}}{\partial x_j}) \tag{4.3}$$

where i represents the i^{th} layer of the composite material. At the interface between the two layers, the VOC mass balance and the concentrations on the two sides take the form:

$$-D_{s,i}\frac{\partial C_{s,i}}{\partial x_j}=-D_{s,k}\frac{\partial C_{s,k}}{\partial x_j} \tag{4.4}$$

$$C_{s,i}=K_{ik}C_{s,k} \tag{4.5}$$

where i and k are two adjacent materials.

In addition to the above equations, appropriate boundary conditions are also needed. Although the boundary conditions for different problems vary, the four types of common boundary conditions of friction and VOC are inlet, outlet, walls, and axis of symmetry.

(a) Inlet

Air velocity (V) and compound concentration (C) are specified for the air supply inlet as:

$$\begin{aligned} V&=V_{supply}\\ C&=C_0 \end{aligned} \tag{4.6}$$

where V_{supply} is air velocity at the supply inlet, and C_0 the inlet concentration (usually 0).

(b) Outlet

A pressure is given and zero gradient of compound concentration in the direction normal to the return outlet:

$$\begin{aligned} P&=P_{return}\\ \frac{\partial C}{\partial x_j}&=0 \end{aligned} \tag{4.7}$$

where P_{return} is the pressure at the return outlet and x_j is the coordinate normal to the outlet.

(c) Walls

Walls include solid walls of a test chamber (or room) and surfaces of the emission material. If V_i is air velocity parallel to a wall and x_j is the coordinate normal to the wall surface, the shear stress τ_w at a wall is expressed by:

$$\tau_w=-\mu\frac{\partial V_i}{\partial x_j} \tag{4.8}$$

The boundary condition for concentration at the emitting material surface is:

$$-D_m \frac{\partial C}{\partial x_j} = -D_a \frac{\partial C}{\partial x_j} \tag{4.9}$$

and at other non-emitting surfaces:

$$\frac{\partial C}{\partial x_j} = 0 \tag{4.10}$$

(d) Axis of symmetry

At the axis of symmetry, we have:

$$\frac{\partial C}{\partial x_j} = 0$$
$$\frac{\partial V_i}{\partial x_j} = 0 \tag{4.11}$$

where V_i is the air velocity perpendicular to the axis of symmetry, x_j.

The initial conditions for VOC are given as follows. In the air, the initial compound concentration is zero. In the solid material, we consider two different types of initial conditions:

$C = C_0$ for a new material: (4.12)

$C = C_0 F(x_j, AGE)$ for an aged material: (4.13)

where:

C_0 = initial concentration of compound in the solid slab, $\mu g/m^3$
AGE = age of the material, day
$F(x_j, AGE)$ = function used to describe the initial concentration profile in the solid

Similar to modeling emissions from "wet" materials, the key to using the mathematical model for a dry material is to first obtain the physical properties of the material. These properties are a) the diffusion coefficient, D_m, b) the partition coefficient, K_{ma}, and c) the initial concentration, C_0. If the material is not totally new, the age of the material, AGE, is also needed. AGE specifies the initial condition of a dry material. AGE = 0 means a uniform initial concentration in the material while a non-zero AGE indicates a non-uniform initial concentration. Once these parameters are determined, they can be used to

study the emissions under different environmental and boundary conditions (*e.g.*, in a building).

Before discussing the methods for obtaining the material properties, it is important to understand the influences of these key parameters on emissions from a dry source. The following section examines such influences.

4.2.2 The influence of C_0, D_m, K_{ma}, and AGE on dry material emissions

In this section, we present results using an example to study the sensitivity of dry material emissions to C_0, D_m, K_{ma}, and AGE.

A dry material with a dimension of $0.212 \times 0.212 \times 0.0159$ m^3 is placed in a small chamber of $0.5 \times 0.4 \times 0.25$ m^3, as shown in Figure 4.1. The chamber is ventilated by 1 ACH and the inlet concentration is 0. The only emitting area from the dry material is from the top surface (0.212×0.212 m^2), and the other faces of the material are well sealed. The physical properties of the material as a reference case are given as follows:

- $C_0 = 5.28 \times 10^7$ $\mu g/m^3$
- $D_m = 7.65 \times 10^{-11}$ m^2/s
- $K_{ma} = 3289$
- AGE = 0

The above parameters were obtained from those of a particleboard that is examined later in section 4.2.4. This section will examine the influence of each individual parameter (all the other parameters remain the same as those of the reference case) on the resulting VOC concentration at the chamber exhaust.

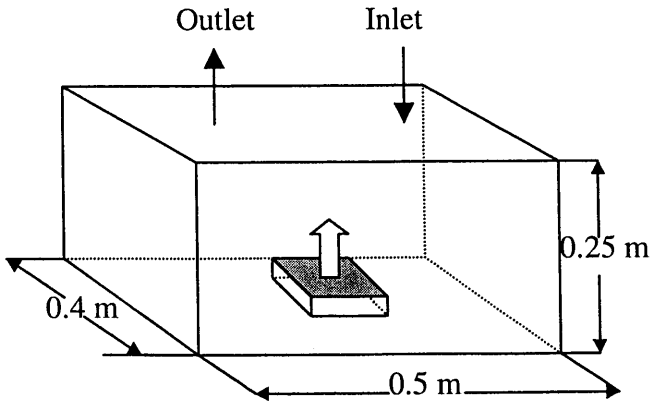

Figure 4.1 A small-scale chamber for measuring dry material emissions.

4.2.2.1 The influence of C_0

The mathematical model (Eqs. (4.1) - (4.13)) indicates that the VOC concentration in the chamber air depends linearly on the C_0. This can be confirmed by the results given in Figure 4.2. The figure shows that when C_0 increases from 5.28×10^7 $\mu g/m^3$ to 1.056×10^8 $\mu g/m^3$ (D_m, K_{ma}, and AGE remain the same as those in the reference case), the concentration also increases by a factor of 2.

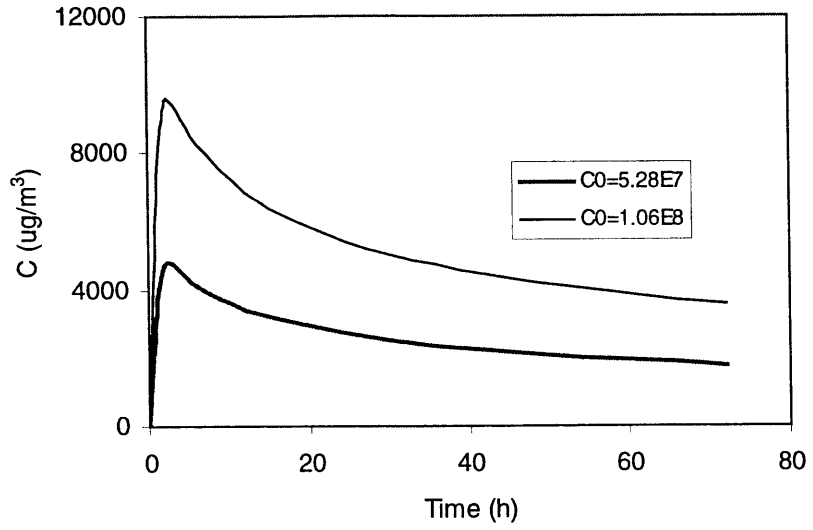

Figure 4.2 The influence of the initial concentration of the source on the resulting VOC concentration in the chamber air. The curve is predicted with the diffusion coefficient D_m = 7.65×10^{-11} m^2/s, partition coefficient K_{ma} = 3289, and material age AGE = 0.

4.2.2.2 The influence of D_m

Figure 4.3 illustrates the effect of D_m on the chamber concentration with time for a constant C_0 of 5.28×10^7 and K_{ma} of 3289 (AGE = 0). The values of D_m vary between 10^{-12} m^2/s and 10^{-10} m^2/s. Results show that D_m significantly influences both the peak concentration and the decay rate of the concentration curve. A higher D_m results in a higher peak concentration and a faster decay rate.

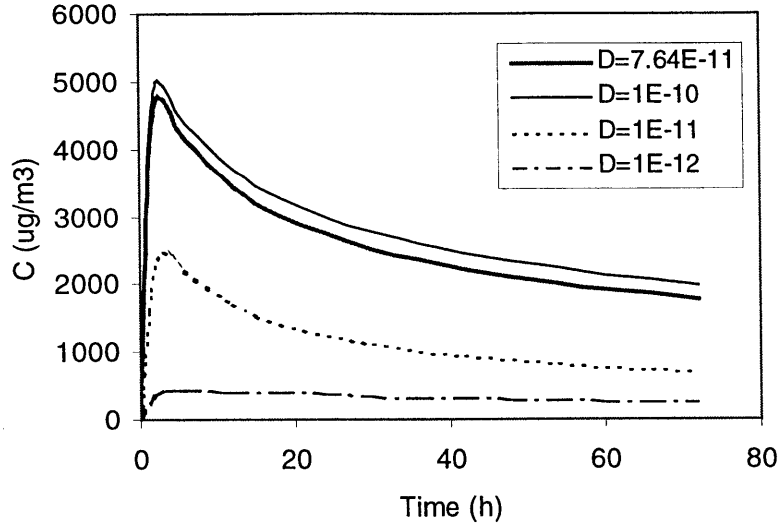

Figure 4.3 The influence of diffusion coefficient on the resulting VOC concentration in the chamber air. The curve is predicted with the initial concentration C_0 = 5.28×10^7 $\mu g/m^3$, partition coefficient K_{ma} = 3289, and material age AGE = 0.

4.2.2.3 The influence of K_{ma}

Figure 4.4 shows the effect of K_{ma} on the chamber concentration with time for a constant C_0 of 5.28×10^7 and D_m of 7.65×10^{-11}(AGE = 0). The values of K_{ma} vary between 1 and 10,000.

Simulation results show that the influence of K_{ma} is two-fold. First, increasing the K_{ma} decreases the emission rate at early times and results in a slower depletion rate of the source. However, the influence of a change in K_{ma} is virtually insignificant below a value of about 1,000. On the other hand, it was observed that although the initial emission and depletion rates vary significantly for different K_{ma}, the chamber concentration after some time is almost identical. This suggests that for a dry source with small diffusivity, K_{ma} may only affect early-stage emissions.

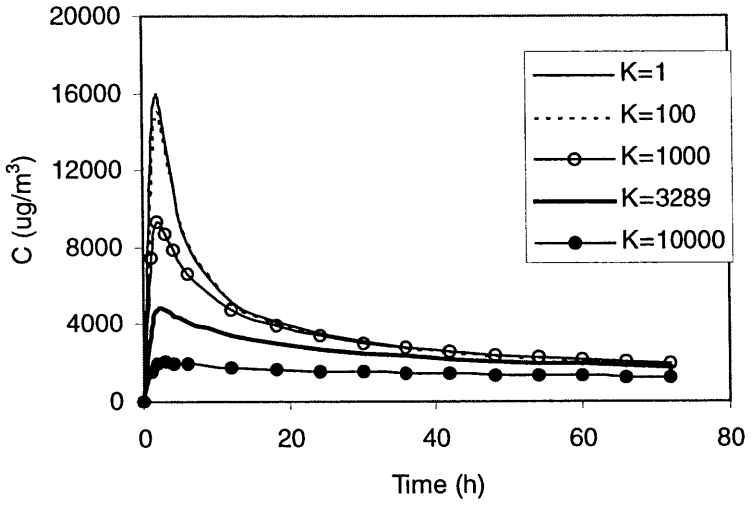

Figure 4.4 The influence of the material-air partition coefficient on the resulting VOC concentration in the chamber air. The curve is predicted with the diffusion coefficient D_m = 7.65×10^{-11} m^2/s, initial concentration C_0 = 5.28×10^7 $\mu g/m^3$, and material age AGE = 0.

To theoretically prove the above prediction, consider a dry material of thickness L that is exposed to air and emits VOCs. For simplicity, consider a 1-D problem only. The governing equation describing the transient diffusion through the material reads:

$$\frac{\partial C_m(y,\tau)}{\partial \tau} = D_m \frac{\partial^2 C_m(y,\tau)}{\partial y^2} \qquad 0<y<L,\ \tau>0 \qquad (4.14)$$

where
$C_m(y, \tau)$ = the VOC concentration at y and time τ
y = the coordinate in which direction that the VOC diffusion in the material takes place

At the material-air interface (y = L):

$$C_m(y=L,\tau) = K_{ma} C_a(y=L,\tau) \qquad (4.15)$$

$$q(y=L,\tau) = -D_m \frac{\partial C_m(y=L,\tau)}{\partial y} \qquad (4.16)$$

where $q(y, \tau)$ is the VOC emission rate (mg/m^2s) at the material-air interface and time τ.

At y = 0 we assume an adiabatic surface whereby:

$$\frac{\partial C_m(y=0,\tau)}{\partial y} = 0 \qquad (4.17)$$

The initial concentration in the solid material is given as uniform:

$$C_m(y,\tau=0) = C_{m0} = \text{const} \qquad 0<y<L \qquad (4.18)$$

Divide both sides of Eqs. (4.14) - (4.17) by C_{m0} and let:

$$\theta_m(y,\tau) = \frac{C_m(y,\tau)}{C_{m0}} \qquad (4.19)$$

and

$$\theta_a(y=L,\tau) = \frac{C_a(y=L,\tau)}{C_{m0}} \qquad (4.20)$$

Laplace transform Eqs. (4.14) - (4.17):

$$s\theta_m(y,s) - 1 = D_m \frac{d^2\theta_m(y,s)}{dy^2} \qquad 0<y<L,\ \tau>0 \qquad (4.21)$$

$$\theta_m(y = L,s) = K_{ma}\theta_a(y = L,s) \qquad (4.22)$$

$$Q(y = L,s) = -D_m \frac{d\theta_m(y = L,s)}{dy} \qquad (4.23)$$

$$\frac{d\theta_m(y = 0,s)}{dy} = 0 \qquad (4.24)$$

The solution to Eq. (4.21) that satisfies Eq. (4.24) is:

$$\theta_m(y,s) = \frac{1}{s} + A\cosh(y\sqrt{\frac{s}{D_m}}) \qquad 0<y<L \qquad (4.25)$$

where s is time in the Laplace domain and A is a constant to be determined by boundary conditions

At y = L, we have from Eq. (4.25):

$$\theta_m(y = L,s) = \frac{1}{s} + A\cosh(L\sqrt{\frac{s}{D_m}}) \qquad (4.26)$$

and

$$\frac{d\theta_m(y = L,s)}{dy} = A\sinh(L\sqrt{\frac{s}{D_m}}) \qquad (4.27)$$

From Eqs. (4.23) and (4.27):

$$Q(y = L,s) = -A\sqrt{D_m s}\sinh(L\sqrt{\frac{s}{D_m}}) \qquad (4.28)$$

From Eqs. (4.22) and (4.26), we can determine A as:

$$A = \frac{K_{ma}\theta_a(y = L,s) - \frac{1}{s}}{\cosh(L\sqrt{\frac{s}{D_m}})} \qquad (4.29)$$

From Eqs. (4.28) and (4.29), we have the emission rate Q(y = L,s) in the Laplace domain:

$$Q(y = L,s) = -\sqrt{D_m s}\tanh(L\sqrt{\frac{s}{D_m}})[K_{ma}\theta_a(y = L,s) - \frac{1}{s}] \qquad (4.30)$$

Eq. (4.30) indicates that the total emission in the Laplace domain, Q(y = L,s), is composed of two parts: due to the surface concentration, $K_{ma}\theta_a(y = L,s)$, and due to a step function, 1/s.

Initially (τ=0), $K_{ma}\theta_a(y = L,s) = \frac{1}{s}$ so Q(y = L,s) = 0.

As $\tau > 0$, the term $K_{ma}\theta_a(y = L,s)$ in Eq. (4.30) decreases as more VOCs are emitted out but the term 1/s remains constant. This means the contribution of the term $K_{ma}\theta_a(y = L,s)$ to emissions becomes less. At the point when

$$K_{ma}\theta_a(y = L,s) << \frac{1}{s} \quad ,$$

the effect of the surface concentration (hence K_{ma}) becomes negligible. The above proves that the K_{ma} does not affect the long-term emission of dry materials. Physically, the VOC concentration at the material surface approaches zero after sufficient time has elapsed.

4.2.2.4 The influence of AGE

The AGE is the time that it takes for a material with uniform initial concentration to reach the same initial VOC distribution as the material tested. Using the same approach of studying the impact of sample application time on "wet" material emissions in Chapter 3, Figure 4.5 gives the predicted VOC concentrations in the chamber outlet for different AGE. Results show that the emission rates for a smaller AGE are higher at the beginning. Meanwhile, the figure also shows that the effect of AGE tends to diminish after a period. This indicates that the AGE affects only the early stage emissions.

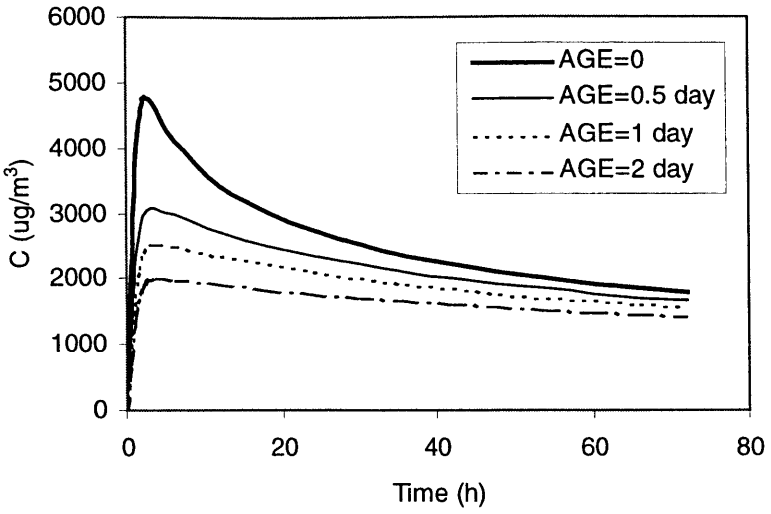

Figure 4.5 Comparison of VOC concentrations at the chamber outlet with different material age, AGE. The curve is predicted with the diffusion coefficient $D_m = 7.65\times10^{-11}$ m^2/s, partition coefficient $K_{ma} = 3289$, and initial concentration $C_0 = 5.28\times10^7$ $\mu g/m^3$.

4.2.3 Identification of material properties for the numerical model

The above sensitivity analysis indicates that in order to predict material emissions, all the material properties (C_0, D_m, K_{ma}, and AGE) must be properly obtained. In case these properties cannot all be accurately given, special attention should be paid to the C_0 and D_m because they determine both the short-term and long-term emission characteristics.

The most direct way of obtaining the material properties is by experimental measurements. Recently, Bodalol *et al.* (1999) developed a method to measure the D_m and K_{ma} of dry sources. The method is promising in that it can provide a database of VOC transport properties for building materials. However, the measurements require a specially designed diffusiometer consisting of two stainless steel chambers (with the test specimen in between). Conducting the experiments is expensive and time consuming (it takes a long time for VOCs to diffuse through the specimen). Moreover, Bodalol (1999) estimated that the measurement equipment has an uncertainty of ±18% for both D_m and K_{ma}. When the measured property values were used to predict emissions from the same material and VOCs, a much larger simulation error was observed (Bodalol, 1999).

Due to the limitations of the direct measurement approach, material properties can also be estimated by the use of emission chamber data (concentration vs. time curve) together with emission modeling through curve fitting, as demonstrated in Chapter 3. Since many chamber measurements have been conducted and published, obtaining material properties from the existing emission data is much cheaper than obtaining it from direct

measurements. A major problem for this method is that it may involve obtaining two or more coupled unknowns using one set of data. However, results from the previous section indicate that the influence of C_0 on emissions can be separated from that of D_m, K_{ma}, and AGE. Among the last three, K_{ma} and AGE can be estimated in light of the following:

(a) Most materials tested are stored in a sealed tedlar bag from the time they are manufactured until they are tested. In such a case, AGE = 0.

(b) The short-term emissions of a dry material are not sensitive to the value of K_{ma} within a certain range (*e.g.*, 1~1,000) and the long-term emissions are independent of K_{ma}. This allows the use of some approximations to estimate K_{ma}, as demonstrated below.

If both AGE and K_{ma} can be pre-determined, the curve fitting will be for D_m only. In this way, the uncertainties of estimating two or more coupled parameters using one set of data can be eliminated.

In summary, the following procedures can be followed to obtain the material properties (D_m, K_{ma}, C_0) and material age (AGE) based on the measured emission data (C vs. τ) for a single sample of dry material.

Step 1: Analyze the emission data and identify the compound(s) emissions to be studied. Identify physical properties of the compound(s), such as molecular weight, vapor pressure, etc.

Step 2: Estimate AGE by tracking the material history and storage method.

Step 3: Pre-determine the material-air partition coefficient. Recently, Bodalal *et al.* (1999) measured D_m and K_{ma} for several solid materials and found that although D_m depends heavily on both material and compound properties, the partition coefficient for different materials can be approximated based solely on the vapor pressure of the compound. Figure 4.6 shows the correlations for different materials and compounds given by Bodalal (1999). When the material and compound to be studied do not match the data available, the following correlation (for plywood) may be used:

$$K_{ma} = 10600 / P^{0.91} \qquad (4.31)$$

where P is the vapor pressure of the compound in mmHg.

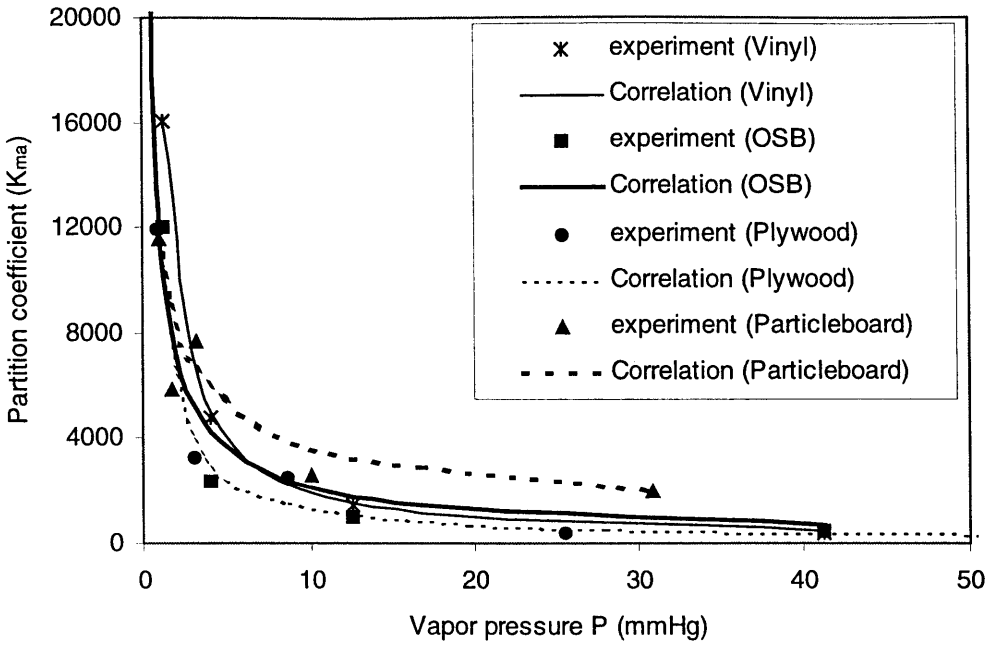

Figure 4.6 Measured partition coefficient of different materials (Bodalal, 1999).

Step 4: Establish the computational domain, boundary and initial conditions.

Step 5: Use numerical simulation to obtain D_m by adjusting its value until the predicted chamber concentration agrees with the measured data. Since the initial concentration C_0 (which is unknown by now) does not affect the shape of the emission curve, at this stage we can assume an arbitrary value, $C_{0,ini}$ and compare the relative concentration (C/C_{max}) between the model prediction and the data. A least-square analysis is usually employed to obtain a "best fit" between the simulation results and the data. The D_m is obtained when a best fit is achieved.

Step 6: Obtain the initial concentration, C_0. Notice that the chamber concentration is proportional to C_0 for the same K_{ma} and D_m; the value of C_0 can be obtained by:

$$C_0 = C_{0,ini} \frac{C_{max,data}}{C_{max,sim}} \tag{4.32}$$

where $C_{max,data}$ and $C_{max,sim}$ are the maximum concentration by measurement and simulation, respectively.

In the following two sections, the use of the above procedures are illustrated with two examples. The first example, using particleboard, demonstrates the general approach. The second one, using an SBR carpet, further investigates the impact of temperature on material emissions.

4.2.4 Application Example 1: VOC emissions from two particleboard samples

Particleboard is a panel product made of wood particles bounded together under heat and pressure, usually using an ureaformaldehyde (UF) resin adhesive. The adhesive produces a water-resistant bound. The bound is layered with the finer particles in the surface layers and coarser particles in the core layer.

Particleboards have long been identified as VOC emitters (*e.g.*, Matthew, 1983). Recently, Magee (1998) measured the VOC emissions from two new particleboards. In the experiments, a small-scale chamber of $0.5 \times 0.4 \times 0.25$ m^3 was used for measuring the particleboard emissions. The chamber, illustrated in Figure 4.1, is similar to the NRC small-scale chamber for measuring "wet" material emissions but has no inner chamber or local velocity control. Two different specimens of particleboard (PB1 and PB2) were tested. A sample holder was used in all the tests, limiting the exposure of the test specimens to a single face. Details of the test specimens and their geometrical dimensions are shown in Table 4.1. The test conditions were:

- Temperature: 23 ± 0.5 °C
- Relative humidity: 50 ± 0.5 %
- Air exchange rate: 1.0 ± 0.05 h^{-1}
- Loading ratio: 0.729 m^2/m^3

Table 4.1 Test specimens of the particleboard.

Specimen	Type/Grade	Length/width/height (m)	Manufacturing details
PB1	Industrial	0.212×0.212×0.0159	Single opening line; 100s press UF Resin: 11.5% face, 8.9% core Scavenger: 15.0% face, 5.0 % core
PB2	Industrial	0.212×0.212×0.0159	Multi-opening line; 125s press UF Resin: 11.2% face, 9.4% core Scavenger: 35% face, 20 % core Wax: 1.2% face, 0.9% core

The tests lasted 96 hours for PB1, and 840 hours for PB2. The VOCs were screened by GC/MS and quantified by tube sampling and analyzed by GC/FID. Major compounds identified for the two different particleboards were the same: hexanal, α.pinene, camphene, and limonene.

For each particleboard tested, the emissions of TVOC and two major compounds: hexanal and α.pinene were simulated. Since both particleboards tested were new, the material age AGE = 0. K_{ma} was calculated using Eq. (4.31), and D_m and C_0 were obtained by curve fitting, as shown in Table 4.2.

Table 4.2 Physical properties of particleboard emissions

(a) PB1

Compound	TVOC	Hexanal	α.Pinene
D_m (m^2/s)	7.65×10^{-11}	7.65×10^{-11}	1.2×10^{-10}
C_0 ($\mu g/m^3$)	5.28×10^{7}	1.15×10^{7}	9.86×10^{6}
K_{ma}	3289	3289	5602
AGE	0	0	0

(b) PB2

Compound	TVOC	Hexanal	α.Pinene
D (m^2/s)	7.65×10^{-11}	7.65×10^{-11}	1.2×10^{-10}
C_0 ($\mu g/m^3$)	9.86×10^{7}	2.96×10^{7}	7.89×10^{6}
K_{ma}	3289	3289	5602
AGE	0	0	0

Figures 4.7 and 4.8 compare the predicted VOC concentrations and the data using the properties listed in Table 4.2. An examination of the material property data revealed several interesting features:

(1) The VOC emission profiles between the two particleboards are very different. However, the property data in Table 4.2 indicate that the two particleboards actually shared the same partition coefficient (K_{ma}) and diffusion coefficient (D_m). The only difference is the initial concentration, C_0. The high initial concentration of the PB2 seems to be connected to the high percentage of scavenger (see Table 4.1) used during the manufacturing process. This suggests that an effective way to reduce emissions from the material is to use as little scavenger as possible to reduce C_0.

(2) For the two types of particleboards studied, K_{ma} and D_m for TVOC can be represented by those of hexanal, the most abundant compound in the particleboards.

(3) For both the two particleboards examined, emissions of α.pinene decayed faster than TVOC and hexanal. Hence, the D_m for α.pinene is larger than that of hexanal (1.2×10^{-10} vs. 7.65×10^{-11}). This finding however is contrary to the molecular diffusion theory. Based on the diffusion theory, compounds with larger molecular weight (α.pinene) should have a smaller diffusion coefficient. The reason for this unusual phenomenon is not clear.

The above example shows that the numerical approach can predict the VOC emissions from the particleboards. Results presented in section 4.2.2 also suggest that for materials with a small diffusion coefficient (*e.g.*, the particleboards), the partition coefficient K_{ma} affect emissions only during the initial period. When K_{ma} =1, the VOC concentrations on both sides of the material-air interface will be continuous and the mass transfer will be analogous to a conjugate heat transfer problem. Hence, for a relatively long-term emission problem, we can conveniently set K_{ma} =1 and use a conventional CFD code to solve the VOC emission problem without getting into the complicated non-linear couplings between the interfacial mass transfer. In the following section, we investigate the impact of temperature on emissions from a carpet by using this simplification.

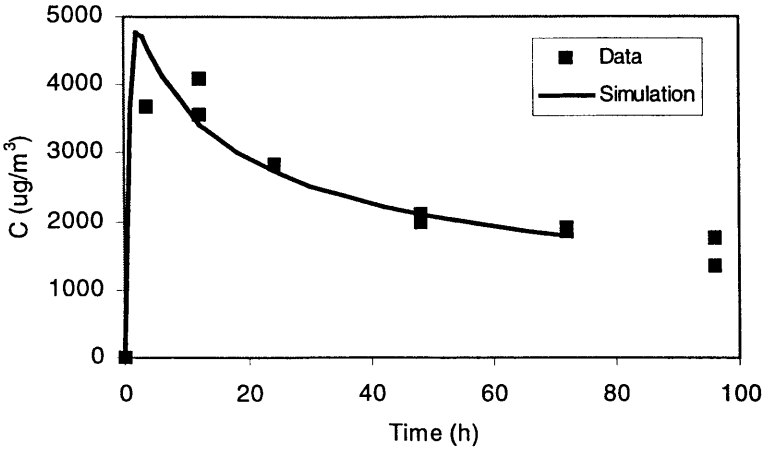

(a)

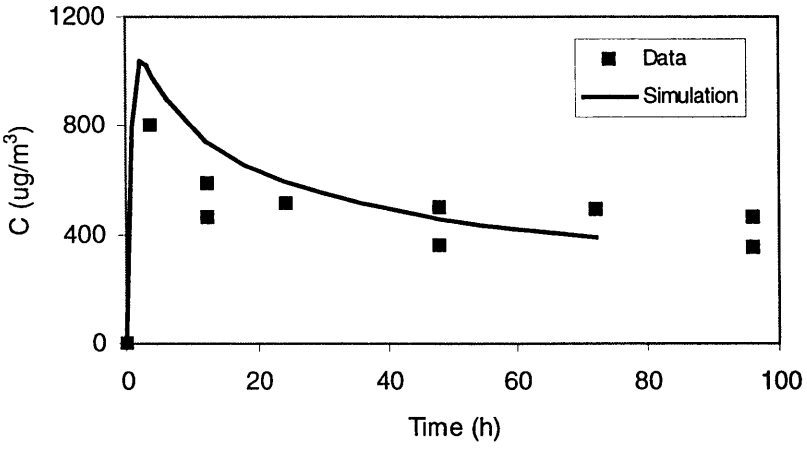

(b)

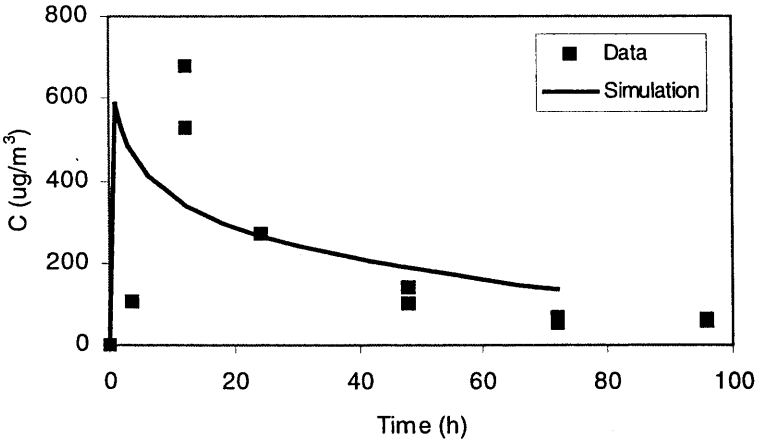

(c)

Figure 4.7 Comparison of measured and simulated VOC concentrations emitted from PB1: (a) TVOC, (b) Hexanal, (c) α.pinene.

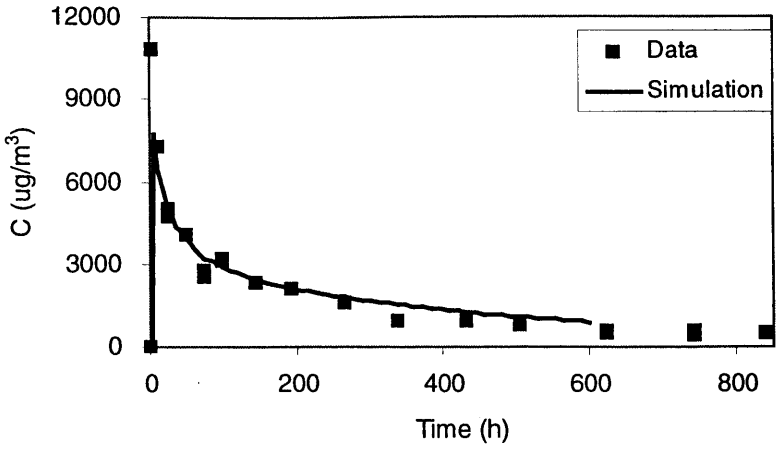

(a)

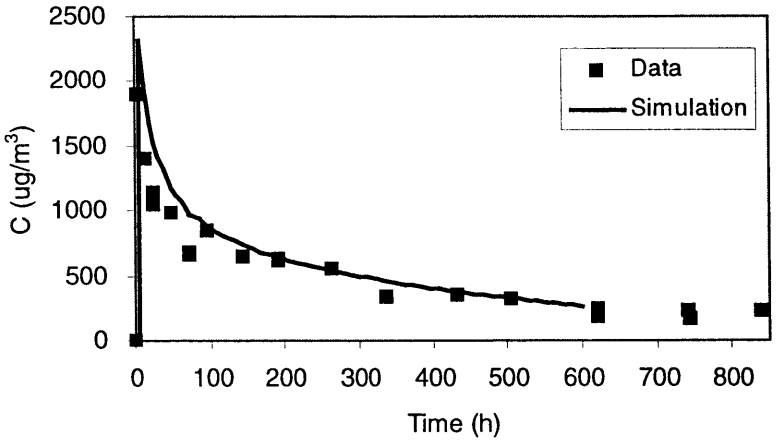

(b)

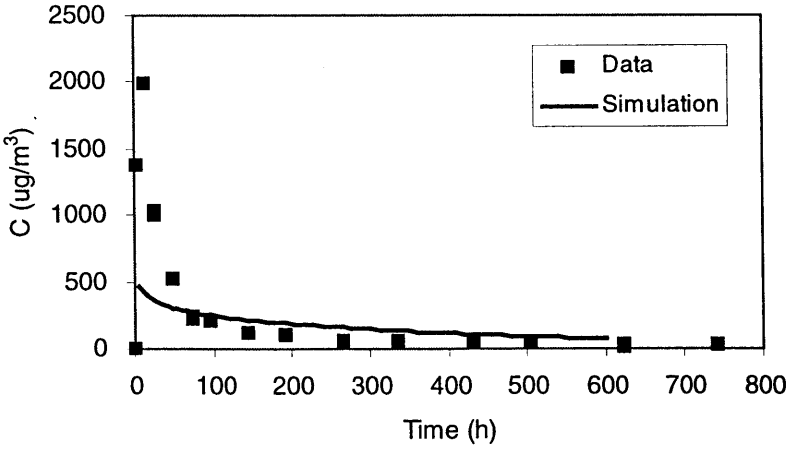

(c)

Figure 4.8 Comparison of measured and simulated VOC concentrations emitted from PB2: (a) TVOC, (b) Hexanal, (c) α.pinene.

4.2.5 Application Example 2: VOC emissions from a carpet

The example that is used in this section is for VOC emissions from a commonly used carpet. Bluyssen *et al.* (1995) have conducted chamber tests to study VOC emissions from a polypropene Styrene-Butadiene Rubber (SBR) bitumen-backed carpet under different temperatures. The study suggests that temperature can significantly influence the carpet emission profiles. Hence, our study focuses on studying the temperature effect on the carpet emissions.

4.2.5.1 Experimental data

VOC emissions form the SBR carpet were measured using a small-scale dessicator. The dessicator, shown in Figure 4.9, has a volume of 6.3 liters. The carpet tested had a gross thickness of 5 mm (2 mm for the bitumen backing and of 3 mm for the fiber). The test conditions were:

- Air exchange rate: 1.0 h^{-1}
- Relative humidity: 45%
- Loading: 0.15 m × 0.15 m (3.57 m^2/m^3)
- Temperature: 23 °C, 30 °C, and 40 °C

Three tests were conducted under different temperatures (23 °C, 30 °C, 40 °C). Each test was for 22 days. The desiccator was placed in a climate chamber (23 °C) or a stove (30 °C and 40 °C). The time-dependent VOC concentrations at the outlet were measured daily by GC/FID. For the SBR carpet, emissions of TVOC and three groups of most abundant compounds, n-alkanes (tot.n-alk.), n-undecane (n-undec.), and aromatic hydrocarbons (tot.arm.) were studied.

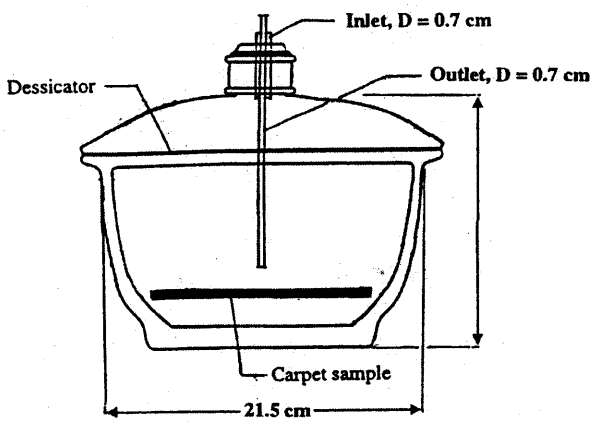

Figure 4.9 Configuration of the small-scale test chamber (dessicator).

4.2.5.2 Simplifications Used in Carpet Emissions

The carpet material we studied consisted of fibers (porous), backing (solid), and installation material such as glue. Generally, emissions from glues occur rapidly, whereas those from the solid part of carpet may last a few months or even years. Due to the complexity in VOC emissions, it is difficult to perform detailed microscopic modeling of the emission processes from a carpet installation. To solve the problem, we introduced two key assumptions to simplify the carpet emissions.

The first assumption was that the impact of the carpet fiber on emissions can be neglected. Due to the fact that the diffusivity in highly porous carpet fiber is usually several orders of magnitude larger than that of solid backing, the mass transfer resistance imparted by the fiber layer compared to that of the backing material is generally small. Further, since the fiber material has more area to be exposed to the air, VOCs in the fiber (if any) should be quickly depleted. As evidence, Little *et al.* (1994) measured the emissions of a typical residential carpet with nylon fibers and a secondary backing consisting of a coarse polypropylene mesh bonded to primary backing with SBR latex adhesive. Using a test in which the fibers and backing materials were separated and tested individually, they found that the fibers contained about 4 - 8% of the total VOCs present in the carpet. The VOC emitted during the first 90 minutes of the test was about 16% of total emission and the emission rates of the fiber decreased far more rapidly than those of the backing. The measurement findings support the assumption that emissions from the fibers are insignificant.

Our second simplification in the study was in regard to the partition coefficient (K_{ma}). Theoretically, we can use Eq. (4.31) to estimate K_{ma} and follow the same procedures as we used for the particleboards to simulate emissions. However, a preliminary examination of the carpet indicates that it has a much smaller diffusion coefficient than

the particleboards. Based on the conclusion presented in section 4.2.2.3, the K_{ma} can be set to 1 so that a conventional CFD code can be used to simulate emissions by using the heat and mass transfer analogy.

4.2.5.3 Determination of material properties and AGE

Based on the period during which the carpet was stored before being tested, we determined that all of the carpet samples had the same AGE of 3 days. Note that the value was not determined in a rigorous way and hence may not reflect the actual initial status of the carpet tested. This may be acceptable for a relatively long period of emissions thus the effect of inaccurate estimation of AGE is insignificant. For an accurate simulation of short-term emissions, a more rigorous method to determine AGE is needed.

After pre-determining K_{ma} and AGE, C_0 and D_m can then be obtained by fitting the simulated chamber concentration with the measured data. A commercial CFD program, PHOENICS (CHAM, 1996), was used to simulate the carpet emissions in the small chamber by using a 2-D cylindrical coordinate. A solution domain, including the location of the carpet and all its boundaries, is shown in Figure 4.10. The CFD program discretizes the space of the test chamber into 23 (r direction) by 62 (y direction) non-uniform computational cells, and the discretized equations were solved with the SIMPLE algorithm (Patankar, 1980). The convergence criteria at each time step were to ensure that the total normalized residual was less than 1% for flow and 2% for VOC concentrations.

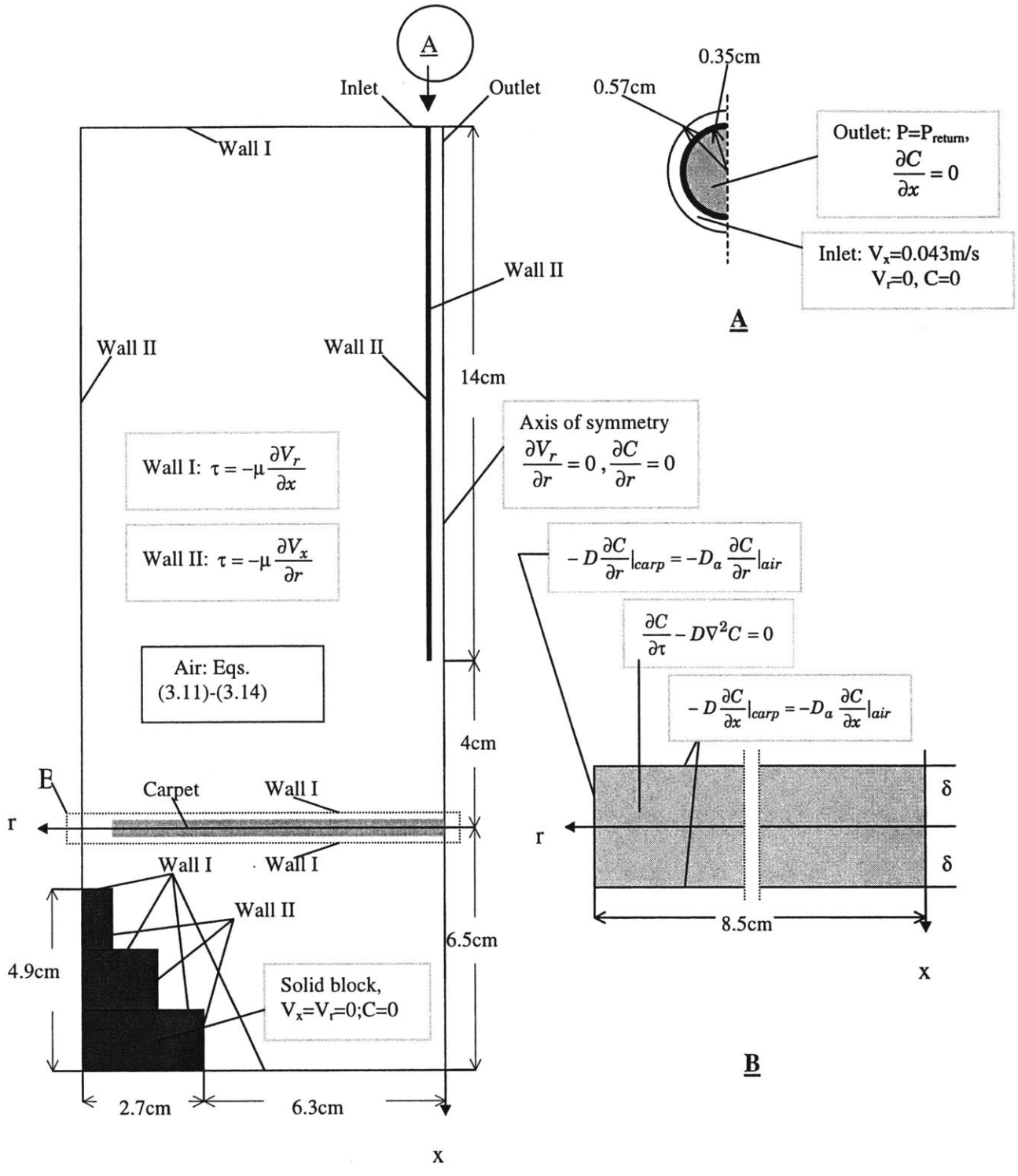

Figure 4.10 CFD solution domain of carpet emission in an axi-symmetrical test chamber.

Table 4.3 lists the parameters of D_m, C_0, K_{ma}, and AGE at different temperatures for TVOC and three single VOCs obtained by matching the model predictions with the data.

Table 4.3: Values of D_m, C_0, K_{ma}, and AGE for different compounds.

(a) TVOC

Temperature	**23 °C**	**30 °C**	**40 °C**
D_m (m^2/s)	1.1×10^{-14}	4.2×10^{-14}	7×10^{-14}
C_0 ($\mu g/m^3$)	1.92×10^{8}	1.60×10^{8}	2.62×10^{8}
K_{ma}	1	1	1
AGE (day)	3	3	3

(b) n-alkanes

Temperature	**23 °C**	**30 °C**	**40 °C**
D_m (m^2/s)	4.0×10^{-14}	1.6×10^{-13}	2.3×10^{-13}
C_0 ($\mu g/m^3$)	2.5×10^{7}	1.8×10^{7}	2.5×10^{7}
K_{ma}	1	1	1
AGE (day)	3	3	3

(c) n-undecane

Temperature	**23 °C**	**30 °C**	**40 °C**
D_m (m^2/s)	5.0×10^{-14}	1.9×10^{-13}	2.5×10^{-13}
C_0 ($\mu g/m^3$)	7.2×10^{6}	5.7×10^{6}	7.5×10^{6}
K_{ma}	1	1	1
AGE (day)	3	3	3

(d) Aromatic hydrocarbons

Temperature	**23 °C**	**30 °C**	**40 °C**
D_m (m^2/s)	4.5×10^{-13}	5.5×10^{-13}	6.0×10^{-13}
C_0 ($\mu g/m^3$)	1.3×10^{6}	3.5×10^{6}	5.0×10^{6}
K_{ma}	1	1	1
AGE (day)	3	3	3

4.2.5.4 The influence of temperature on carpet emissions

Figure 4.11 shows the test data and the computed results using the numerical model under various temperatures. Except for aromatic hydrocarbons at 30 °C and 40 °C, the simulated results of the VOCs agreed reasonably with the data over the 22-day period. Note that the agreement was obtained by matching the simulated concentration with the experimental data by adjusting D_m and C_0.

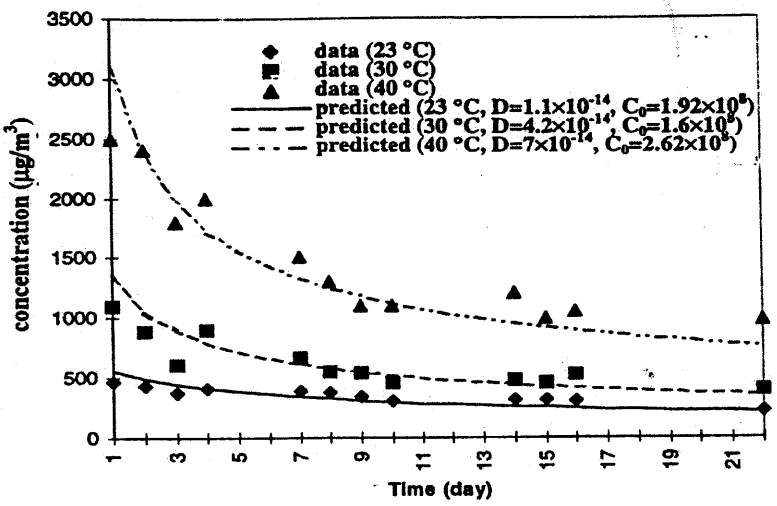

(a) TVOC

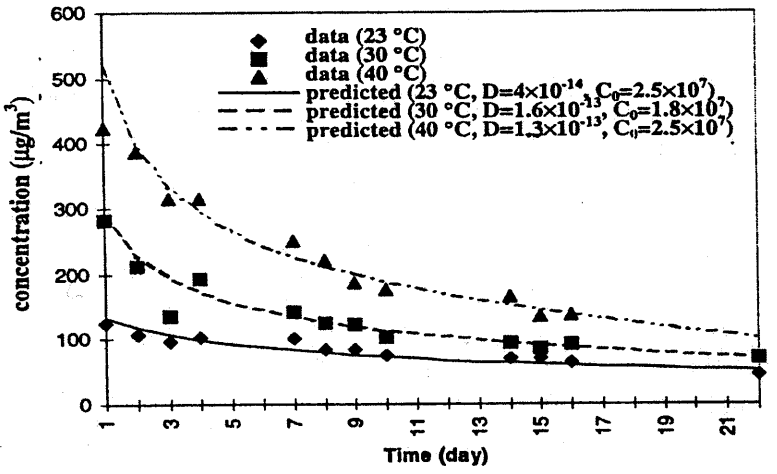

(b) n-alkanes

Figure 4.11 Comparison of predicted VOC concentrations with the chamber data under different temperatures. D is the diffusion coefficient (m^2/s), and C_0 is the initial compound concentration ($\mu g/m^3$) of the carpet polymer.

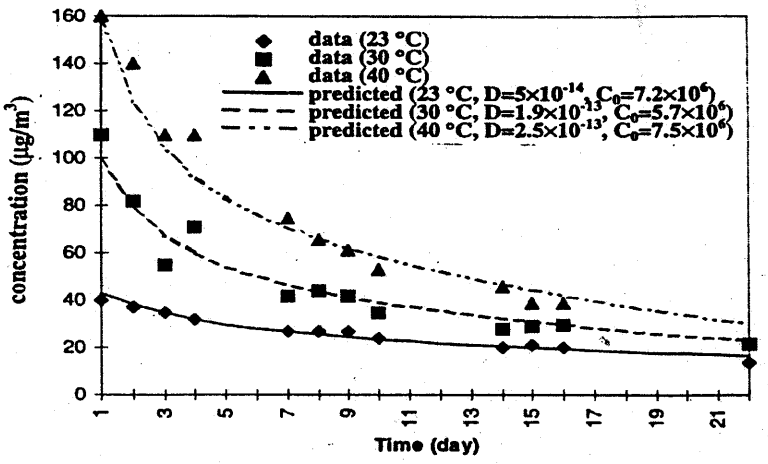

(c) n-undecane

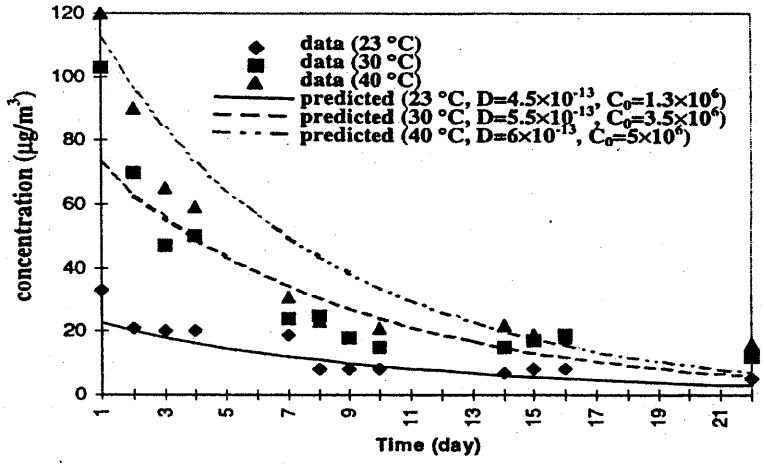

(d) aromatic hydrocarbons

Figure 4.11 (Continued) Comparison of predicted VOC concentrations with the chamber data under different temperatures. D is the diffusion coefficient (m^2/s), and C_0 is the initial compound concentration ($\mu g/m^3$) of the carpet polymer.

The experimental data by Bluyssen *et al.* (1995) revealed two important phenomena of VOC emissions from the carpet: (a) the initial emission rate and the decay constant increased with the temperature, and (b) the decay constant decreased as the boiling point of the compounds increased (Bluyssen *et al.*, 1995). The D_m determined the decay rate of VOCs. The results showed that the diffusion coefficients for different compounds were highly dependent on the temperature of the material. For the three groups of compounds studied (tot.n-alk., n-undec., and tot.arm.), the values of D_m varied between 4×10^{-14} m^2/s and 4.5×10^{-13} m^2/s at 23 °C. At 40 °C, the values were several times larger. The same applies to the D_m for TVOC, which is 1.1×10^{-14} m^2/s, 4.2×10^{-14} m^2/s, and 1.0×10^{-13} m^2/s for 23 °C, 30 °C, and 40 °C, respectively. The values of E_d for different groups of compounds (see Eq. (4.2)), obtained from the computations, are listed in Table 4.4.

Table 4.4: Predicted values of E_d for different groups of compounds. See Eq. (4.2) for more detail.

Compounds	**n-alkanes**	**n-undecane**	**Aromatic hydrocarbons**	**TVOC**
E_d (J/mol)	8.148×10^4	7.483×10^4	1.413×10^4	8.522×10^4

Note that C_0 varies for each group of compounds at different temperatures. Since C_0 indicates the total amount of compounds in the carpet polymer, its value should not change with temperature if there is no chemical reaction to create or consume the compounds. It is generally believed that a chemical reaction is unlikely under the temperatures tested, although this has not been rigorously validated. The predictions show that, except for aromatic hydrocarbons, C_0 at 23 °C was approximately equal to C_0 at 40 °C. At 30 °C, however, the value was 28%, 25%, and 39% lower for n-alkalane, n-undecane, and TVOC, respectively, compared to that at 40 °C. This suggests that the carpet sample tested at 30 °C may have a longer AGE. C_0 for TVOC at 23 °C was about 27% lower than that at 40 °C. Apart from the experimental and modeling errors and AGE difference, another reason for the difference is that some other compounds may have been emitted at 40 °C, a higher temperature.

4.3 Development of a Long-term Model for Dry Materials

The CFD-based short-term simulation calculates the VOC emissions of a dry material in detail. It is mainly used for obtaining the material properties based on the measured emission data from a test chamber. If the material emission lasts for a long period of time (*i.e.*, 1 year), it would be too expensive and time consuming to do numerical simulations for the entire period although not impossible. The following section discusses the development of a simplified model for predicting long-term emissions.

4.3.1 The long-term model

As far as long-term emissions are concerned, the diffusion coefficient D_m in the solid must be very small. We can therefore assume that the emission is dominated solely by the internal diffusion of the solid material and that the mass transfer resistance in the air phase boundary layer is negligible. Further, we have also demonstrated that the partition coefficient, K_{ma}, does not affect the long-term emission behavior of VOCs. Thus, it is possible to simplify the long-term emission simulations with the following assumptions:

(a) The VOC concentration at the material surface is 0 (the emission resistance at both the material-air interface and air phase boundary layer is ignored).

(b) Since the time scale considered is much longer than the materials age (AGE), the uniform initial condition (Eq. (4.12)) is used.

(c). VOC diffusion in the material is 1-D.

The assumption (c) above simplifies Eq. (4.1) into the following 1-D form:

$$\frac{\partial C}{\partial \tau} = D_m \frac{\partial^2 C}{\partial y^2} \tag{4.33}$$

where y is the direction in which VOC diffusion occurs.

Based on the above assumptions, the compound concentration at a cross section y and time τ in the material can be obtained by solving Eqs. (4.12) and (4.33) (or by inverse Laplace transformation of Eq. (4.30) with $\theta_a(y = L,s) = 0$) to yield:

$$\frac{C}{C_0} = \sum_{n=0}^{\infty} \frac{2(-1)^n}{(n+\frac{1}{2})\pi} \cos[(n+\frac{1}{2})\pi \frac{y}{\delta}] \exp[-(n+\frac{1}{2})^2 \pi^2 Fo] \tag{4.34}$$

where

δ = thickness of the solid slab, m

Fo = Fourier number, $Fo = D_m \tau / \delta^2$

The normalized compound emissions (ratio of TVOC emitted to the total amount of TVOC in the carpet) at time τ is obtained by integrating Eq. (4.34) from 0 to δ:

$$\frac{M_\tau}{M_\infty} = 1 - \sum_{n=0}^{\infty} \{ \frac{2}{[(n+\frac{1}{2})\pi]^2} \exp[-(n+\frac{1}{2})^2 \pi^2 Fo] \} \quad (4.35)$$

where

M_τ = total amount of compound emitted up to time τ, μg

M_∞ = total amount of compound in the material, μg. $M_\infty = C_0 A \delta$ and A is the total surface area of the material (m^2).

The average emission factor (emission rate per unit emission area) between time τ_1 and τ_2 is:

$$E_{f12} = \frac{3600 M_\infty (\frac{M_2}{M_\infty} - \frac{M_1}{M_\infty})}{A(\tau_2 - \tau_1)} \quad (4.36)$$

where

E_{f12} = average compound emission factor between time τ_1 and τ_2, $\mu g/m^2 h$

τ_1, τ_2 = time, h

$\frac{M_2}{M_\infty}$ = normalized compound emissions at time τ_2

$\frac{M_1}{M_\infty}$ = normalized compound emissions at time τ_1

After obtaining the emission factor, the average compound concentration at the chamber outlet can be calculated using the steady-state mass balance in the chamber:

$$C_{o,12} = \frac{E_{f12} A}{NV} \quad (4.37)$$

where

$C_{o,12}$ = average compound concentration at the chamber outlet between time τ_1 and τ_2, $\mu g/m^3$

Note Eqs. (4.34) - (4.37) are only valid for long-term emission estimations of materials with one-dimensional diffusion. For a large Fourier number (or time τ), the series in Eqs. (4.34) and (4.35) converge very quickly and usually the first few terms are sufficient. Through an order of magnitude analysis, they are appropriate for monthly emission analyses. If the emission does not last for at least several months, the assumptions used for the long-term simplification may not be satisfied and the short-term simulation should be performed.

4.3.2 Application example

Using the above long-term model and the material properties (D_m, C_0) obtained from the short-term simulation, it is possible to study long-term emissions for different groups of VOCs. The following demonstrates the long-term emission study of the SBR carpet.

Figure 4.12 gives the monthly average TVOC concentrations predicted at the outlet of the dessicator under different temperatures. The emissions do last a few years, though the carpet half-thickness is only 1 mm. Figure 4.12 also shows the impact of temperature on VOC emissions. At 23 °C, it takes 68 months for the average TVOC concentration to drop to less than 1 $\mu g/m^3$, a value with a negligible effect to IAQ. However, it takes just 23 months at 30 °C and 16 months at 40 °C for a TVOC concentration to drop to the same level.

If the carpet tested is applied to buildings, the emissions will be different from those in the test chamber. This is because, in the chamber, the carpet was exposed to air on both sides (double-side emission), whereas in buildings only one surface emits VOCs to the air (single-side emission). In this case the carpet thickness, δ, should be the thickness of the entire carpet polymer (2mm) instead of half of it (1mm). Regarding the effect of carpet thickness on the emissions, Figure 4.13 illustrates the predicted average TVOC emission rates for δ = 1 mm and δ = 2 mm; both are assumed to be single-side emissions. Emissions from a carpet with δ = 2 mm will last much longer than that with δ = 1 mm.

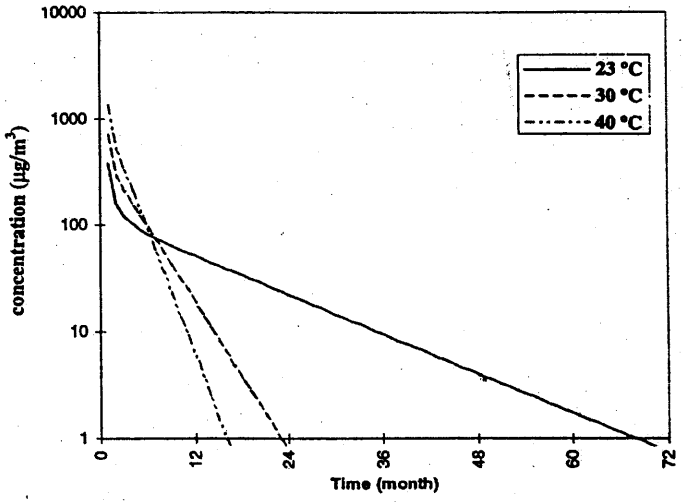

(a) In the first six years

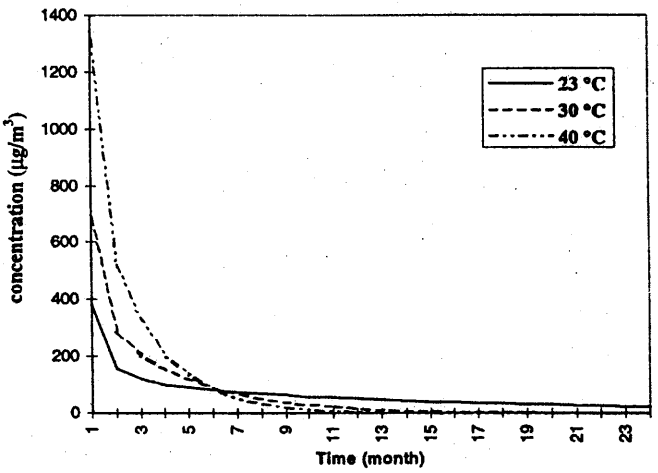

(b) In the first two years

Figure 4.12 Predicted monthly average TVOC concentrations at the chamber outlet under different temperatures.

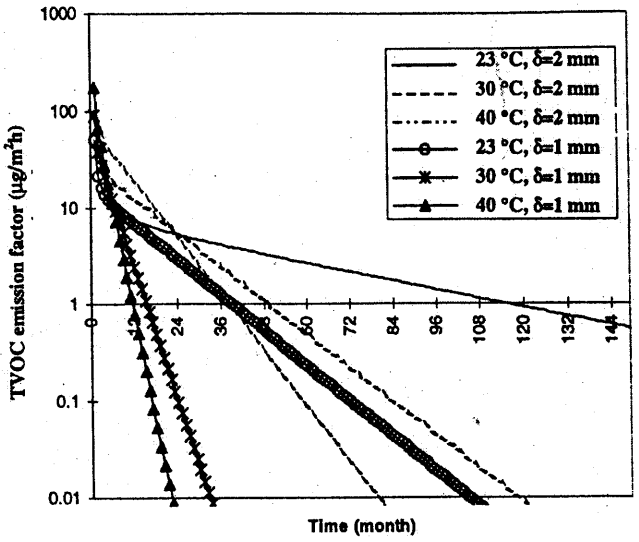

(a) In the first 12 years

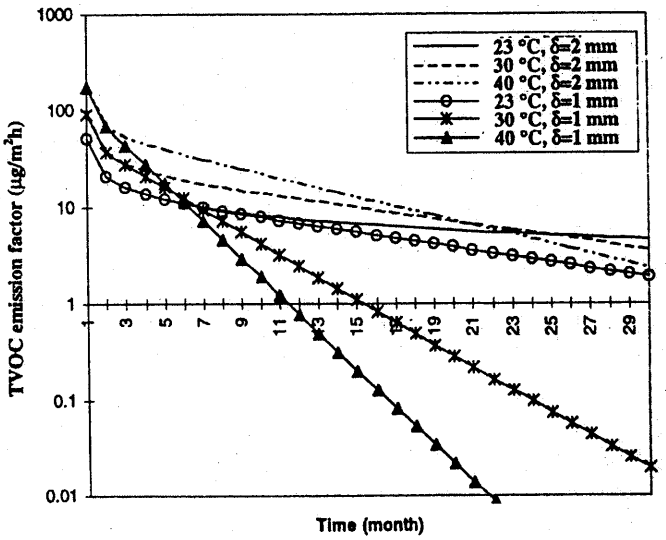

(b) In the first two years

Figure 4.13 Predicted monthly average TVOC emission factor at different temperatures. Single-side emission. δ is the carpet thickness.

Figure 4.14 shows the normalized TVOC emissions (ratio of TVOC emitted to the total amount of TVOC in the carpet) as a function of time. At 23 °C, it takes 119 months for 90% of the TVOC to be emitted. However, only 32 and 19 months are needed for the carpet to emit the same fraction of TVOC at 30 °C and 40 °C, respectively. Note that the VOC emitted is normalized by the total amount of TVOC in the carpet. The actual emissions may be significant even when the curves asymptotically approach 1.0 (100%).

One may try to bake the VOC out of a new material by increasing the temperature for a short time and to achieve low VOC emissions afterwards. For the 2 mm thick carpet studied, the baking out process will not work for TVOC even though it may work for some single VOCs with low boiling points. The TVOC emission rate at 40 °C is higher for about 20 months than at 30 °C, and the emission rate at 30 °C will be higher for about 2 years than at 23 °C. It seems that the most effective way of reducing the VOC emissions would be to lower the temperature.

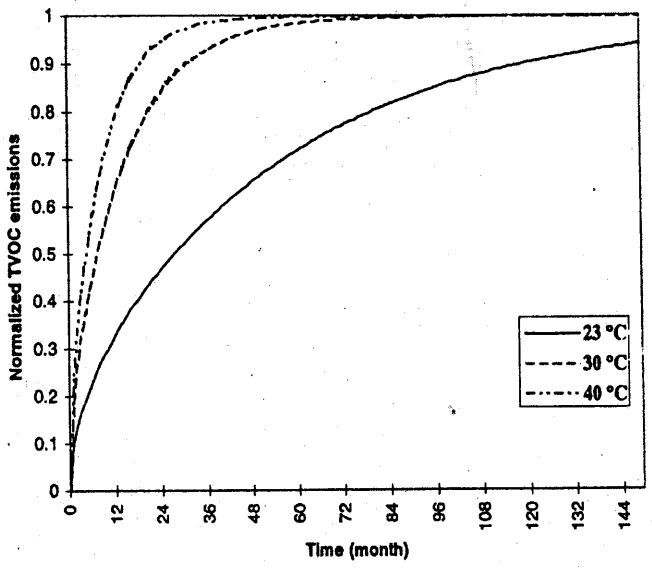

Figure 4.14 Normalized TVOC emissions (ratio of TVOC emitted to the total amount of TVOC in the carpet). Carpet thickness $\delta = 2$ mm, single-side emission.

4.4 Conclusions

This chapter presents two models for simulating VOC emissions from dry materials. One is a numerical model that uses the CFD technique for short-term predictions, and the other is an analytical model for long-term predictions. The short-term model is a detailed one. It uses the following parameters to describe emission characteristics: the initial VOC concentrations in the material (C_0), the solid-phase diffusion coefficient (D_m), the material-air partition coefficient (K_{ma}), and the age of the material (AGE). The parameters were obtained by fitting the predicted VOC concentrations with the small-scale chamber data. The long-term model, which employs some simplifications, uses Eqs. (4.35) and (4.36) to predict the long-term emissions.

The emission studies for two different particleboard samples show that:

(1) For the particleboard studied, different parameters have different impacts on emissions. The emission rate is in proportion to C_0. D_m influences both short-term and long-term emissions. A higher D_m results in a higher initial emission rate and a faster decay rate. On the other hand, K_{ma} and AGE affect only the short-term emissions of the particleboard. It has virtually no impact to long-term emissions.

(2) Using the numerical model developed here, a fairly good agreement of VOC concentrations between the experimental data and model prediction can be achieved by pre-determining K_{ma} and AGE and adjusting D_m and C_0. These material properties obtained can be used to study material emissions in buildings, and help to reduce the material emissions by reformulating the products.

Short-term and long-term emission studies for the SBR bitumen-backed carpet under different temperatures show that:

(1) Temperature has a significant effect on VOC emissions from the carpet. The higher the temperature, the higher the initial emission rates and the quicker the depletion of VOCs. Under different temperatures, VOC emissions can be modeled by changing the diffusion coefficient. A formulation of the Arrhenius relation was used to correlate the dependence of D_m on temperature.

(2) If the carpet studied is applied to buildings, the TVOC emissions can last as long as 12 years at 23 °C. The emissions will last for about 4 years for 30°C and 3 years for 40 °C. In addition, The TVOC emission rates at 40 °C will be higher for about 20 months than those at 30 °C, and at 30 °C will be higher for about 2 years than that at 23 °C. It is therefore impractical to bake the VOC out in a short time (*i.e.*, two weeks). An effective way of reducing the emissions would be to lower the room air temperature in buildings.

Chapter 5

Modeling of VOC Sorption on Building Materials

The sorption (adsorption and desorption) of VOCs by different building materials can significantly affect VOC concentrations in indoor environments. Detailed simulation of VOC sorption in buildings and its impact on indoor air quality can be carried out by a numerical approach (e.g., computational fluid dynamics). However, due to the extremely small magnitude of the diffusion coefficient (i.e., 1×10^{-12} m^2/s) of VOCs in the materials, direct numerical simulation of VOC diffusion in the materials requires very fine grids to determine high VOC concentration gradients, especially near the material-air interface. This chapter develops a new model for simulating VOC adsorption and desorption rates of homogeneous building materials with constant diffusion coefficients and material-air partition coefficients. The model presented in this chapter analytically solves the VOC sorption rate at the material-air interface. It can be used as a "wall function" for solving the VOCs with a numerical program to study indoor air quality. We validate the sorption model in a simple case with an analytical solution as well as the experimental data obtained from sorption experiments.

5.1 Introduction

5.1.1 Objectives

The previous chapters dealt primarily with the VOC emissions from building materials. In this chapter we examine a problem opposite to emissions: VOCs sorption on building materials. Sorption, including adsorption and desorption, is traditionally described as a surface phenomena. In the case of adsorption, VOC molecules are attached to a material surface by physical or chemical forces. In the process of desorption, VOCs that accumulate on the material surface are released into air. In this regard, desorption is similar to emission so it is also called a secondary emission.

Sorption of chemical molecules by a liquid or solid material is ubiquitous in the environment and pollution-control engineering. The lingering odors of winter clothes stored during the summer with naphthalene crystals (moth balls), and the use of activated carbon to remove hazardous VOCs from drinking water are but two examples of sorption.

The sorption of VOCs on material-air interfaces is also very important to the indoor environment. Researchers have found that re-emission of adsorbed VOCs can elevate VOC concentrations in the indoor environment (Tichenor *et al.*, 1988; Berglund *et al.*, 1988). Materials capable of depositing, adsorbing, and/or accumulating pollutants can influence indoor air quality during the entire service life of a building (Nielsen, 1987). Therefore, an accurate characterization of sorption of building materials and the sorption impact on indoor air quality (IAQ) is important.

At present, the studies of the sorption effect are mainly conducted by experiments using environmental chambers. In a typical chamber experiment, the material is placed in the chamber and exposed to a VOC source (a single VOC or VOC mixture) until a stable concentration of that VOC source in the test chamber is reached. The exposure is then stopped. The sorption of the material can be measured by monitoring the VOC concentration at the chamber outlet and comparing the results with the predicted concentration without a sink.

Although the sorption of building materials can be detected by well-designed experiments, sorption models are needed to represent the experimental data and study the impact of sorption on IAQ. This chapter presents a new sorption model based on the fundamental mass transfer theory. The model explicitly quantifies the essential mechanisms of VOC sorption, while maintaining the mathematical equations in an analytically solvable form to provide a readily-accessible solution. It can perform the following tasks:

(1) It can predict the VOC adsorption and desorption by permeable materials with homogeneous diffusivity without the need of sorption measurements.

(2) When incorporated into a numerical program, the model can address the impact of environmental conditions (temperature, airflow, VOC concentration in air) on sorption.

(3) The model can also be used in conjunction with broader studies to identify factors that have a critical impact on IAQ.

Before presenting the new sorption model, the following two sections briefly discuss the physical/chemical processes associated with sorption and how current sorption models deal with those processes.

5.1.2 Sorption fundamentals

Figure 5.1 shows that a typical adsorption process of a permeable building material involves mass transfer in three different regions. In the air, VOCs move from the bulk air to the material surface through a thin boundary layer. At the material-air interface, VOCs are adsorbed on the material surface. The VOCs adsorbed can then penetrate into the material by diffusion. The process is simply the opposite process of dry material emissions. Desorption, in which the material emits VOCs after it absorbs enough VOCs during the adsorption, is similar to emission.

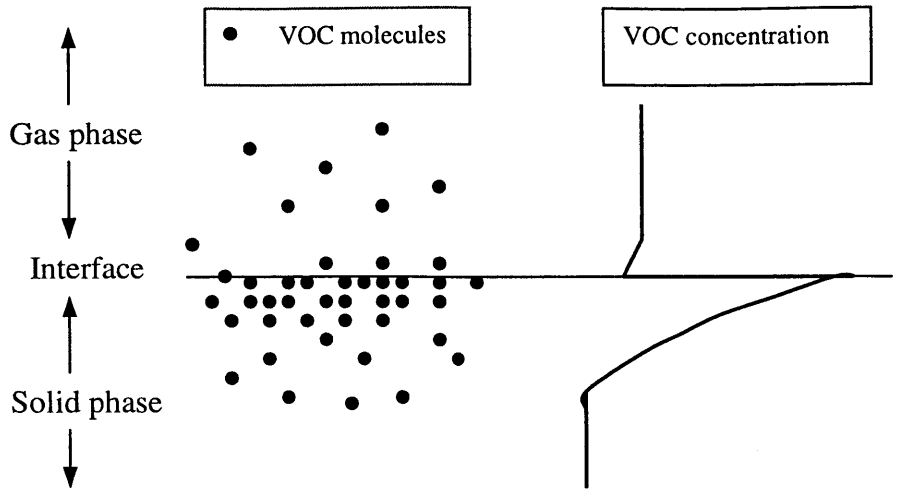

Figure 5.1 The general mass transfer regions of an adsorption process.

All the three processes, including VOC transport (diffusion and convection) in the gas-phase boundary layer, phase change at the interface, and VOC diffusion in the solid material, have been discussed in Chapter 3. However, it is useful to take a closer look at the physical and chemical changes on the material-air interface. According to Clark (1997), sorption on a material-air interface is often categorized as two types: physisorption and chemisorption. In physisorption, the adsorbate (the adsorbing VOC molecule) is bound to the adsorbent (the solid surface) by intermolecular van der Waals forces or electrostatic forces. Chemisorption is thought to result from the formation of a chemical bond between the adsorbent and the adsorbate. Generally, physisorption is considered a relatively reversible process while chemisorption is not. It should be noted that both types of sorption can occur simultaneously; experimental results may not be able to identify what type of sorption is occurring.

5.1.3 Earlier work in modeling the VOC sorption process

Due to the complex nature of the sorption process, not all the sorption mechanisms are readily modeled. Frequently, the sorption process is assumed to be totally reversible and only the mechanism that dominates the sorption is considered. To date, researchers have developed two types of sorption models: the sorption isotherm models (Daniels and Alberty, 1961; Dunn and Tichenor, 1988) and the diffusion models (Matthews *et al.*, 1987; Axley, 1991; Axley and Lorenzetti, 1993; Dunn and Chen, 1993).

The sorption isotherm models assume the adsorption and desorption are confined on the material surface and an equilibrium is achieved between phases at the interface. Axley (1991) compared several isotherm models that have been developed. Among those models, the most promising for examining the indoor environment are the Langmuir isotherm model and the linear isotherm model, a simplified asymptote of the Langmuir model at low VOC concentrations. The Langmuir isotherm model represents the equilibrium VOC concentrations on the material surface by:

$$C_{ad} = \frac{K_l C_g}{1 + K_l C_g} \tag{5.1}$$

where
C_{ad} = adsorbed VOC concentration on the material surface
C_g = VOC concentration in the gas (air)
K_l = Langmuir sorption coefficient

At low gas phase concentration that is common in indoor environments, the Langmuir model can be simplified to a linear form as:

$$C_{ad} = K_l C_g \tag{5.2}$$

The isotherm models, together with the VOC mass balance in a test chamber, have been used to describe the sorption characteristics based on the chamber data (Dunn and Tichenor, 1988; Tichenor *et al.*, 1991). These models, although simple in principle, have limitations. First, they assume that the adsorption or desorption processes occur only at the surface of a solid material. In other words, the models neglect the mass transfer at the gas phase boundary layer and assume that VOCs that accumulate at the surface do not diffuse into the material. Although this assumption may apply to the sorption of non-permeable materials such as stainless steel and glass, it may not apply for sorption of permeable materials such as carpets or gypsum boards. The latter actually represent the mainstream building materials used indoors.

The second limitation of the isotherm models is that investigators must run sorption experiments to obtain the sorption coefficient (K_l) for a material-VOC system. A sorption measurement usually needs to monitor the VOC concentration in an environmental chamber with the presence of the sorption material for several hundred hours. Hence, the measurements are very expensive and time consuming.

Another type of sorption model, the diffusion model, takes the VOC diffusion mechanisms into consideration. Axley (1991) developed the Boundary Layer Diffusion Controlled (BLDC) adsorption model to account for the diffusion in the gas phase boundary layer, but the model ignores the diffusion in the material and assumes a uniform concentration in solid material. Dunn and Chen (1993) applied a series of diffusion models to estimate the sink effect of ethylbenzene and tetrachloroethylene adsorbed on pillows and carpets. Although the models consider the concentration gradient in the solid, they assume an infinite (nonsaturable) sink and well-mixed chamber air (*i.e.*, the diffusion in the gas-phase boundary layer was ignored). In addition, the model has very complicated forms. Matthews *et al.* (1987) applied a hybrid diffusion model of the boundary layer and bulk diffusions to study the sorption dynamics of the formaldehyde

(Ch_2O) on gypsum board, but the model was largely empirical in nature. It must be used with a specific sorption experiment. Jayjock *et al.* (1995) developed a sorption-degradation model. The model considers the degradation of chemical compounds in the sink in addition to the sorption process, but introduces a degradation rate constant of the compound in the sink that is difficult to determine.

In summary, current sorption studies have been heavily based on expensive sorption experiments. Similar to the problem of applying the emission data from small-scale chambers to buildings, there is ambiguity as to whether the model parameters obtained from a sorption experiment can be used in buildings. Further, current sorption models significantly simplify the sorption process in order to achieve a simple solution. The simplifications may not be realistic for detailed studies of sorption and its impact on IAQ in buildings. The next section describes our effort to remedy the gaps.

5.2 Development of a New Sorption Model

Chapters 3 and 4 have shown that emissions from a dry source are actually controlled by several external conditions (*e.g.*, temperature, airflow) and internal properties of the material (K_{ma} and D_m). It is expected that sorption will be determined by these external and internal parameters as well. Recognizing that obtaining K_{ma} and D_m would be easier than conducting sorption measurements (which need considerably longer time and more effort than emission measurements), it would be much cheaper and more convenient if the sorption could also be represented by these properties. This forms the basic idea of the sorption model to be developed.

Similar to the simulation of VOC emissions from a dry source, detailed simulation of the sorption process can also be done by numerically solving the governing equations of sorption (which are essentially the same as those for emissions). However, due to the extremely small magnitude of the diffusion coefficient of VOCs in materials, direct numerical simulation of VOC diffusion in materials requires very fine grids to determine the high VOC concentration gradients especially near the material-air interface. This can be avoided if the VOC sorption rate, $q(0,\tau)$, can be modeled based on the air phase concentration at the interface, $C_a(0,\tau)$, and the physical properties of the building material (Figure 5.2). The model can then be used as a "wall function" for solving the VOCs with a numerical program to study IAQ.

To obtain a simple form of the aforementioned sorption model, the following assumptions are made for the sorption:

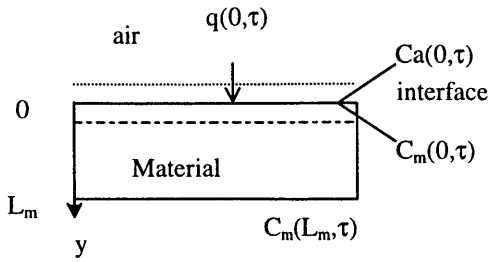

Figure 5.2: VOC adsorption on a solid material

(1) The mass transfer rate between the air and material is very small. Hence, the heat generation/release associated with the sorption is negligible.

(2) Fick's law applies to mass diffusion in both air and the material.

(3) The material is homogeneous and the VOC diffusion coefficient in the material and the material-air partition coefficient are constant. Further, the VOC sorption occurs in a very thin layer of interior building materials. Hence the diffusion inside the material can be assumed to be 1-D.

With the above assumptions, the following sections discuss the development of the sorption model for a solid building material.

5.2.1 Mathematical formulation

Chapters 3 and 4 have given the mass transfer equation for emissions. The sorption model is based on the same equations at the material-air interface and diffusion inside the material, as will be described below.

At the material-air interface:

$$C_m(0,\tau) = K_{ma} C_a(0,\tau) \tag{5.3}$$

where 0 represents the material-air interface (y = 0), τ is time, and K_{ma} is the dimensionless partition coefficient.

For a solid material with homogeneous diffusivity, the 1-D transient diffusion process is governed by:

$$\frac{\partial C_m(y,\tau)}{\partial \tau} = D_m \frac{\partial^2 C_m(y,\tau)}{\partial y^2} \tag{5.4}$$

where D_m is the VOC diffusion coefficient in the material (m^2/s), and y is the coordinate representing the direction that the VOC diffusion in the material occurs (m). The VOC mass transfer rate $q(y, \tau)$ (mg/m^2s) at an arbitrary displacement y of material and time τ is given by:

$$q(y,\tau) = -D_m \frac{\partial C_m(y,\tau)}{\partial y} \tag{5.5}$$

If the thickness of the material is L_m, the initial and boundary conditions for the solid material are:

$$C_m(y,\tau = 0) = 0 \tag{5.6}$$

$$q(0,\tau) = -D_m \frac{\partial C_m(0,\tau)}{\partial y} = -D_a \frac{\partial C_a(0,\tau)}{\partial y} \tag{5.7}$$

$$C_m(L_m,\tau) = 0 \tag{5.8}$$

where D_a is the VOC diffusion coefficient in air (m^2/s). Eq. (5.7) represents a mass balance at the material-air interface and Eq. (5.8) indicates two possibilities on the other side of the material ($y = L_m$). The first possibility is that the material is thick compared to the diffusion distance and the other side remains unaffected by the diffusion. The second is that the VOCs have already penetrated the material but the other side is exposed to an environment with 0 VOC concentration and a large mass transfer coefficient. In most cases, the diffusion process in a solid material is very slow and the first possibility exists.

Based on the above mathematical formulation, a model can be developed to describe the change of VOC sorption rate, $q(0, \tau)$, as the air phase VOC concentration at the interface, $C_a(0, \tau)$, varies. This will be shown in the following section.

5.2.2 A new sorption model based on the Laplace transformation

By using the Laplace transformation, Eqs. (5.4) and (5.5) can be rewritten as follows:

$$D_m \frac{\partial^2 C_m(y,s)}{\partial y^2} - s \cdot C_m(y,s) = 0 \tag{5.9}$$

$$Q(y,s) = -D_m \frac{\partial C_m(y,s)}{\partial y} \tag{5.10}$$

where s is the Laplace operator, $C_m(y,s)$ and $Q(y,s)$ are the Laplace transformation of $C_m(y, \tau)$ and $q(y, \tau)$, respectively.

The solution to Eqs. (5.9) and (5.10) with the initial and boundary conditions (Eqs. (5.3), (5.6), (5.7) and (5.8)) reads:

$$Q(0,s) = \frac{A(s)}{B(s)} C_a(0,s) \tag{5.11}$$

where $A(s) = K_{ma} \cosh(\sqrt{\frac{s}{D_m}} L_m)$ and $B(s) = \frac{1}{\sqrt{D_m s}} \sinh(\sqrt{\frac{s}{D_m}} L_m)$

Eq. (5.11) is the response of the VOC sorption rate on the air-phase VOC concentration at the interface in the Laplace domain. The VOC sorption rate in the time domain can be obtained by an inverse Laplace transformation of Eq. (5.11):

$$q(0,\tau) = L^{-1}[\frac{A(s)}{B(s)} C_a(0,s)] \tag{5.12}$$

Eq. (5.12) is solvable if $C_a(0, \tau)$ is a simple function, *e.g.*, a step or ramp function. However, in indoor environments, $C_a(0, \tau)$ is usually a complex function of time. A direct solution of Eq. (5.12) is generally not available. To solve the problem, we discretize the $C_a(0, \tau)$ into the sum of a series of discrete functions composed of the peak value at each sampling point multiplied by a unit triangle function, $f(j\Delta\tau)$ ($j = 0,1,2, \ldots, n$), where $\Delta\tau$ is a time step. As shown in Figure 5.3, the sum of such a set of overlapping triangle functions is a first order approximation of $C_a(0, \tau)$. The sorption rate at a given time $n\Delta\tau$ is affected by the air-phase boundary concentration at time $n\Delta\tau$ as well as the boundary concentrations in the previous time, *i.e.*,

$$q(0,n\Delta\tau) = \sum_{j=0}^{n-1} X(j) C_a[0,(n-j)\Delta\tau] \tag{5.13}$$

where X(j) is the system response under the unit triangle function $f(j\Delta\tau)$ ($j= 0, 1, 2, \ldots, n$), and $C_a[0,(n-j)\Delta\tau]$ is the air phase boundary concentration at time $n\Delta\tau$, $(n-1)\Delta\tau$, ... $\Delta\tau$, respectively.

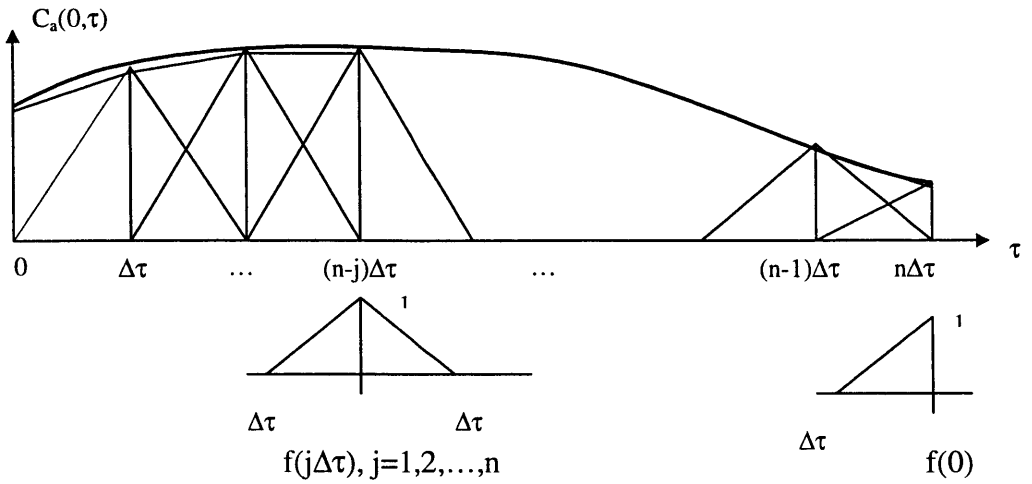

Figure 5.3 Discretization of the $C_a(0,\tau)$ with a series of unit triangle functions.

To calculate the system response at different time steps, we first obtain the system response under a unit ramp function:

$$g(\tau) = \frac{\tau}{\Delta\tau} \tag{5.14}$$

Based on Eq. (5.12), the system response under such a unit ramp function is:

$$G(\tau) = L^{-1}\left[\frac{A(s)}{B(s)}\frac{1}{s^2\Delta\tau}\right] \tag{5.15}$$

B(s) has an infinite number of real roots as follows:

$$s_i = -\mu_i = -\frac{\pi^2 i^2}{L_m^{\ 2}} D_m,\ i = 1,2,3,\ldots \tag{5.16}$$

By using the Heaviside expansion (Beyer, 1975), Eq. (5.15) can be expressed as:

$$G(\tau) = \lim_{s\to 0}\frac{d}{ds}\left[s^2\frac{A(s)}{B(s)}\frac{1}{s^2\Delta\tau}e^{s\tau}\right] + \sum_{i=1}^{\infty}\frac{A(s)}{\frac{d}{ds}[B(s)\cdot s^2]\Delta\tau}e^{s\tau}\Big|_{s=-\mu_i} \tag{5.17}$$

From Eqs. (5.16) and (5.17), we obtain:

$$G(\tau) = \frac{K_{ma} D_m \tau}{L_m \Delta\tau} + \frac{2K_{ma} L_m}{\pi^2 \Delta\tau} \sum_{i=1}^{\infty} \frac{1 - e^{-\mu_i \tau}}{i^2} \tag{5.18}$$

X(0) is the response of $g(\tau)$ at time $\tau = \Delta\tau$:

$$X(0) = G(\Delta\tau) = \frac{K_{ma} D_s}{L_m} + \frac{2K_{ma} L_m}{\pi^2 \Delta\tau} \sum_{i=1}^{\infty} \frac{1 - e^{-\mu_i \Delta\tau}}{i^2} \tag{5.19}$$

For calculating the response of $f(j\Delta\tau)$, j=1, 2, …, n, we decompose $f(j\Delta\tau)$ into the sum of three ramp functions as:

$$f(j\Delta\tau) = g[(j+1)\Delta\tau] - 2g[j\Delta\tau] + g[(j-1)\Delta\tau] \tag{5.20}$$

From Eqs. (5.18) and (5.20), the system response at time $\tau = j\Delta\tau$ is then:

$$X(j) = G[(j+1)\Delta\tau] - 2G[j\Delta\tau] + G[(j-1)\Delta\tau] = \sum_{i=1}^{\infty} W_i e^{\mu_i \Delta\tau} e^{-\mu_i (j\Delta\tau)} \tag{5.21}$$

where $W_i = -\frac{2K_{ma} L_m}{\pi^2 i^2 \Delta\tau}(1 - e^{-\mu_i \Delta\tau})^2$.

Now we have the sorption rate at time $\tau = n\Delta\tau$:

$$q(0, n\Delta\tau) = X(0) C_a[0, n\Delta\tau] + \sum_{j=1}^{n-1} \{ \sum_{i=1}^{\infty} W_i e^{\mu_i \Delta\tau} e^{-\mu_i (j\Delta\tau)} C_a[0, (n-j)\Delta\tau] \} \tag{5.22}$$

When we let $q_i(0, n\Delta\tau) = \sum_{j=1}^{n-1} W_i e^{-\mu_i (j\Delta\tau)} C_a[0, (n-j)\Delta\tau]$ be the sorption rate corresponding to the i^{th} root, we have:

$$q(0, n\Delta\tau) = X(0) C_a[0, n\Delta\tau] + \sum_{i=1}^{\infty} q_i(0, n\Delta\tau) \tag{5.23}$$

where $q_i(0,n\Delta\tau)$ is an unknown but can be obtained progressively as follows:

$$q_i(0, n\Delta\tau) = W_i C_a[0, (n-1)\Delta\tau] + e^{-\mu_i \Delta\tau} q_i[0, (n-1)\Delta\tau] \tag{5.24}$$

and initially, $q_i(0,0)=0$.

Eqs. (5.23) and (5.24) represent the new sorption model. Because the model links the material sorption rate to the VOC history in the air, it can take the VOC deposition on the material surface and the VOC diffusion in the material into account. Once the values of the D_m, K_{ma}, and the air phase concentration are determined, the sorption rate can be obtained by using the above model.

The sorption model can easily be incorporated into an existing numerical model. The use of the model does not need to solve the differential equations for the solid material and hence can significantly reduce computing costs. Since B(s) has an infinite number of roots, there should be an infinite number of $q_i(0,\tau)$ terms corresponding to each root. However, Eq. (5.24) indicates that all the roots greater than some cut-off value have a negligible effect, because the contribution at a time step is always reduced by a factor ($e^{-\mu_i \Delta\tau}$) of the previous sorption rate. If the truncation error is smaller than ε_t, namely,

$$e^{-\mu_i \Delta\tau} < \varepsilon_t \tag{5.25}$$

The maximum number of roots needed is:

$$M = \frac{L_m}{\pi}\sqrt{\frac{\ln(1/\varepsilon_t)}{D_m \Delta\tau}} \tag{5.26}$$

Eq. (5.26) indicates that, the smaller the L_m and the bigger D_m, $\Delta\tau$, and ε, the fewer roots there will be. For example, if $L_m = 0.01$ m, $\varepsilon_t = 10^{-10}$, $\Delta\tau = 60$ s, and $D_m = 2.5\times10^{-12}$ m^2/s, which is common for a solid material, the total number of roots will be less than 1250.

5.3 Validation of the New Sorption Model Using an Analytical Solution

The above sorption model is derived for an arbitrarily varying air phase concentration, $C_a(0,\tau)$. In some simple circumstances, the sorption problem can be solved analytically. Hence, it is natural to validate the model first under such simple circumstances. In the following, the mass diffusion of a semi-infinite plate with constant surface concentration will be used to validate the sorption model.

As shown in Figure 5.4, a semi-infinite material with constant diffusivity D_m is exposed to air with a constant surface concentration, C_a. We assume that the material-air partition coefficient $K_{ma} = 1$ so the surface concentration at the material side is also constant, *i.e.*, $C_m = C_a$ = constant.

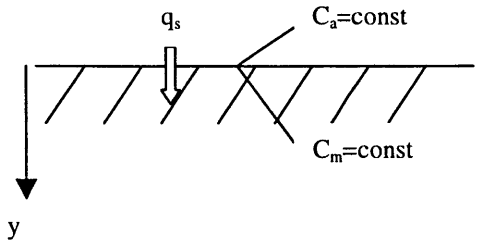

Figure 5.4 A semi-infinite material exposed to a constant surface concentration.

The time-dependent mass transfer rate at the interface, $q_s(\tau)$, has an analytical solution (Mills, 1995) of:

$$q_s(\tau) = D_m \frac{C_a}{\sqrt{\pi D_m \tau}} \tag{5.27}$$

where $\sqrt{\pi D_m \tau}$ is the penetration length of mass transfer. Eq. (5.27) indicates that the mass transfer rate from a constant surface concentration to a semi-infinite material can be modeled as a steady-state mass diffusion by using the time-dependent penetration length as the material thickness.

Assume we are given the following:

$D_m = 2.5\times10^{-12}$ m^2/s
$K_{ma} = 1$
$C_a = 5.33\times10^{8}$ mg/m^3

The solution obtained by using the sorption model ($\Delta\tau$ = 60 sec, L_m = 0.01 m, M = 1250 from Eq. (5.26)) and the analytical results are shown in Table 5.1.

Table 5.1 Comparison of the mass transfer rate through a semi-infinite material by using the new sorption model and analytical solution.

Time (min)	Penetration length (m)	q-analytical	q-model	q-error (%)
1	2.17E-05	61.38272	50.85101	17.15745
2	3.07E-05	43.40414	39.01938	10.10217
3	3.76E-05	35.43933	32.8948	7.17996
4	4.34E-05	30.69136	28.98086	5.57323
5	4.85E-05	27.45119	26.20067	4.55542
6	5.32E-05	25.05939	24.09401	3.85237
7	5.74E-05	23.20049	22.42612	3.33772
8	6.14E-05	21.70207	21.06308	2.94437
9	6.51E-05	20.46091	19.92196	2.63403
10	6.86E-05	19.41092	18.94838	2.38289
....	....	....	....	....
91	2.07E-04	6.43466	6.41701	0.27432
....	....	....	....	....
96	2.13E-04	6.26485	6.24854	0.26028
....	....	....	....	....
100	2.17E-04	6.13827	6.12293	0.24993
....	....	....	....	....
171	2.84E-04	4.69405	4.68716	0.14695
....	....	....	....	....
176	2.88E-04	4.62690	4.62029	0.14275
....	....	....	....	....
180	2.91E-04	4.57520	4.56881	0.13964
....	....	....	....	....
300	3.76E-04	3.54393	3.54094	0.08451
....	....	....	....	....
500	4.85E-04	2.74512	2.74371	0.05150
....	....	....	....	....
1000	6.86E-04	1.94109	1.94057	0.02669

The above results indicate that there were significant errors for the first few time steps. But the error quickly decayed after about 10 time steps and remained negligible afterwards. The reason is that in the sorption model, we used a series of unit triangle functions to represent a continuous C_m. The actual C_m for the analytical solution was a step function, whereas the C_m used in the sorption model was a ramp function instead of a step function for the first half $\Delta\tau$ as shown in Figure 5.5. This difference results in the solution error for the sorption model. However, results show that errors can decay quickly with time, hence they should not be a concern for application purposes.

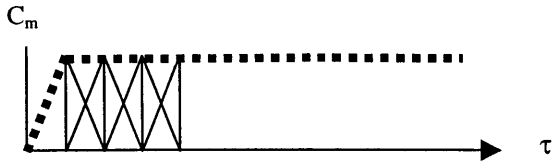

Figure 5.5 The input function (dashed line) used in place of the step function.

A straightforward way to demonstrate the above problem is to use a step function instead of the unit triangle function for the first time step. Following the procedures given in section 5.2, the solution for the sorption rate with a step function is:

$$q(0,\Delta\tau) = \frac{2K_{ma}L_m}{\pi^2} + \sum_{i=1}^{M}\left(\frac{\mu_i e^{-\mu_i \Delta\tau}}{i^2} + \frac{K_{ma}D_m}{L_m}\right) \tag{5.28}$$

Eq. (5.28) now provides the exact same result as the analytical solution for the first time step.

In the above example, the material thickness, L_m = 0.01 m, is used to represent a semi-infinite thickness. In order to evaluate what L_m can be used to represent a semi-infinite thickness, let's do a sensitivity study by changing the L_m into different values, *i.e.*, L_m = 0.0001 m, 0.001 m, 0.01 m, and 0.1 m. The corresponding M for these L_m are, respectively, 13, 125, 1,250, and 12,500. Table 5.2 shows the sorption rate obtained using different L_m.

The results indicate that at the beginning, all the values of L_m represent a "semi-infinite" thickness well. However, starting from the 17th time step (τ = 17 min), the numerical results for L_m = 0.0001m begin to deviate from the analytical values. An analysis of the results indicates that the above transition happened when L_m was at about the same magnitude of the penetration length (L_p). Physically, this means that a smaller material thickness L_m can be used to represent a "semi-infinite" thickness as long as L_m is bigger than the penetration length.

The above results are useful in reducing the computational cost of the new sorption model. As indicated by Eq. (5.26), the total number of roots to be considered is in proportion to the L_m. For the VOC sorption of many building materials, the penetration length is usually very small. Hence, it is possible to reduce the computational time by reducing the L_m to a value that is slightly greater than the penetration length, but not less.

Table 5.2 The mass transfer rate through a semi-infinite material represented by different material thickness (L_m).

Time (min)	L_p (m)	q-analytical	q for L_m=0.0001m	q for L_m=0.001m	q for L_m=0.01m	q for L_m=0.1m
1	2.17E-05	61.38272	50.85096	50.85107	50.85101	50.85101
2	3.07E-05	43.40414	39.01930	39.01937	39.01938	39.01938
3	3.76E-05	35.43933	32.89476	32.89487	32.89480	32.89480
4	4.34E-05	30.69136	28.98088	28.98097	28.98086	28.98086
5	4.85E-05	27.45119	26.20102	26.20078	26.20067	26.20067
6	5.32E-05	25.05939	24.09582	24.09411	24.09401	24.09401
7	5.74E-05	23.20049	22.43257	22.42625	22.42612	22.42612
8	6.14E-05	21.70207	21.07998	21.06319	21.06308	21.06308
9	6.51E-05	20.46091	19.95813	19.92207	19.92196	19.92196
10	6.86E-05	19.41092	19.01515	18.94847	18.94838	18.94838
11	7.20E-05	18.50759	18.21544	18.10504	18.10492	18.10492
12	7.52E-05	17.71967	17.53323	17.36511	17.36501	17.36501
13	7.83E-05	17.02450	16.94903	16.70910	16.7090	16.70900
14	8.12E-05	16.40522	16.44751	16.12227	16.12218	16.12218
15	8.41E-05	15.84989	16.01625	15.59322	15.59313	15.59313
16	8.68E-05	15.34568	15.64503	15.11309	15.11300	15.11300
17	8.95E-05	14.88750	15.32528	14.67475	14.67467	14.67467
18	9.21E-05	14.46805	15.04976	14.27247	14.27238	14.27238
19	9.46E-05	14.08216	14.81225	13.90156	13.90149	13.90149
20	9.71E-05	13.72559	14.60751	13.55816	13.55807	13.55807
21	9.95E-05	13.39481	14.43097	13.23901	13.23893	13.23893
22	1.02E-04	13.08684	14.27873	12.94138	12.94129	12.94129
23	1.04E-04	12.79918	14.14746	12.66297	12.66291	12.66291
24	1.06E-04	12.52970	14.03427	12.40180	12.40173	12.40173
25	1.09E-04	12.27654	13.93664	12.15615	12.15607	12.15607
26	1.11E-04	12.03814	13.85246	11.92454	11.92447	11.92447
27	1.13E-04	11.81311	13.77986	11.70568	11.70561	11.70561
28	1.15E-04	11.60024	13.71725	11.49845	11.49839	11.49839
29	1.17E-04	11.39849	13.66327	11.30186	11.30180	11.30180
30	1.19E-04	11.20690	13.61670	11.11500	11.11495	11.11495
...	...	...	...	...	...	...
51	1.55E-04	8.595300	13.33792	8.553552	8.553512	8.553512
52	1.57E-04	8.512251	13.33613	8.471704	8.471656	8.471656
53	1.58E-04	8.431577	13.33458	8.392144	8.392112	8.392112
54	1.60E-04	8.353130	13.33325	8.314797	8.314757	8.314757
55	1.61E-04	8.276844	13.33211	8.239541	8.239501	8.239501
56	1.62E-04	8.202611	13.33111	8.166299	8.166251	8.166251
57	1.64E-04	8.130340	13.33026	8.094964	8.094932	8.094932
58	1.65E-04	8.059946	13.32951	8.025491	8.025451	8.025451
59	1.67E-04	7.991350	13.32889	7.957757	7.957709	7.957709
60	1.68E-04	7.924480	13.32834	7.891717	7.891677	7.891677

The above Table raises another question: what if the material thickness is smaller than the penetration length? In such a case, the VOCs have penetrated the material and the sorption will be determined by the VOC boundary conditions on the other side of the material. When the boundary condition given by Eq. (5.8) does not apply, the sorption problem needs to be solved by considering the interaction from both surfaces. The solution domain needs to be extended to a multi-zone. In such circumstances, similar sorption models can still be derived by following the same principle. However, this should not be a concern for many building materials because the diffusion in these materials is usually very slow.

5.4 Experimental Validation of the Sorption Model

The above example shows that the new sorption model works well for an ideal case when the boundary condition (surface concentration) is constant. In the following example, the new sorption model is incorporated into a numerical code to simulate sorption by considering the change of VOC concentrations in air. The simulation will reproduce the results of the sorption experiments. The simulated results are then compared with the experimental data for validation.

5.4.1 Sorption data from a small-scale test chamber

In a study aimed at characterizing the sink strength of different indoor materials, An *et al.* (1999; Zhang, 1998) measured the sorption effect by using an environmental test chamber. The 0.05 m^3 environmental chamber was the same as the one for measuring the emissions from the particleboards (see Figure 4.1). Five typical indoor building materials, vinyl floor tile, painted gypsum wallboard, ceiling tile, carpet, and unpainted gypsum board were tested. Each material was tested with five VOCs as shown in Table 5.1. The table also gives the molecular weight and some physicochemical properties of the VOCs used to determine the diffusion and partition coefficients.

Table 5.3 Selected VOCs and their physicochemical properties (Lyman *et al.*, 1990).

VOCs	Molecular weight	Boiling point (°C)	Vapor pressure (mmHg)
Ethylbenzene	116.25	136.3	8.27
Cyclohexanone	126.2	155	2.84
1,4-dichlorobensene	147	173	1.41
Benzaldehyde	253.21	178	1.06
Dodecane	170.34	216	0.27

For each test, a specimen holder was used to confine the sorption to the top surface; the surface area was 0.2×0.45 m^2. The edges of the materials were sealed with wax. The

sample was placed in the test chamber supplied with clean air. At the start of each test, the testing VOC was injected into the inlet flow. The material was placed in the chamber and exposed to the VOC source. The sink strength of the material was indicated by the difference of VOC concentrations between the inlet and outlet (we refer to this stage as the adsorption phase). Once an apparent stable concentration of that VOC in the test chamber was reached, the exposure was stopped. Again, by monitoring the VOC concentration for a period of time, the desorption of the VOC by the material was measured. During the experiments, the chamber air samples were collected by adsorption tubes and analyzed by a GC/FID. The test conditions were:

- Temperature: 23 ± 1 °C
- Relative humidity: 50 ± 2 %
- Air exchange rate: 0.5 ± 0.01 h^{-1}
- Chamber loading factor: 0.57 m^2/m^3

The experimental results indicated that the sorption strength of the five materials was different. Even for the same material, the sorption of different VOCs was also significantly different. It was found that the sorption capacity increased linearly with the inverse of the VOC vapor pressure (An *et al.*, 1999).

For the five materials tested for sorption, Bodalal (1999) experimentally measured the diffusion coefficient and partition coefficient of the unpainted gypsum board and gave the following correlations for D_m (m^2/s):

$$D_m = \frac{3.32 \times 10^6}{3600 M^{6.6}} \tag{5.29}$$

where M is the molecular weight of the tested VOC.

The correlation for K_{ma} was not given but can be estimated by:

$$K_{ma} = 10600 / P^{0.91} \tag{5.30}$$

(see Eq. (4.31))

From Eqs. (5.29) and (5.30), the D_m and K_{ma} for each compound can be calculated. After obtaining these parameters, we can simulate the sorption and compare the predicted results with the measured data. The next section demonstrates the simulation and comparison results for unpainted gypsum board. Section 3.4.3 in Chapter 3 gave the method for incorporating the sorption model into a numerical code.

5.4.2 Simulation of VOC sorption of unpainted gypsum board and comparison with the data

The simulation of the sorption process is similar to the simulation of VOC emissions of dry materials. The sorption model (Eqs. (5.23) and (5.24)) was incorporated into a numerical code to simulate both the air phase concentration and material sorption. In this way, no numerical grids were needed for the solid material.

Based on the experimental data, three compounds, ethylbenzene, benzaldehyde, and dodecane, which represent low, medium, and high sorption rates, were selected for the sorption simulation. D_m and K_{ma}, obtained by using Eqs. (5.29) and (5.30) for these compounds, are listed in Table 5.4.

Table 5.4 D_m and K_{ma} for simulating VOC sorption of unpainted gypsum board.

Compound	**Ethylbenzene**	**Benzaldehyde**	**Dodecane**
D_m (m^2/s)	2.154×10^{-11}	3.932×10^{-11}	1.73×10^{-12}
K_{ma}	1550	10053	34895

Figure 5.6 shows the comparison of the VOC concentrations at the chamber outlet for the model predictions and the chamber observations for ethylbenzene, benzaldehyde, and dodecane, respectively. In general, the predicted concentrations during the adsorption phase (0 - 310 hours) and desorption phase (310 - 500 hours) agree with the measured results. However, the different compounds have different discrepancies. For both ethylbenzene and benzaldehyde, the model tends to over-predict the strength of both adsorption and desorption, resulting in lower chamber concentrations during the adsorption phase and higher concentrations during the desorption phase. The dodecane behaves just the opposite, and the model tends to underestimate the strength of sorption.

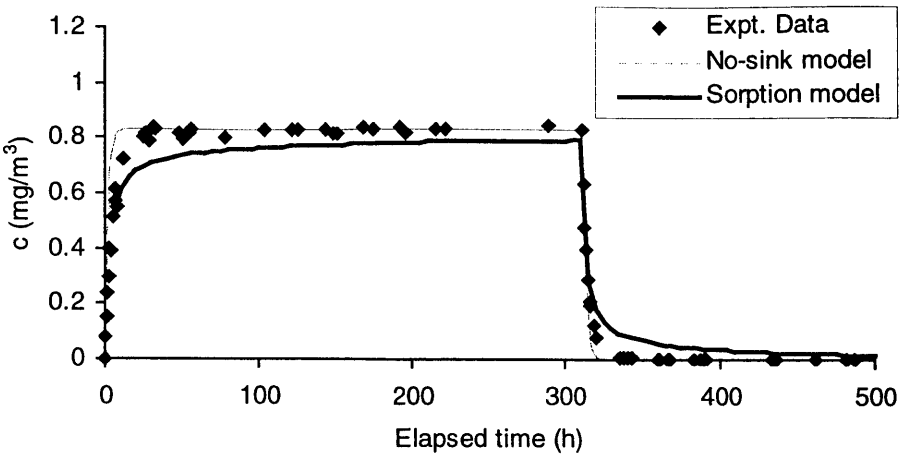

(a)

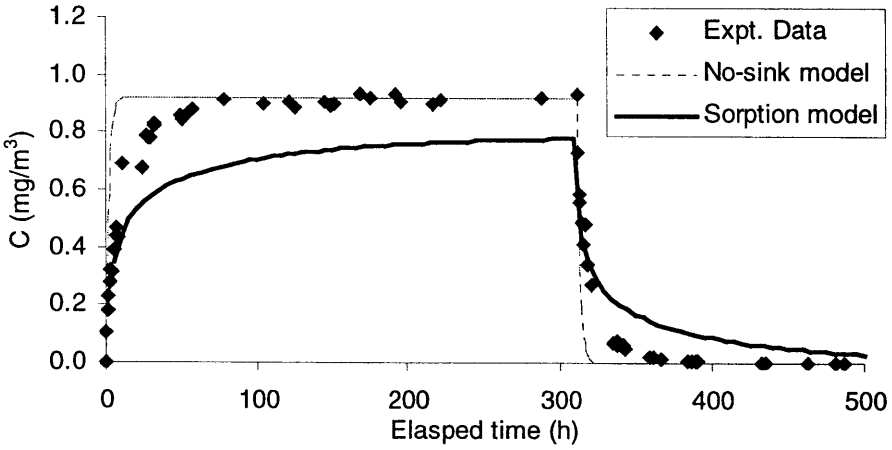

(b)

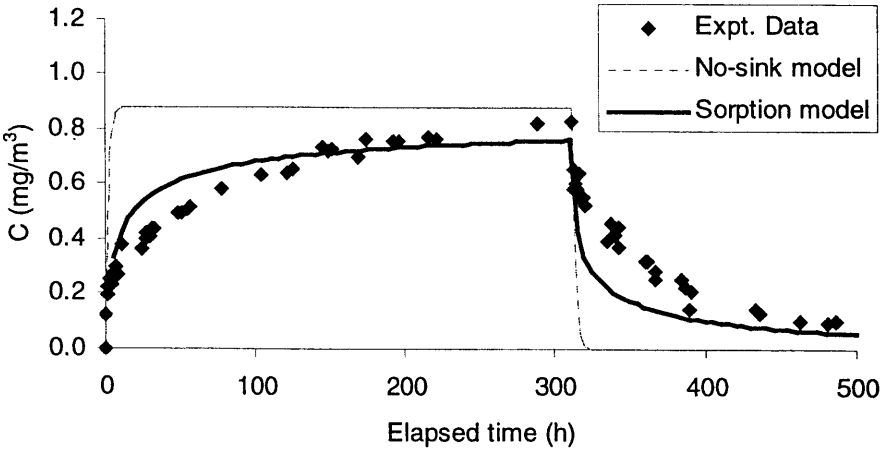

(c)

Figure 5.6 Comparison of measured and simulated sink effects of unpainted gypsum board: (a) Ethylbenzene, (b) Benzaldehyde, (c) Dodecane.

The discrepancies between the predicted and measured concentrations comes from two different reasons. First, An *et al.* (1999) found that the chamber walls themselves also had a considerable sink effect, especially for dodecane. This may partly explain the discrepancy between the predicted and measured results for dodecane, but not for ethylbenzene and benzaldehyde. The discrepancies for the latter compounds may be primarily due to the possible inaccurate values used for the D_m and K_{ma}, which actually determine the sorption. For example, a much better agreement for benzaldehyde can be achieved by using $D_m = 2\times10^{-12}$ m^2/s and $K_{ma} = 3000$, as illustrated in Figure 5.7. Despite the discrepancies found above, the new model can predict the sorption effect directly based solely on material and compound properties (D_m and K_{ma}) without resorting to sorption measurements.

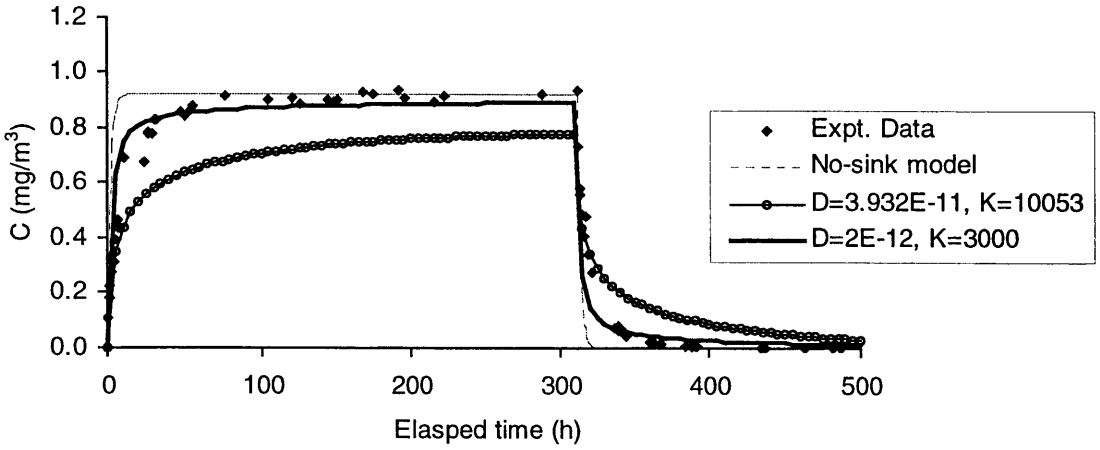

Figure 5.7 A better agreement between the model prediction and experiment can be achieved by adjusting the material properties (D_m and K_{ma}). The results shown here are benzaldehyde sorption on unpainted gypsum board.

To further evaluate the strength of the material on adsorbing or desorbing VOCs, Figure 5.8 gives the percentage of the total incoming VOC rate (from the inlet air) uptaken during the adsorption period. The figure also gives the amount of VOCs released (represented by the percentage of the VOC rate released to the total VOC rate from the inlet during the adsorption phase) during the desorption period. The results indicate that the gypsum board can adsorb a significant portion of the VOCs. At the beginning, about 25% (for ethylbenzene) to 55% (for dodecane) of the VOCs from the inlet air was adsorbed by the material. At 310 hours, the percentage dropped to 3.9% for ethylbenzene and 11.5% for dodecane. From 310 hours, the supply VOCs stopped and the material began to release the adsorbed VOC to the air and serve as a secondary source. At the beginning of the desorption phase (τ=315 hours), the release rate was about 20% (of the VOC rate from the inlet during the adsorption phase) for ethylbenzene and 32% for dodecane. As time passed, the release rate decreased but this would last a long period of time.

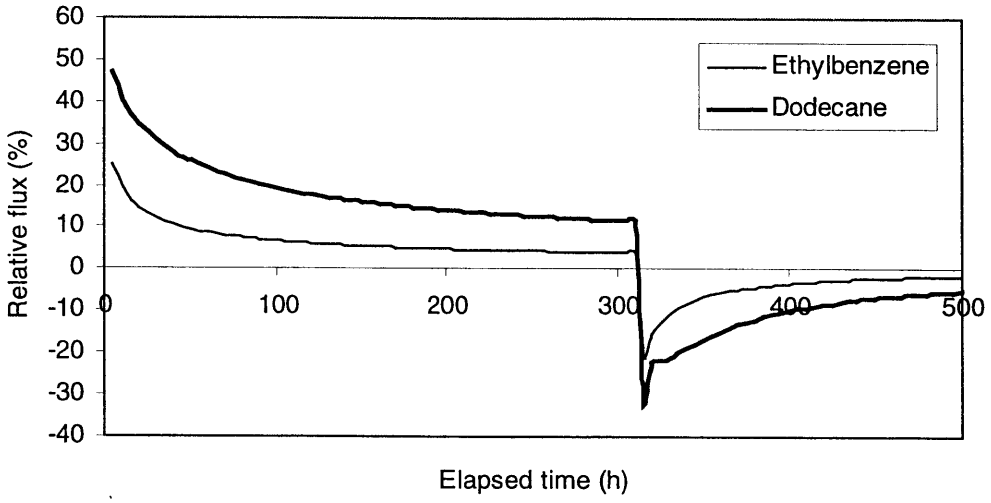

Figure 5.8 Simulated sink effect for ethylbenzene and dodecane by unpainted gypsum. Results show the percentage of the incoming VOC rate (from the inlet air) uptaken during the adsorption period (0-310 h) and the VOCs released (represented by the percentage of the VOC rate released to the total VOC rate from the inlet during the adsorption phase) during the desorption period (> 310 h).

The above results show that building materials exhibit a significant sink effect for VOCs. Such effects are expected to affect the VOC concentrations and exposures in buildings, as many materials could act as sinks to VOCs. This is further investigated in Chapter 6.

5.5 Conclusions

This chapter describes a new VOC sorption model for homogeneous building materials with a constant diffusion coefficient and partition coefficient. The model solves analytically the VOC sorption rate at the material-air interface as a function of the air-phase concentration. The model carries information on the physical representation of the entire sorption process. A validation of the model using an analytical solution confirms its validity. The sorption model has also been incorporated into a numerical program to study VOC sorption on an unpainted gypsum board. Results show that despite the discrepancies, the model can simulate the general trend of the sorption curve.

The significance of the new sorption model that we developed lies in the fact that it provides a relatively simple relationship for the prediction of sorption based solely on the physical properties (diffusion coefficient and partition coefficient) of the material. The model can be used to study sorption processes of building materials without resorting to expensive sorption measurements.

Chapter 6

Study of Indoor Air Quality (IAQ) in a Room with Different Ventilation Systems

In this chapter, a numerical study is carried out to predict the indoor air quality in a full-scale model room. The study is for different emission sources, sinks, and ventilation systems. A computer program, ACCESS-IAQ, is developed to simulate the airflow pattern, the time history of the contaminant concentrations in the occupied zone, and the inhalation exposures. The program has been used to investigate the effectiveness of displacement ventilation on VOC removal in a small office by comparing the performance of displacement ventilation with three different types of mixing ventilation systems. Results show that displacement ventilation may not provide better IAQ than mixing systems if the VOC sources are distributed on the floor. Further, for the Type B source (wood stain) and sinks (gypsum board from four vertical walls) with displacement ventilation, simulation results show that the walls adsorbed significant amount of VOCs during the first hour and acted as secondary sources afterwards. As a result, the sink lowered the peak concentration by about 6% and elevated the concentrations after the peak time.

6.1 Introduction

In previous chapters, the emission characteristics of different building materials and the sorption of building materials have been studied. The ultimate goal of the study is to provide healthy and comfortable indoor environments. For this purpose, an integrated study of indoor air quality (IAQ), personal exposures, as well as thermal comfort in buildings is also required.

Thermal comfort is determined by the indoor air temperature, velocity, relative humidity, and radiant temperature for a certain activity and clothing level. IAQ and personal exposures are the results of the interaction of pollutant sources, sinks, air movement, and thermal conditions in buildings. Pollutant sources may be located in rooms, in the HVAC systems, or outside the buildings (by air supply or infiltration). Sinks may be located in the same locations. Sinks may also act as sources when the pollutants collected in the sinks are re-emitted.

Several IAQ models have been developed to predict indoor air pollutant concentrations. Molhave (1982) used the VOC emission rates of 42 indoor materials, measured in a test chamber, and he calculated the steady-state indoor air concentrations of pollutants originating from these materials. Neretnieks *et al.* (1993) developed a compartment model to describe the emission, sorption, and re-emission of VOCs from/to various building materials and furniture in a room. The compartment model assumes that the system to be modeled is represented by a number of compartments in contact with each other. Each object (*e.g.*, a wall) in the system consists of one or more compartments, and the concentration in each compartment is assumed to be uniform. Haghighat *et al.* (1994) numerically studied the IAQ in a newly painted partitioned office by using a CFD code

with the k-ε turbulence model. The emission source in the model was simulated by using the VB model (Guo and Tichenor, 1992). No sinks were considered in their study.

Based on the results of indoor contaminant concentrations, the models for exposure assessment of an individual or a population are also available. For example, Hayes (1989) developed a single compartment model for analysis of a population exposed to a wide range of indoor air pollutants. Sparks *et al.* (1991) developed another model, EXPOSURE, for analysis of individual (as opposed to population) exposure. The model can be used to provide guidance to individuals on reducing their exposure to pollutants from indoor sources. It can also provide individual guidance in the effectiveness of IAQ control options of specific situations. The existing IAQ and exposure models, although very useful for guiding policy analysis and individual or population risk assessment, are not suitable for detailed IAQ and exposure analysis due to the following two problems:

(1) The use of oversimplified or empirical models for emission sources/sinks

In previous chapters, we have demonstrated that, depending on the material type, material emissions and sorption are determined by many external (environmental) or internal (VOC or material properties) factors. Accurate modeling of emissions and sorption needs comprehensive mass transfer models. However, existing IAQ and exposure models use oversimplified (sometimes empirical) emission or sorption models. For example, Molhae (1982) transfers directly the emission rates measured from a small-scale chamber to buildings. EXPOSURE (Sparks *et al.*, 1991) uses the first-order decay model to represent all sources and a modified Langmuir model for sinks. Haghighat *et al.* (1994) uses the VB model for VOC emissions from paint. It has been shown in Chapter 3 that the VB model only applies to the initial period when evaporation dominates the emissions. The compartment model by Neretnieks *et al.* (1993) seems too coarse to simulate internal diffusion in building materials. The use of an inaccurate emission source or sinks models cannot provide accurate and reliable information for IAQ and exposure assessment.

(2) The use of the well mixing assumption

The type of mixing between the pollutants and the room air must be specified in an IAQ model. Because mixing is complex, the existing models usually use simplifying assumptions, such as the well mixing assumption. While this assumption may be acceptable in some circumstances, it may not be generalized in buildings. Concentrations can vary spatially within the rooms of a building due to the distributions of contaminant sources, sinks, the placement of fans, location and discharge characteristics of supply or exhaust openings, internal barrier to air flow, and thermal gradients in the room, etc. Many researchers have measured or calculated the non-uniform contaminant distributions in a room (*e.g.*, Haghighat *et al.*, 1994; Brohus, 1997; Yang *et al.*, 1998a, 1998b). For an IAQ study, failure to account for the possible incomplete mixing may result in an inaccurate estimation of the actual VOC distributions and hence the exposures in buildings. Further, mixing may also affect the emission or sorption rates by building

materials. This problem will be more pronounced for "wet" sources because the local VOC distributions affect the mass transfer rate at the material-air interface.

The above review indicates that current IAQ studies usually employ significant and sometimes unrealistic simplifications to the emission sources, sinks and mixing conditions. Given that a wide variety of emission sources and sinks may co-exist in buildings, a simple IAQ analysis as such is useful for a quick approximation of the IAQ levels in buildings. On the other hand, indoor environment design requires a more accurate IAQ model. The model should remedy the gaps in existing models while keeping the computational cost within a reasonable range. In this chapter, we combine the emission and sorption models developed in Chapters 3 - 5 for a detailed study of IAQ and exposure in buildings. The study is conducted for a model room with different emission sources, sinks, and ventilation systems. The results can provide designers with detailed information for selecting appropriate ventilation systems and analyzing IAQ.

6.2 Model for IAQ Studies

Similar to the study of emission sources or sinks, the IAQ study also solves the conservation equations of continuity, momentum, energy, and VOC concentrations in both room air and the material side. However, an IAQ model is more complicated than an emission or sorption model because of several reasons. First, a room usually contains several emission sources and sinks. Interactions among these sources and sinks must be considered simultaneously. Second, the flow and thermal conditions in a building are far more complicated than those in a standard test chamber. The results presented in previous chapters have shown that room air (airflow and temperature) can play an important role on material emissions, sorption, and VOC transport in buildings.

Therefore, all the emission sources, sinks, and their interaction with room air need to be combined in an IAQ study to predict the time history of pollutant concentrations in a room. The predictions of the concentration results are then used by an exposure model to predict individual exposures. An IAQ model is a combination of:

- A room air model
- Material emission models
- Material sorption models
- An exposure model

6.2.1 The room air model

Previous studies have shown that simulating room air and the air phase VOC transport usually takes major computing time for an emission or sorption study. This is also true for IAQ simulations because an IAQ study in buildings is a 3-D transient problem. Hence, the room air model must be computationally effective.

Most indoor airflows involve all three types of convection: forced, natural, and mixed (a combined forced and natural). For example, the flow from an air diffuser with the same temperature as the room air is forced convection and the thermal plume around a person is natural convection. In a typical air-conditioned room with equipment (computers, etc.) or exterior hot/cold walls or windows, the airflow is mixed convection. Mixed convection is more complicated than forced convection and natural convection since it combines the complexity of both. In order to simulate room airflow that is most turbulent, a suitable turbulence model is needed so that the flow can be simulated with currently available computer capacities.

Many turbulence models are available for different types of flow. The "standard" k-ε model (Launder and Spalding, 1974) is widely used but sometimes provides poor results for indoor airflow and heat transfer. To consider the low-velocity and buoyant characteristics of room airflow, many researchers have employed low-Reynolds-number (LRN) turbulence models that consider the damping effects (Blay et. Al., 1992; Chen, 1995; Murakami *et al.*, 1996). Some researchers have used more advanced turbulence models, such as the Reynolds-stress models (RSM) (Peeters and Henkes, 1992; Chen, 1996) for indoor airflow simulation. It is well known that LRN turbulence models demand fine grids near walls and raise computing costs significantly. A non-steady, three-dimensional airflow calculation by a LRN model requires a computing capacity close to that of the Large Eddy Simulation (LES). Using more advanced models such as RSMs in a similar case requires very high computing capacity, since in addition to considering LRN effects, RSMs must solve many differential equations simultaneously. Further, Chen (1996) pointed out that RSMs do not perform much better than the standard k-ε model but they have a much higher computing cost.

In order to solve the above problem, recently Xu (1998) developed a new two-layer turbulence model. The two-layer model uses a one-equation (k) model for the near wall region and the "standard" k-ε model in the outer region. The near wall models have been developed with the aid of the data of natural and forced convection flows by Direct Numerical Simulation (DNS). Studies show that the two-layer model can predict airflows most accurately, better than many k-ε models. The computing cost is significantly lower than that of the LRN k-ε models and is only slightly higher than that of the "standard" k-ε model. Hence, in our IAQ study, we use the new two-layer model. Details of the model are given by Xu (1998).

6.2.2 The emission source models

The behavior of sources plays a major role in determining the indoor concentration as a function of time. Generally, sources can be divided into three categories:

(1) Constant sources such as moth cakes
(2) Slow decaying sources such as many dry materials
(3) Quick decaying sources such as "wet" materials

Chapters 3 and 4 give details of the emission models for these materials.

6.2.3 The material sorption models

Indoor sinks can also play an important role in determining indoor pollutant concentrations. The significant impact of sinks is that they become sources when the original pollutant source is removed or when the strength of the original source drops below some value. These sinks may be reversible or irreversible. In our study, only reversible sinks that can re-emit all the VOCs collected are considered.

Chapter 5 discusses two types of sinks models: the sorption isotherm models (*e.g.*, the Langmuir model) and the new sorption model we developed. The sorption isotherm models assume that sorption is confined to the material surface and ignore the internal diffusion inside the sink material, while the latter considers internal diffusion. Since most building materials are permeable sinks, they will be considered in this study. Chapter 5 gives the new sorption model developed for those materials and Chapter 3 shows the method to incorporate the sorption model into a numerical program.

6.2.4 The exposure model

The personal exposures are determined by both the indoor pollutant concentrations and the way the concentrations affect an occupant. Because the most common route for exposure to indoor air pollutants is by inhalation, it is convenient to use inhalation exposure given by Sparks (1991):

$$E_i = C(\tau)bv \tag{6.1}$$

where
E_i = inhalation exposure, mg/h
$C(\tau)$ = pollutant concentration at time τ, mg/m^3
b = breathing rate, breath/hour
v = volume per breath, m^3/breath

The exposure defined by Eq. (6.1) is instantaneous, *i.e.*, the exposure at any instant time, τ. The cumulative inhalation exposure between time τ_1 and τ_2 is:

$$E_{ic} = \int_{\tau 1}^{\tau 2} C(\tau)bv d\tau \tag{6.2}$$

For exposure by mechanisms other than inhalation, the instantaneous exposure, E, to a pollutant at time τ is the concentration, $C(\tau)$, in the room with the person at time τ:

$$E = C(\tau) \tag{6.3}$$

Similarly, the cumulative exposure from τ_1 to τ_2 is given by:

$$E_c = \int_{\tau 1}^{\tau 2} C(\tau) d\tau \tag{6.4}$$

In order to determine the time a person is exposed to the concentration, the individual's activity pattern is also required. An activity pattern is defined by the time a person enters and leaves the building (Sparks, 1991).

The IAQ model proposed above is suitable for the detailed study of material emission, sorption, and their impact on IAQ. Based on the model, a computer program, ACCESS-IAQ (A Code for Characterizing Emission Sources, Sinks, and Indoor Air Quality), has been developed by us (Appendix). The program can be used for the following purposes:

(1) Study the VOC emissions from different types of building materials ("wet" or dry materials). The model inputs are the flow and thermal boundary conditions and material properties (*e.g.*, diffusion coefficient and partition coefficient).

(2) Study the VOC sorption by building materials.

(3) Study the combined problem of indoor air flow, thermal comfort, IAQ, and exposures. The computer code allows the user to select the appropriate turbulence models and treat the mass transfer near a solid wall in different ways (*e.g.*, the use of wall functions), and specify multiple sources and sinks.

(4) Evaluate the effects of different ventilation systems on VOC removal and exposures.

The following section describes the results of a numerical study of IAQ in a room with different ventilation systems.

6.3 Case Study

Our case study is about VOC removal in a small office with sources and sinks from the interior building materials. The effectiveness of a displacement ventilation and two mixing ventilation systems on VOC removal is evaluated by comparing the VOC concentrations and personal exposure at the breathing level in the room. The effects of sinks on IAQ and exposure will also be quantitatively studied.

6.3.1 Configuration and flow conditions of the model room

The full-scale environmental chamber built at Massachusetts Institute of Technology will be used as the model room. The 5.16 m × 3.65 m × 2.44 m room, shown in Figure

6.1, is assumed to be occupied by two persons and equipped with two tables, two computers, two file cabinets and six overhead lights. A 3.65 m × 1.04 m window was mounted on the wall connecting the office to another room where the temperature was controlled to simulate outdoor conditions. All other walls were insulated to minimize the heat gain/loss.

Each occupant in the test room was simulated by a box, 0.4 m long, 0.35 m wide, and 1.1 m high, heated by three light bulbs. The supply air temperature was controlled at 17.0 °C. Other temperatures of the interior surfaces were measured and given by Chen *et al.* (1998). The window surface temperature was 27.3 - 28.1 °C (for summer condition). The surface temperature on the floor was a fixed 23.5 °C. Surface temperatures on the other walls were 23.3 - 26.6 °C. The internal heat sources and the ventilation rate are listed in Table 6.1.

Table 6.1 Specification of the internal heat sources and ventilation rate of the model room.

Type	**Area (m^2)**	**Person (number)**	**Equipment (W/m^2)**	**Lighting (W/m^2)**	**Total internal load (W/m^2)**	**Ventilation rate (ACH)**
Small office	18.8	2	14.9	10.8	33.7	4

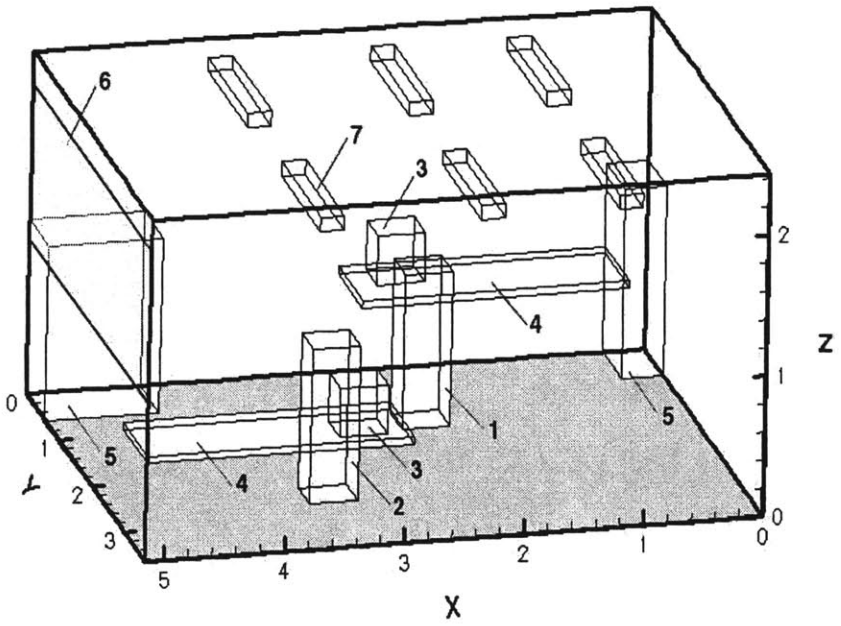

Figure 6.1 Configuration of the model office. 1 = occupant 1; 2 = occupant 2; 3 = computers; 4 = tables; 5 = furniture; 6 = window; 7 = lights.

The above configuration was taken after an experimental setup by Chen *et al.* (1998). They used the above experimental setup and CFD technique to generate a database and develop design guidelines for the so-called displacement ventilation system. Unlike a traditional mixing ventilation system, displacement ventilation supplies fresh air directly to the occupied zone with low velocity and large volume. When the cold air meets with a heat source like a person, an upward plume is generated and the plume can bring the contaminant directly to the exhaust without mixing with the room air. In this way, the IAQ in the room could be improved. Chen *et al.* (1998) studied the displacement ventilation system in detail and demonstrated its capabilities to improve IAQ and also reduce energy consumption in buildings. However, the study assumed that the contaminant sources were associated with a heat source. While this is true in circumstances where contaminants are mainly generated by occupants or equipment, it may not be generalized to building material emissions because many VOC sources are not associated with heat sources. It is important to evaluate the effectiveness of displacement ventilation under such conditions. On the other hand, different types of mixing ventilation systems are still popular. It is necessary to compare the performance of displacement ventilation with different mixing ventilation systems in terms of VOC removal in buildings. Hence, the objectives of the case study are:

(1) To evaluate the effectiveness of displacement ventilation for VOC removal when VOC sources are distributed on the floor and not associated with heat sources.

(2) To compare the performance of displacement ventilation with different types of mixing ventilation for VOC removal and exposures.

6.3.2 Simulation cases

To achieve the objectives mentioned above, we designed a series of simulation cases for IAQ study. The cases use different emission sources, sinks, and ventilation systems, as will be specified below.

Internal VOC sources:

- Type A: A source with constant flux. The source represents constant or slow decaying sources such as the SBR carpet studied in Chapter 4. The source flux of 1.0 mg/m^{2}s, is assumed to distribute throughout the entire open area of the floor (area 17.714 m^2).

- Type B: A wood stain applied to the oak substrate as studied in Chapter 3. The source represents "wet" materials applied to a realistic substrate. The wood stain is also distributed on the open area of the floor (area 17.714 m^2). A total of 1.331 kg of wood stain is applied to have a same film thickness as that of the reference case (Case1-2b) tested in the small-scale chamber (see Chapter 2). The physical properties of the wood stain are given in Table 3.7 of Chapter 3.

VOC sinks:

- No sinks in the room.

- Sinks on the four vertical walls in the room. The sinks are the unpainted gypsum board as studied in Chapter 5. Since the dominant VOC from the wood stain is decane, the diffusion coefficient $D_m=5.67\times10^{-12}$ m^2/s and partition coefficient $K_{ma}=8652$ (calculated by Eqs. (5.29) and (5.30)) are used for TVOC. The total sink area is 43 m^2.

Ventilation systems:

- Displacement ventilation: supply from a displacement diffuser on the rear-wall (opposite to the window) near the floor and exhaust on the ceiling (Figure 6.2).

- Mixing type I: supply from two four-way diffusers on the ceiling and exhaust from a rear-wall grille near the floor (Figure 6.3).

- Mixing type II: supply from two linear diffusers on the ceiling and exhaust from a rear-wall grill near the floor (Figure 6.4).

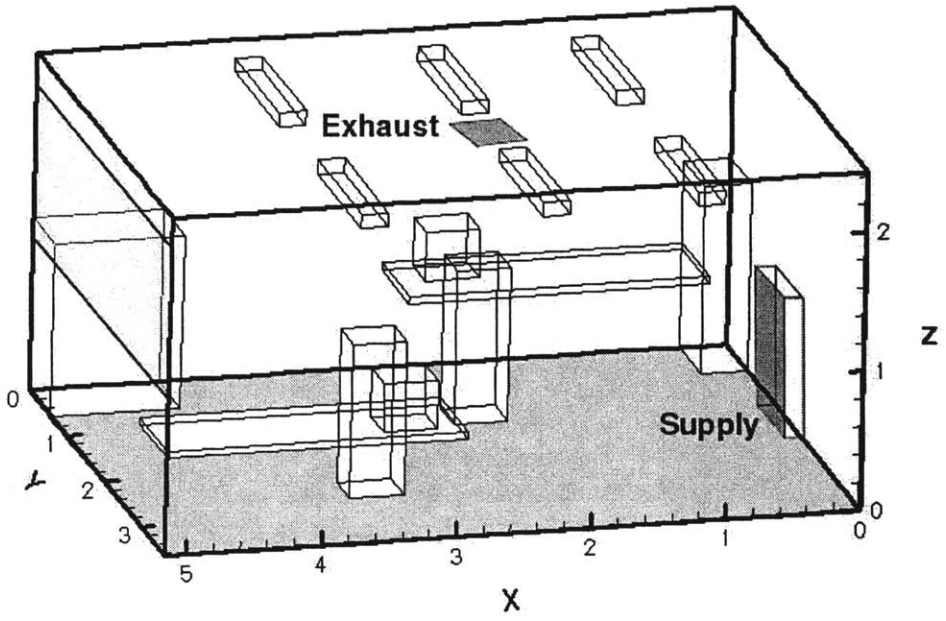

Figure 6.2 Schematic of the model office with displacement ventilation.

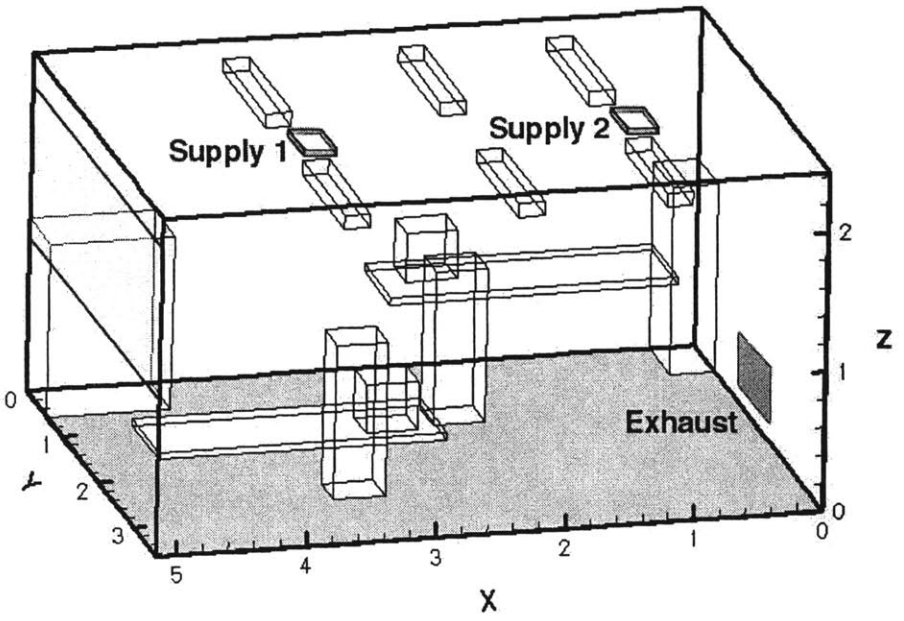

Figure 6.3 Schematic of the model office with mixing ventilation type I (supply from two four-way diffusers on the ceiling and exhaust from a rear-wall grill near the floor).

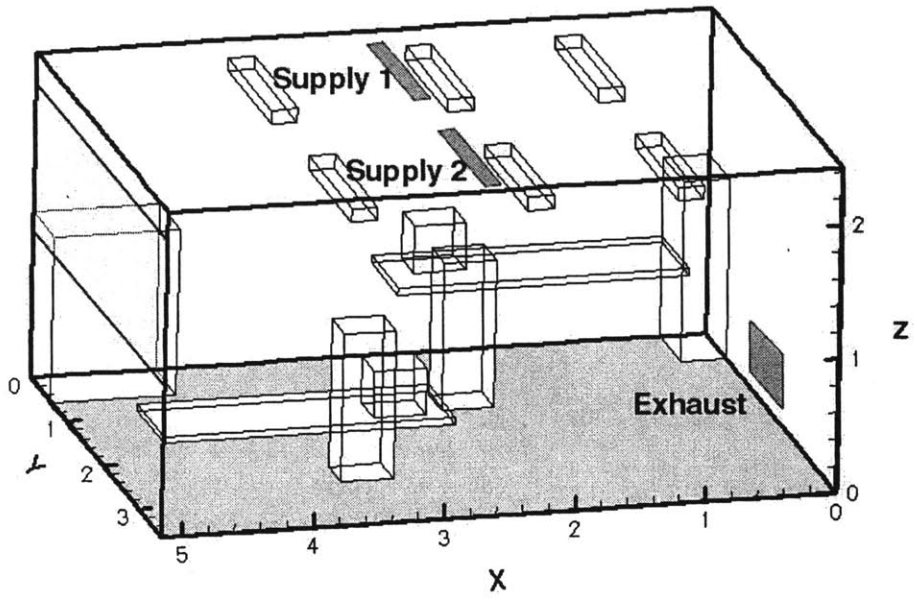

Figure 6.4 Schematic of the model office with mixing ventilation type II (supply from two linear diffusers on the ceiling and exhaust from a rear-wall grill near the floor).

The study is geared for the selected combinations of the above sources, sinks, and ventilation systems. Table 6.2 lists a total of 7 cases simulated. Among those, Cases 1 to 3 compare the performance of different ventilation systems on VOC removal for the type A source without sinks. Cases 4 to 6 are for type B source with sinks. Case 7 further examines the sink effect by comparing the results with those of Case 4.

Table 6.2 Cases for IAQ studies in the small office.

Case Number	Source type	Sinks	Ventilation system
1	A (constant flux)	No	Displacement
2	A (constant flux)	No	Mixing type I
3	A (constant flux)	No	Mixing type II
4	B (wood stain + oak)	Gypsum board	Displacement
5	B (wood stain + oak)	Gypsum board	Mixing type I
6	B (wood stain + oak)	Gypsum board	Mixing type II
7	B (wood stain + oak)	No	Displacement

6.3.2 Results and discussion

6.3.2.1 The flow field

It has been pointed out that both airflow and temperature may affect material emissions, sorption, and IAQ. They should be accurately predicted. However, temperature is not a concern for the cases in Table 6.2 because the temperatures of both the emission source and sinks are close to constant (23.5 °C). Hence, only the results of air flow field will be given.

Among the three ventilation systems (displacement and two mixing), Xu (1998) simulated the air velocity and temperature distributions for the displacement ventilation case by using the two-layer turbulence model. The simulated results agree well with the measured airflow patterns (using smoke), velocity and velocity fluctuation (using hot sphere anemometers), and temperature (using thermal-couples). The velocity vectors at two sections, one at the room center (y = 1.83 m) and the other across the occupant 1 (y = 1.03 m) for the displacement ventilation system are shown in Figure 6.5. At the room center, cold air from the supply diffuser spreads on the floor level and induces a reverse flow in the layer between 0.5 m and 1.0 m above the floor. Figure 6.5(b) shows the thermal plume generated by the occupant. The plume entrains air from both the floor level and the recirculated area (about 1.0 m above the floor).

Predicted velocity vectors for the two mixing ventilation systems are given in Figures 6.6 and 6.7, respectively. For mixing type I (use of two four-way diffusers on the ceiling), a

jet flow with high velocity is found near the diffusers. The jet flow generates recirculation between the two diffusers. Due to the cold downward flow from the diffusers, the upward plume by the occupant is very weak. For mixing type II, cold air from the two linear diffusers reaches directly to the floor level. As a result, there is no upward plume on the left side of the occupant. Also for mixing type II, the cold air near the occupant may cause a draft problem, which is unfavorable in terms of thermal comfort.

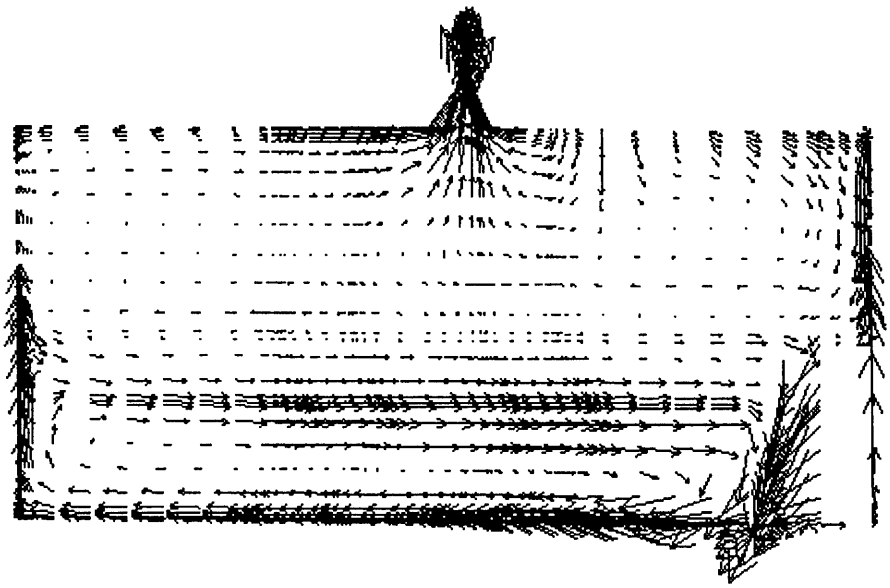

(a)

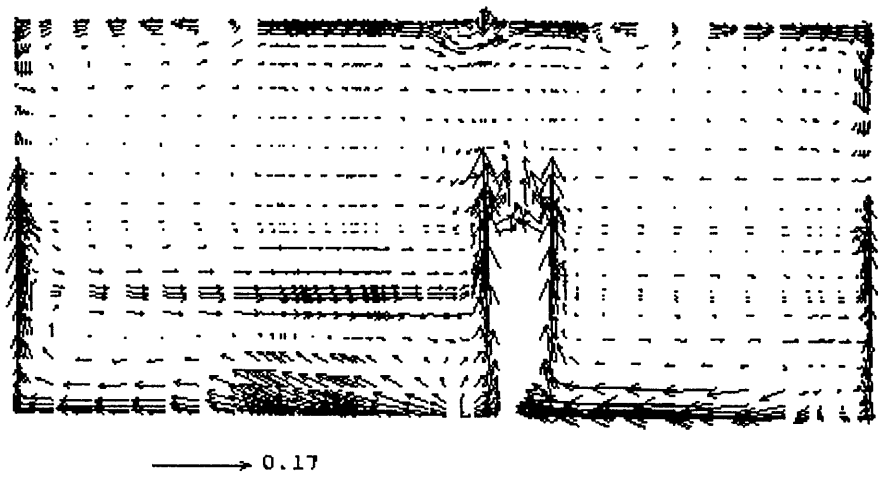

(b)

Figure 6.5 Predicted velocity vectors for displacement ventilation: (a) room center (y = 1.83m), (b) across occupant 1 (y = 1.03m).

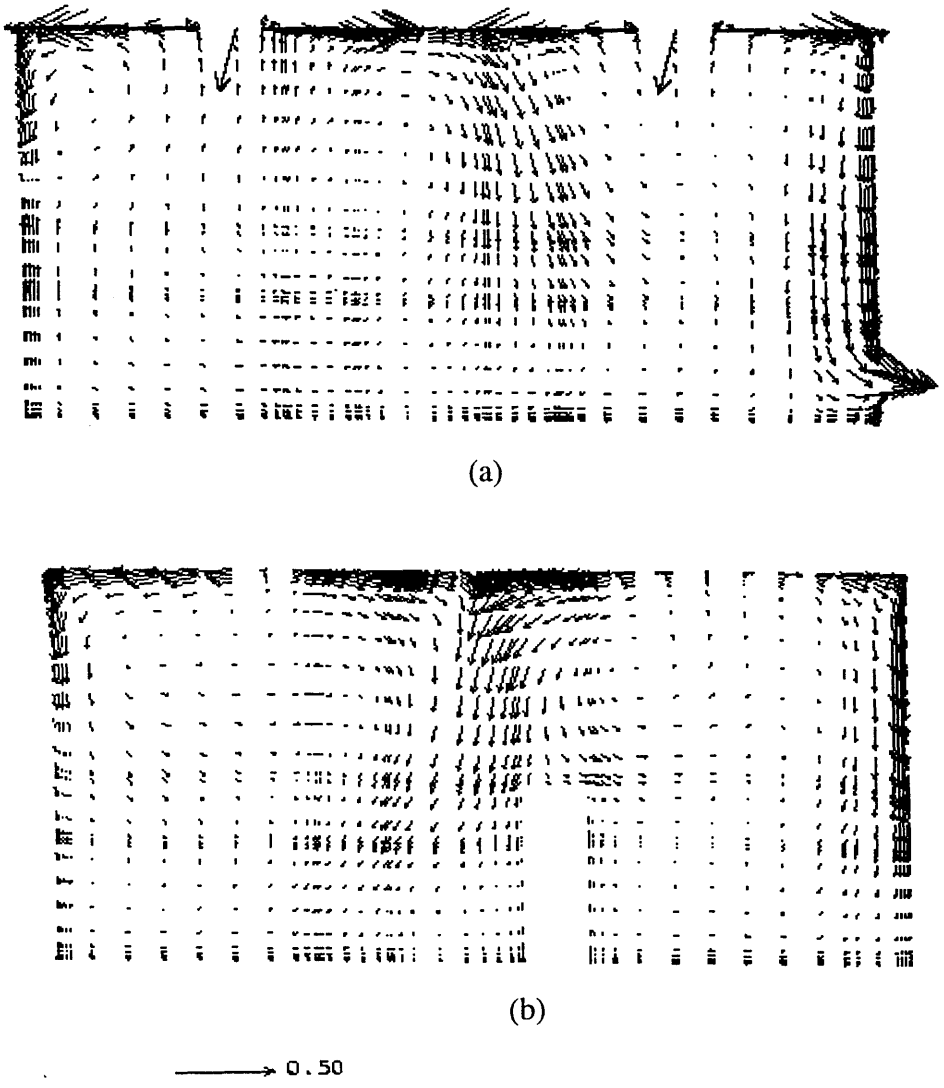

Figure 6.6 Predicted velocity vectors for mixing ventilation type I: (a) room center (y = 1.83m), (b) across occupant 1 (y = 1.03m).

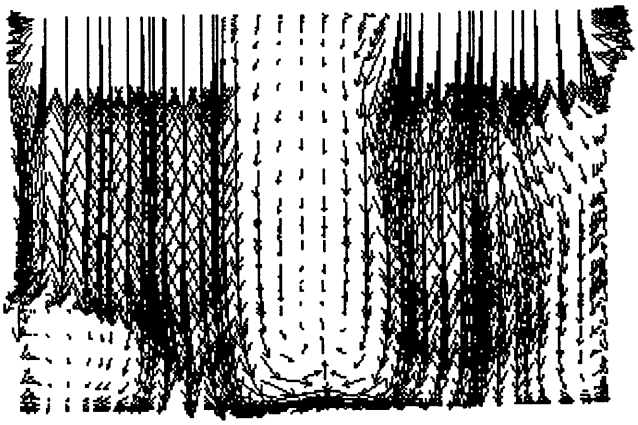

(a)

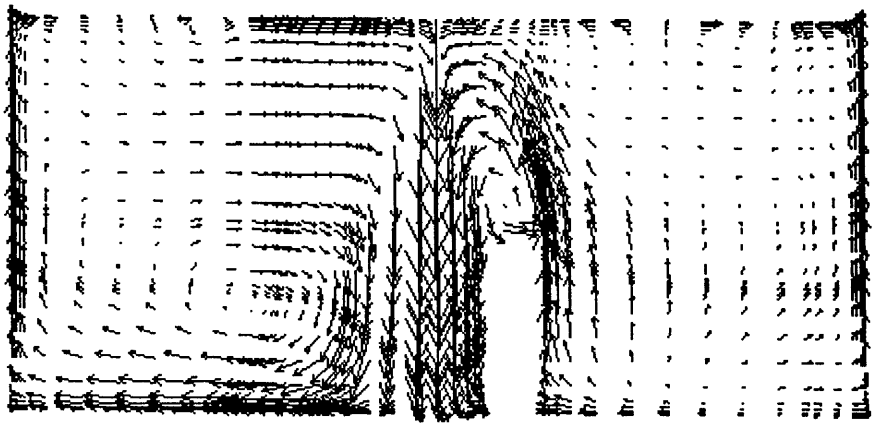

(b)

Figure 6.7 Predicted velocity vectors for mixing ventilation type II: (a) across the supply diffusers (x = 2.5m), (b) across occupant 1 (y = 1.03m).

When the three different ventilation systems are compared, the major part of the displacement ventilation is a horizontal flow. Mixing type I has an irregular flow pattern while mixing type II has a generally downward flow toward the floor. These different airflow patterns may exert an influence on the contaminant distributions and personal exposure. This will be further investigated in the subsequent section.

6.3.2.2 VOC concentration for type A (constant flux) source without a sink

Since ventilation systems may affect both emissions (particularly from "wet" sources), sorption, and VOC transport, evaluation of the VOC concentrations using a constant source without a sink helps us understand the impact of a ventilation system on VOC transport alone.

Figure 6.8 illustrates the vertical VOC distributions in front of occupants 1 and 2, at the room center, and the average VOC concentrations at each horizontal plane with the three ventilation systems. The two mixing systems have relatively uniform distributions in the vertical (z) direction, with differences in concentration between different locations (*e.g.*, occupants 1 & 2). Mixing type I has a higher concentration than mixing type II.

The displacement ventilation system has a larger concentration stratification in the z direction, and the concentrations are also more sensitive to different locations. For displacement ventilation, concentrations near the floor (source) are very high. Then the concentrations quickly drop to their minimum values at the height of about 0.1 - 0.2 m, due to the direct supply of fresh air to the lower region of the room. The concentrations then increase with the height and form a vertical stratification. For both occupants 1 and 2, the peak concentration of VOC occurred at the ceiling level. At the room center, however, the peak occurred at about 1.0 m. This may be due to the backward flow (see Figure 6.5) that entrained the contaminant back to this region. The average concentration also has a peak at about 1.0 m above the floor level.

From the IAQ point of view, the VOC concentrations at the breathing level (about 1.0 m from the floor) is of particular interest. For the three different locations and room average shown in Figure 6.8, mixing type I and displacement ventilation both have considerably higher concentrations at the breathing level than mixing type II. Apparently, the latter benefits from a favorable downward flow of air so the pollutants have less chance to be transported to the breathing zone.

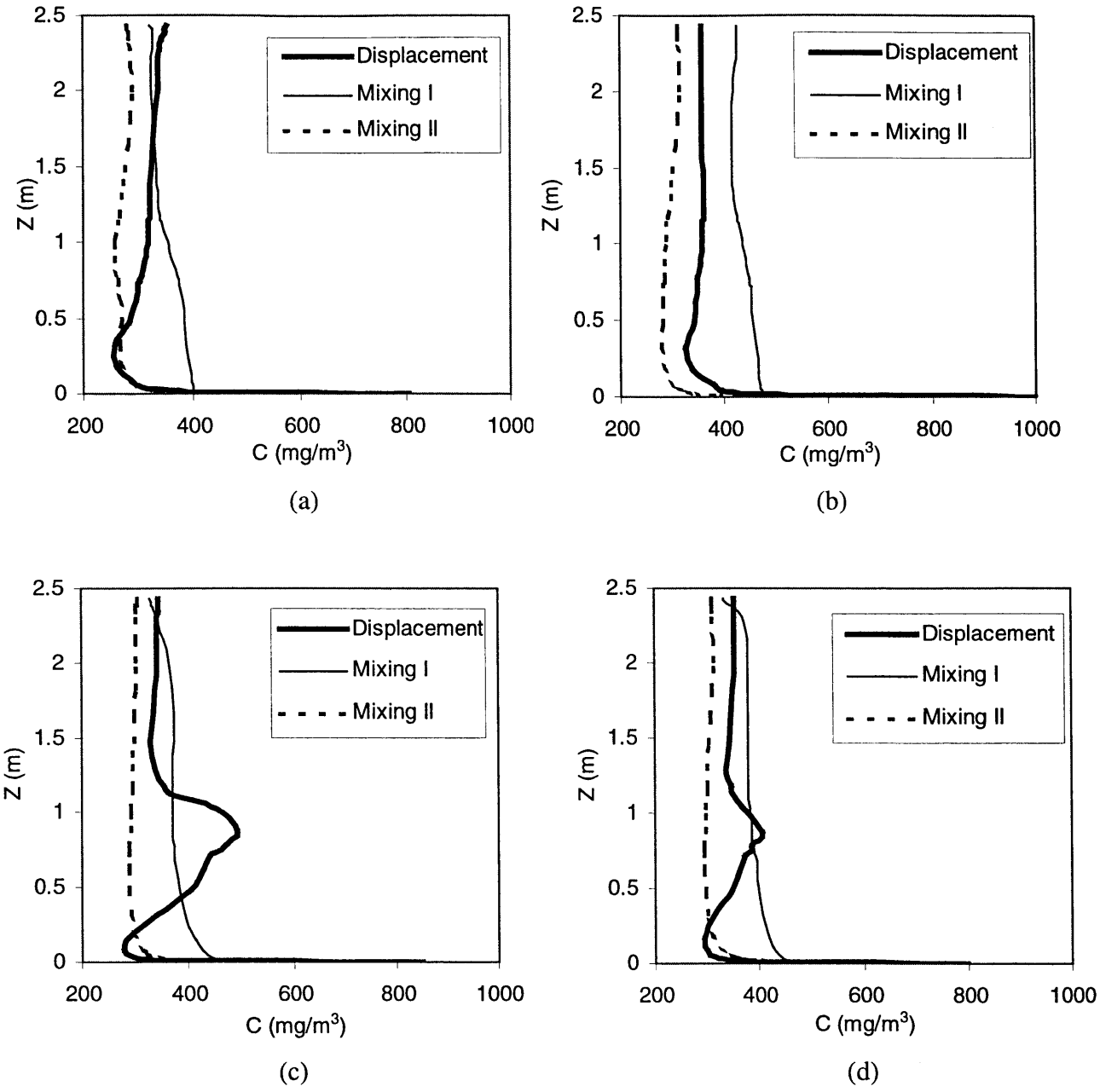

Figure 6.8 Comparison of vertical VOC distributions with a constant emission (type A) source in the floor without a sink: (a) Occupant 1, (b) Occupant 2, (c) Room center, (d) Room average

6.3.2.3 VOC concentration and exposure for type B (wood stain and oak) source with sinks (gypsum boards)

The above results show that even with the same emission source rate, the IAQ of different ventilation systems is significantly different. Now we move a step forward to the type B source with sinks, which represent a scenario closer to a real room.

Unlike the type A source, the emissions, sorption, and VOC concentrations for type B source and sinks are time-dependent. The history of concentrations at the breathing level during the first four days after the wood stain is applied is presented in Figures 6.9 to 6.11. The VOC concentrations at different locations (Occupants 1 & 2, room average) first increase rapidly and reach a peak in about 0.5 hour. After that, the concentrations begin to decay. For all the four ventilation systems, the VOC concentrations at the three locations drop from the peak value of 1500 - 3000 mg/m^3 to lower than 2 mg/m^3 four days after the wood stain is applied.

Figures 6.9 to 6.11 also compare the relative VOC concentrations among the three ventilation systems. For occupants 1 and 2, mixing type I (use of two four-way diffusers on the ceiling) generates the highest VOC concentration, while mixing type II (use of two linear diffusers on the ceiling) generates the lowest concentration during the 96 hours period. The average concentration at the breathing level (z = 1.0 m) follows the same trend. This again indicates that mixing type II is preferred over mixing type I or displacement ventilation for better IAQ.

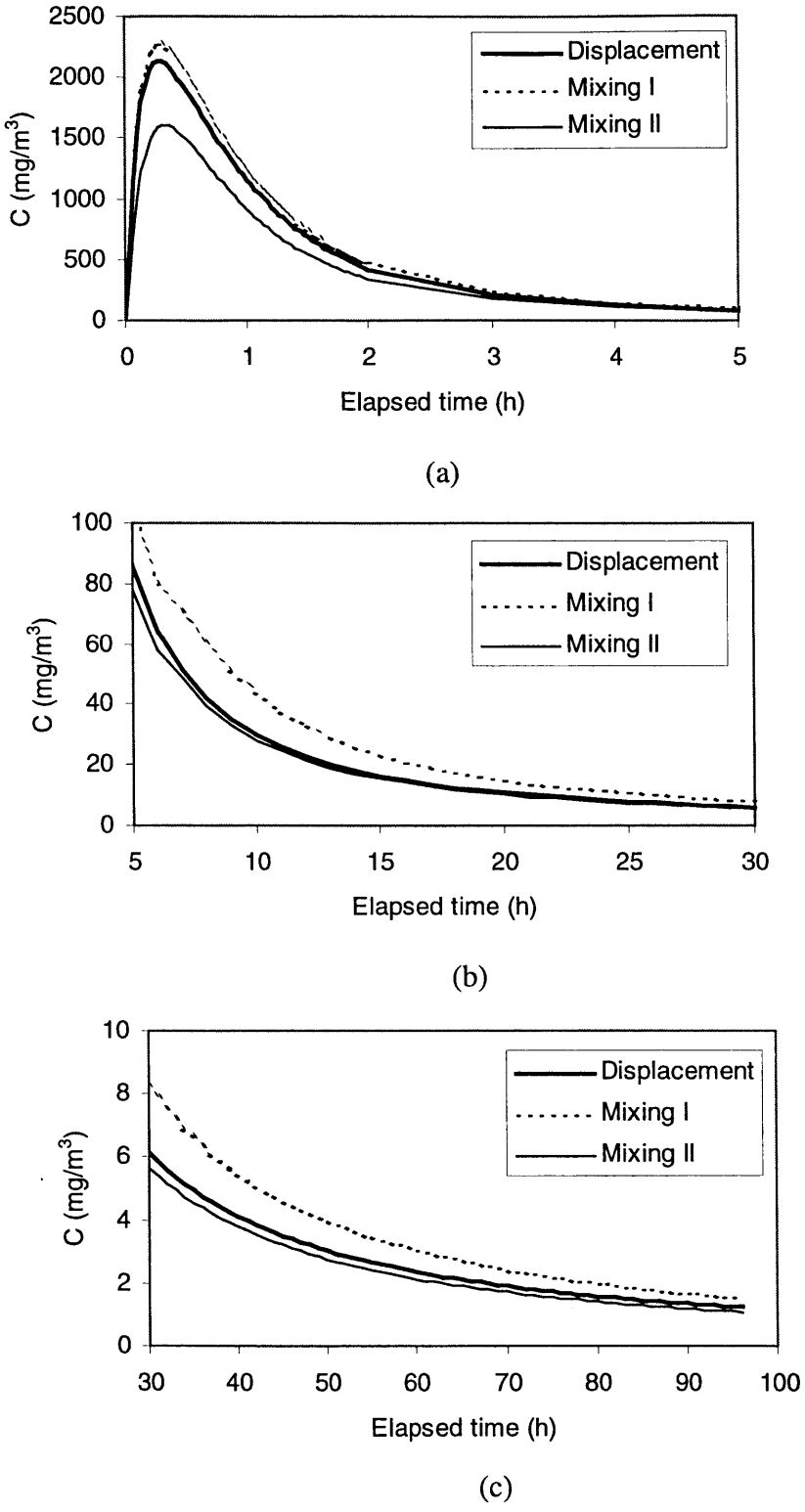

Figure 6.9 Predicted VOC concentrations at the breathing level for occupant 1 for type B source (wood stain and oak) from the floor and sinks (gypsum board) from the vertical walls: (a) 0 – 5 h, (b) 5 – 30 h, (c) 30 – 96 h.

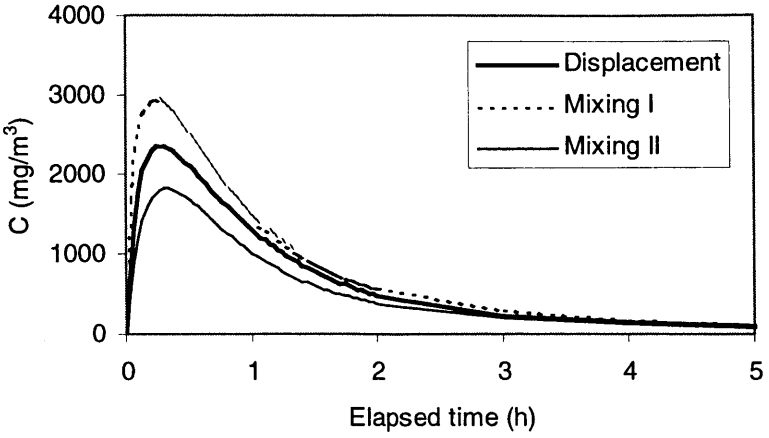

(a)

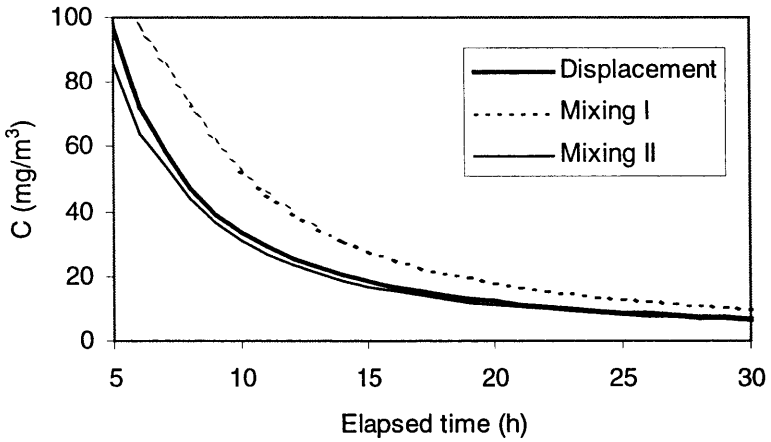

(b)

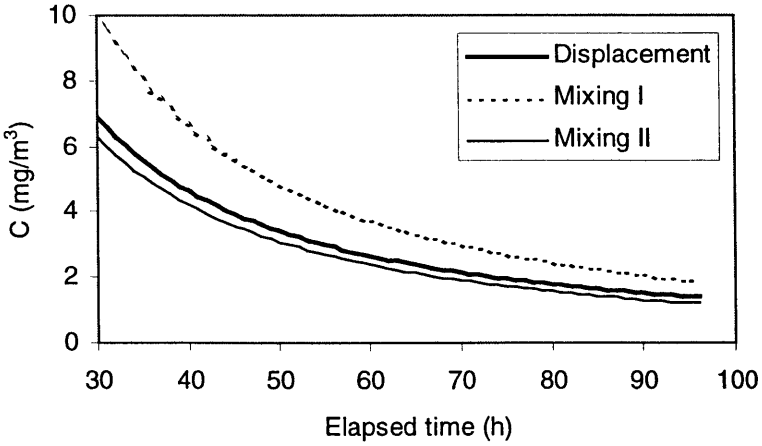

(c)

Figure 6.10 Predicted VOC concentrations at the breathing level of occupant 2 for type B source (wood stain and oak) from the floor and sinks (gypsum board) from the vertical walls: (a) 0 – 5 h, (b) 5 – 30 h, (c) 30 – 96 h.

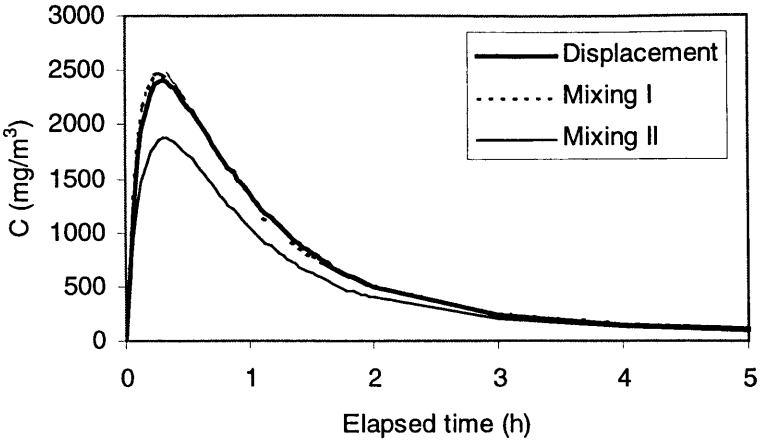

(a)

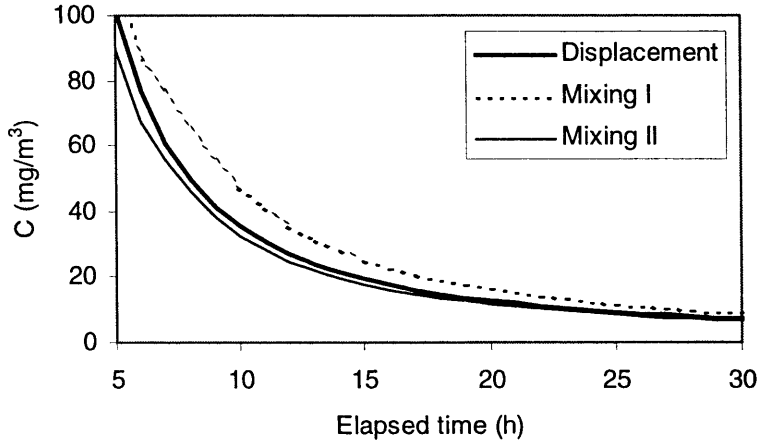

(b)

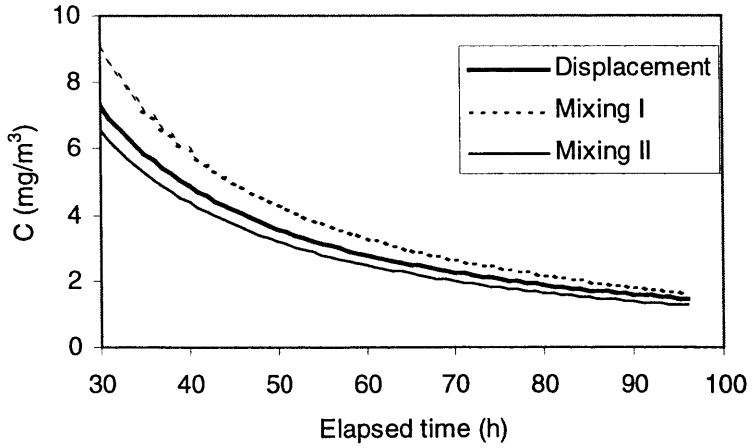

(c)

Figure 6.11 Predicted VOC concentrations at the breathing level of room average for source type B (wood stain and oak) from the floor and sinks (gypsum board) from the vertical walls: (a) 0 – 5 h, (b) 5 – 30 h, (c) 30 – 96 h.

It is useful now to consider the health effects due to the presence of the VOCs in this office. Andersson *et al.* (1997) reviewed numerous human experimental investigations in which subjects were exposed in exposure chambers to VOC mixtures or individual VOCs. The experimental investigations found that odors are significant at TVOC concentrations of 3 to 25 mg/m^3, and irritation to eyes, nose, and mouth at TVOC concentrations of 5 to 25 mg/m^3. Using 3 mg/m^3 as the odor threshold and 5 mg/m^3 as the irritation threshold, TVOC concentrations during the first 10 hours are about 8 to 600 times higher than the irritation threshold. Obviously, a significant health effect will result if a person stays in the room during this period. However, due to the decay of the emission source, VOC concentrations will finally decay to the values below the irritation or odor thresholds. The results show that about 57, 65 and 53 hours are required for displacement ventilation, mixing type I, and mixing type II, respectively, to reduce the average TVOC concentrations in the breathing zone below the odor threshold (3 mg/m^3). In other words, the room air is not healthy before being ventilated for these periods.

The VOC exposures can further be obtained based on the time-dependent VOC concentrations in the room. Figure 6.12 gives the cumulative inhalation exposures for occupants 1 and 2, assuming these occupants stay in the room 24 hours per day. The results show that displacement ventilation generates lower VOC exposures than mixing type I (use of two four-way diffusers on the ceiling), but higher exposures than mixing type II (use of two linear diffusers on the ceiling).

Figure 6.13 compares the daily accumulated exposure for occupant 1. The results show that a significant portion of the exposure comes from the first day when the emission rates and room VOC concentrations are very high. To avoid excessive exposure, the activity pattern of the occupants is now assumed to change to 10 hours of stay (9 am – 7 pm), starting from the second day (the ventilation system still operates 24 hours/day). Figure 6.14 shows that the exposures decrease by a factor of 20 - 30. A comparison of the daily accumulated exposure for occupant 1 is given in Figure 6.15. Note that, displacement ventilation now generates considerably lower exposure than mixing types I and slightly higher exposure than mixing type II.

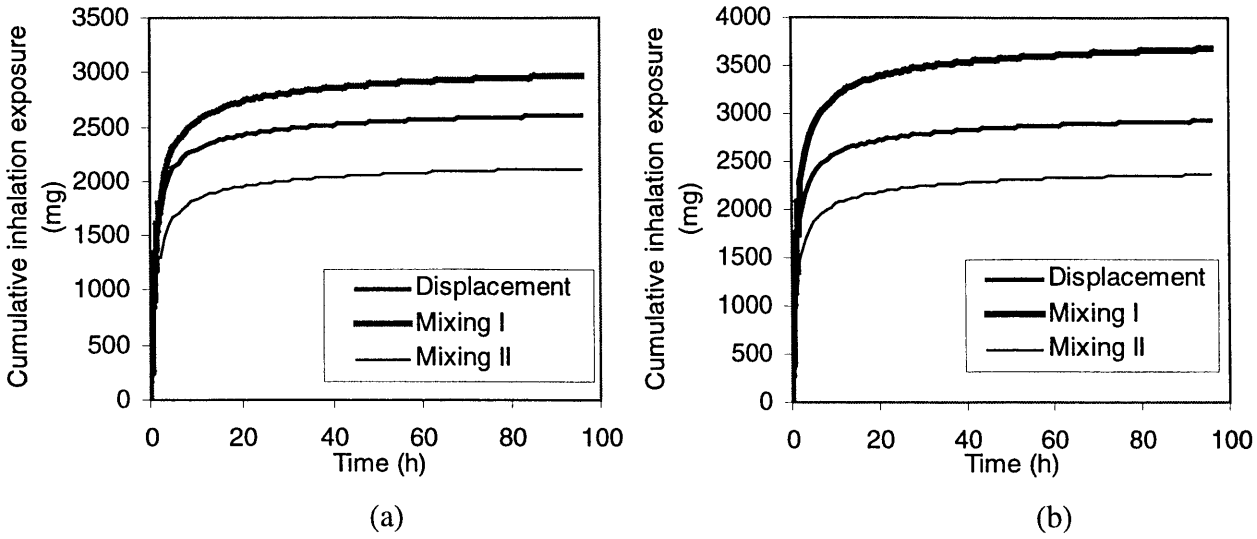

Figure 6.12 Cumulative inhalation exposures for the occupants, assuming the occupants stay 24 hours a day: (a) Occupant 1, (b) Occupant 2.

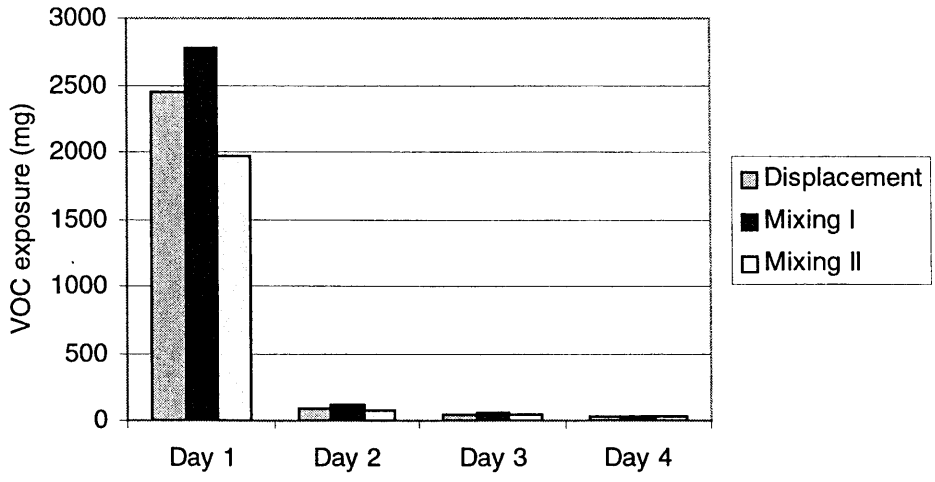

Figure 6.13 Daily cumulative VOC exposures for occupant 1, assuming the occupant stays 24 hours a day.

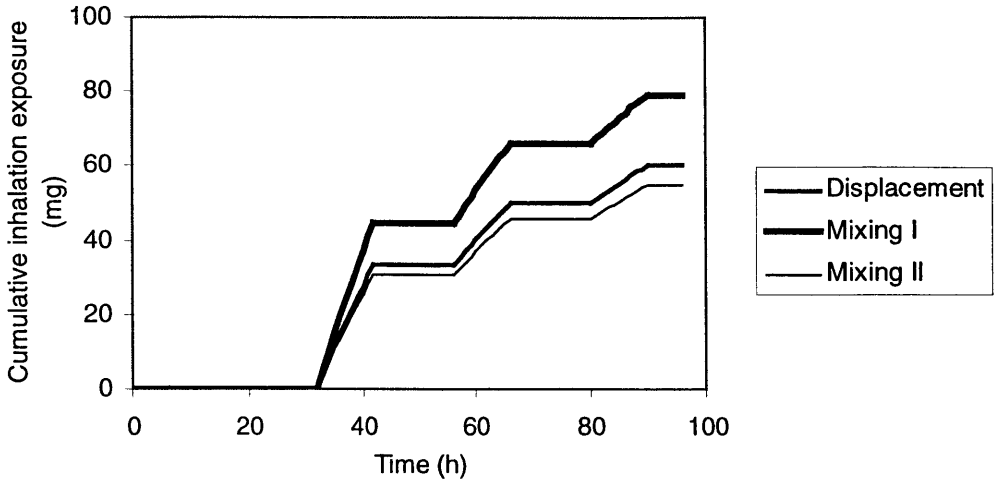

Figure 6.14 Cumulative inhalation exposures for occupant 1, assuming the occupant stays 9 am – 7 pm, starting from the second day.

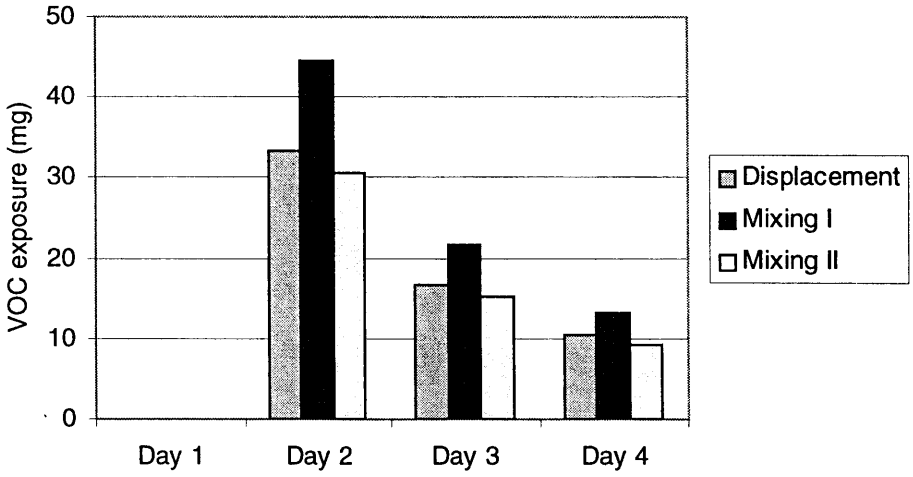

Figure 6.15 Daily cumulative VOC exposures for occupant 1, assuming the occupant stays 9 am - 7 pm, starting from the second day.

6.3.2.4 Analysis of type B source and the sinks and their impact on IAQ

The emission sources, sinks, and the ventilation systems all contribute to the VOC concentration in the room. Figure 6.16 compares the history of the VOC emission rates from the type B source (wood stain). The results show that mixing type I has the highest initial emission rate, followed by mixing type II, and displacement ventilation has the lowest value. The order is reversed after about 0.5 hour for about three days. After three days there are then no noticeable differences among the three ventilation systems. The results reflect that mixing type I generates a higher gas phase mass transfer coefficient on the floor than the other two ventilation systems. As indicated in Chapter 3, the gas phase mass transfer coefficient is determined by combined factors of air velocity, turbulence, and flow direction near the surface of the emission source exerted by the ventilation systems.

In addition to influencing the VOC emission rates from the source, different ventilation systems can also affect the sorption rate of the sinks. Figure 6.17 compares the simulated sorption rates by the four walls in the model room. A negative value of the sorption rate means that there is uptake of VOCs by the sinks, whereas a positive one means a release of VOCs from the sinks. The results indicate that the walls adsorbed significant amounts of VOCs during the first hour when the VOC concentrations in the room are high. After that, the walls begin to release VOCs and acted as a secondary source.

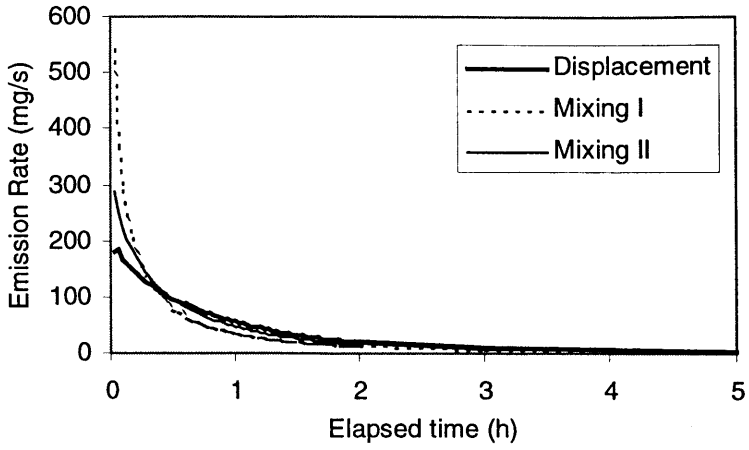

(a)

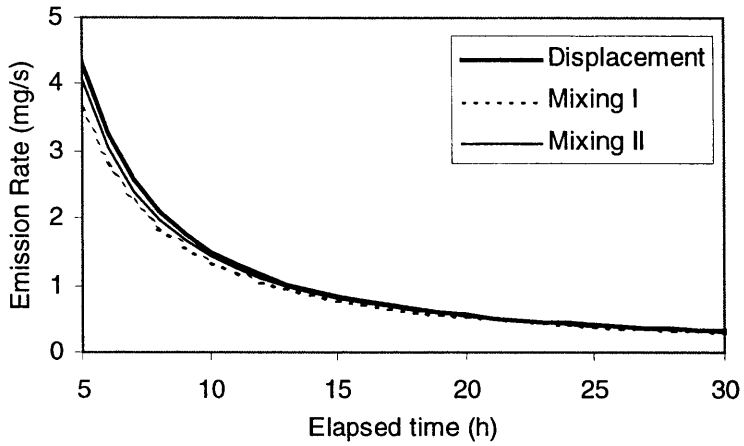

(b)

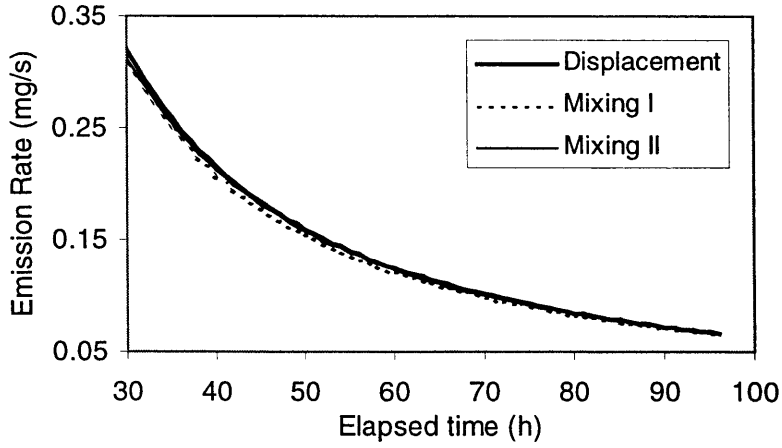

(c)

Figure 6.16 Predicted TVOC emission rates from the type B source (wood stain and oak) under different ventilation systems: (a) 0 – 5 h, (b) 5 – 30 h, (c) 30 – 96 h.

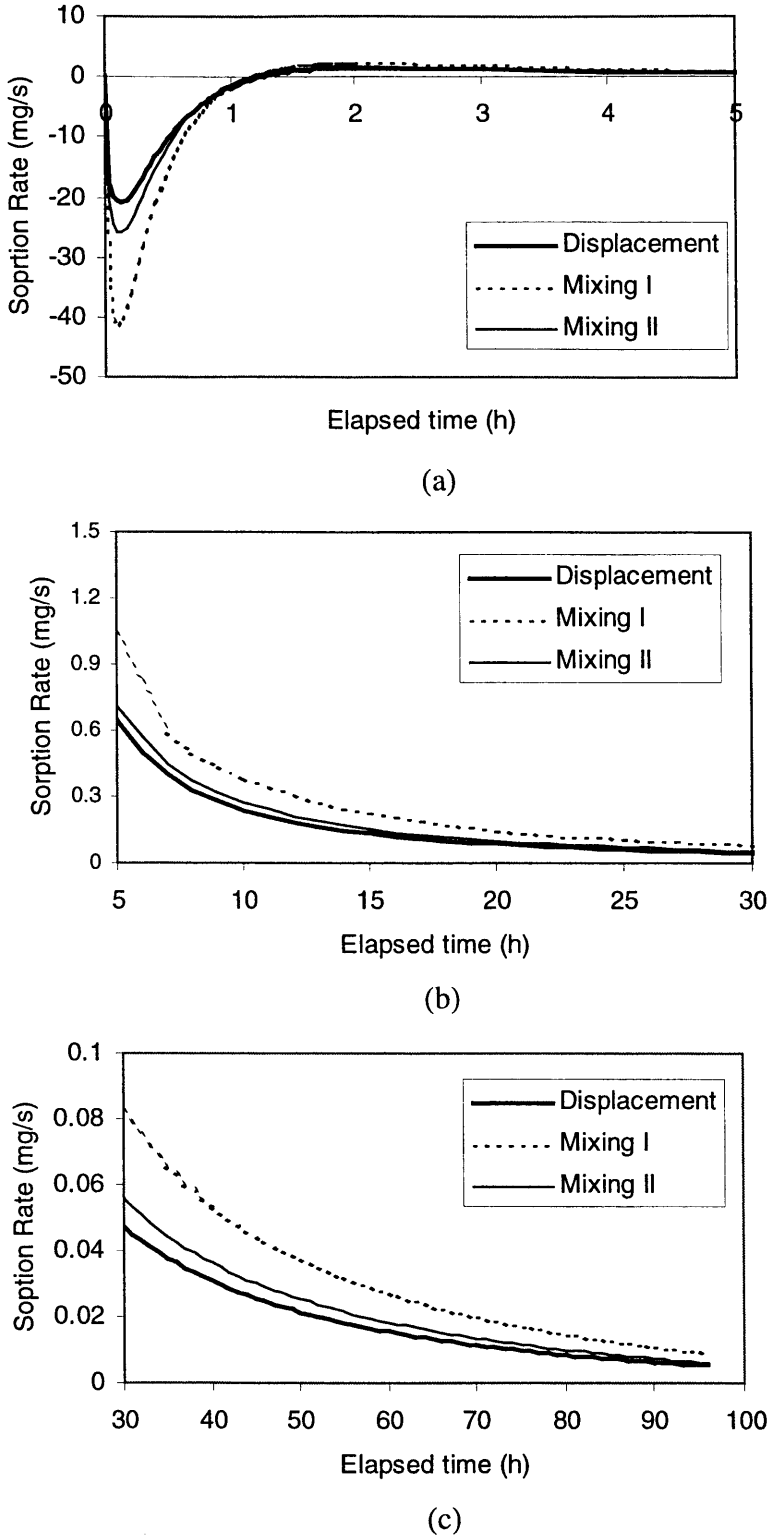

Figure 6.17 Predicted VOC sorption rates by the sinks under different ventilation systems: (a) 0 – 5 h, (b) 5 – 30 h, (c) 30 – 96 h.

To evaluate the sorption capacity by the sinks, Figure 6.18 compares the VOC concentrations at occupant 1 with and without the sinks (for the displacement ventilation). Because the sinks adsorb some VOCs at the early phase, the peak concentration of the no-sink case is about 6% higher than that of the case with sinks. After 2 hours, the concentration of the case without a sink decreases more than that with sinks. At the 96^{th} hour, the release of the adsorbed VOCs from the sinks elevates the concentration by about 10%, compared to the case without sinks.

Figure 6.19 further demonstrates the relative strength of the sink by showing the percentage of the desorption rate of the sinks to the emission rate from the source. The results indicate that the re-emission accounts to about 10% - 15% of the emissions during the initial 96 hours. Note, however, that the above results are based on the model room studied. The model room considers the gypsum wallboard on the four walls as the only sinks whereas in buildings, more and perhaps stronger sinks may exist. Under such circumstances the sink effect is expected to be more significant than what was revealed in the above.

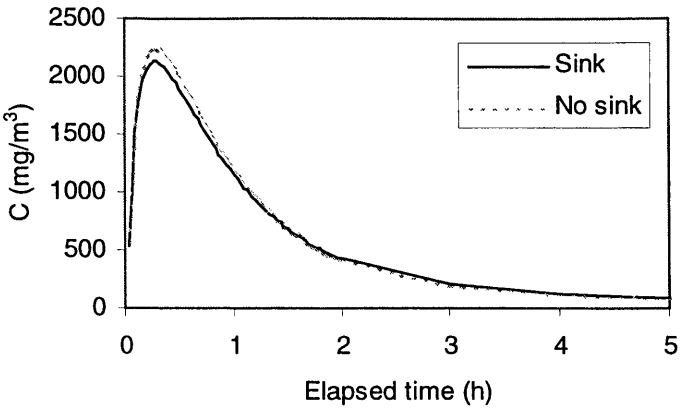

(a)

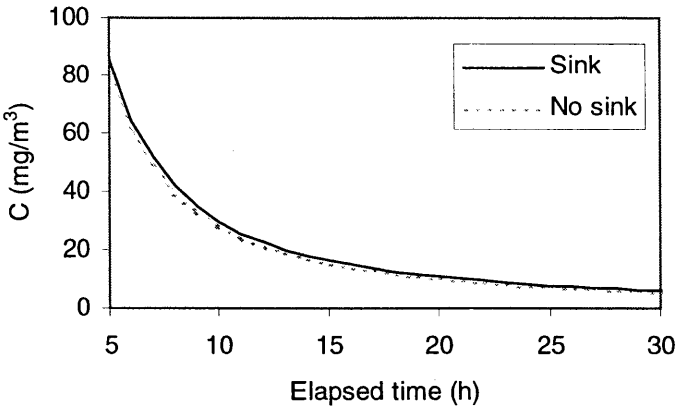

(b)

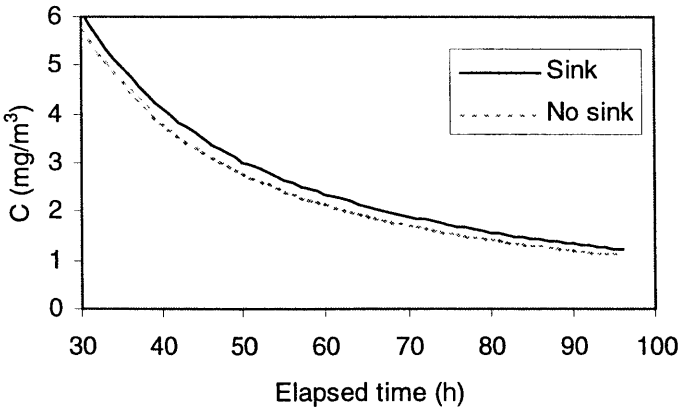

(c)

Figure 6.18 Comparison of VOC concentrations at occupant 1 (type B source) with and without sinks (displacement ventilation): (a) 0 – 5 h, (b) 5 – 30 h, (c) 30 – 96 h.

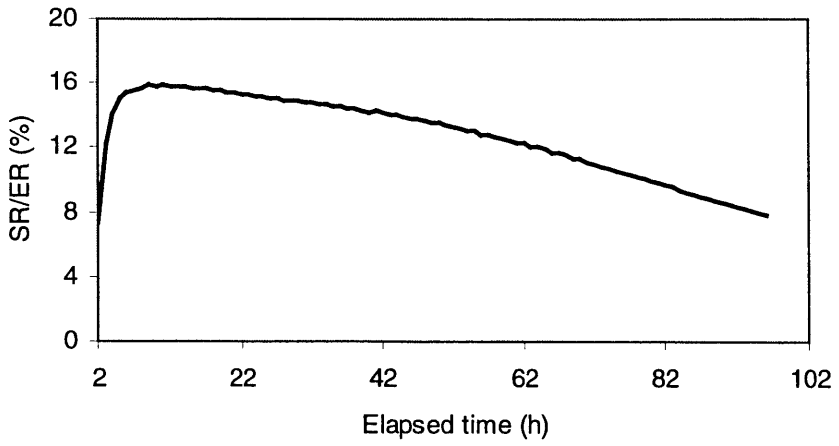

Figure 6.19 Percentage of desorption rate by the sinks compared to the emission rate from the source.

It should be noted that the primary aim of the above case study is to demonstrate the method of an integrated study of material emissions, sorption, and IAQ. The model room considered may be too ideal compared to a real room. Experimental measurements are expected to validate the applicability of the modeling. To acquire more reliable results from the simulations, work is needed to identify and simplify the emission sources and sinks included in a building and the associated material properties (*e.g.*, diffusion coefficient, partition coefficient). Nevertheless, the approach presented should apply to more complicated scenarios.

6.4 Conclusions

Based on the numerical models of material emission and sorption developed in Chapters 3 - 5, this chapter studies the combined problem of material emissions, sorption, IAQ, and VOC exposure in buildings. The model for our IAQ study combines a room airflow model, material emission models, VOC sorption models, and an exposure model. A computer program, ACCESS-IAQ, was developed for the general purposes of studying emission sources, sinks, and IAQ. The program has been used to investigate the effectiveness of displacement ventilation for VOC removal in a small office by comparing the performance of displacement ventilation with two different types of mixing ventilation systems. The following conclusions can be drawn from the small office studied:

(1) For VOC sources with constant flux distributed uniformly across the floor (type A source) without a sink, displacement ventilation generates concentration stratification in the vertical direction. For the three different locations considered (occupants 1 and 2,

room center) and the room average, displacement ventilation has considerably higher concentrations at the breathing level than mixing types II (use of two linear diffusers on the ceiling), but lower concentrations than mixing type I (use of two four-way diffusers on the ceiling).

(2) For the type B source (wood stain) in the floor area with sinks (gypsum board) from the four vertical walls, the relative concentrations among the three ventilation systems follow a similar trend of that with type A source. Further, for the type B source and sinks with displacement ventilation, simulation results show that the walls adsorb significant amounts of VOCs during the first hour and act as secondary sources afterwards. As a result, the sinks lower the peak concentration of about 6% and elevate the concentrations after the peak time. At the 96^{th} hour, release of the adsorbed VOC from the sinks elevated the indoor concentration by approximately 10%.

(3) For the type B source with sinks, displacement ventilation creates lower cumulative inhalation exposure than mixing type I but higher exposure than mixing type II.

(4) Based on the simulation results, displacement ventilation may not provide better IAQ than the mixing ventilation if the VOC sources are distributed on the floor.

Chapter 7

Conclusions and Recommendations

This chapter summarizes the results and conclusions obtained from this study. Some limitations of the current work and future perspectives for material emission and indoor air quality (IAQ) studies are also discussed.

The objective of this thesis work is to study the VOC emission characteristics of various building materials and their impact on indoor air quality (IAQ). The objective has been achieved by using both experimental and modeling approaches. The approaches have broad applicability to most building materials and products that release VOCs into indoor environments.

The major conclusions from the study are summarized as follows.

7.1 Experimental Approach

The effects of environmental conditions (temperature, airflow, VOC concentration in the air) and the substrate on the VOC emissions from two "wet" materials (wood stain and decane) have been systematically measured. We found that:

(1) Airflow (velocity and velocity fluctuation) distributions created different impacts on the "wet" material emissions during the three different emission periods. In the first and second period (0 to 6 h for wood stain), the cases with larger velocity and velocity fluctuation demonstrated a larger initial emission rate and also a faster decay rate. No general trend could be observed during the third period.

(2) Temperature also impacted "wet" material emissions differently during the three periods. In the first period (0 to 0.2 h for wood stain), higher emission rates and faster decay rates were observed for higher temperatures. The impact of temperature during the second period (0.2 to 8 h for wood stain) could not be identified, although it appeared that the cases with higher temperatures also decayed faster. During the third period (> 8 h), results obtained based on the electronic balance and GC/FID analysis did not agree.

(3) Different substrates (oak board and glass) can significantly affect "wet" material emissions. Both the initial emission rate and emission decay rate resulting from the glass substrate were considerably higher than those from the oak substrate during the 6 hour test period. When the wood stain was applied to the porous oak board, the initial emission rates of TVOC during the first 2 hours decreased by as much as about 60% comparing to the use of glass plate as the substrate. In order to evaluate the time-varying VOC emission characteristics of "wet" products, a realistic substrate such as wood should be used.

(4) The emission data measured in a small-scale chamber cannot be applied directly to a building due to the different flow and thermal conditions between a small-scale chamber and a building.

(5) The experimental measurements may not provide reliable results during the third period when emission rates become very low compared to those during the first and second periods.

7.2 Modeling Approach

Several models have been developed to simulate VOC emissions from building materials and furnishings.

7.2.1 A numerical model for simulating emissions of "wet" coating material applied to porous substrates

(1) The comprehensive model considers the VOC mass transfer processes in four different layers: air, material-air interface, material film, and the substrate. It can physically address the impact of temperature and airflow on "wet" material emissions. The model has been validated in a full-scale environmental chamber.

(2) The numerical simulations have confirmed that the emissions from the "wet" materials applied to an absorptive substrate are dominated by evaporation at the beginning and internal diffusion afterwards, which had been hypothesized based on previous experimental data.

(3) The use of the numerical model requires material properties such as VOC diffusivities in the material film and the substrate. This thesis used small-scale chamber data to obtain these properties. With these property values, the numerical model can be used to study "wet" material emissions in actual building environments.

(4) By using the numerical model that we developed, the effects of air velocity, film thickness, temperature, and sample application time on "wet" material emissions have been investigated independently. For the wood stain studied, simulation results indicate that air velocity and sample application time only significantly affect the emission profiles in the early stage (0 - 4 hours). Film thickness, on the other hand, affects long-term ($\tau > 0.2$ h) emissions. Temperature can affect both the short-term and long-term emissions. In order to obtain repeatable and reproducible measurements, all these parameters must be well controlled.

7.2.2 A numerical model for simulating short-term emissions of dry materials

(1) The model uses the following parameters to describe emission characteristics: the initial VOC concentrations in the material (C_0), the solid-phase diffusion coefficient (D_m), the material-air partition coefficient (K_{ma}), and the age of the material (AGE). Numerical simulations show that D_m and C_0 influence both short-term and long-term emissions. K_{ma} and AGE, on the other hand, affect only the short-term emissions of a dry material. They have virtually no impact to long-term emissions.

(2) Using the numerical model we developed, a fairly good agreement of VOC concentrations between the experimental data and model prediction were achieved by pre-determining K_{ma} and AGE and adjusting D_m and C_0. These material properties obtained can be used to study material emissions in buildings, and can help to reduce the material emissions by reformulating the products.

(3) Temperature has a significant effect on VOC emissions from the carpet. The higher the temperature, the higher the initial emission rates and the quicker the depletion of VOCs. Under different temperatures, VOC emissions can be modeled by changing the diffusion coefficient. A formulation of the Arrhenius relation was used to correlate the dependence of D_m on temperature.

7.2.3 An analytical model for estimating long-term emissions of dry materials

(1) The long-term emission model, which assumes that emissions are predominately controlled by a 1-D diffusion process, can be used to quickly estimate the long-term emission source rate of a dry material with a small diffusion coefficient (*e.g.*, $<1\times10^{-12}$ m^2/s).

(2) The long-term emission period is dependent on D_m and C_0. The emissions last longer for a smaller D_m or larger C_0. For dry materials with very small D_m such as the SBR carpet ($D_m \sim 10^{-14}$ to 10^{-13} m^2/s), VOC emissions can last several years. Increasing temperature can increase the D_m and shorten the emission period. However, increasing air temperature within a certain range (*e.g.*, 23 °C – 40 °C) may not bake the VOCs out. For the SBR carpet studied, TVOC emission rates at 40 °C will be higher for about 20 months than those at 30 °C, and at 30 °C they will be higher for about 2 years than those at 23 °C.

7.2.3 A model for detailed simulation of VOC sorption on building materials

(1) Based on the mass transfer theory, the new sorption model analytically solves the VOC sorption rate at the material-air interface as a function of the air-phase concentration and material properties (diffusion coefficient and partition coefficient). The model carries information on the physical representation of the entire sorption process.

(2) A validation of the model using an analytical solution confirms its validity. The sorption model has also been incorporated into a numerical program to study VOC sorption on an unpainted gypsum board. Results show that despite the discrepancies, the model can simulate the general trend of the sorption curve. A better agreement between the predicted and measured sorption effect can be achieved by adjusting the partition coefficient and diffusion coefficient.

(3) The significance of the new sorption model that we developed lies in the fact that it provides a relatively simple way for the prediction of sorption based solely on the physical properties (diffusion coefficient and partition coefficient) of the material. The model can be used to study sorption processes of building materials without resorting to expensive sorption measurements.

7.3 Model Applications

We have used the mass-transfer-based models for emissions and sorption to study IAQ and VOC exposure in a model room. The following conclusions are based on the IAQ study of a small office with two occupants and different types of emission sources, sinks, and ventilation systems.

(1) For VOC sources with constant flux distributed uniformly in the floor (type A source) without a sink, displacement ventilation generates concentration stratification in the vertical direction. For the three different locations considered (occupants 1 and 2, room center) and the room average, displacement ventilation has considerably higher concentrations at the breathing level than mixing type II (use of two linear diffusers on the ceiling), but lower concentrations than mixing type I (use of two four-way diffusers on the ceiling).

(2) For the type B source (wood stain) in the floor area with sinks (gypsum board) from the four vertical walls, the relative concentrations among the three ventilation systems follow a similar trend of that with type A source. Further, for the type B source and sinks with displacement ventilation, simulation results show that the walls adsorb significant amounts of VOCs during the first hour and act as secondary sources afterwards. As a result, the sinks lower the peak concentration of about 6% and elevate the concentrations after the peak time. At the 96^{th} hour, release of the adsorbed VOC from the sinks elevated the indoor concentration by approximately 10%.

(3) For the type B source with sinks, displacement ventilation creates lower cumulative inhalation exposure than mixing type I but higher exposure than mixing type II.

(4) Displacement ventilation may not provide better IAQ than the mixing ventilation if the VOC sources are distributed on the floor.

7.4 Limitations of the Current Work

Apart from the limitations that are already mentioned, the current work is still subject to further improvements in several areas:

(1) The emission, sorption, and IAQ models directly result from the current level of understanding regarding the fundamental processes that control the transport of VOCs. Our knowledge on the complicated emission and sorption process is limited. Detailed theoretical and experimental work on the possible chemical reactions within different materials, surface physics at the material-air interface that adsorbs and desorbs contaminants, and the impact of the humidity on both emissions and sorption is needed.

(2) The work in this thesis is focused on the VOC emissions and sorption of a single material. It needs to be extended to the material assemblies with more complicated initial and boundary conditions (*e.g.*, an air gap between two individual materials).

(3) The IAQ study conducted is based on a simplified model room. The study needs to be extended to more complicated scenarios. To do that, an accurate and effective procedure that can identify and simplify different emission sources and sinks is needed. The standard method to determine the required material properties for the IAQ study is also required.

7.5 Future Perspectives

IAQ is a high priority environmental problem that affects everyone's daily life. In the future, the public's interest and investment in a deeper understanding of IAQ problems caused by material emissions will continue to grow. Several related areas need further scrutiny:

(1) A deep understanding of the health effects of different VOCs, especially the possible long-term health effects of complex mixtures of VOCs at the levels observed in indoor environments.

(2) A complete and useful database of material properties (diffusion coefficient, partition coefficient) and their related correlations.

(3) Development of improved IAQ and exposure models to take a person's breathing system into account.

(4) Development of active VOC control and mitigation strategies other than the use of ventilation systems alone.

(5) Consideration of particles, fibers, pollen, and other gaseous contaminants with a density different from the surrounding room air on IAQ.

References

An, Y., Zhang, J.S. and Shaw, C.Y, 1999, Measurements of VOC adsorption /desorption characteristics of typical interior building material surfaces, *International Journal of HVAC&R Research* (in Press).

Andersson, K., Bakke, J.V., Bjorseth, O., Bornehag, C.-G., Hongslo, J.K., Kjellman, M., Kjaergaard, S., Levy, F., Molhave, L., Skerfving, S. and Sundell, J., 1997, TVOC and health in non-industrial indoor environments, *Indoor Air*, **7**:78-91.

Ashford, N.A. and Miller C.S., 1998, *Chemical Exposures: Low Levels and High Stakes*, Second Edition, John Wiley Press.

ASHRAE, 1996, *ASHRAE Standard 89R: Ventilation for Acceptable Indoor Air Quality (Draft)*, ASHRAE, Atlanta.

ASTM, 1990, *Standard Guide for Small-scale Environmental Chamber Determinations of Organic Emissions from Indoor Materials/products*, ASTM, D5116, American Society of Testing and Materials, Philadelphia.

Axley, J.W, 1991, Adsorption modeling for building contaminant dispersal analysis, *Indoor Air*, **1**:147-171.

Axley, J. W. and Lorenzetti, D., 1993, Sorption transport models for IAQ analysis, *Modeling indoor air quality and exposure*, ASTM STP 1205, 105-127.

Barrer, R.M., 1957, *J. Phys. Chem., Wash.* **61**, 178.

Berglund, B., Johansson, I., and Lindvall, T., 1988, Adsorption and desorption of organic compounds in indoor materials, *Proceedings of Healthy Buildings '88*, Vol. **3**, 299-309.

Beyer, W H., 1975, *Handbook of Mathematical Sciences*, 5th Edition, CRC Press, Inc.

Blay, D., Mergui, S., and Niculae, C., 1992, Confined turbulent mixed convection in the presence of a horizontal buoyant wall jet, *Fundamentals of mixed convection*, HTD **213**: 65-72.

Bluyssen, P.M., van der Wal, J.F., Cornelissen, H.J.M., Hoogeveen, A.W., and Wouda, P., 1995, European database of indoor air pollution sources: the effect of temperature on the chemical and sensory emissions of indoor materials, TNO-Report 95-BBI-R0826, The Netherlands.

Bodalal, A., Zhang, J.S., Plett, E.G., 1999, A method for measuring internal diffusion and

partition coefficients of volatile organic compounds for building materials. Building and Environment, 1-24 (NRCC-41957). (In press)

Bodalal, A., 1999, Fundamental mass transfer modeling of emission of volatile organic compounds from building materials, Ph.D. Thesis, Department of Mechanical and Aerospace Engineering, Carleton University, Canada.

Brohus, H., 1997, Personal exposure to contaminant sources in ventilated rooms. Ph.D. Thesis, Department of Building Technology and Structural Engineering, Aalborg University, Denmark.

Brown, S.K., Sim, M.R., Abramson, M.J. and Gray, C.N., 1994, Concentrations of volatile organic compounds in indoor air – a review, *Indoor Air*, **4**:123-134.

Cantrel, L., Chaouche, R., and Chopin-Dumas, J., 1997, Diffusion coefficients of molecular iodine in aqueous solutions, *J. Chem. Eng. Data*, **42**, 216-220.

CEC, 1992, *Guidelines for ventilation requirements in buildings*, Commission of the European Communities, report No. 11, Luxembourg.

CHAM, 1996, PHOENICS Version 2.1, CHAM Ltd, UK.

Chang, J.C.S., 1992, Modeling of he fast organic emissions from a wood-finishing product – floor wax, *Atmospheric Environment*, Vol. **26A**, No. 13, 2365-2370.

Chang, J.C.S. and Guo, Z., 1992, Characterization of organic emissions from a wood finishing product — wood stain, *Indoor Air*, **2**:146-153.

Chang, J.C.S., Tichenor, B.A., Guo, Z. and Kreb, K., 1997, Substrate effects on VOC emissions from a latex paint, *Indoor Air*, **7**:241-247.

Chen, J.J. and Lin, J.D., 1998, Simultaneous heat and mass transfer in polymer solutions exposed to intermittent infrared radiation heating, *Numerical Heat Transfer, Part A*, **33**:851-873.

Chen, P. and Pei, C.T., 1989, A mathematical model of drying processes. *International Journal of Heat and Mass Transfer*, **32**(2):297-310.

Chen, Q., 1995, Comparison of different k-e models for indoor airflow computations, *Numerical Heat Transfer, Part B*, **28**:353-369.

Chen, Q., 1996, Prediction of room air motion by Reynolds-stress models. *Building and Environment*, **31**(3):233-244.

Chen, Q., Glicksman, L., Yuan, X., Hu, S., Hu, and Y., 1999, Performance Evaluation and Development of Design Guidelines for Displacement Ventilation, Final report to ASHRAE TC 5.3 – Room Air Distributions in ASHRAE Research Project – RP – 949, Department of Architecture, Massachusetts Institute of Technology, Cambridge, MA.

Chirife, 1983, Fundamentals of the drying mechanism during air dehydration of foods, in *Advances in Drying* (Edited by A.S. Mujumdar), Vol. **2**, 73-80, Hemisphere, Washington DC.

Christianson, J., Yu, J.W. and Neretnieks, I., 1993, Emission of VOC's from PVC-flooring — models for predicting the time dependent emission rates and resulting concentrations in the indoor air, *Proceedings of Indoor Air'93*, **2**, 389-394.

Clark, M.M., 1997, *Transport Modeling for Environmental Engineers and Scientists*, John Wiley & Sons, New York.

Colombo, A. and De Bortoli, M., 1992, Comparison of models used to estimate parameters of organic emissions from materials tested in small environmental chambers, *Indoor Air*, **2**:49-57.

Crank, J. and Park, G.S. (Eds), 1968, *Diffusion in polymers*, Academic Press, London and New York.

Daniels, F. and Alberty, R., 1961, *Physical Chemistry*, John Wiley & Sons, New York.

De Bellie, L., Haghighat, F. and Zhang, Y., 1995, Review of the effect of environmental parameters on material emissions, Proceedings of the 2nd International Conference on Indoor Air Quality, Ventilation, and Energy Conservation in Buildings, Montreal, Canada, 111-119.

DIN-1946, 1994, *Raumlufttechnik, Gesundheitstechnische Anforderungen (VDI-LUFTUNGSREGELN).*

Dunn, J.E., 1987, Models and statistical methods for gaseous emission testing of finite sources in well-mixed chambers, *Atmospheric Environment*, **21**(2):425-430.

Dunn J. and Tichenor, B., 1988, Compensating for sink effects in emissions test chambers by mathematical modeling, *Atmospheric Environment*, **22**:885-894.

Dunn, J. E. and Chen, T., 1993, Critical evaluation of the diffusion hypothesis in the theory of porous media VOC sources and sinks, *Modeling indoor air quality and exposure*, ASTM STP 1205, 64-80.

EDP, 1994, *European Draft Prestandard prENV 1752*, European Committee for Standardization, Brussels.

Esmen, T., 1985, The status of indoor air pollution, *Environmental health Perspectives*, **62**:259-265.

European Commission, 1997, *European Data Base on Indoor Air Pollution Sources in Buildings*, Final Report.

Fisk, W. and Rosenfeld, A.H., 1997, Estimates of improved productivity and health from better indoor environments, *Indoor Air*, **7**:158-172.

Glasstone, S., Laider, K.J., and Eyring, H., 1941, *The Theory of Rate Processes*, Chapter 9, McGraw-Hill Book Company, Inc., New York.

Guo, Z. and Tichenor, B.A., 1992, Fundamental mass transfer models applied to evaluating the emissions of vapor-phase organics from interior architectural coatings, *Proceedings of EPA/AWMA Symposium*, Durham, NC.

Guo, Z., Fortman, R., Marfiak, S., Tichenor, B.A., Sparks, L., Chang, J.C.S. and Mason, M., 1996a, Modeling the VOC emissions from interior latex paint applied to gypsum board, proceedings of Indoor Air'96, Vol. **1**, 987-991, Nagoya, Japan.

Guo, Z., Tichenor, B.A., Krebs, K.A., and Roache, N.F., 1996b, Considerations on revision of emissions testing protocols, Characterizing sources of indoor air pollution and related sink effects, ASTM STP 1287, Bruce A. Tichenor, Ed., American Society for Testing and Materials, 225-236.

Guo, Z., Sparks, L.E., Tichenor, B.A. and Chang, J.C.S., 1999, Predicting the emissions of individual VOCs from petroleum-based indoor coatings, *Atmospheric Environment* (in Press).

Haghighat, F., Jiang, Z. and Zhang, Y., 1994, The impact of ventilation rate and partition layout on the VOC emission rate: time-dependent contaminant removal, *Indoor Air*, **4**:276-283.

Haghighat, F. and De Bellis, L., 1998, Material emission rates: literature review, and the impact of indoor air temperature and relative humidity, *Building and Environment*, **33**(5):261-277.

Harlow, F.H. and Welch, J.E., 1965, Numerical calculation of time-dependent viscous incompressible flow of fluid with free surface, *Physics Fluids*, Vol. **8**, 2182-2189.

Hart, G.H. and Int-Hout, D., 1980, The performance of a continuous linear air diffuser in the perimeter zone of an office environment, *ASHRAE Transactions*, Vol. **86**, Part 2, 107-124.

Hayes, S.R., 1989, Estimating the effect of being indoors on total personal exposure to outdoor air pollution, *J. Air & Waster management Assoc.*, **39**:1453.

Haymore, C. and Odom, R., 1993, Economic effects of poor IAQ, *EPA Journal*, **19**(4), 28-29.

Hodgson, A.T., Wooley, J.D., and Daisey, J.M., 1993, Emissions of volatile organic compounds from new carpets measured in a large-scale environmental chamber, *J. Air Waste Manage. Assoc.*, **43**:316-324.

Jayjock, M.A., Doshi, D.R., Nungesser, E.H. and Shade, W.D., 1995, Development and evaluation of a source/sink model of indoor air concentrations from isothiasolone-treated wood used indoors, *Am. Ind. Hyg. Assoc. J.*, **56**:546.

Jost, W., 1960, *Diffusion in Solids, Liquids, Gases*, Academic Press Inc., Publishers, New York.

Launder, B.E. and Spalding, D.B., 1974, The numerical computation of turbulent flows, *Computer Methods in Applied Mechanics and Energy*, **3**, 269-289.

Lide, D.R. (Editor-in-Chief), 1995, *Handbook of Chemistry and Physics*, 76th Ed, CRC Press.

Little, J.C., Hodgson, A.T., and Gadgil, A.J., 1994, Modeling emissions of volatile organic compounds from new carpets, *Atmospheric Environment*, **28**(2):227-234.

Lyman, W.J., Reehl, W.F. and Rosenblatt, D.H., 1990, *Handbook of chemical property estimation method*, American Chemical Society, Washington, DC.

Mage, D.T. and Gammage, R.B., 1985, Evaluation of changes in indoor air quality occurring over the past several decades. In: Gammage, R.B. and Kaye, S.V. (Eds) Indoor Air and Human health, Chelsea, MI, Lewis Publishers, Inc. 5-36.

Magee, R.. 1998. Measurements of VOC emissions from particleboards, Private communications.

Matthews, T.G., Reed, T.J., Timberg, B.J., Daffron, C.R. and Hawthorne, A.R., 1983, Formaldehyde emissions from combustion sources and solid formaldehyde resin containing products: Potential impact on indoor formaldehyde concentrations and possible corrective measures, *Proceedings of An Engineering Foundation*

Conference on Management of Atmospheres in Tightly Enclosed Spaces, Santa Barbara, ASHRAE, 23-43.

Matthews, T.G., Hawthorne, A.R. and Thompson, C.V., 1987, Formaldehyde sorption and desorption characteristics of gypsum wallboard, *Environmental Science and Technology*, **21**(7), 629-634.

Merrill, R., Steiber, R. and Nelms, L., 1987, Screening methods for the identification of organic emissions from indoor air pollution sources, *Atmospheric Environment*, **21** (2): 331-336.

Mills, A.F., 1995, *Heat and Mass Transfer*, Irvine.

Molhave, L., 1982, Indoor air pollution due to organic gases and vapours of solvents in building materials, *Environment International*, Vol. **8**, 117-127.

Molhave, L., Liu, Z., Jorgensen, A.H., Pedersen, U.F., and Kjargaard, S.K., 1993, Sensory and physiological effects on humans of combined exposures to air temperatures and volatile organic compounds, *Indoor Air*, **3**:155-169.

Molhave, L., Jensen, J.G. and Larsen, S., 1998, Acute and sub-acute subjective reaction to volatile organic compounds, *Atmospheric Environment*, **25A**:1283-1293.

Murakami, S., Kato, S., Chikamoto, T., Laurence, D., and Blay, D., 1996, New low-Reynolds number k-e model including damping effect due to buoyancy in a stratified flow field, *Int. J. Heat Mass Transfer,* **39**(16):3493-3496.

National Research Council, 1999, MEDB-IAQ: Material Emission Database and a single-zone IAQ model – a tool for building designers, engineers, and managers, IRC/NRC CMEIAQ Final Report 4.2, Ottawa, Canada.

Neretnieks, I., Christiansson, J., Romero, L., Dagerholt, L. and Yu, J.W., 1993, Modeling of emission and re-emission of volatile organic compounds from building materials with indoor air applications, *Indoor Air*, **3**:2-11.

Nielsen, P., 1987, Potential pollutants – their importance to the Sick Building Syndrome –and their release mechanism, *Proceedings of Indoor Air'87*, Vol. **2**, 598-602.

Okazaki, M., Shioda, K., Masuda, K. and Toei, R., 1974, Drying mechanisms of coated film of polymer solution, *Journal of Chemical Engineering of Japan*, Vol. **7**, No. 2, 99-105.

Patankar, S.V. and Spalding, D.B., 1970, *Heat and Mass Transfer in Boundary Layers*, Intertext Books, London.

Patankar, S.V., 1980, *Numerical Heat Transfer and Fluid Flow*, Hemisphere Publishing Corp, New York.

Peeters, T.W. and Henkes, R.A.W.M., 1992, The Reynolds-stress model of turbulence applied to the natural-convection boundary layer along a heated vertical plate, *Int. J. Heat Mass Transfer,* **35**, 403-420.

Pettankofer, M.V., 1892, Uber das Verhalten der Luft zum Wohnhause, Beziehungen der Luft zu Kleidung, Wohnung und Boden. – Viehweg, Braunschweig, S. 39 – 74.

Reid, R.C., Prausnitz, J.M., and Sherwood, T.K., 1977, *The Properties of Gases and Liquids*, McGraw-Hill Book Company.

Sano, Y. and Yamamoto, S., 1990, Calculation of concentration-dependent mutual diffusion coefficient in desorption of film, *Journal of Chemical Engineering of Japan*, Vol. **23**, No. 3, 331-338.

SBE, 1995, Statens Bygningstekniske Etat, *Guidelines to Norweigian Building Code* (draft).

Schwope, A.D., Lyman, W.J., and Reid, R.C., 1989, Methods for assessing exposure to chemical substances, *Vol. 11: Methodology for estimating the migration of additives and impurities from polymetric materials*, U.S. Environmental Protection Agency, Office of Toxic Substances, Washington, DC, EPA/560/5-85-015.

Sherwood, T.K., 1929, The drying of solids: I, *Ind. Eng. Chem.*, Vol. **21**, 12-16.

Sparks, L.E., 1991, EXPOSURE Version 2 A Computer Model for Analyzing the Effects of Indoor Air Pollutant Sources on Individual Exposure, EPA Report EPA/600/8-91/013, U.S. Environmental Protection Agency, Washington D.C.

Sparks, L.E., Tichenor, B.A., Chang, J. and Guo, Z., 1996, Gas-phase mass transfer model for predicting volatile organic compound (VOC) emission rates from indoor pollutant sources, *Indoor Air*, **6**:31-40.

Sparks, L.E., Guo, Z., Chang, J.C.S and Tichenor, B.A, 1999, Volatile organic compound emissions from latex paint – Part 1 chamber experiments and source model development, *Indoor Air*, **9**:10-17.

Svanstrom, 1997, Blowing Agents in Rigid Polyurethane Foam, Ph.D. Thesis, Department of Chemical Environmental Science, Chalmers University of Technology, Sweden.

Tichenor, B., Sparks, L., White, J. and Jackson, M., 1988, Evaluating sources of indoor air pollution, paper presented at 81st Annual Meeting of the Air Pollution Control Association, Dallas, TX.

Tichenor, B.A., Guo, Z., Dunn, J.E., Sparks, L.E. and Mason, M.A., 1991, The interaction of vapor phase organic compounds with indoor sinks, *Indoor Air*, **1**:23-35.

Tichenor, B.A., 1996, Overview of source/sink characterization methods, Characterizing sources of indoor air pollution and related sink effects, ASTM STP 1287, Bruice A. Tichenor, Ed., American Society for Testing and Materials, 1996, 9-19.

Topp, C., Nielsen, P.V. and Heiselberg, P., 1997, Evaporation controlled emission in ventilated rooms, *Proceedings of Healthy Buildings/IAQ'97*, Washington DC.

U.S. EPA, 1988, Total Exposure Assessment Methodology (TEAM) Study, NTIS PB88-10052, U.S. Environmental Protection Agency, Washington, DC.

U.S. EPA, 1990, Reducing risk: setting priorities and strategies for environmental protection, Science Advisory Board, U.S. Environmental Protection Agency, Washington, DC.

U.S. EPA, 1991, Sick building syndrome (SBS), Indoor Air Facts No. 4 (revised), U.S. Environmental Protection Agency, Washington, DC.

van der Wal, J.F., Moons, A.M.M. and Cornelissen, H.J.M., 1991, Indoor air quality in renovated Dutch homes, *Indoor Air*, **1**:621-633.

Van Amerongen, G.J., 1950, *J. Polym. Sci.*, **5**, 307.

Van Amerongen, G.J., 1964, *Rubb. Chem. Technol.*, **37**, 1065.

Wallace, L.A., Pellizzari, E.P., Leaderer, B., Zelon, H. and Sheldon, L., 1987, Emissions of volatile organic compounds from building materials and consumer products, *Atmospheric Environment*, **21**(2): 385-393.

Wijeysundera, N.E., Zheng, B.F., Iqbal, M. and Hauptmann, E.G., 1996, Numerical simulation of the transient moisture transfer through porous insulation, *Int. J. Heat Mass Transfer*, **39**(5):995-1004.

Wilkes, C., Koontz, M., Ryan, M. and Cinalli, C., 1996, Estimation of emission profiles for interior latex paints, *Proceedings of Indoor Air'96*, Nagoya, Japan.

Wolkoff, P., Clausen, P.A., and Nielsen, P.A., 1993, Application of fields and laboratory emission cell (FLEC) recovery study, case study of damaged linoleum, and liquid wax, *Indoor Air*, **3**:543-549.

Wolkoff, P., 1995, Volatile organic compounds: sources, measurements, emissions, and the impact on indoor air quality, *Indoor Air*, **5**, Supplement 3.

World Health Organization, 1989, Indoor air quality: organic pollutants, Copenhagen, WHO regional office for Europe (EURO Report and Studies I111).

Xu, W., 1998, New Turbulence Models for Indoor Airflow Simulation, Ph.D. Thesis, Department of Architecture, Massachusetts Institute of Technology

Yang, X., Chen, Q. and Zhang, J.S., 1997, Study of VOC emissions from building materials using computational fluid dynamics, *Proceedings of Healthy Buildings/IAQ'97*, 587-592, Washington DC.

Yang, X., Chen, Q. and Zhang, J.S., 1998a, Impact of early stage incomplete mixing on estimating VOC emissions in small test chambers, *Indoor Air*, **8**:180-189.

Yang, X., Chen, Q. and Bluyssen, P.M., 1998b, Prediction of short-term and long-term volatile organic compound emissions from SBR bitumen-backed carpet under different temperatures, *ASHRAE Transactions*, **104**(2), 1297-1308.

Yokhot, V., Orzag, S.A., Thangam, S. Gatski, T.B., and Speziale, C.G., 1992, Development of turbulence models for shear flows by a double expansion technique, *Physics Fluids A*, **4**(7), 1510-1520.

Yuan, X., Chen, Q., Glicksman, L.R., Hu, Y., and Yang, X., 1999, Measurements and computations of room airflow with displacement ventilation, *ASHRAE Transactions*, **105**(1).

Zhang, J.S., 1998, VOC sorption data of unpainted gypsum board, Private communications.

Zhang, J.S., Shaw, C.Y., Nguyen-Thi, L.C., Macdonald, R.A. and Kerr, G., 1995, Field measurements of boundary layer flows in ventilated rooms, *ASHRAE Transactions*, **101**(2).

Zhang, J.S., Shaw, C.Y., Kanabus-Kaminska, J.M., MacDonald, R.A., Magee, R.J., Lusztyk, E. and Weichert, H.J., 1996a, Study of air velocity and turbulence effects on organic compound emissions from building materials/furnishings using a new small test chamber, *Characterizing Sources of Indoor Air Pollution and Related Sink Effects, ASTM STP 1287, Bruce A. Tichenor, Ed.,* ASTM, 184-199.

Zhang, J.S., Kanabus-Kaminska, J.M. and Shaw, C.Y., 1996b, A full-scale test chamber for material emission studies and indoor air quality modeling, *Characterizing Sources of Indoor Air Pollution and Related Sink Effects, ASTM STP 1287, Bruce A. Tichenor, Ed.,* ASTM, 58-66.

Zhang, J.S., Nong, G., Shaw, C.Y. and Wang, J.M., 1999, Measurements of volatile organic compound (VOC) emissions from wood stains by using an electronic balance, *ASHRAE Transactions* **105**(1).

Zhang Y. and Haghighat, F., 1997, The impact of surface air movement on material emissions, *Building and Environment*, **32**(6):551-556.

Appendix: The program Structure of ACCESS-IAQ

A computer simulation of IAQ should be a general-purpose program that can be easily adapted for a solution of the particular problem. At the same time, the program must provide a structure in which the user can easily make the necessary changes. The computer program ACCESS-IAQ has been developed to meet those requirements.

The program ACCESS-IAQ has five elements and several data files as shown in Figure A.1. In the following, the functions of these elements will be briefly explained. Contents of the data files are listed in Table A.1.

(1). PHOENICS: The program PHOENICS is a stand-alone CFD code developed by the CHAM, Ltd. (CHAM, 1996). PHOENICS is included in ACCESS-IAQ because it is used to simulate the distributions of air velocity, temperature, and turbulence by using appropriate turbulence models (*e.g.*, the two-layer turbulence model). Other CFD codes can be used in place of PHOENICS as long as they can accurately predict the flow and thermal conditions in a space.

(2). SORPTION: This program pre-calculates the sorption properties of each sink material based on the sorption model developed in Chapter 5. The values that are pre-calculated using SORPTION include X(0), W_i, and μ_i (see Eqs. (5.16), (5.19), and (5.21) for the meaning of these variables).

(3). IAQ: The program IAQ solves the 3-D transient problems of material emission, sorption, and VOC transport in a space. It is equipped with all the mass transfer equations given in Chapters 3 - 5 as well as three options of equation solvers: Gauss-Seidel, TDMA, and Strong Implicit Procedure (SIP). Gauss-Seidel solver is very stable but slow compared to the other two solvers (hence needs significantly longer computing time). It is used only when both the other two solvers fail to converge.

(4). POSTC: The results from IAQ are huge data files containing all the detailed information of VOC emission, sorption, and concentrations. The program POSTC is used to extract the information that is needed from the detailed result file.

(5). EXPC: This spreadsheet program calculates the total exposures based on the simulated concentration history and human activities.

The current version of ACCESS-IAQ has no graphical interface for both input and output. However, the simulation results (*e.g.*, concentration distributions) can be conveniently loaded into other CFD programs (*e.g.*, PHOENICS) or plotting tools (*e.g.*, TECPLOT) to be visualized graphically.

Table A.1 Contents of the data files used in ACCESS-IAQ

Data file	Type (input/output) and connection	Contents
q1	Input of PHOENICS	• Grid information of the computation domain • Flow and thermal boundary conditions • Specification of the turbulence model
iaq.dat	Input of IAQ	• Specification of VOC sources • VOC boundary conditions
eigen.dat	Input of SORPTION	• Specification of VOC sinks
Phi	Output of PHOENICS Input of IAQ	• Grid information of the computational domain • Results of distributions of velocity, temperature, and turbulence properties
eigen.out	Output of SORPTION Input of IAQ	• Pre-calculated results for sorption
cresult.dat	Output of IAQ Input of POSTC	• Simulated results of concentration distributions and mass transfer rates of sources and sinks at different times
cneed.dat	Output of POSTC	• Simulated results based on the user's specific needs (*e.g.*, concentration distributions around an occupant)
exp.dat	Output of EXPC	• Results of VOC exposures at specified locations

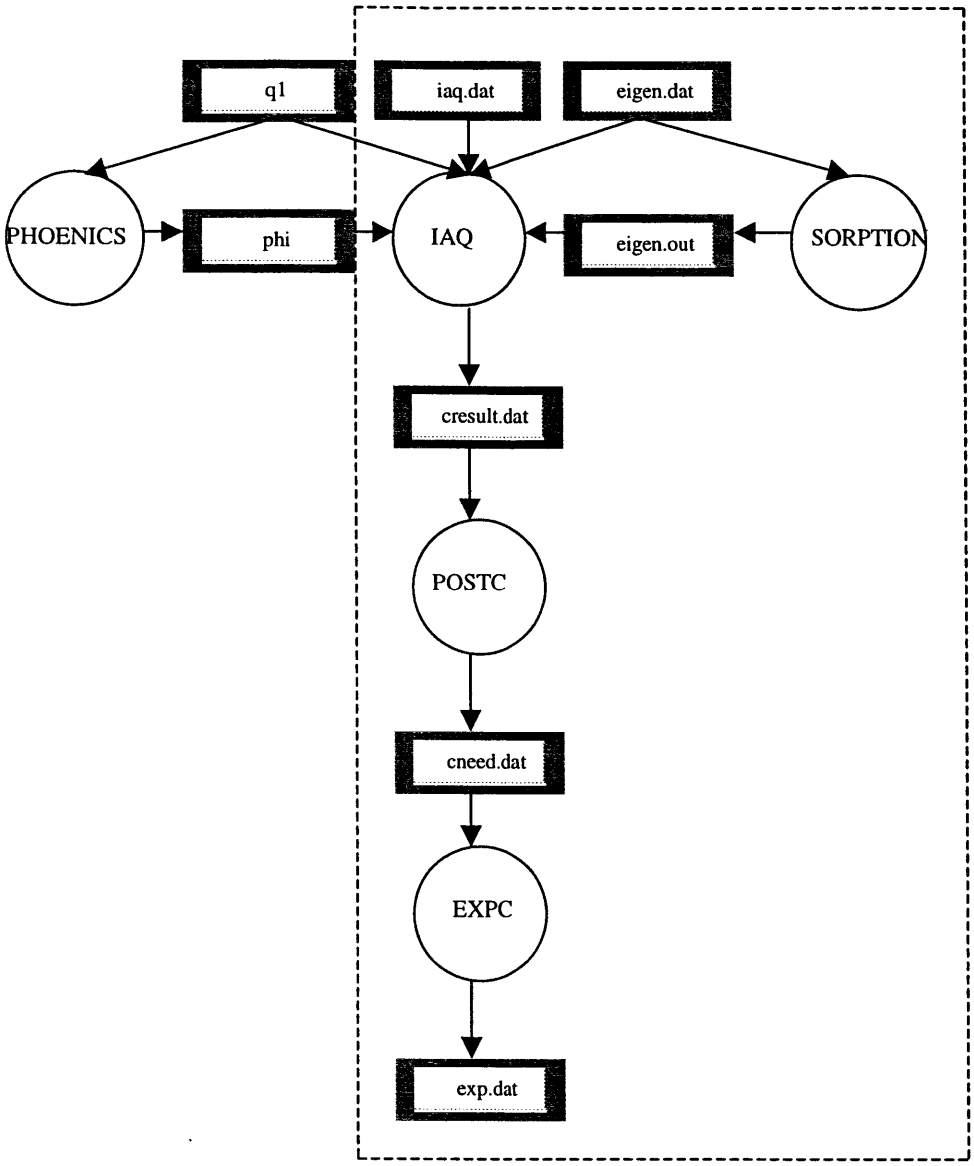

Figure A.1 Schematic representation of separate programs and data connections for ACCESS-IAQ. Contents in the dashed square are developed by the author. PHOENICS is a commercial CFD program.

Nomenclature

a, b, c, d, f	constants determined by the Least Square Regression Analysis
$a_{\phi,E}$, $a_{\phi,W}$, $a_{\phi,N}$, $a_{\phi,S}$, $a_{\phi,H}$, $a_{\phi,L}$, $a_{\phi,\tau}$, $a_{\phi,P}$	coefficients in discretized equations
A, B	properties of compounds
AGE	age of the material, day
b	breathing rate, breath/hour
c_1, c_2, k_1, k_2	constants determined by the Least Square Regression
C_0	initial concentration of compound in the solid slab, $\mu g/m^3$
C_a	air phase VOC concentration, mg/m^3
C_a^+	dimensionless concentration, $\frac{(C_{a,int} - C_a)u_\tau}{q_{int}}$
$C_{a,0}$	VOC vapor pressure, mg/m^3
C_{ad}	adsorbed VOC concentration on the material surface, mg/m^3
$C_{a,int}$	air phase VOC concentration at material-air interface, mg/m^3
$C_{l,0}$	initial VOC concentration in the "wet" source, mg/m^3
C_m	VOC concentration in the material film, mg/m^3
$C_{m,0}$	initial VOC concentration in the material film, mg/m^3
$C_{m,int}$	surface concentration on the material side, mg/m^3
$C_{o,12}$	average compound concentration between time τ_1 and τ_2, $\mu g/m^3$
COEF	coefficient
C_s	VOC concentration in the substrate, mg/m^3
C_∞	VOC concentration in the bulk flow, mg/m^3
D_0	initial diffusion coefficient in the material film, m^2/s
D_a	VOC diffusion coefficient in the air, m^2/s
$D_{a,eff}$	effective air phase diffusion coefficient
D_e, D_w, D_n, D_s, D_h, D_l	diffusive coefficient at each face of the current cell (Table 3.3)
D_m	effective diffusion coefficient in the material film, m^2/s
$D_{m,0}$	initial VOC diffusivity in the material film, m^2/s
D_s	VOC diffusion coefficient in the substrate, m^2/s
E	constant, E=9 for a moderate pressure-gradient flow
$E(\tau_{i+1/2})$	average emission rate between τ_i and τ_{i+1}, g/h
E_d	activation energy, J/mol
E_{f12}	average compound emission factor between time τ_1 and τ_2, $\mu g/m^2h$
E_i	inhalation exposure, mg/h
F_e, F_w, F_n, F_s, F_h, F_l	convective flux at each face of the current cell (Table 3.3)
Fo	Fourier number, $D_m\tau/\delta^2$
g	weight of non-VOC content, g
h	inner chamber height, m
h_c	mass transfer coefficient, m/h
k	turbulent kinetic energy, m^2/s^2
K_l	Langmuir sorption coefficient
K_{ma}	material-air partition coefficient
L	characteristic length of the source, m

L_p	penetration length, m
M	molecular weight of the compound, g/mol
M_τ	total amount of compound emitted up to time τ, μg
M_∞	total amount of compound in the material, μg
P	VOC vapor pressure, mmHg
Pr	Prandtl number
Pr_t	turbulent Prandtl number
q	VOC emission or sorption rate, mg/m^2s
q_s	source term
Q	VOC emission or sorption rate in the Laplace domain
Q_{int}	heat transfer rate, W/m^2
R	universal gas constant (=8.3145 $Jmol^{-1}K^{-1}$)
Re_h	Reynolds number based on h, $Vh\rho/\mu$
Re_L	Reynolds number based on L, $VL\rho/\mu$
s	Laplace operator
S	VOC source term, mg/m^3s
Sc	Schmidt number of VOC
Sc_t	turbulent Schmidt number
Sh	Sherwood number, $h_cL/(3600D_a)$
S_ϕ	source term for ϕ
T	absolute temperature, K
T^+	dimensionless temperature, $\frac{(T_{a,int}-T_a)u_\tau}{Q_{int}}$
$T_{a,int}$	surface temperature, °C
u_j (j=1,2,3)	three components of air velocity
u_τ	friction velocity, $\sqrt{\frac{\tau_w}{\rho}}$
u^+	dimensionless velocity, $\frac{u}{u_\tau}$
v	volume per breath, m^3/breath
V	air velocity, m/s
VAL	value
W	weight of the "wet" material remaining in the substrate, g
x,y,z	coordinates
x_j (j=1,2,3)	coordinates
X_0	coefficient to calculate the sorption rate on a solid material
X(j)	system response under the unit triangle function $f(j\Delta\tau)$
y	distance between the first grid node and the wall, m
y^+	dimensionless wall distance, $\frac{yu_\tau\rho}{\mu}$

Greek Symbols

α	liquid expansion factor
θ_m	dimensionless concentration
τ	time, sec (or h)
τ_w	wall shear stress, kg/ms^2
δ	thickness of the solid slab, m
μ	molecular viscosity of air, Pa.s
μ_i	roots of B(s) (see Eq.(5.15)), $\frac{\pi^2 i^2}{L_m^2} D_m$
μ_t	turbulent viscosity, $\rho C_\mu \frac{k^2}{\varepsilon}$
ε	dissipation rate of turbulent kinetic energy
ε_t	truncation error
ρ	air density, kg/m^3
ρ_l	liquid density, mg/m^3
κ	von Karman constant (0.435)
$\phi_E, \phi_W, \phi_N, \phi_S$	
$\phi_H, \phi_L, \phi_P, \phi_{P^-}$	parameter ϕ in each cell
$\Delta\tau$	time step sec (or h)
Δy_m	grid size (in y direction) of the first near-interface grid
$\Gamma_{\phi,eff}$	effective diffusion coefficient for ϕ

Abbreviations

1-D, 2-D, 3-D	One, two, three dimensional
ACCESS-IAQ	A Code for Characterizing Emission Sources, Sinks, and Indoor Air Quality
ACH	Air Change per Hour
ASTM	American Society of Testing and Materials
BLDC	Boundary Layer Diffusion Controlled
CFD	Computational Fluid Dynamics
DNS	Direct Numerical Simulation
FID	Flame Ionization Detector
GC	Gas Chromatography
HVAC	Heating, Ventilating, and Air-Conditioning
IAQ	Indoor Air Quality
LES	Large Eddy Simulation
LRN	Low-Reynols-Number
MCS	Multiple Chemical Sensitivity
MS	Mass Spectrometry
RNG	Re-Normalization Group
RSM	Reynolds-Stress Models
SBR	Styrene-Butadiene Rubber

SBS	Sick Building Syndrome
TDMA	Tri-Diagonal Matrix Algorithm
TVOC	Total Volatile Organic Compound
US EPA	U.S. Environmental Protection Agency
VB	Vapor pressure and Boundary layer
WHO	World Health Organization
VOC	Volatile Organic Compound